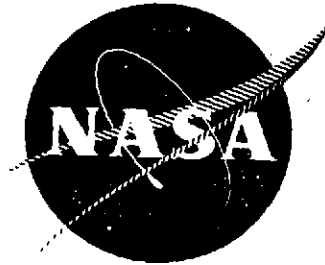


NASA-CR-121093
Final Report
F-C3452-1



STEADY-STATE AND DYNAMIC PERFORMANCE OF A
GAS-LUBRICATED SEAL

By

R. Colsher
W. Shapiro

The Franklin Institute Research Laboratories

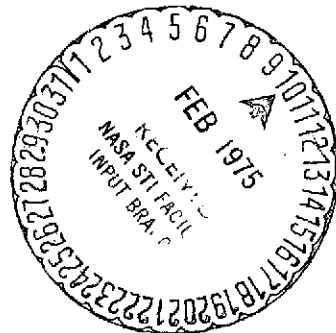
Prepared for

National Aeronautics and Space Administration

NASA Lewis Research Center

Contract Nos. NAS3-16863
and NAS3-14418

Reproduced by
**NATIONAL TECHNICAL
INFORMATION SERVICE**
US Department of Commerce
Springfield, VA. 22151



PRICES SUBJECT TO CHANGE

(NASA-CR-121093) STEADY-STATE AND DYNAMIC
PERFORMANCE OF A GAS-LUBRICATED SEAL Final
Report (Franklin Inst. Research Labs.,
Philadelphia) 158 p
CSCL 131
G3/37 07755
N75-15993
Unclas

1. Report No. CR121093		2. Government Accession No.		3. Recipient's Catalog No.	
4. Title and Subtitle Steady State and Dynamic Performance of Gas-Lubricated Seals				5. Report Date November 1972	
				6. Performing Organization Code	
7. Author(s) R. Colsher and W. Shapiro				8. Performing Organization Report No. F-C3452-1	
9. Performing Organization Name and Address Franklin Institute Research Laboratories Benjamin Franklin Parkway Philadelphia, Pa. 19103				10. Work Unit No.	
				11. Contract or Grant No. NAS-3-16863	
12. Sponsoring Agency Name and Address National Aeronautics and Space Administration Washington, D.C. 20546				13. Type of Report and Period Covered Contractor Report	
				14. Sponsoring Agency Code	
15. Supplementary Notes Project Manager, Lawrence P. Ludwig, Fluid Systems Components Division, NASA Lewis Research Center, Cleveland, Ohio. Final					
16. Abstract Steady-state and dynamic performance of a gas-lubricated, self-acting face seal was determined using numerical methods based on a variable grid, finite-difference, time-transient procedure. Results were obtained for a gas turbine main shaft seal operating at 206.9 newton per square centimeter (300 psi) sealed air pressure and 152.4 meters per second (500 ft/sec) sliding velocity. Analysis of the seal dynamics revealed that the response of the seal nosepiece to runout of the seat face is markedly affected by secondary seal friction and by nosepiece inertia. The nosepiece response was determined for various levels of secondary seal friction and seat face runout magnitudes.					
17. Key Words (Suggested by Author(s)) Seal, Mainshaft Seal, Self-Acting Seal, Gas Film Seal				18. Distribution Statement	
19. Security Classif. (of this report) Unclassified		20. Security Classif. (of this page) Unclassified		21. No. of Pages	
				22. Price*	

* For sale by the National Technical Information Service, Springfield, Virginia 22151

SUMMARY

Steady-state and dynamic analyses of a face seal with hydrodynamic lift augmentation are described. The primary purpose was to determine limits and effects of the rotating seat runout and secondary seal friction on dynamic response. The analyses resulted in the generation of a seal tracking map as a function of the two independent variables, runout and friction. It was determined that dynamic response is limited by two phenomena, excessive friction and seal inertia. If friction levels exceed fluid film forces the nosepiece will not follow and contact will occur since runout excursions are greater than the self-generated film thickness. Excessive inertia will not allow the nosepiece to respond in phase with the seat resulting in contact or failure. The theory of the computerized analyses employed is comprehensively described in the Appendices. Response history for varying operating conditions are also appended.

FOREWORD

The work described herein was done at the Franklin Institute Research Laboratories, under NASA contracts NAS3-16863 and NAS3-14418 with Mr. Lawrence Ludwig, Fluid Systems Component Division, NASA-Lewis Research Center, Program Manager.

CONTENTS

<i>Section</i>	<i>Title</i>	<i>Page</i>
	FOREWORD.	iii
	SUMMARY	iv
1	INTRODUCTION	1-1
2	STEADY-STATE PERFORMANCE	2-1
	2.1 Cases 2, 3 and 4	2-1
	2.2 Case 1	2-13
3	DYNAMIC PERFORMANCE	3-1
	3.1 Case 1	3-1
	3.2 Tracking Map, Case 1	3-12
	3.3 Cases 2, 3, and 4.	3-15
4	CONCLUSIONS	4-1
	4.1 Conclusions	4-1
	4.2 Recommendations	4-1
5	REFERENCES.	5-1
6	NOMENCLATURE	6-1
	APPENDIX A - ANALYTICAL APPROACH USED TO OBTAIN SEAL PERFORMANCE	
	APPENDIX B - DYNAMIC RESPONSE RESULTS, CASES 1, 2, 3 AND 4	
	APPENDIX C - COMPUTATION OF PISTON RING FRICTION	

FIGURES

<i>Number</i>	<i>Title</i>	<i>Page</i>
1	Shaft Seal Configuration.	1-2
2	Schematic of Seal Face	1-4
3	Force Balance on Seal	1-5
4	Seal Force vs. Axial Clearance for Cases 2 and 4.	2-5
5	Seal Force vs. Axial Clearance for Case 3	2-6
6	Seal Moment vs. Axial Clearance for Cases 2 and 4	2-7
7	Seal Moment vs. Axial Clearance for Case 3	2-8
8	Seal Power Loss vs. Axial Clearance for Cases 2 and 4	2-9
9	Seal Power Loss vs. Axial Clearance for Case 3	2-10
10	Seal Leakage vs. Axial Clearance for Cases 2 and 4	2-11
11	Seal Leakage vs. Axial Clearance for Case 3	2-12
12	Fluid-Film Force vs. Axial Clearance, Case 1.	2-15
13	Power Loss vs. Axial Clearance, Case 1	2-16
14	Leakage vs. Axial Clearance, Case 1	2-17
15	Rotation About X-Axis vs. Shaft Revolutions, Run 3e, Case 1	3-4
16	Rotation About Y-Axis vs. Shaft Revolutions, Run 3e, Case 1	3-5
17	Fluid-Film Force vs. Shaft Revolutions, Run 3e, Case 1	3-6
18	Minimum Clearance vs. Shaft Revolutions, Run 3e, Case 1	3-7
19	Fluid-Film Moment About X-Axis vs. Shaft Revolutions, Run 3e, Case 1	3-8

FIGURES (cont)

<i>Number</i>	<i>Title</i>	<i>Page</i>
20	Fluid-Film Moment About Y-Axis vs. Shaft Revolutions, Run 3e, Case 1.	3-9
21	Typical Tracking Map	3-13
22	Partial Tracking Map at the Specified Operating Condition for Case 1.	3-14

TABLES

<i>Number</i>	<i>Title</i>	<i>Page</i>
1	Operating Parameters	1-7
2	Steady-State Performance, Cases 2 and 4	2-2
3	Steady-State Performance, Case 3	2-3
4	Steady-State Performance For No Misalignment, Case.	2-14
5	Summary of Dynamic Runs, Case 1	3-2

1. INTRODUCTION

Shaft face seals for advanced turbine engines for aircraft have received considerable research and development effort aimed at extending seal speed and pressure capability (reference 1). In particular, seals with self-acting lift augmentation (references 1 and 2) promise a seal with the rotating speed capability of labyrinth seals and the low leakage capability of contact seals. This self-acting lift seal is similar in construction to a conventional face seal except for the addition of a self-acting geometry that acts to keep the primary faces separated. Thus, the seal has long life high-speed potential. For ideal operation, rubbing would occur only on startup and shutdown. Further, the self-acting geometry tends to operate with a small separation of the primary faces. For this reason, the mass leakage flow through the primary seal can be much less than that of a conventional labyrinth seal.

The lift force of the self-acting geometry provides positive gas-film stiffness, and potentially can compel the nosepiece to dynamically track the runout motions of the seal face provided inertia of the nosepiece and the secondary seal ring friction are compatible. It is of particular interest to be able to predict whether the combination of seal geometry and operating conditions are such that dynamic tracking will result; it was the primary purpose of this work to predict dynamic response of a particular seal configuration (NASA designed) and to describe the methods employed.

The seal configuration is shown on Figure 1. A hydrodynamic film is generated by a series of Rayleigh-step pads that maintain separation of an integral sealing-ring dam at a small but finite distance to inhibit leakage and prevent wear.

The stationary nosepiece is made of carbon graphite for good wearing qualities in case of a high-speed rub. The opposing seal-seat runner is made of TZM to minimize thermal distortions.

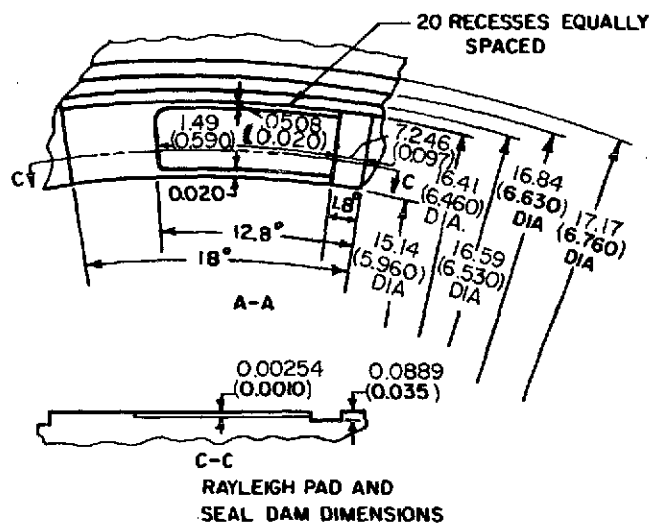
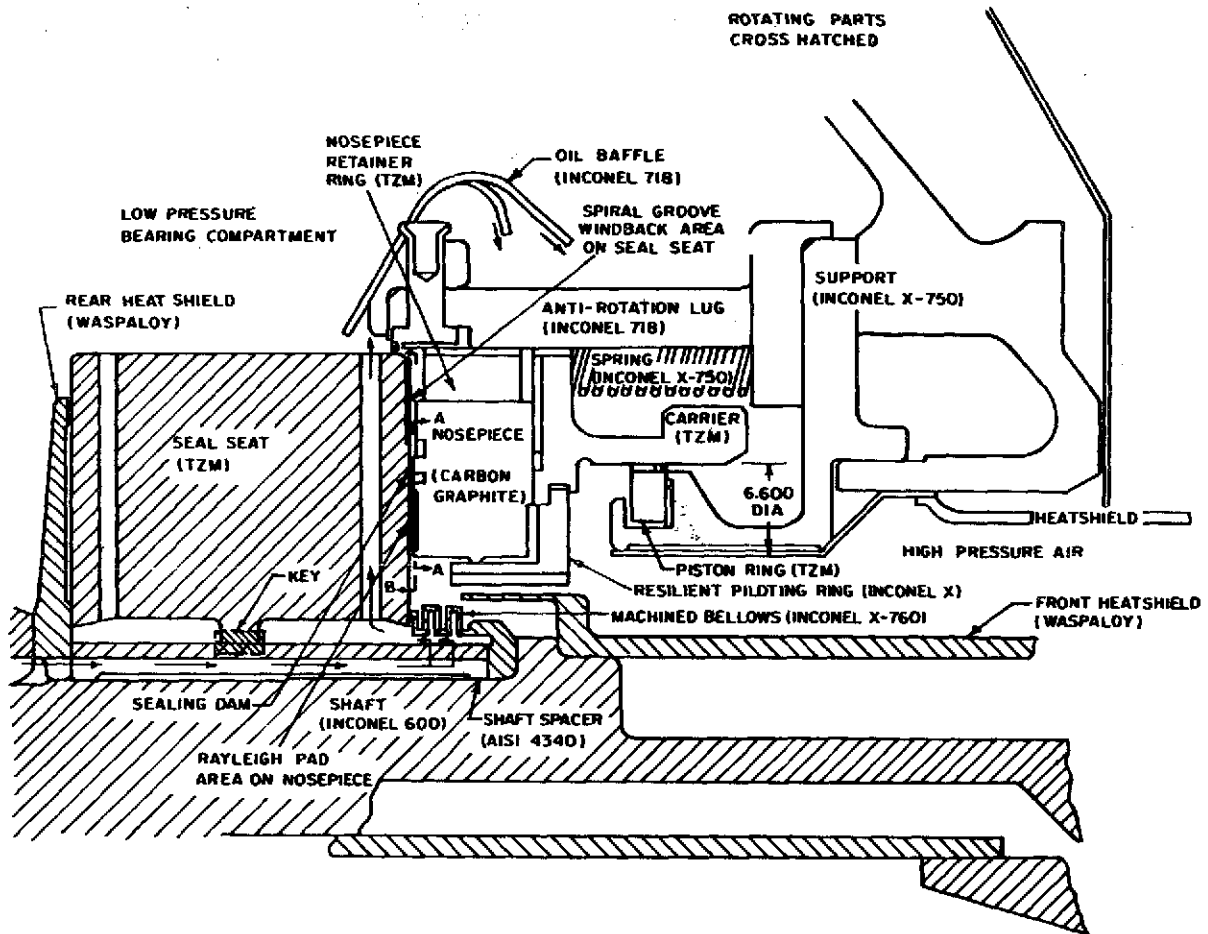


Figure 1. Shaft Seal Configuration

Careful attention has been paid to the prevention of thermal distortions of the members in the high temperature environment. Cooling passages are provided through the rotating collar. Radiation heat shields reduce thermal gradients and seat deformations. A machined bellows provides a coolant seal between the shaft and the seal seat and permits differential expansion of the parts while simultaneously avoiding clamping deformations of the seat. The carbon graphite nosepiece is mounted in a resilient piloting ring so as not to impose undue thermal and pressure loadings and to minimize eccentricity between the sealing dam and the secondary sealing diameter. The secondary seal consists of a TZM piston ring which mates against a TZM carrier. Antirotation lugs and closing springs are indicated. The high pressure side is on the interior diameter and leakage is from the inside out.

The general face configuration of the seal is shown on Figure 2. It consists of 20 equally spaced shrouded Rayleigh-step pads which are fed by the high pressure fluid. A groove on the exterior of the pads ensure that the high pressure environment completely surrounds the pads. Outside of the groove is the sealing dam which seals the high pressure fluid. The dimensions of each pad and sealing ridge are shown in view A-A and C-C of Figure 1.

Basic operation of the seal is schematically depicted on Figure 3. The force tending to close the seal consists of high pressure fluid acting to the secondary seal diameter and the mechanical spring force. The opening forces are provided by the Rayleigh-step lift pads and the pressure gradient through the sealing dam. The secondary seal friction force acts in a closing direction whenever the seal ring is moving away from the runner but tends to keep the seal open when it is moving in a closing direction. Therefore the faces of the seat and seal ring tend to be non-parallel as illustrated in Figure 3. The lift-pads are the only positive stiffness mechanism. If the clearance over the pad closes down, then the fluid-film force increases and a greater opening force is produced. Similarly, if the clearance opens, the lift-pad forces reduce, and the seal returns to its equilibrium position by unbalanced closing forces (provided that secondary friction forces do not prevent motion).

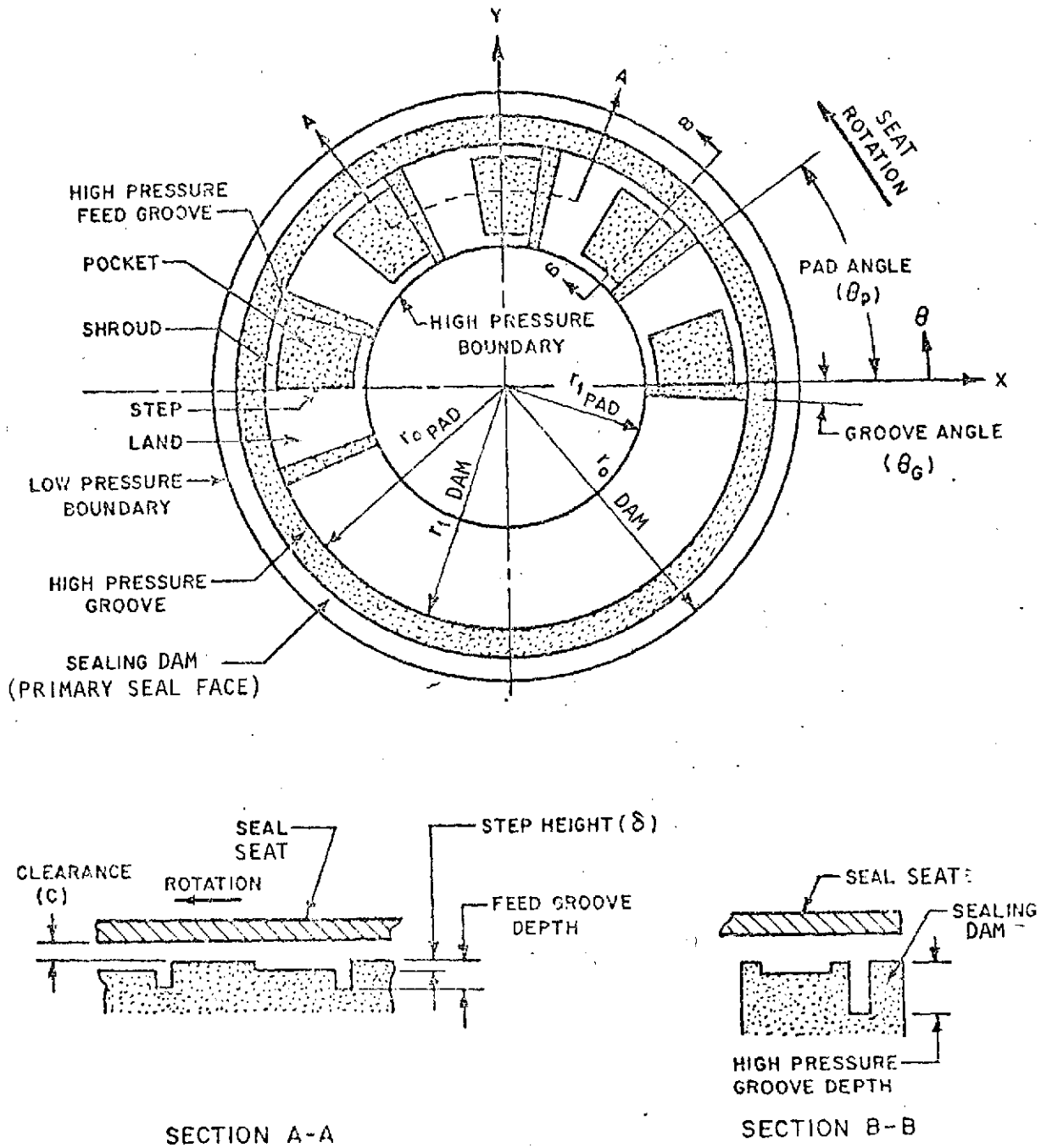


Figure 2. Schematic of Nosepiece Face

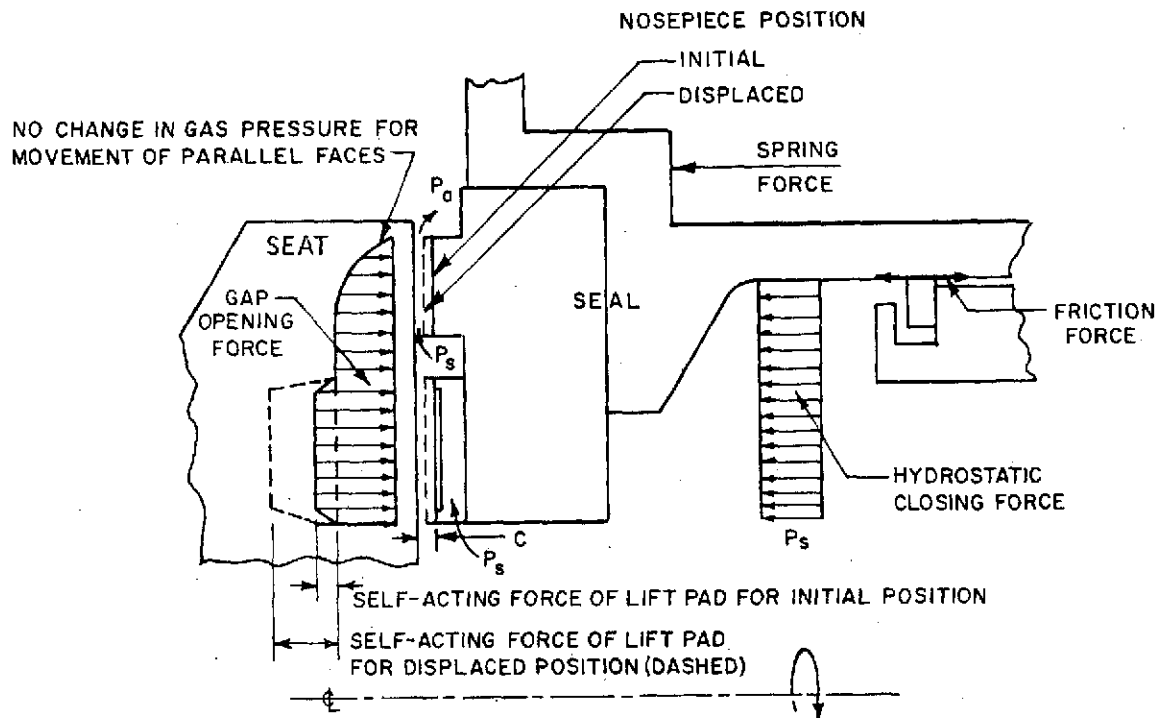


Figure 3. Forces on Nosepiece.

Table 1 indicates the various operating conditions that were examined. The most extensive dynamic results were obtained for Case 1 in which variations in secondary seal friction and runout of the seat face were evaluated. This case was conducted subsequent to the others and was accomplished under separate contract (NAS3-14418).

Table 1. Operating Parameters

	CASE 1	CASE 2
Sealed air pressure	2069 kN/m ² (300 psig)	1379 kN/m ² (200 psig)
Sealed air temperature	810.92°K (1000°F)	810.93°K (1000°F)
Sliding speed	152.4 m/sec (500 ft/sec) 1785.5 rad/sec (17,050 rpm)	1428.4 rad/sec (13,640 rpm) 121.9 m/sec (400 ft/sec)
Sump pressure	0 kN/m ² (0 psig)	0 kN/m ² (0 psig)
Face runout of rotating shaft	25.4 + 63.5μm (.001 + .0025 in)	25.4μm (0.001 in)
Maximum angular misalignment corresponding to a face runout measured at a radius of 8.204 cm (3.23 in.) (outside radius of step pad)	155 + 387μ rad.	155μ rad.
Spring load	88.96N (20 lbs)	66.72N (15 lbs)
Equilibrium self-acting load*	166.4N (37.41 lbs)	123.6N (27.78 lbs)
Initial axial clearance	8.120μm (0.00032 in)	8.38μm (0.00033 in)
Nosepiece weight	7.78N (1.75 lbs)	10N (2.25 lbs)
Nosepiece moment of inertia	.0033 kg-m ² (.029 lb-sec ² -in)	.00435 kg-m ² (0.0381 lb-sec ² -in)
Coefficient of sliding friction	0.1 + 1.0	.15
Frictional force	0 + 222.4N (0 + 50 lbs)	17.79N (4 lbs)
Frictional moments	0 + 11.86N-m (0 + 105 in-lbs)	5.93N-m (53 in-lbs)
Fluid viscosity	3.69 x 10 ⁻⁸ kNs/m ² (5.35 x 10 ⁻⁹ lb-sec/in ²)	.69 x 10 ⁻⁸ kNs/m ² (5.35 x 10 ⁻⁹ lb-sec/in ²)
	CASE 3	CASE 4
Sealed air pressure	344.75 kN/m ² (50 psig)	1379 kN/m ² (200 psig)
Sealed air temperature	338.7°K (150°F)	810.93°K (1000°F)
Sliding speed	1428.4 rad/sec (13,640 rpm) 121.9 m/sec (400 ft/sec)	1785.5 rad/sec (17,050 rpm) 152.4 m/sec (500 ft/sec)
Sump pressure	0 kN/m ² (0 psig)	0 kN/m ² (0 psig)
Face runout of rotating shaft	25.4μm (0.001 in)	25.4μm (0.001 in)
Maximum angular misalignment corresponding to a face runout measured at a radius of 8.204 cm (3.23 in.) (outside radius of step pad)	155μ rad.	155μ rad.
Spring load	66.72N (15 lbs)	66.72N (15 lbs)
Equilibrium self-acting load*	89.4N (20.09 lbs)	123.6N (27.78 lbs)
Initial axial clearance	8μm (0.000315 in)	10.16μm (0.00040 in)
Nosepiece weight	10N (2.25 lbs)	4.98N (1.12 lbs)
Nosepiece moment of inertia	.00435 kg-m ² (0.0381 lb-sec ² -in)	.00217 kg-m ² (0.019 lb-sec ² -in)
Coefficient of sliding friction	.15	.15
Frictional force	4.89N (1.1 lbs)	17.79N (4 lbs)
Frictional moments	1.64N-m (14.5 in-lbs)	5.99N-m (53 in-lbs)
Fluid viscosity	2.01 x 10 ⁻⁸ kNs/m ² (2.92 x 10 ⁻⁹ lb-sec/in ²)	3.69 x 10 ⁻⁸ kNs/m ² (5.35 x 10 ⁻⁹ lb-sec/in ²)

*Obtained by performing load balance on seal using the loads shown in Figure 3.

ORIGINAL PAGE IS
OF POOR QUALITY

2. STEADY-STATE PERFORMANCE

The more extensive steady-state information was generated for Cases 2, 3 and 4. The theory used for developing steady-state performance is described in reference 3 and in Appendix A.

2.1 CASES 2, 3 AND 4

Performance prediction consisted of determining the self-acting force, righting moment, power loss due to the viscous drag, and leakage across the sealing dam as a function of axial clearance and angular misalignment about a diameter. The axial clearance was defined in the film thickness before misalignment measured at the land region of the lift pads (C in Figure 3).

Steady-state operating conditions are enumerated below:

	<u>Cases 2 & 4</u>	<u>Case 3</u>
Sealed air pressure	1379 kN/m ² (200 psig)	344.75 kN/m ² (50 psig)
Sealed air temperature	810.92°K (1000°F)	338.7°K (150°F)
Sliding speed (mean)	121.92 m/sec (400 ft/sec)	121.92 m/sec (400 ft-sec)
Sump pressure	0 kN/m ² (0 psig)	0 kN/m ² (0 psig)
Spring load	66.72N (15 lbs)	66.72N (15 lbs)
Viscosity	3.81x10 ⁻⁸ kNs/m ² (5.53x10 ⁻⁹ lb-sec/in. ²)	2.01x10 ⁻⁸ kNs/m ² (2.92x10 ⁻⁹ lb-sec/in. ²)

Tables 2 and 3 contain significant results for each condition examined. These tables contain performance for both the step pads and sealing dam. Note that the change in load capacity for the sealing dam with respect to clearance and tilt is insignificant. While the change in moment is large, the overall magnitude is insignificant when compared to the moment of the step pads. With the particular variable

Table 2. Steady-State Performance, Cases 2 and 4

Shrouded Step Pads Performance (20 Pads)										Sealing Dam Performance										
C	$\alpha_{R/O}/C$	Fluid Film Force		X-MOM		Y-MOM		Power Loss		Load		X-MOM		Y-MOM		Power Loss		Leakage		
μm	(in.)	N	(lbs)	N-m	(in.-lbs)	N-m	(in.-lbs)	W	(hp)	N	(lbs)	N-m	(in.-lbs)	N-m	(in.-lbs)	W	(hp)	m ³ /min	(SCFM)	
25.4	(0.001)	0.0	8.10	(1.82)	0.0	(0.0)	0.0	(0.0)	40.27	(0.054)	585.36	(131.6)	0.0	(0.0)	0.0	(0.0)	14.17	(0.019)	3.51	(123.9)
		0.25	9.25	(2.08)	.24	(2.10)	.0108	(0.096)	41.01	(0.055)	585.36	(131.6)	.032	(0.286)	.000203	(0.0018)	14.17	(0.019)	3.85	(135.9)
		0.50	14.68	(3.30)	.71	(6.25)	.0497	(0.44)	45.49	(0.061)	585.80	(131.7)	.076	(0.676)	.00116	(0.0103)	16.41	(0.022)	4.57	(172.1)
		0.75	36.52	(8.21)	2.27	(20.1)	.146	(1.29)	56.67	(0.076)	587.14	(132.0)	.172	(1.52)	.00562	(0.0497)	21.63	(0.029)	6.58	(232.3)
20.32	(0.0008)	0.0	14.06	(3.16)	0.0	(0.0)	0.0	(0.0)	49.22	(0.066)	585.36	(131.6)	0.0	(0.0)	0.0	(0.0)	17.15	(0.023)	1.81	(63.43)
		0.25	16.46	(3.70)	.42	(3.67)	.0259	(0.229)	50.71	(0.068)	585.36	(131.6)	.027	(0.237)	.00429	(0.022)	17.00	(0.024)	1.97	(69.63)
		0.50	25.80	(5.80)	1.21	(10.7)	.0825	(0.730)	55.93	(0.075)	585.80	(131.7)	.072	(0.639)	.00407	(0.036)	20.13	(0.027)	2.50	(88.15)
		0.75	57.60	(12.95)	3.57	(31.6)	.2045	(1.81)	69.35	(0.093)	587.14	(132.0)	.172	(1.52)	.00847	(0.075)	26.65	(0.036)	3.37	(119.0)
15.24	(0.0006)	0.0	30.51	(6.86)	0.0	(0.0)	0.0	(0.0)	64.13	(0.086)	585.36	(131.6)	0.0	(0.0)	0.0	(0.0)	23.15	(0.031)	.758	(26.76)
		0.25	34.78	(7.82)	.84	(7.42)	.053	(0.465)	68.62	(0.088)	585.36	(131.6)	.032	(0.281)	.00169	(0.015)	23.76	(0.032)	.831	(29.36)
		0.50	51.15	(11.50)	2.27	(20.13)	.137	(1.21)	72.33	(0.097)	585.80	(131.7)	.076	(0.676)	.00407	(0.036)	26.05	(0.036)	1.05	(37.17)
		0.75	95.85	(21.55)	5.59	(49.50)	.297	(2.63)	90.23	(0.121)	587.14	(132.0)	.172	(1.52)	.015	(0.133)	35.79	(0.048)	1.42	(50.18)
10.16	(0.0004)	0.0	82.91	(18.64)	0.0	(0.0)	0.0	(0.0)	93.96	(0.126)	585.36	(131.6)	0.0	(0.0)	0.0	(0.0)	34.30	(0.046)	.225	(7.929)
		0.25	90.65	(20.38)	1.91	(16.9)	.101	(0.892)	96.94	(0.130)	585.36	(131.6)	.032	(0.287)	.00328	(0.029)	35.70	(0.048)	.246	(8.700)
		0.50	177.61	(39.44)	4.55	(40.3)	.229	(2.03)	106.64	(0.143)	585.36	(131.6)	.076	(0.677)	.00938	(0.083)	40.27	(0.054)	.312	(11.01)
		0.75	173.29	(38.96)	8.88	(78.6)	.463	(4.10)	130.50	(0.175)	587.14	(132.0)	.172	(1.522)	.0338	(0.299)	53.60	(0.072)	.421	(14.87)
5.08	(0.0002)	0.0	294.50	(66.3)	0.0	(0.0)	0.0	(0.0)	181.05	(0.244)	585.36	(131.6)	0.0	(0.0)	0.0	(0.0)	60.35	(0.093)	.0281	(0.9911)
		0.25	302.91	(68.1)	3.84	(34.0)	.185	(1.64)	186.43	(0.250)	585.36	(131.6)	.032	(0.283)	.0133	(0.118)	70.84	(0.095)	.0308	(1.088)
		0.50	327.37	(73.6)	7.98	(70.6)	.434	(3.84)	201.34	(0.270)	585.80	(131.7)	.076	(0.677)	.0378	(0.335)	81.54	(0.108)	.0303	(1.377)
		0.75	363.18	(83.0)	12.64	(111.9)	.89	(7.88)	240.86	(0.323)	587.14	(132.0)	.181	(1.60)	.134	(1.19)	106.64	(0.143)	.0526	(1.859)
2.54	(0.0001)	0.0	582.69	(131)	0.0	(0.0)	0.0	(0.0)	328.85	(0.441)	585.36	(131.6)	0.0	(0.0)	0.0	(0.0)	137.95	(0.185)	.0035	(0.1238)
		0.25	582.69	(131)	3.66	(32.4)	.356	(3.15)	336.31	(0.451)	585.36	(131.6)	.032	(0.285)	.053	(0.470)	142.43	(0.191)	.0038	(0.1359)
		0.50	591.58	(133)	7.38	(65.3)	.807	(7.14)	363.16	(0.487)	585.80	(131.7)	.081	(0.714)	.151	(1.34)	160.33	(0.215)	.0049	(0.1721)
		0.75	622.72	(140)	12.15	(107.5)	1.63	(14.4)	439.22	(0.589)	588.47	(132.3)	.311	(2.75)	.522	(4.62)	214.02	(0.287)	.0066	(0.2323)

$$T_s = 810.92^\circ\text{K} (1000^\circ\text{F})$$

$$\mu = 3.69 \times 10^{-8} \text{ kNs/m}^2 (5.35 \times 10^{-9} \text{ lb-sec/in.}^2)$$

$$N = 1428.4 \text{ rad/sec (13,640 rpm)}$$

$$P_s = 1482.4 \text{ kN/m}^2 (215 \text{ psia})$$

$$P_a = 103.4 \text{ kN/m}^2 (15 \text{ psia})$$

Table 3. Steady-State Performance, Case 3

Shrouded Step Pads Performance (20 Pads)										Sealing Ridge Performance									
C μm (in.)	P ₀ R ₀ /C (in.)	Fluid Film Force		X-MOM		Y-MOM		Power Loss		X-MOM		Y-MOM		Power Loss		Leakage			
		N (lbs)	N-m (in.-lbs)	N-m (in.-lbs)	N-m (in.-lbs)	N-m (in.-lbs)	N-m (in.-lbs)	W (hp)	N (lbs)	N-m (in.-lbs)	N-m (in.-lbs)	N-m (in.-lbs)	N-m (in.-lbs)	W (hp)	N (lbs)	m ³ /min (SCFM)			
25.4 (0.001)	0.0	4.42 (0.994)	0.0 (0.0)	0.0 (0.0)	0.0 (0.0)	0.0 (0.0)	0.0 (0.0)	21.63 (0.029)	137.89 (31.0)	0.0 (0.0)	0.0 (0.0)	0.0 (0.0)	0.0 (0.0)	7.46 (0.010)	1.34 (0.010)	(47.24)			
	0.25	5.08 (1.141)	.127 (1.124)	.0127 (0.1124)	.0127 (0.1124)	.0127 (0.1124)	.0127 (0.1124)	22.37 (0.030)	137.89 (31.0)	.0088 (0.078)	.00019 (0.0017)	.00019 (0.0017)	.00019 (0.0017)	7.46 (0.010)	1.47 (0.010)	(51.83)			
	0.50	-- (--)	-- (--)	-- (--)	-- (--)	-- (--)	-- (--)	-- (--)	137.89 (31.0)	.0211 (0.187)	.00077 (0.0068)	.00077 (0.0068)	.00077 (0.0068)	8.45 (0.012)	1.86 (0.012)	(65.62)			
	0.75	-- (--)	-- (--)	-- (--)	-- (--)	-- (--)	-- (--)	-- (--)	138.33 (31.1)	.0476 (0.421)	.0029 (0.0253)	.0029 (0.0253)	.0029 (0.0253)	11.93 (0.016)	2.51 (0.016)	(85.59)			
20.32 (0.0008)	0.0	8.01 (1.80)	0.0 (0.0)	0.0 (0.0)	0.0 (0.0)	0.0 (0.0)	0.0 (0.0)	26.85 (0.036)	137.89 (31.0)	0.0 (0.0)	0.0 (0.0)	0.0 (0.0)	0.0 (0.0)	9.69 (0.013)	.684 (0.013)	(24.17)			
	0.25	9.16 (2.06)	.226 (2.00)	.0188 (0.166)	.0188 (0.166)	.0188 (0.166)	.0188 (0.166)	27.59 (0.037)	137.89 (31.0)	.009 (0.080)	.00044 (0.0039)	.00044 (0.0039)	.00044 (0.0039)	9.69 (0.013)	.752 (0.013)	(26.55)			
	0.50	14.32 (3.22)	.662 (5.86)	.0465 (0.412)	.0465 (0.412)	.0465 (0.412)	.0465 (0.412)	34.30 (0.046)	137.89 (31.0)	.022 (0.195)	.0011 (0.0095)	.0011 (0.0095)	.0011 (0.0095)	11.19 (0.015)	.951 (0.015)	(33.57)			
	0.75	32.60 (7.33)	2.01 (17.77)	.107 (0.947)	.107 (0.947)	.107 (0.947)	.107 (0.947)	38.03 (0.051)	138.33 (31.1)	.048 (0.425)	.0047 (0.042)	.0047 (0.042)	.0047 (0.042)	14.91 (0.020)	1.28 (0.020)	(45.37)			
15.24 (0.0006)	0.0	16.99 (3.82)	0.0 (0.0)	0.0 (0.0)	0.0 (0.0)	0.0 (0.0)	0.0 (0.0)	35.05 (0.047)	137.89 (31.0)	0.0 (0.0)	0.0 (0.0)	0.0 (0.0)	0.0 (0.0)	12.68 (0.017)	.289 (0.017)	(10.20)			
	0.25	13.22 (4.32)	.462 (4.09)	.031 (0.271)	.031 (0.271)	.031 (0.271)	.031 (0.271)	35.79 (0.048)	137.89 (31.0)	.0087 (0.077)	.00082 (0.0073)	.00082 (0.0073)	.00082 (0.0073)	12.68 (0.017)	.317 (0.017)	(11.20)			
	0.50	28.51 (6.41)	1.26 (11.18)	.072 (0.637)	.072 (0.637)	.072 (0.637)	.072 (0.637)	39.52 (0.053)	137.89 (31.0)	.0211 (0.187)	.0022 (0.0199)	.0022 (0.0199)	.0022 (0.0199)	14.91 (0.020)	.401 (0.020)	(14.17)			
	0.75	54.62 (12.28)	3.19 (28.25)	.148 (1.31)	.148 (1.31)	.148 (1.31)	.148 (1.31)	49.22 (0.066)	138.33 (31.1)	.0475 (0.420)	.0081 (0.0718)	.0081 (0.0718)	.0081 (0.0718)	19.39 (0.026)	.542 (0.026)	(19.13)			
10.16 (0.0004)	0.0	45.99 (10.34)	0.0 (0.0)	0.0 (0.0)	0.0 (0.0)	0.0 (0.0)	0.0 (0.0)	51.45 (0.069)	137.89 (31.0)	0.0 (0.0)	0.0 (0.0)	0.0 (0.0)	0.0 (0.0)	18.64 (0.025)	.0856 (0.025)	(3.024)			
	0.25	50.44 (11.34)	1.08 (9.52)	.052 (0.46)	.052 (0.46)	.052 (0.46)	.052 (0.46)	52.95 (0.071)	137.89 (31.0)	.0088 (0.078)	.0018 (0.016)	.0018 (0.016)	.0018 (0.016)	19.39 (0.026)	.094 (0.026)	(3.318)			
	0.50	66.32 (14.91)	2.60 (23.0)	.114 (1.01)	.114 (1.01)	.114 (1.01)	.114 (1.01)	58.16 (0.078)	137.89 (31.0)	.021 (0.186)	.0051 (0.045)	.0051 (0.045)	.0051 (0.045)	21.63 (0.029)	.119 (0.029)	(4.200)			
	0.75	98.92 (22.24)	5.12 (45.3)	.214 (1.89)	.214 (1.89)	.214 (1.89)	.214 (1.89)	70.84 (0.095)	138.33 (31.1)	.048 (0.426)	.018 (0.161)	.018 (0.161)	.018 (0.161)	29.08 (0.039)	.161 (0.039)	(5.670)			
5.08 (0.0002)	0.0	169.02 (38.0)	0.0 (0.0)	0.0 (0.0)	0.0 (0.0)	0.0 (0.0)	0.0 (0.0)	99.18 (0.133)	137.89 (31.0)	0.0 (0.0)	0.0 (0.0)	0.0 (0.0)	0.0 (0.0)	38.03 (0.051)	.0107 (0.051)	(0.3779)			
	0.25	173.92 (39.1)	2.26 (20.0)	.080 (0.711)	.080 (0.711)	.080 (0.711)	.080 (0.711)	101.42 (0.136)	137.89 (31.0)	.0088 (0.078)	.0072 (0.064)	.0072 (0.064)	.0072 (0.064)	38.78 (0.052)	.0117 (0.052)	(0.4147)			
	0.50	187.71 (42.2)	4.63 (41.0)	.181 (1.60)	.181 (1.60)	.181 (1.60)	.181 (1.60)	109.62 (0.147)	137.89 (31.0)	.021 (0.188)	.0204 (0.181)	.0204 (0.181)	.0204 (0.181)	43.25 (0.058)	.0149 (0.058)	(0.5250)			
	0.75	209.95 (47.2)	7.21 (63.8)	.356 (3.15)	.356 (3.15)	.356 (3.15)	.356 (3.15)	131.24 (0.176)	138.33 (31.1)	.056 (0.495)	.073 (0.642)	.073 (0.642)	.073 (0.642)	58.16 (0.078)	.0201 (0.078)	(0.7087)			
2.54 (0.0001)	0.0	332.27 (74.7)	0.0 (0.0)	0.0 (0.0)	0.0 (0.0)	0.0 (0.0)	0.0 (0.0)	178.97 (0.240)	137.89 (31.0)	0.0 (0.0)	0.0 (0.0)	0.0 (0.0)	0.0 (0.0)	75.32 (0.101)	.00134 (0.101)	(0.0472)			
	0.25	334.04 (75.1)	1.99 (17.6)	.132 (1.17)	.132 (1.17)	.132 (1.17)	.132 (1.17)	183.44 (0.246)	137.89 (31.0)	.0093 (0.082)	.029 (0.253)	.029 (0.253)	.029 (0.253)	77.55 (0.104)	.00147 (0.104)	(0.0518)			
	0.50	-- (--)	-- (--)	-- (--)	-- (--)	-- (--)	-- (--)	-- (--)	138.33 (31.1)	.026 (0.226)	.081 (0.721)	.081 (0.721)	.081 (0.721)	87.25 (0.117)	.00186 (0.117)	(0.0656)			
	0.75	-- (--)	-- (--)	-- (--)	-- (--)	-- (--)	-- (--)	-- (--)	139.67 (31.4)	.167 (1.48)	.269 (2.38)	.269 (2.38)	.269 (2.38)	117.07 (0.157)	.00251 (0.157)	(0.0866)			

$$T_s = 338.71^\circ\text{K} (150^\circ\text{F})$$

$$\mu = 2.01 \times 10^{-8} \text{ kg/m}^2 (2.92 \times 10^{-9} \text{ lb-sec/in.}^2)$$

$$N = 1428.38 \text{ rad/sec (13,640 rpm)}$$

$$P_s = 448.2 \text{ kN/m}^2 (65 \text{ psia})$$

$$P_o = 103.4 \text{ kN/m}^2 (15 \text{ psia})$$

ORIGINAL PAGE IS
OF POOR QUALITY

grid computerized analysis employed it was possible to obtain solutions for very small film thickness of 2.54 μm (.0001 in), a condition which is usually numerically unstable without the variable grid option. The angular misalignment (rotation) at the nosepiece was taken about the X-X axis (see Figure 2). Therefore, the Y-MOM in the tables indicate the cross-coupling effect, that is a tilt about the X-X axis also produces a righting moment about the Y-Y axis. The cross-coupling effects however, are small in comparison with the primary righting moment (X-MOM). Figures 4 through 11 show the performance of the seal as a function of the land clearance and angular misalignment about a diameter for Cases 2, 3 and 4.

Figures 4 and 5 show the fluid-film force generated by the hydrodynamic action in the Rayleigh-step pad. Note that as the clearance reduces, the force continues to rise and also that the force increases with increased values of the misalignment angle, $\alpha_x R_o/C$.

For the righting moment characteristics shown on Figures 6 and 7, a peak is reached at somewhat less than two tenths of a mil land clearance. When the average clearance is small the angular misalignment produces step height to land clearance ratios that are far from optimum on the tight clearance pads while closer to optimum on the large clearance pads. This effect essentially indicates that the force on the tight clearance pads increases at a slower rate than the force on the larger clearance pads at small average clearances thus causing the righting moment to level off. In general, over the operating range of this seal, the righting moment is increased with increased angles of angular misalignment. These curves include the moment effect of the sealing dam.

The power loss curves illustrated in Figure 8 and 9 show an increase in power loss with reductions in clearance and with increasing angular misalignments. Power loss consists of frictional losses in the step pad and sealing dam.

The leakage in standard cubic feet per min (SCFM) is shown on Figures 10 and 11. Leakage computations were made on the basis of laminar viscous flow which can be shown to be the case over most of the operating range of this seal. In actual operation seal clearances were very small

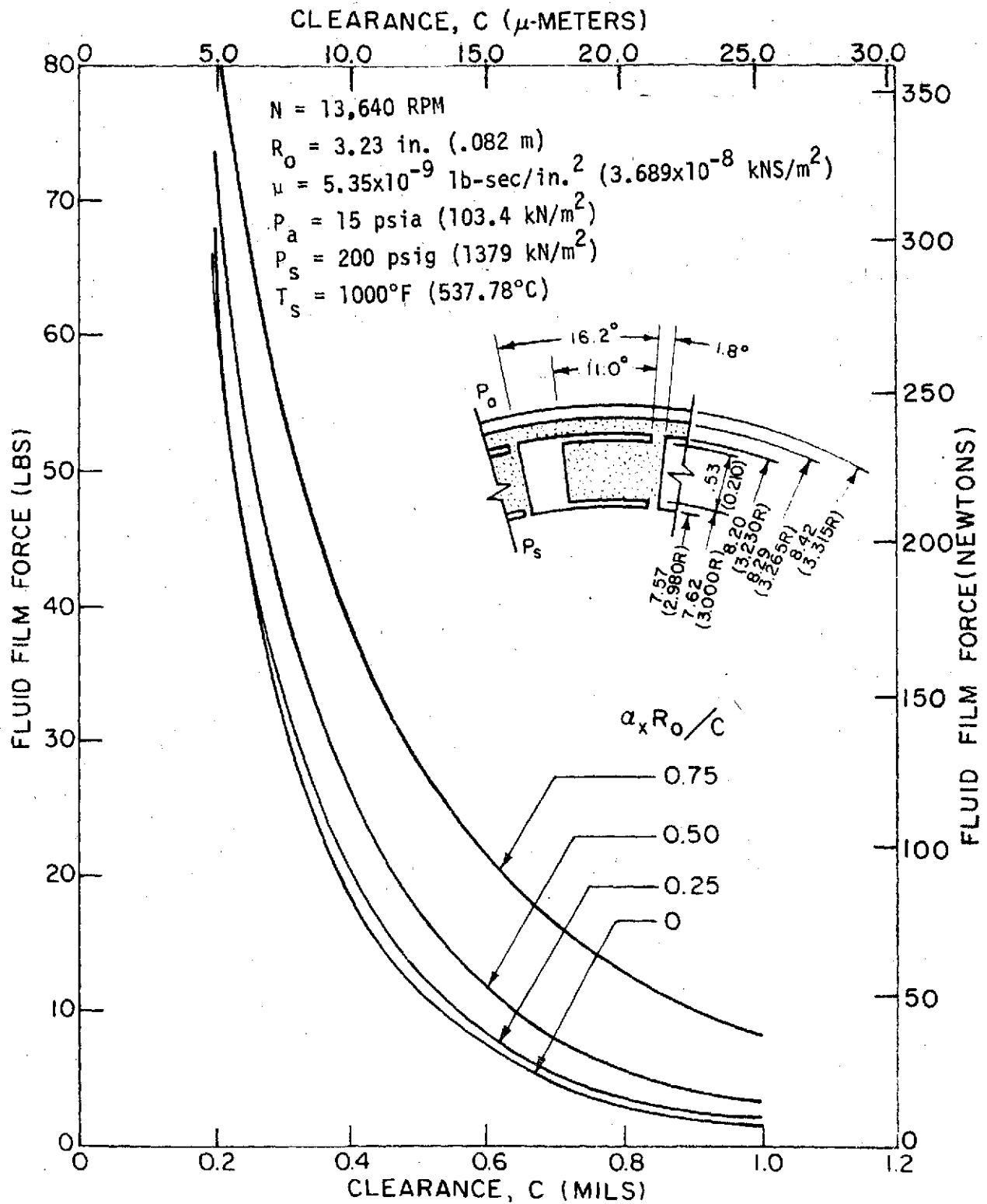


Figure 4. Seal Force vs. Axial Clearance for Cases 2 and 4

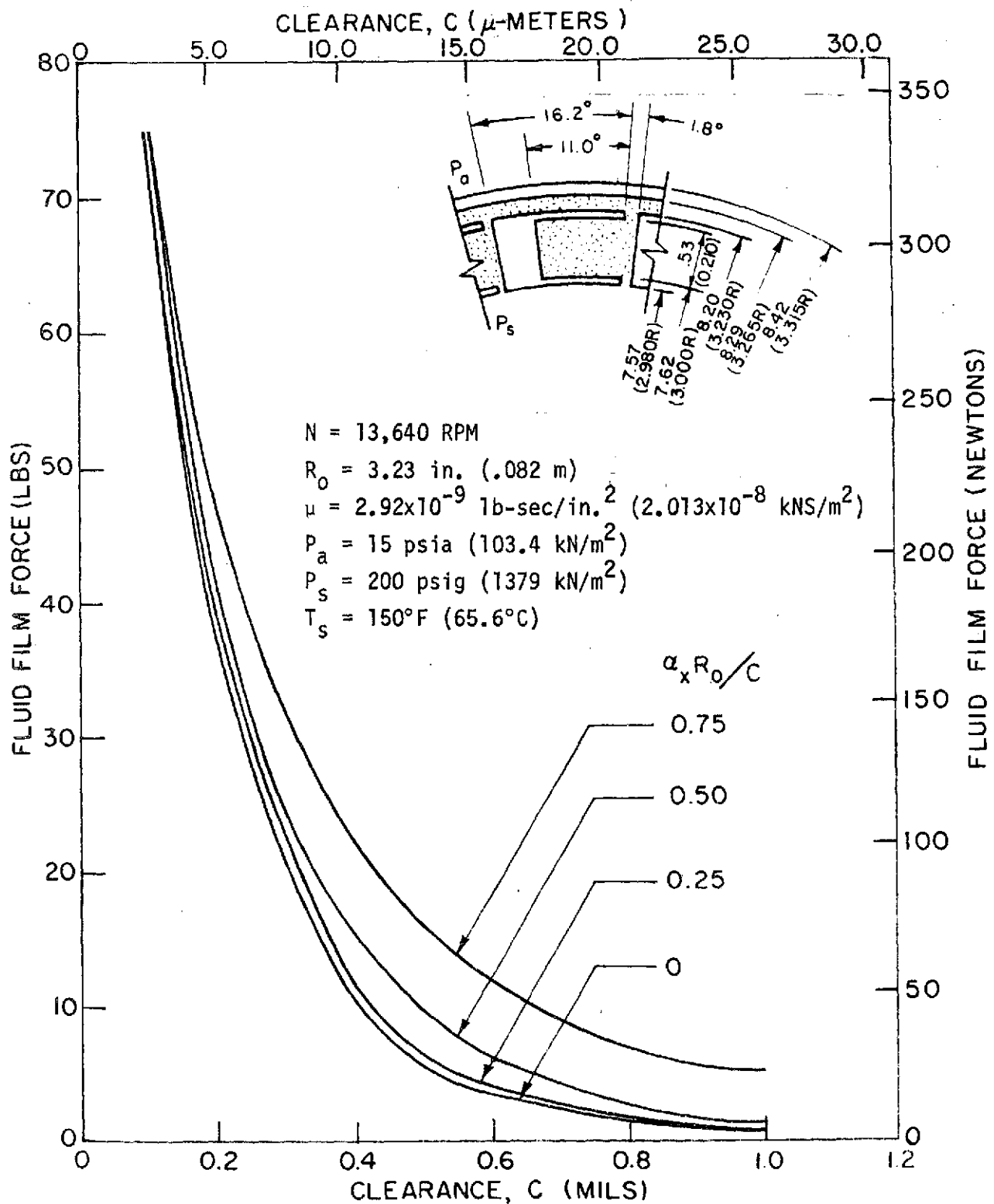


Figure 5. Seal Force vs. Axial Clearance for Case 3

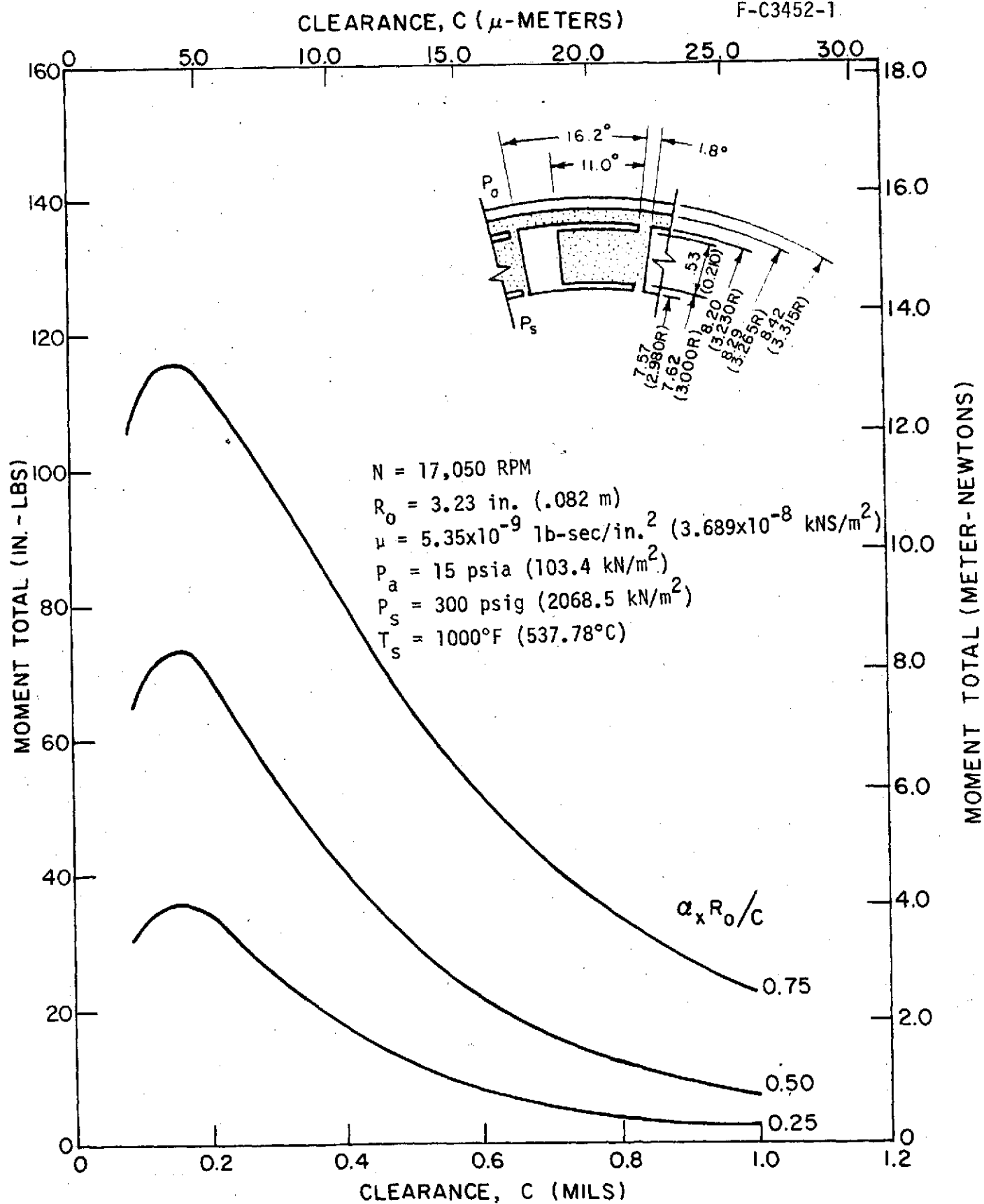
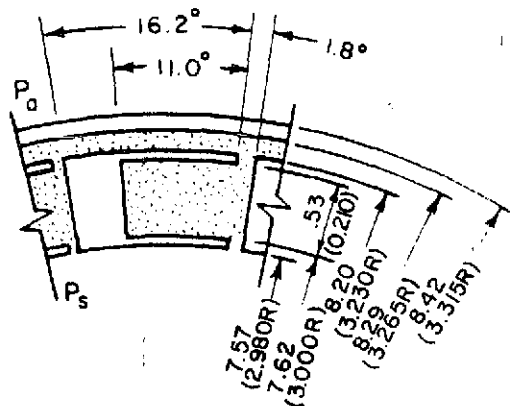


Figure 6. Seal Moment vs. Axial Clearance for Cases 2 and 4



2-8

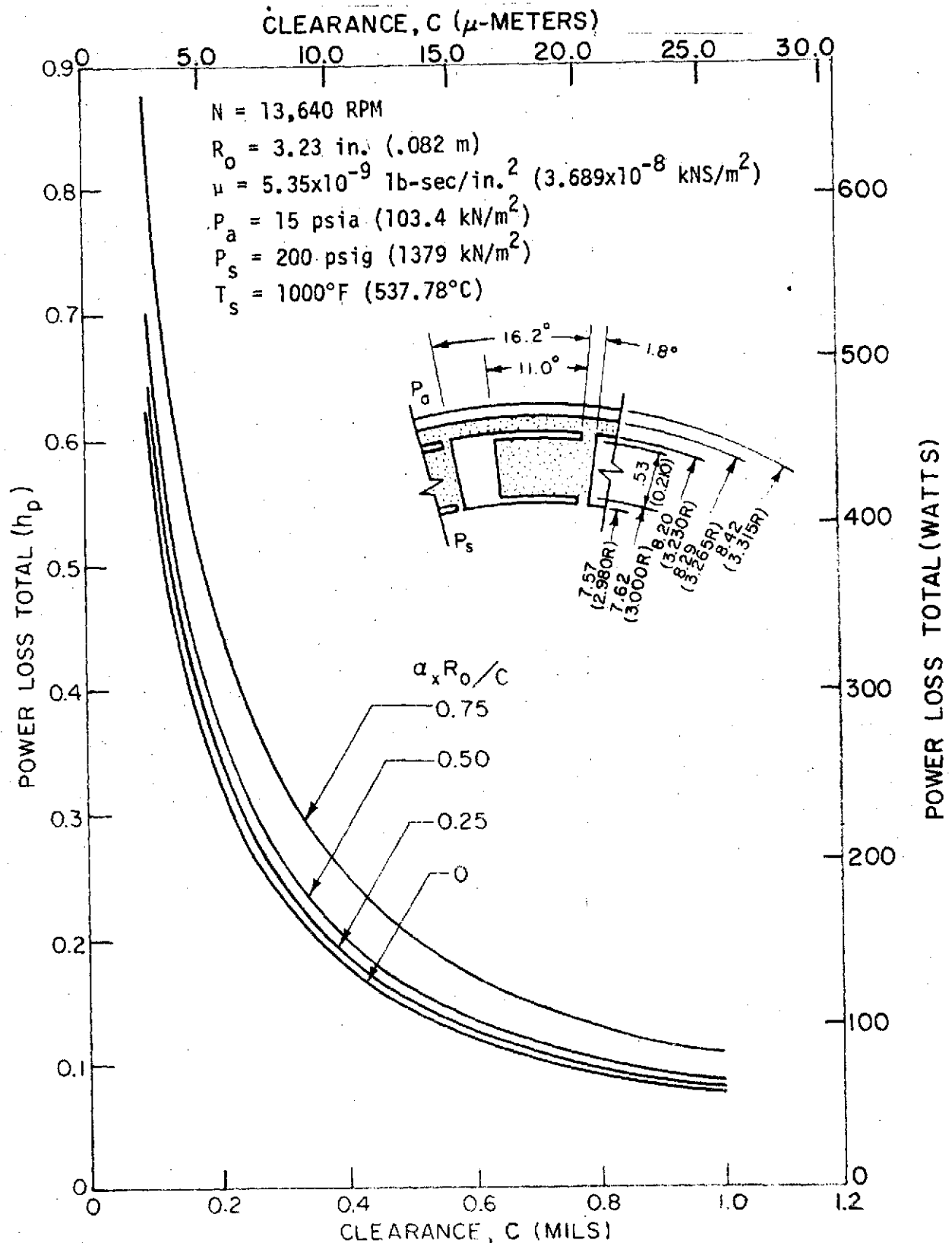


Figure 8. Seal Power Loss vs. Axial Clearance for Case 2 and 4

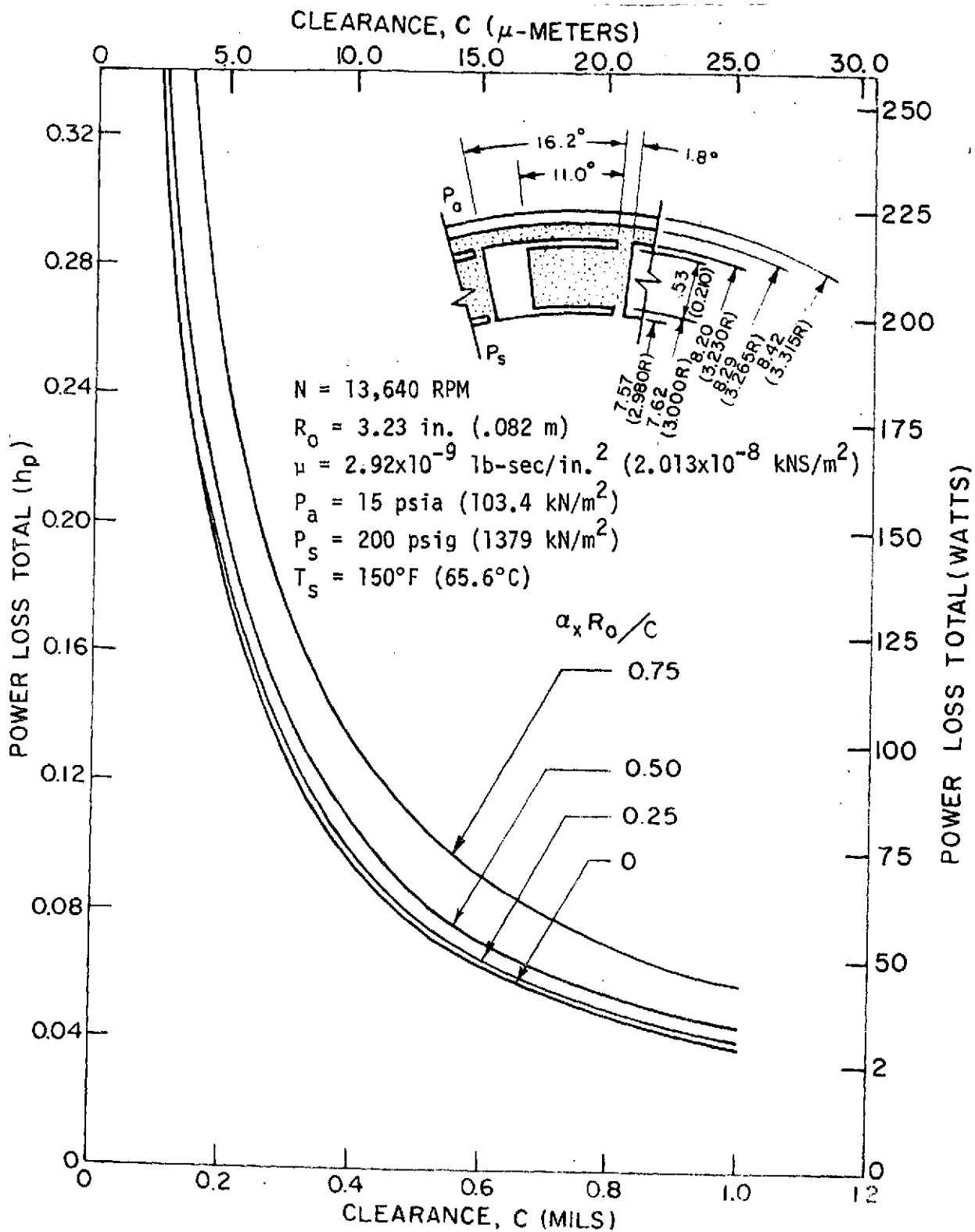
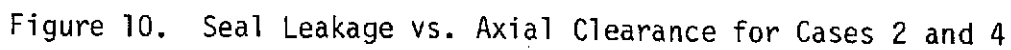
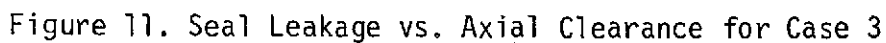


Figure 9. Seal Power Loss vs. Axial Clearance for Case 3





and laminar viscous flow theory predominates. The leakage curve is shown on semilog paper because of the cubic relationship between clearance and leakage. Here again, leakage increases with misalignment.

2.2 CASE 1

For Case 1, steady-state results consisted of determining performance as a function of axial clearance.

The operating condition considered was:

Sealed air pressure	2068.5 kN/m ² (300 psig)
Sealed air temperature	810.93°K (1000°F)
Sliding speed (mean)	152.4 m/sec (500 ft/sec) 1785.5 rad/sec (17,050 rad/min)
Sump pressure	0 kN/m ² (0 psig)
Viscosity	3.81 x 10 ⁻⁸ kNs/m ² (5.53 x 10 ⁻⁹ lb-sec/in ²)
Axial clearance	2.54 + 25.4µm (.0001 + .001 in)

Table 4 summarizes results and performance curves are plotted on Figures 12, 13 and 14.

Table 4. Steady-State Performance For No Angular Misalignment
Case 1

Shrouded Step Pads Performance (20 Pads)

Sealing Dam Performance

Clearance		Fluid Film Force		Power Loss		Load		Power Loss		Leakage	
μm	(in.)	N	(lbs)	W	(hp)	N	(lbs)	W	(hp)	m^3/min	SCFM
25.4	(.0010)	9.83	(2.210)	60.63	(0.0813)	885.77	(199.14)	21.55	(0.0289)	7.55	(266.47)
20.32	(.0008)	17.93	(4.032)	73.68	(0.0988)	885.77	(199.14)	26.92	(0.0361)	3.86	(136.43)
15.24	(.0006)	38.32	(8.614)	95.52	(0.1281)	885.77	(199.14)	35.94	(0.0482)	1.63	(57.556)
10.16	(.0004)	103.19	(23.20)	140.19	(0.1880)	885.77	(199.14)	53.91	(0.0723)	.483	(17.054)
7.62	(.0003)	188.73	(42.43)	185.38	(0.2486)	885.77	(199.14)	71.89	(0.0964)	.204	(7.195)
5.08	(.0002)	364.34	(81.91)	270.91	(0.3633)	885.77	(199.14)	107.83	(0.1446)	.0604	(2.132)
2.54	(.0001)	160.64	(160.64)	482.32	(0.6468)	885.77	(199.13)	215.58	(0.2891)	.0075	(0.2664)

Temperature 810.92°K (1000°F)
Viscosity $3.69 \times 10^{-8} \text{ kN}\cdot\text{s}/\text{m}^2$ ($5.35 \times 10^{-9} \text{ lb}\cdot\text{sec}/\text{in}^2$)
Speed 1785.5 rad/sec (17050 rpm)
Sealed Pressure 2172 kN/m^2 (315 psia)
Sump Pressure 103.4 kN/m^2 (15 psia)

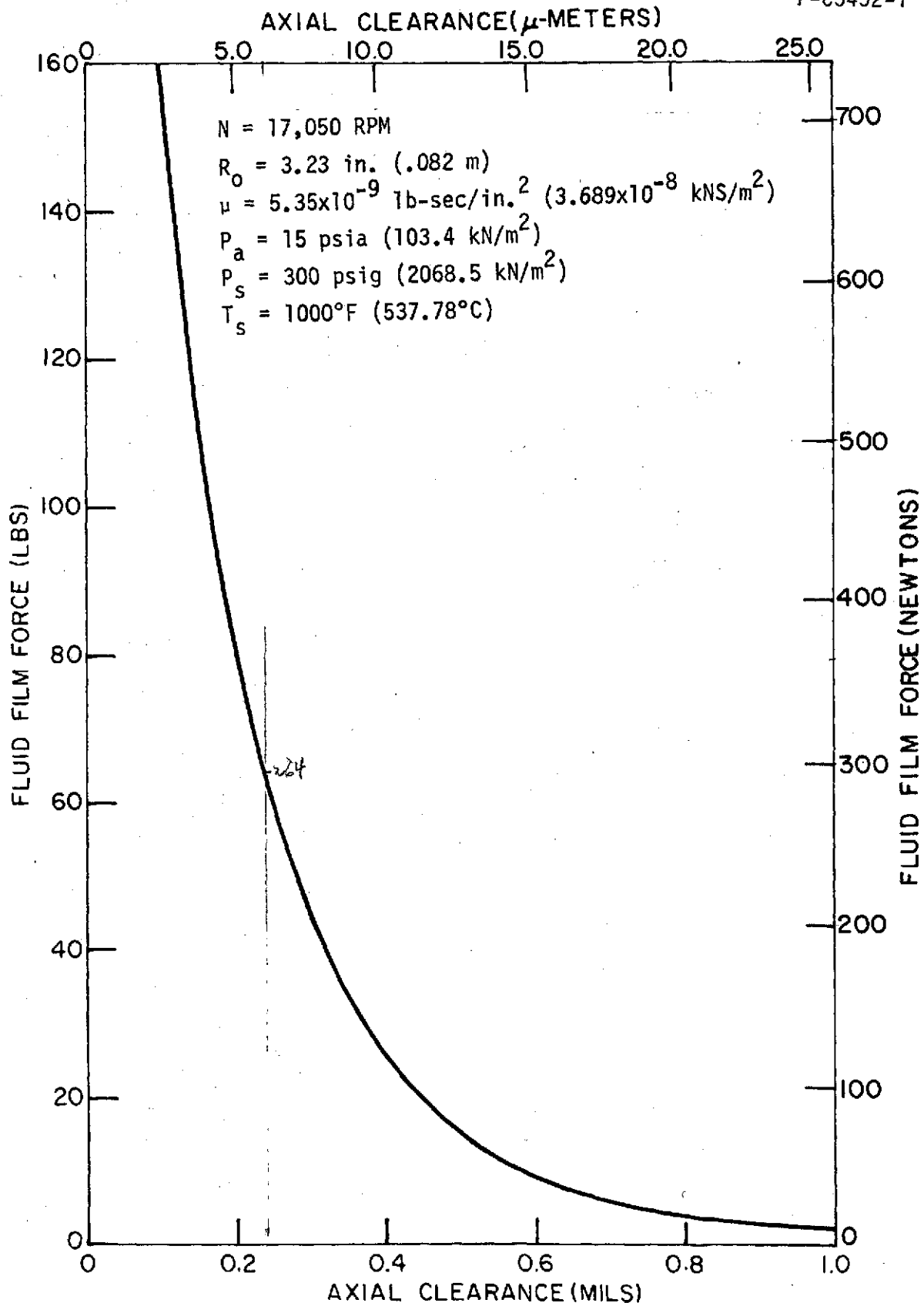


Figure 12. Fluid-Film Force vs. Axial Clearance, Case 1

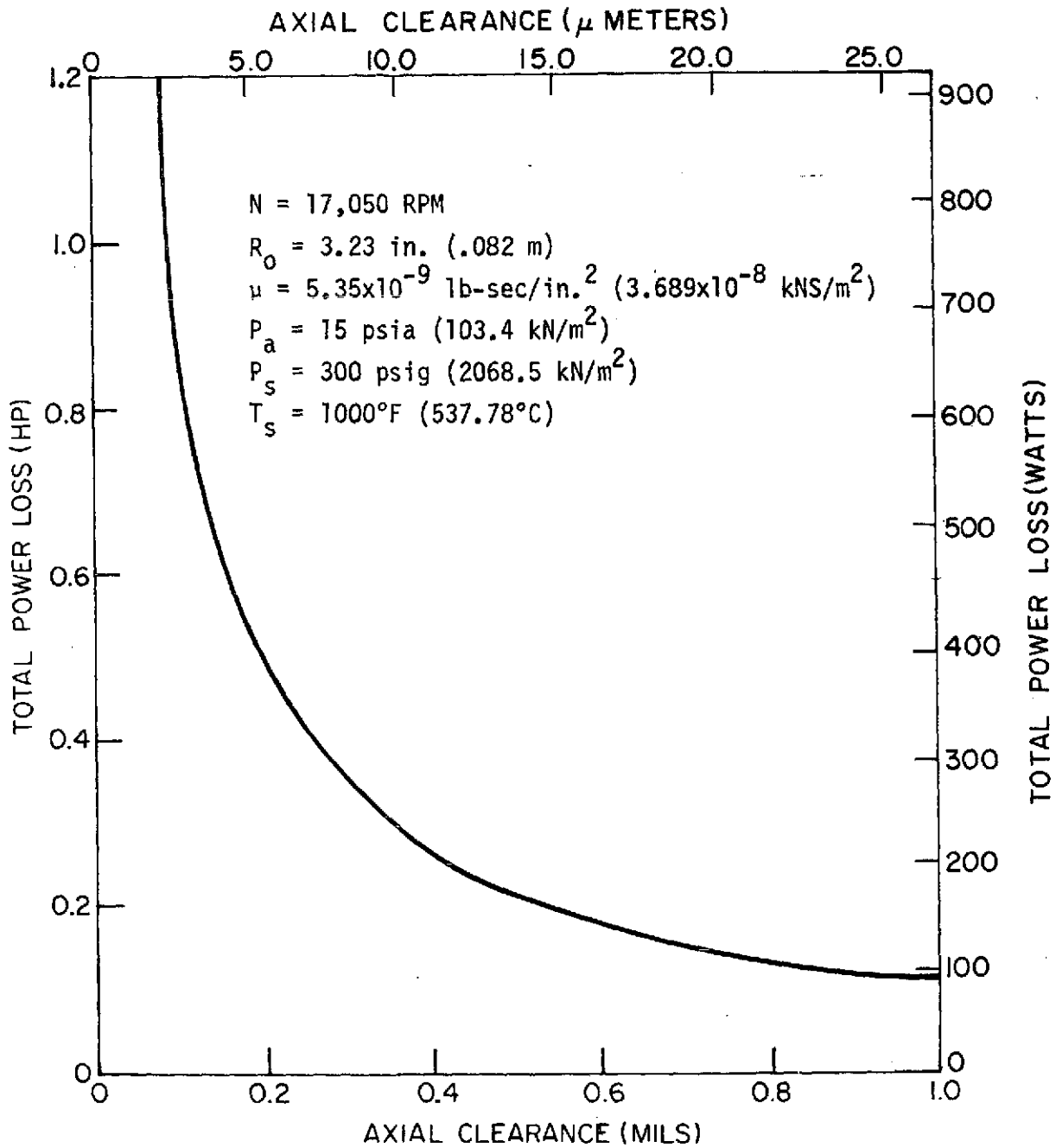


Figure 13. Power Loss vs. Axial Clearance, Case 1

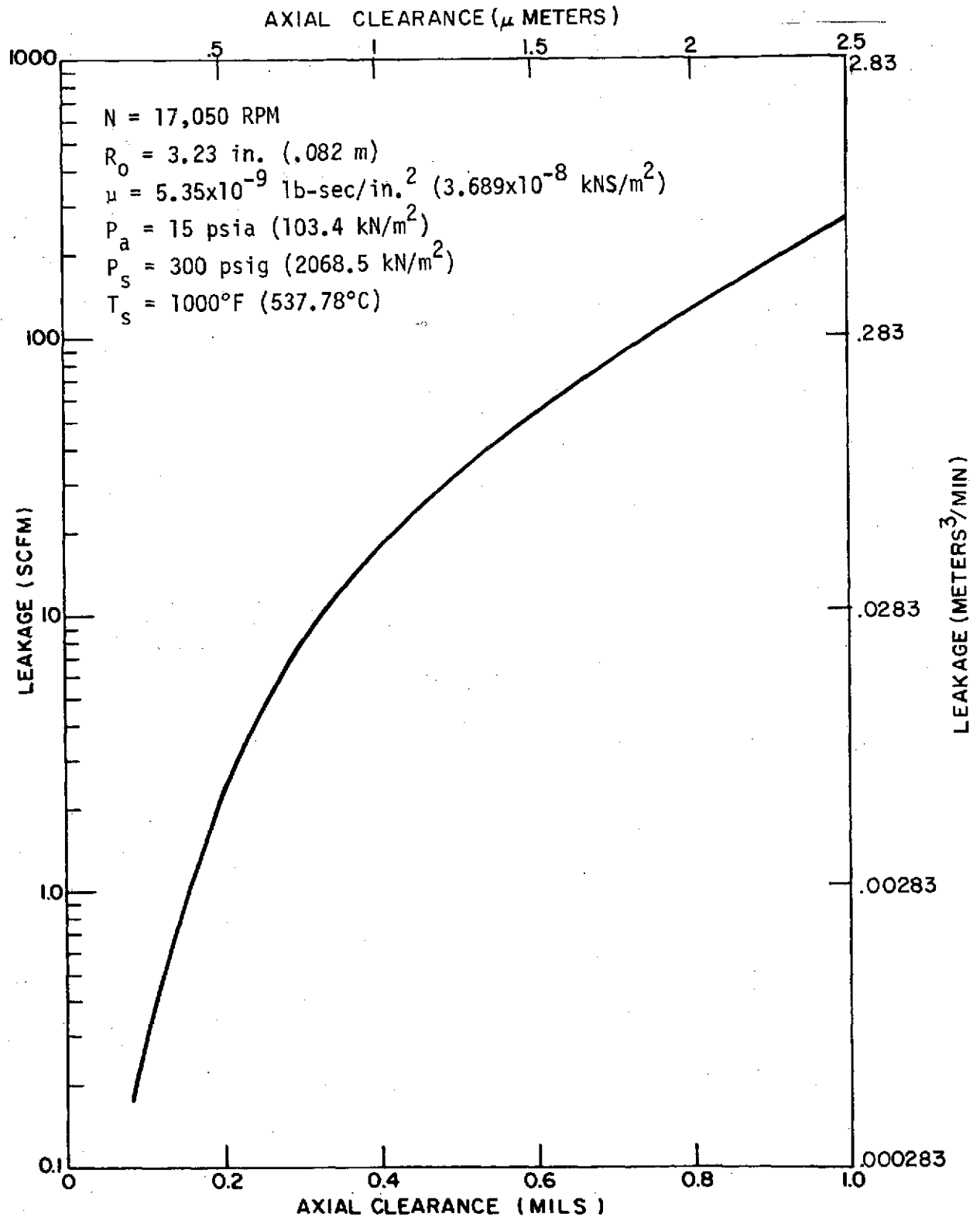


Figure 14. Leakage vs. Axial Clearance, Case 1

3. DYNAMIC PERFORMANCE

The dynamic analysis produces responses of the seal assembly to nutations of the seal runner. The seal is permitted three degrees of freedom consisting of axial translations and rotations about orthogonal axes passing through the contact point of the piston ring and seal assembly. Coulomb friction between the seal and the piston ring retards seal motions. The analysis accounts for the frictional effects of the secondary seal piston ring. Methods are described in Appendix A and in references 2 and 6.

3.1 CASE 1

Comprehensive analysis of Case 1 was completed as a function of misalignment of collar or seat face and frictional resistance of the piston ring secondary seals.

For each dynamic run, the following performance was determined as a function of shaft revolutions:

- Seal axial translation
- Seal X rotation, or rotation about the X axis
- Seal Y rotation, or rotation about the Y axis
- Minimum film thickness
- Axial self-acting fluid film force
- Fluid film moment about the X axis
- Fluid film moment about the Y axis

The initial conditions for the analysis were determined from a steady-state force balance. The self-acting fluid-film force was computed as 166.4N (37.41 lbs), and from Figure 12, the initial clearance was 8.128 μm (0.00032 in.).

Table 5 is a summary of the dynamic cases that were run. The variables included runout or misalignment of the runner and coefficient of friction of the secondary seal piston ring. The remarks column of Table 5 indicates

Table 5. Summary of Dynamic Runs, Case 1

RUN	RUNOUT		ANGULAR ⁽¹⁾ MIS- ALIGNMENT		FRICTION			COEFFI- CIENT OF FRICTION	MEAN AXIAL ⁽²⁾ CLEARANCE		ANGULAR ⁽³⁾ AMPLITUDE	MEAN MINIMUM CLEARANCE		REMARKS
	(in.)	(μ m)	(μ -rad)	(lbs)	(N)	(in-lbs)	(N-m)		(mils)	(μ m)		(mils)	(μ m)	
1a	(0.001)	25.4	.155	(0.0)	0.0	(0.0)	0.0	0	(.318)	8.077	.160.	(.244)	6.198	Stable ⁽⁴⁾
b	(0.001)	25.4	.155	(6.0)	26.69	(13.0)	1.469	.17	(.326)	8.28	.159.	(.277)	7.036	Stable
c	(0.001)	25.4	.155	(14.0)	62.27	(29.0)	3.276	.39	(.320)	8.128	.148.	(.265)	6.731	Stable
2a	(0.0015)	38.1	.232	(0.0)	0.0	(-0.0)	-0.0	0	(.312)	7.925	.252.	(.186)	4.724	Stable
3a	(0.002)	50.8	.310	(0.0)	0.0	(0.0)	0.0	0	(----)	-----	----	-----	-----	Failed ⁽⁵⁾ at 0.3 revolutions
b	(0.002)	50.8	.310	(1.0)	4.448	(2.0)	.4519	.03	(----)	-----	----	-----	-----	Failed at 0.3 revolutions
c	(0.002)	50.8	.310	(4.0)	17.79	(8.0)	.9038	.11	(----)	-----	----	-----	-----	Failed at 0.5 revolutions
d	(0.002)	50.8	.310	(6.0)	26.69	(13.0)	1.469	.17	(.327)	8.306	.331.	(.185)	4.699	Stable
e	(0.002)	50.8	.310	(14.0)	62.27	(29.0)	3.276	.39	(.377)	9.576	.351.	(.265)	6.731	Stable
4a	(0.0025)	63.5	.387	(0)	0.0	(0)	0	0	(----)	-----	----	(----)	-----	Failed at 0.3 revolutions
b	(0.0025)	63.5	.387	(6.0)	26.69	(13.0)	1.469	.17	(----)	-----	----	(----)	-----	Failed at 0.7 revolutions
c	(0.0025)	63.5	.387	(8.0)	35.58	(17.0)	1.921	.22	(----)	-----	----	(----)	-----	Failed at 0.9 revolutions
d	(0.0025)	63.5	.387	(11.0)	48.93	(23.0)	2.599	.30	(.368)	9.347	.445.	(.210)	5.334	Stable
e	(0.0025)	63.5	.387	(14.0)	62.27	(29.0)	3.276	.39	(.395)	10.033	.410.	(.258)	6.553	Stable
f	(0.0025)	63.5	.387	(28.0)	124.54	(59.0)	6.666	.77	(.504)	12.802	.400.	(.230)	5.842	Stable
i	(0.0025)	63.5	.387	(40.0)	177.92	(84.0)	9.49	> 1	(.506)	12.852	.387.	(.250)	6.35	Stable
j	(0.0025)	63.5	.387	(50.0)	222.4	(105.0)	11.863	> 1	(.503)	12.776	.375.	(.210)	5.334	Stable
5a	(0.0025)	63.5	.387	(4.0)	17.79	(52.0)	5.875	.11	(.521)	13.233	.423.	(.288)	1.216	Stable
6a	(0.0025)	63.5	.387	(8.0)	35.58	(105.0)	11.863	.22	(----)	-----	----	(----)	-----	Failed at 0.6 revolutions

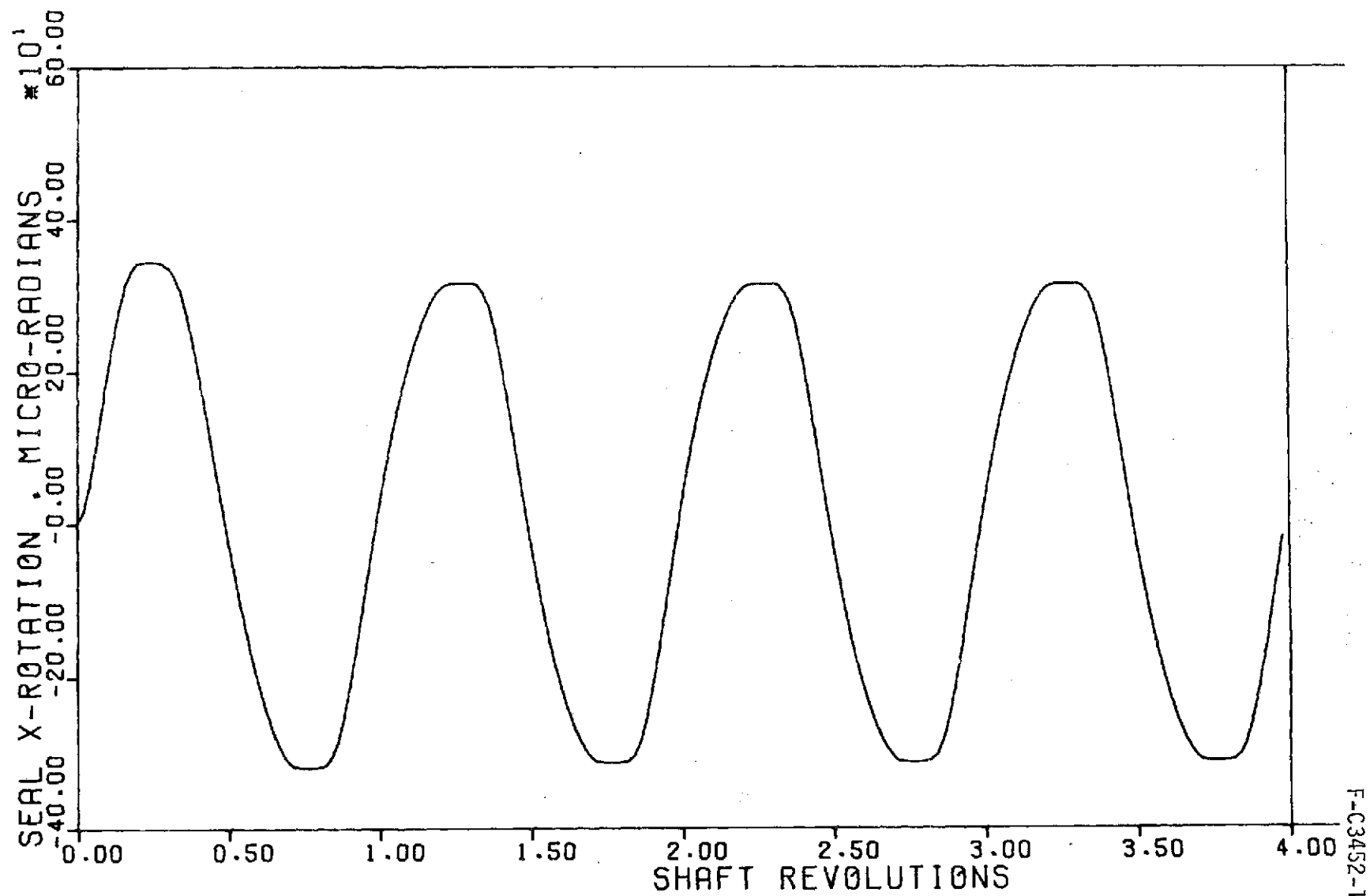
1. Angular misalignment of seal seat corresponding to a face runout measured at a radius of 8.20 cm (3.23 in.) (outside radius of step pad)
2. Mean axial clearance is the initial clearance plus the mean displacement of the seal from the initial clearance.
3. Angular amplitude of seal pivoting about piston ring.
4. When seal tracks seal seat.
5. When the runner contacts the seal.

whether the seal was able to track the nutating runner, or contact (implies failure) occurred.

The computer plots for run 3e of Table 5 are shown on Figures 15 through 20. Figure 15 shows rotational response of the seal ring about the X or horizontal axis as a function of shaft revolutions. At the extremity of each half cycle, the rotational response remains fixed for a finite period. The frictional resistance of the seal ring prevents motion until the fluid-film torque exceeds the frictional resistance torque. The magnitude of the response is 351 micro-radians while the seal seat force runout was 310 micro-radians. Thus, there is a slight magnification, although the period is in phase with the excitation. Figure 16 shows a similar curve for rotation about the Y-axis. Figure 17 depicts the axial fluid-film force response as a function of shaft revolutions. Four distinct cycles are noted for each shaft revolution. This occurs because the seal-ring sticks once every half cycle, about each of its axes of rotation, resulting in an upsurge in the fluid-film force and moment response. Since the seal is tilted, as an initial condition, it has greater load capacity than computed on the basis of uniform clearance. Initially, the load peaks up to 284N (64 lbs) which is sufficient to axially translate the seal-ring away from the collar. It thus takes on a new equilibrium position about which it oscillates. At the new position, (greater film thickness) the fluid-film no longer has the capacity to overcome friction and the seal ring remains stationary in the axial mode. Figure 18 shows variations in minimum film thickness as a function of shaft revolutions. Again, the four per revolution response is evident. Figures 19 and 20 show fluid-film moments. Here, the predominant frequency is once per revolution, with four local peaks each revolution as a result of the sticking phenomenon.

Dynamic plots of each of the runs of Case 1 are included in Appendix B. A brief description of each run follows:

Run 1. Runout = 25.4 μ m (.001 in.)



F-C3452-1

Figure 15. Rotation About X-Axis vs. Shaft Revolutions, Run 3e, Case 1

Pressure = 300 psig (2068.5 kN/m²) Runout = 0.002 in. (50.8 μm)
Temperature = 1000°F (537.78°C) Friction = 14.0 lbs (62.272 N), 29.0 in.-lbs (3.276 Nm)
Speed = 500 ft/sec (152.4 m/sec) Initial Clearance = 0.00032 in. (8.128 μm)
Nosepiece Wt. = 1.75 lbs (7.784 N)

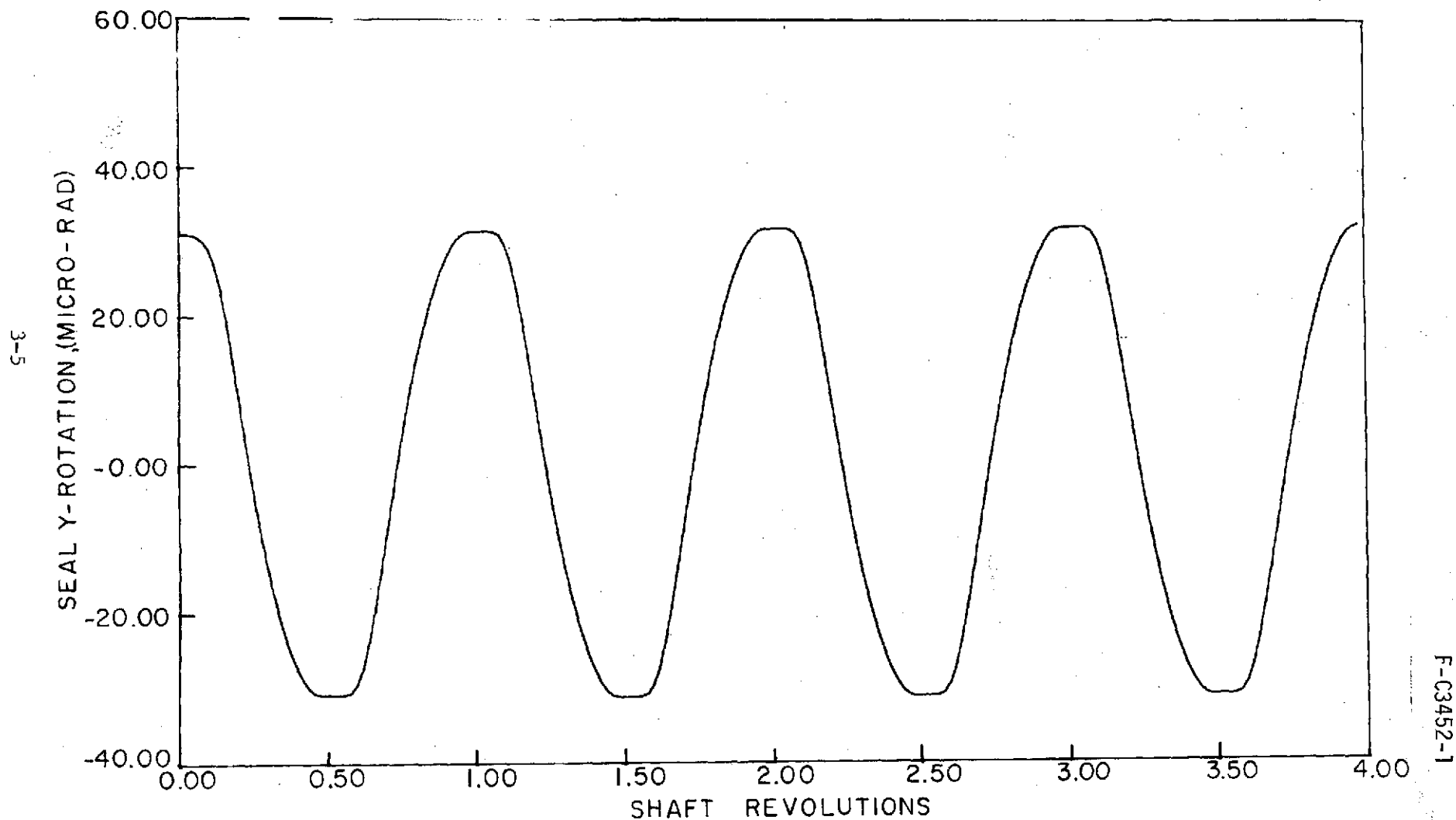


Figure 16. Rotation About Y-Axis vs. Shaft Revolutions, Run 3e, Case 1

Pressure = 300 psig (2068.5 kN/m²) Runout = 0.002 in. (50.8 μ m)
Temperature = 1000°F (537.78°C) Friction = 14.0 lbs (62.272 N), 29.0 in.-lbs (3.276 Nm)
Speed = 500 ft/sec (152.4 m/sec) Initial Clearance = 0.00032 in. (8.128 μ m)
Nosepiece Wt. = 1.75 lbs (7.784 N)

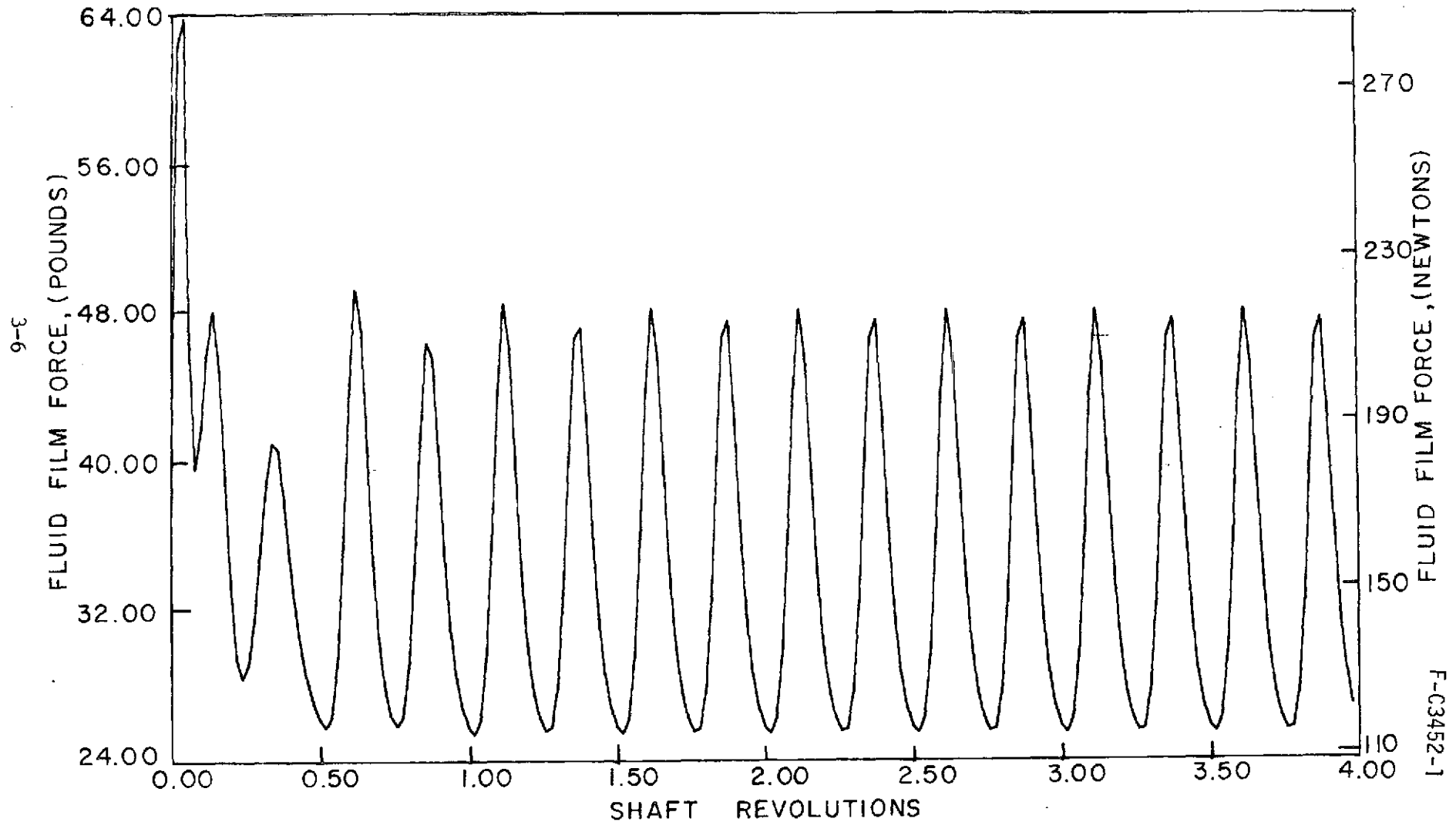


Figure 17. Fluid-Film Force vs. Shaft Revolutions, Run 3e, Case 1

Pressure = 300 psig (2068.5 kN/m²)

Runout = 0.002 in. (50.8 μ m)

Temperature = 1000°F (537.78°C)

Friction = 14.0 lbs (62.272 N), 29.0 in.-lbs (3.276 Nm)

Speed = 500 ft/sec (152.4 m/sec)

Initial Clearance = 0.00032 in. (8.128 μ m)

Nosepiece Wt. = 1.75 lbs (7.784 N)

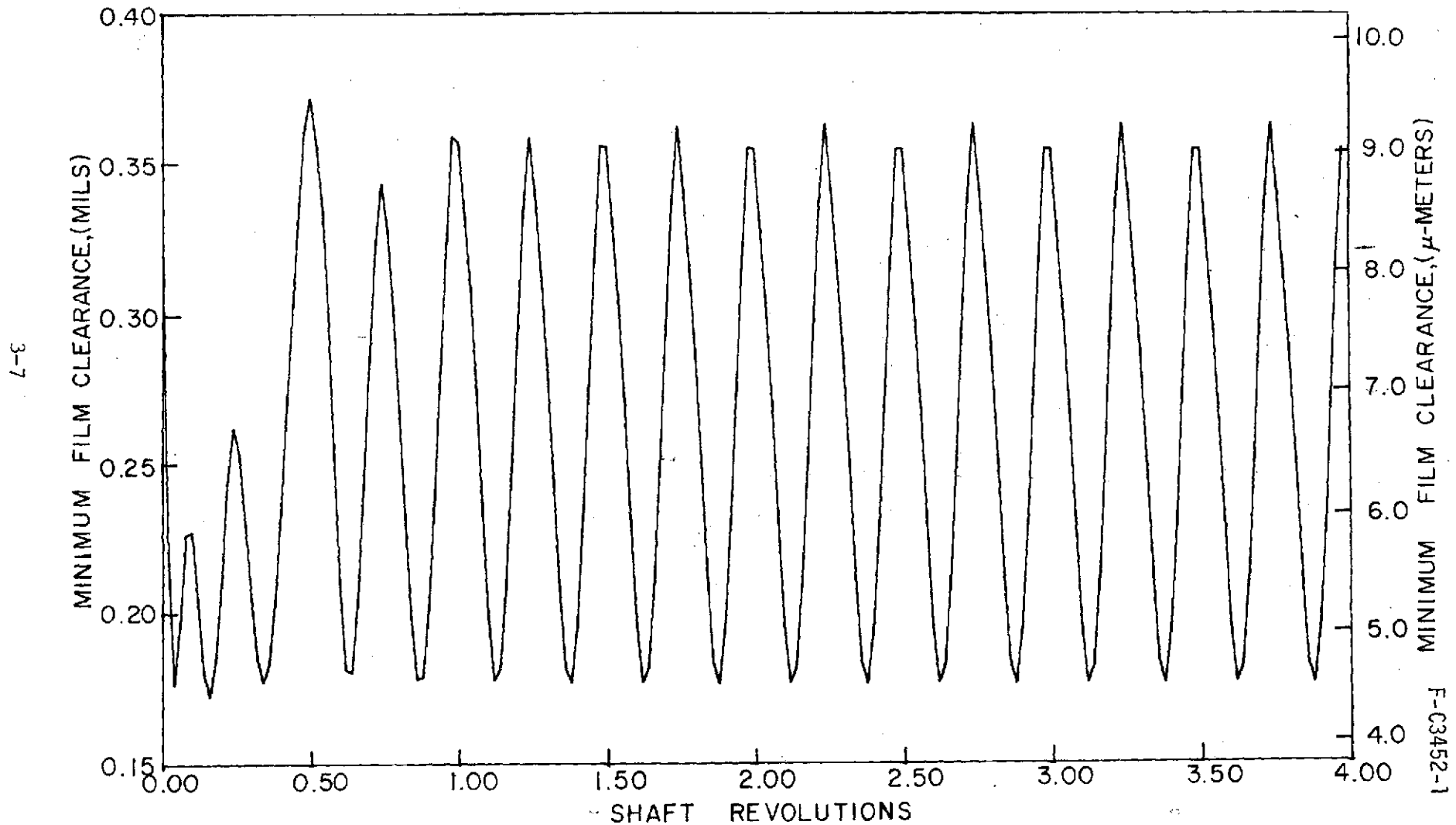


Figure 18. Minimum Clearance vs. Shaft Revolutions, Run 3e, Case 1

Pressure = 300 psig (2068.5 kN/m²)

Runout = 0.002 in. (50.8 μm)

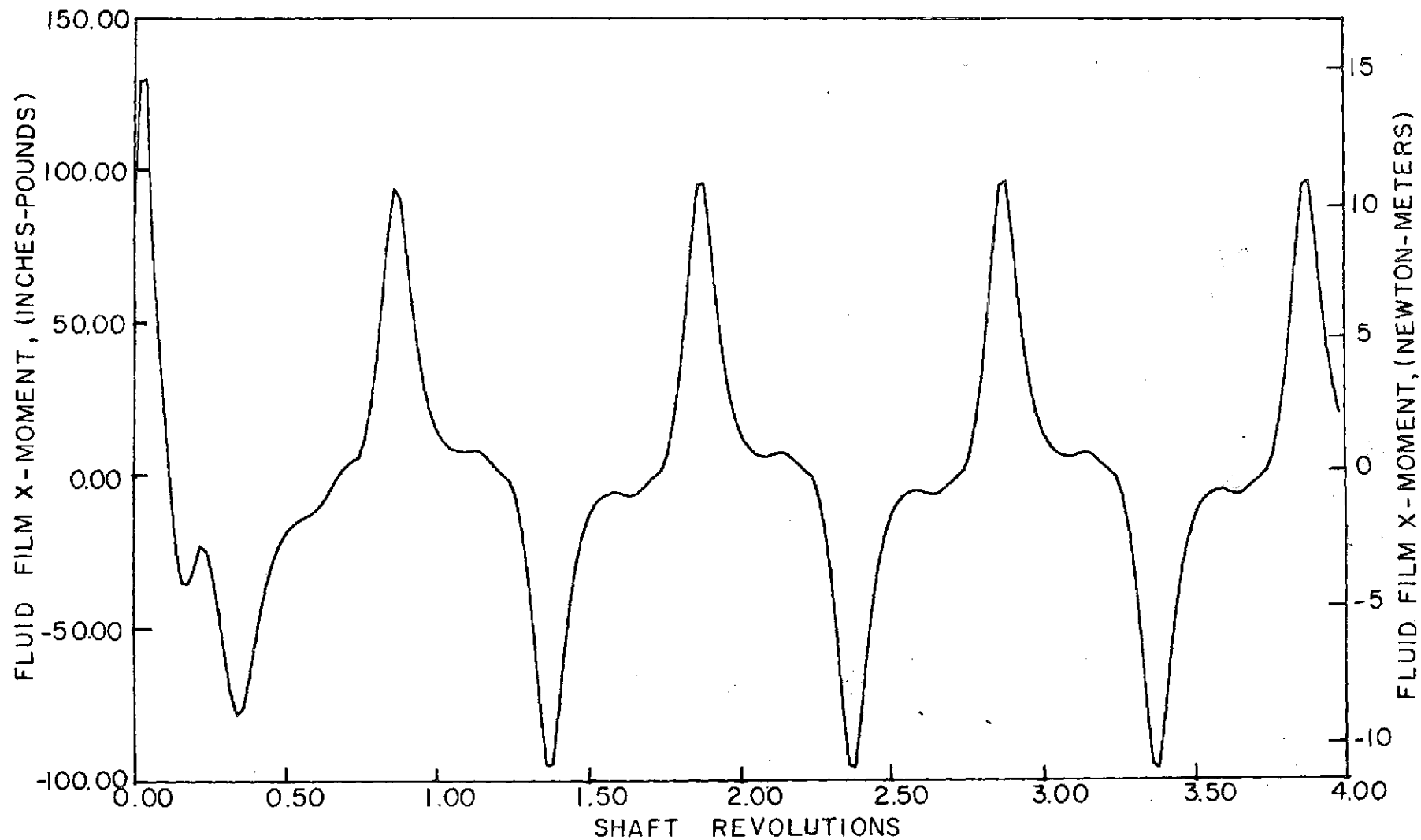
Temperature = 1000°F (537.78°C)

Friction = 14.0 lbs (62.272 N), 29.0 in.-lbs (3.276 Nm)

Speed = 500 ft/sec (152.4 m/sec)

Initial Clearance = 0.00032 in. (8.128 μm)

Nosepiece Wt. = 1.75 lbs (7.784 N)



F-C3452-1

Figure 19. Fluid-Film Moment About X-Axis vs. Shaft Revolutions, Run 3e, Case 1

Pressure = 300 psig (2068.5 kN/m²) Runout = 0.002 in. (50.8 μm)
Temperature = 1000°F (537.78°C) Friction = 14.0 lbs (62.272 N), 29.0 in.-lbs (3.276 Nm)
Speed = 500 ft/sec (152.4 m/sec) Initial Clearance = 0.00032 in. (8.128 μm)
Nosepiece Wt. = 1.75 lbs (7.784 N)

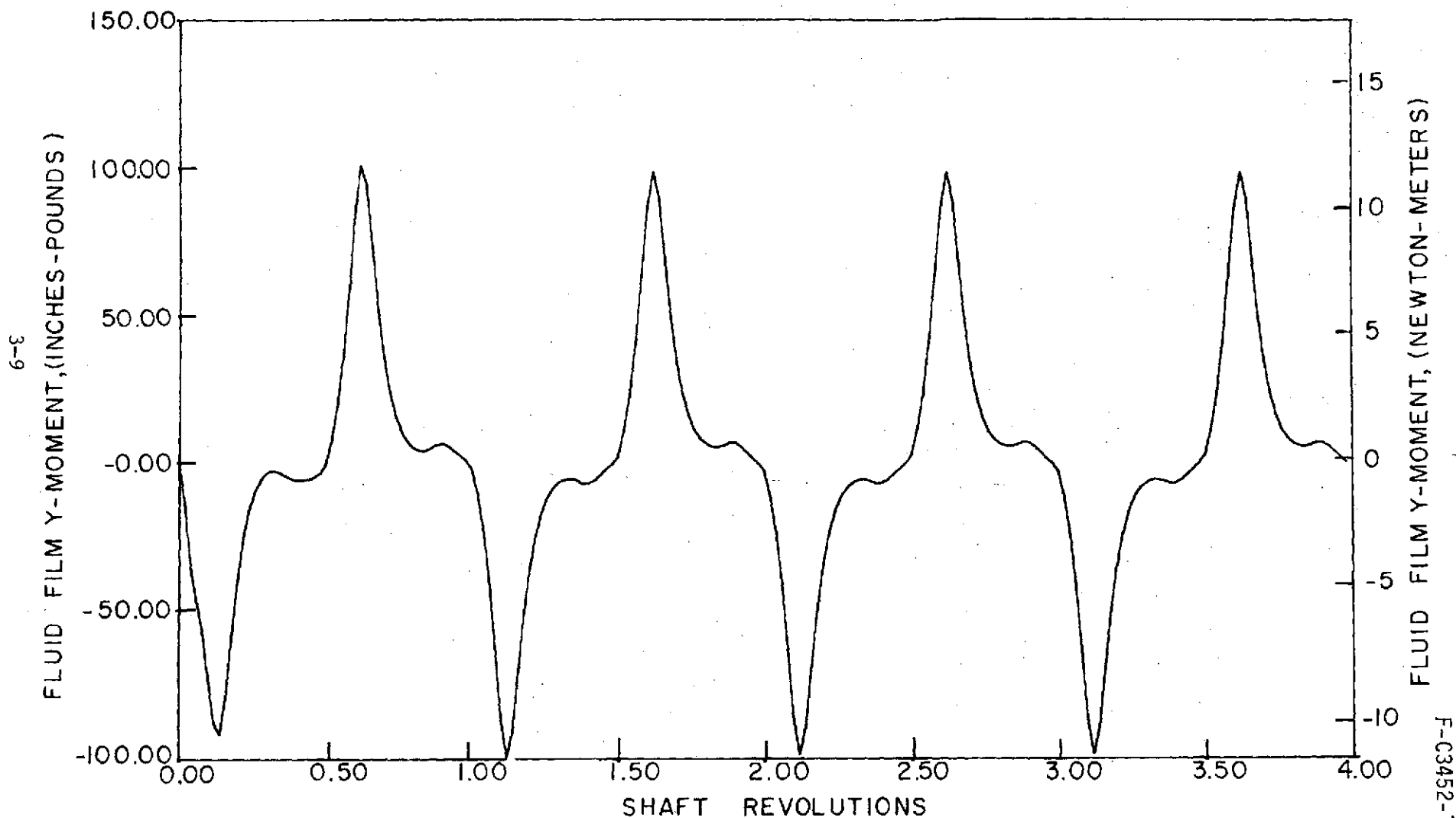


Figure 20. Fluid-Film Moment About Y-Axis vs. Shaft Revolutions, Run 3e, Case 1

Three friction values were examined for this particular runout.

FRICITION	COEFF. OF FRICTION
0.0 N, 0.0 N-m (0.0 lbs, 0.0 in-lbs)	0
26.69 N, 1.47 N-m (6.0 lbs, 13.0 in-lbs)	.20
62.27 N, 3.28 N-m (14.0 lbs, 29.0 in-lbs)	.47

Figures B-1 - B-4 illustrate the dynamic responses and forces as a function of shaft revolution for a friction level of zero. The seal follows the swashing in-phase which is illustrated by the angular rotation curves (Figure B-1, B-2). The seal did not vibrate in the axial mode which was typical of most of the cases studied. The minimum clearance $6.2 \mu\text{m}$ (.244 mils) and the fluid film force 166.4 N (37.4 lbs) remained a constant during this dynamic run. Note that the fluid film force is equal to the equilibrium condition. Fluid film moments are shown in Figures B-3 and B-4. The predominant vibration is once per shaft revolution.

When the friction level was increased to 26.688 N, 1.4687 Nm (6 lbs, 13 in-lbs), the system remained stable but the angular amplitudes, Figures B-5 and B-6, show signs of "sticking" due to angular friction. The seal again did not vibrate in the axial mode mainly because the axial friction of 26.688 N (6 lbs) was larger than the change in fluid film force (B-7) which was approximately 17.792 N (4 lbs). Minimum clearance (Figure B-8) and the force curves show a frequency of four cycles per one shaft revolution. This frequency can also be seen in the moment plots (Figures B-9, B-10) although the predominant frequency is once per rev.

The results for friction of 62.272 N, 3.276 Nm (14 lbs, 29 in-lbs) are shown in Figures B-11 - B-16. The conclusions are basically the same as above with the frictional "sticking" more pronounced for this run.

Run 2. Runout = $38.1 \mu\text{m}$ (.0015 in)

One test was made at zero friction level for this runout. The results are illustrated in Figures B-17 - B-22. The fluid film force (Figure B-17)

settles out to the equilibrium value 166.4 N (37.41 lbs), while the minimum clearance (Figure B-18) maintains a constant value of 4.6 μm (.18 mils). Again the seal did not vibrate in the axial mode.

Run 3. Runout = 50.8 μm (.002 in)

Friction levels of 0.0 N (0.0 lbs), 4.45 N, 0.226 Nm (1.0 lbs, 2.0 in-lbs) and 17.792 N, 0.904 Nm (4.0 lbs, 8 in-lbs) all failed with the least stable occurring at 0.0 N (0.0 lbs). Figures B-23 - B-28 illustrate the results for this run.

Figures B-29 - B-40 show the results of two stable runs as friction levels of 26.688 N, 1.4687 Nm (6 lbs, 13 in-lbs) and 62.272 N, 3.276 Nm (14 lbs, 29 in-lbs) respectfully. The same trends are noticeable in these runs compared with the previous stable runs with friction. There was again no axial vibration of the nosepiece. The nosepiece moves axially to a new position and remains there.

Run 4. Runout = 63.5 μm (.0025 in)

Seal failure occurred at the friction levels of 0.0 N, 0.0 Nm (0.0 lbs, 0.0 in-lbs), 26.688 N, 1.4687 Nm (6.0 lbs, 13.0 in-lbs) and 35.6 N, 1.4687 Nm (8.0 lbs, 13.0 in-lbs) with again the least stable run occurring at zero friction. Figures B-41 - B-46 illustrate the results for zero friction.

Friction levels up to 222.5 N, 11.865 Nm (50 lbs, 105 in-lbs) were found to be stable; although no plots were made for these runs the trends were the same as previously observed.

Run 5. Runout = 63.5 μm (.0025 in)

Up to this point all the cases studied were based on the relationships between friction force and friction moment derived in Appendix C. This generally should be true for this seal design. However, it is not unlikely that the seal could "hang-up" (high friction) in the angular modes. This could occur at large values of runout.

Two runs were studied where the friction moment was increased by approximately a factor of 6, at a friction level of 17.792 N, 5.988 Nm (4.0 lbs, 52 in-lbs). The seal was stable (Figures B-47 - B-53). Notice

that the seal is also vibrating in the axial mode (Figure B-47). The reason for this is that the seal "sticks" in the angular mode due to the large friction moment thus causing the axial film force (Figure B-48) to increase due to angular misalignment. Since the friction force in the axial direction is small compared to the fluid film force fluctuations, the seal will vibrate in the axial mode.

At a friction level of 35.6 N, 11.86 Nm (8 lb, 105 in-lb) the seal failed. The seal and runner contacted at approximately 0.6 revolutions.

3.2 TRACKING MAP, CASE 1

The data obtainable from the dynamic computer runs permits a seal tracking map to be developed.

Figure 21 is a typical theoretical tracking map for a seal which has coulomb friction. Curve 1 represents a threshold based on the maximum friction level. Above this curve, the seal assembly will not track because friction will not permit the seal to move and since nutation amplitudes exceed film thickness, the seal will fail. Curve 2 represents a threshold based on minimum friction. Below this curve, the seal system will not track because there is insufficient coulomb friction to damp seal inertia forces. If the inertia properties of the seal were reduced this curve would shift to the right, increasing the tracking range. The converse is also true. For given inertia properties below a certain value of runout, the system tracks for zero friction. A good seal design would be one in which the inertia properties are selected so that the seal tracks at zero friction and maximum runout. Generally, friction levels will increase with supply pressure. Of course, this is not always possible to do because of the physical limitations of the system. Figure 22 is a tracking map of the NASA seal. The shaded area of this curve is the region where the analysis predicts acceptable tracking. The solid line 2 corresponds to curve 2 of Figure 22. Runouts greater than 63.5 μm (.0025 in.) were not examined, but for friction levels below 42.3 N (9.5 lb) these cases would definitely not track.

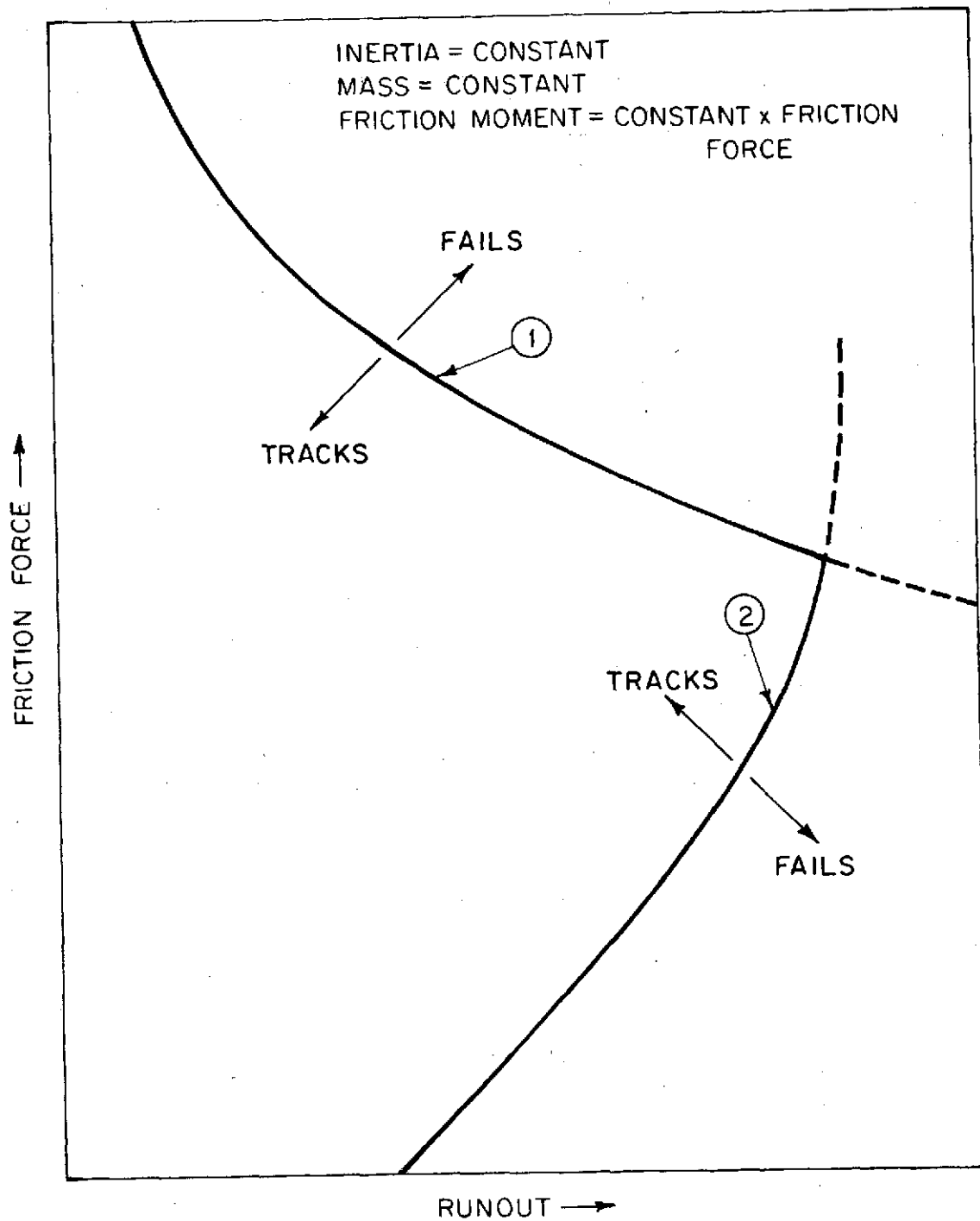


Figure 21. Typical Tracking Map

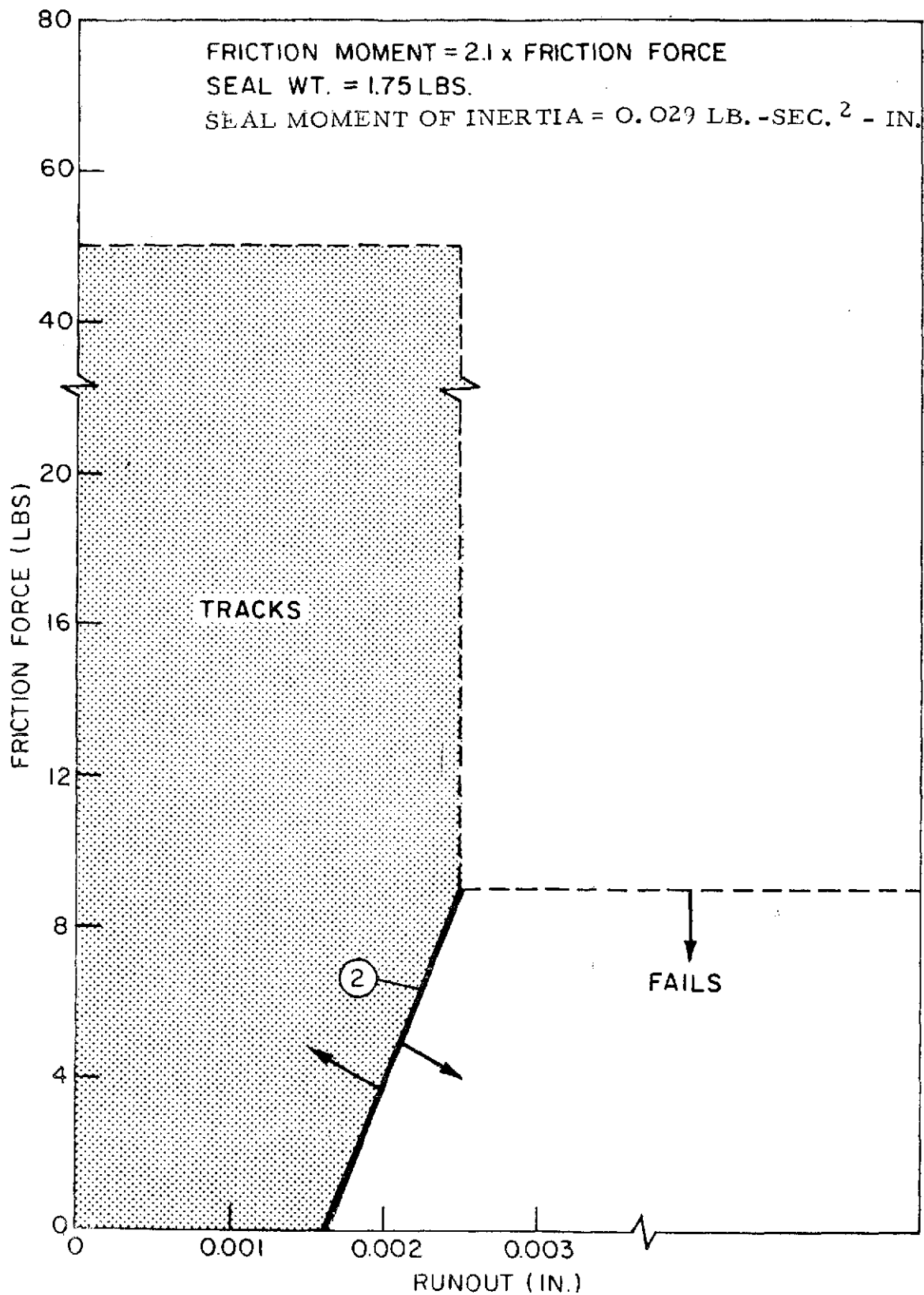


Figure 22. Partial Tracking Map at the Specified Operating Condition for Case 1

At 63.5 μm (.0025 in.) runout, friction levels were increased from 42.3 N (9.5 lbs) to 222.5 N (50 lbs) axially with the system tracking. This establishes that below 222.5 N (50 lbs) friction and above curve 2 of Figure 22 the system will track for runouts less than 63.5 μm (.0025 in.). For this seal design and the assumed relationship between axial and angular friction, curve 1 of Figure 21 lies above 222.5 N (50 lbs). Since 222.5 N (50 lbs) friction corresponds to a coefficient of friction greater than 1, it was not required to determine curve 1 (friction level boundary for this tracking map). Apparently, the seal will track regardless of friction level.

Two additional runs were made at a runout of 63.5 μm (.0025 in.) where the relationship between angular and axial friction was changed to friction moment = 13 x axial frict. (runs 5a and 6a on Table 5). This is not expected to be the case based on the calculations in Appendix C, but results indicate how drastic the stability map can shift with different relationship between friction and friction moment.

3.3 CASES 2, 3, and 4

Dynamic response curves of Cases 2, 3, and 4 are included in Appendix B. Figure B-54 shows seal translation as a function of shaft revolutions. This is the axial motion measured from the initial axial clearance. The minus sign indicates that the axial clearance is becoming larger. The initial clearance for this case was 8.4 μm (.33 mils) and the mean displacement from that position is -5.6 μm (-.22 mils). Therefore, the seal assembly is vibrating axially about 14 μm (.55 mils) axial clearance with an amplitude of 1.02 μm (.04 mils). This motion has a predominant frequency of four times the shaft speed, a common characteristic discussed for Case 1.

Figure B-55 and B-56 show the seal's angular motion about orthogonal axis. Note that the peak to peak amplitude of the seal for each rotation is approximately 200 micro-radians while that of the runner is 310 micro-radians.

Minimum film thickness, as shown on Figure B-57, oscillates about an average of 3.56 μm (.14 mils) with an amplitude of 2.03 μm (.08 mils).

Again the superharmonic of four times the shaft speed occur in this parameter. Similar response occurs for the fluid film forces (Figure B-58) which oscillate about the steady-state loading of approximately 125-134 N (28-30 lbs). The moments (Figure B-59, B-60) have a combined frequency of a four per rev with predominant frequency of once per rev which was the case with angular response.

Case 3 is the same as Case 2 except that the sealing pressure is $1/4$ that of Case 1. This essentially reduces the friction by approximately $1/4$. Figure B-61 through B-67 contain the results for this case. The same overall conclusion made for Case 2 can be made for this case. Seal translation vibrates almost about its equilibrium position of $8\text{ }\mu\text{m}$ (.315 mils) and seal angular motion is approximately the same as the runner amplitude. The minimum clearance oscillates about $5.6\text{ }\mu\text{m}$ (.22 mils) which is larger than Case 1. The main reason for the improved response is the reduction of sliding friction.

Case 4 differs from Case 2 in that seal mass and inertial properties were reduced to $1/2$ their original values and the rotating speed of the runner was increased 25% to 1270 cm/sec (500 in/sec). Figures B-68 through B-74 show seal dynamic performance. The seal for this case follows the runner essentially the same as Case 2 with a larger mean minimum clearance $4.6\text{ }\mu\text{m}$ (.18 mils). Most likely the improvement in minimum clearance is caused by the higher speed which increases the hydrodynamic load capacity of the seal. This is further illustrated by noting that the seal axial motion is vibrating about an axial clearance of $14.7\text{ }\mu\text{m}$, (0.58 mils) which is larger than that of Case 2. Therefore, the reduction of mass and inertia did not seem to improve seal response.

4. CONCLUSIONS AND RECOMMENDATIONS

4.1 CONCLUSIONS

- Dynamic response of the self-acting type face seal is limited by two phenomena.
 1. Friction levels could exceed the force that the fluid film produces, thus causing seal failure.
 2. Seal inertia will not permit tracking if the runner has large angular misalignments. The situation can be improved by introducing friction which will prevent excessive seal motion, and also by reducing the inertia properties of the seal.

The analysis revealed that the NASA designed self-acting seal does not track (nosepiece does not follow seat motions) for seat runouts greater than $63.5 \mu\text{m}$ (0.0025 in). Suitable tracking was predicted for runouts below $63.5 \mu\text{m}$ (0.0025 in) and for the friction levels of 222.5 N(50 lbs) force and 11.865 Nm (105 in-lbs) moment; higher friction levels were not investigated.

Sealed air pressure	2068.5 kN/m ² (300 psig)
Sealed air temperature	810.93°K (1000°F)
Sliding speed (mean)	152.4 m/sec (500 ft/sec) 1785.5 rad/sec (17,050 rad/min)

- If the relationship between axial and angular friction changes (possibly due to seal hang-up in the angular modes causing the seal angular friction to increase), there is a drastic change in the stability map. This infers that it is significant to be able to predict this relation between axial and angular friction as a function of secondary seal geometry.
- Since actual friction values are difficult to determine and ideal geometries are assumed for this analysis, a good seal design would keep runouts below $38.1 \mu\text{m}$ (.0015) and/or reduce inertia properties of seal as much as practical.
- Although no direct comparative experimental information was available, the results qualitatively compare well with observed results. Superharmonic frequencies have been recorded and they were about 4 x running speed, and film thickness and leakage measurements were close to theoretical predictions.

4.2 RECOMMENDATIONS

- The computerized analysis has usefulness as a design tool, and it is recommended that it be utilized in the design process to:
 - a) proportion seal mass and inertia to produce acceptable dynamic response.
 - b) optimize the hydrodynamic geometry.
 - c) determine maximum seat runout and tolerable limit of secondary seal friction.
 - d) establish operating limits of existing configurations.

5. REFERENCES


1. V. P. Povinelli and A. H. McKibbin, "Development of Mainshaft Seals for Advanced Air Breathing Propulsion Systems - Phase II", NASA CR 72737, prepared for NASA Lewis Research Center.
2. V. P. Povinelli and A. H. McKibbin, "Development of Mainshaft Seals for Advanced Air Breathing Propulsion Systems - Phase III", NAS3-7609, prepared for NASA Lewis Research Center.
3. R. Colsher and W. Shapiro, "Predicting Performance of Gas-Lubricated Seals Using Advanced Numerical Techniques", Nonr-2342(00).
4. "The Numerical Solution of Parabolic and Elliptic Differential Equations", Journal, Society Industry, Applied Mathematics, Vol. 3, No. 1 (March 1955), pp. 28-41.
5. Elrod, H. G., Glanfield, G. A., "Computer Procedures for the Design of Flexibly Mounted, Externally Pressurized Gas-Lubricated Journal Bearings", University of Southampton, Department of Mech. Engineering Report, Sept. 1970.
6. W. Shapiro, R. Colsher, "Dynamic Analysis of a Gimbal-Mounted, Rayleigh-Step Thrust Bearing", Proceedings of Gas Bearing Symposium, University of Southampton, Southampton, England, 1971.
7. W. Shapiro, R. Colsher, "Implementation of Time-Transient and Step-Jump Dynamic Analysis of Gas-Lubricated Bearings", Transactions of ASME, Journal of Lubrication Technology, Vol. 92, Series F, No. 3, July 1970, pp. 518-529.
8. P. R. Shepler, "Split-Ring Seals", Machine Design, Chapter 5, March 9, 1967, pp. 18-23.

6. NOMENCLATURE

Δa	- area of typical grid region surrounding a grid point, cm^2 (in^2)
ΔA	- non-dimensional area of typical grid region surrounding a grid point = $\Delta a/r_o^2$
C	- equilibrium or initial parallel clearance between runner and seal measured at the seal centerline, cm (in)
F_a	- self-acting force due to the hydrodynamic effects of the step pads, N (lbs)
$F_{a_{eq}}$	- equilibrium self-acting force due to the hydrodynamic effects of the step pad, N (lbs)
F_f	- sliding friction force, N (lbs)
F_L	- seal leakage, N/sec (lbs/sec)
F_{SCFM}	- seal leakage, m^3/min (SCFM)
G	- gas constant, J /K°-mole ($\text{in}^2/\text{°R-sec}^2$)
h	- film thickness, cm (in)
H	- non-dimensional film thickness = h/c
I_x	- inertia of seal assembly around X-X axis, N-m-sec^2 (in-lbs-sec^2)
I_y	- inertia of seal assembly around Y-Y axis, N-m-sec^2 (in-lbs-sec^2)
m_s	- mass of seal assembly, $\text{N-sec}^2/\text{m}$ ($\text{lbs-sec}^2/\text{in}$)
M	- number of grid points in radial directions
M_{fr}	- viscous friction loss, N-m (in-lbs)
\bar{n}	- unit normal vector
N	- number of grid points in circumferential direction
N	- rotational speed, rpm
p	- film pressure, N/m^2 (psia)
p_a	- ambient pressure, N/m^2 (psia)
p_s	- sealed pressure, N/m^2 (psia)

P	- non dimensional film pressure, p/p_a
P_f	- power loss, watt (hp)
Q	- independent variable = p^2
r	- radial coordinate, cm (in)
Δr	- radial grid interval
$r_o = R_o$	- outside radius, cm (in)
r_l	- inside radius, cm (in)
r_{pr}	- radius of piston ring, cm (in)
R	- non-dimensional radial coordinate = r/r_o
ΔR	- non-dimensional radial grid interval, $\Delta r/r_o$
S	- surface
t	- time, sec
Δt	- time step interval, sec
T	- non-dimensional time = $t\omega/2\Lambda$
ΔT	- non-dimensional time step interval = $\Delta t \omega/2\Lambda$
T_a	- self-acting moment, N-m (in-lbs)
T_s	- temperature of sealed gas, °K (°R)
T_f	- sliding friction torque, N-m (in-lbs)
v	- volume, cc (in ³)
\bar{V}	- velocity vector
z_s	- seal translation, cm (in)
α_x	- angular tilt about X-X axis, radian
α_{r_x}	- runner nutation about x-x axis, radian
α_{r_y}	- runner nutation about y-y axis, radian
α_{s_x}	- angular rotation of seal about x-x axis, radian
α_{s_y}	- angular rotation of seal about y-y axis, radian

- Δ - non-dimensional step height = δ/c
- θ - circumferential coordinate measured counter clockwise from positive x axis, radians
- θ_p - pad angle, radians
- $\Delta\theta$ - circumferential grid interval, radians
- Λ - compressibility number = $6\mu\omega r_o^2/p_a c^2$
- μ - viscosity, kNs/m^2 (lb-sec/in^2)
- ρ - mass density kg/m^3 ($\text{lbs/sec}^2/\text{in}^4$)
- ω - runner rotational speed, rad/sec
- δ - step height, cm (in)



F-C3452-1

Appendix

A

ANALYTICAL APPROACH USED TO OBTAIN
SEAL PERFORMANCE



THE FRANKLIN INSTITUTE RESEARCH LABORATORIES
THE BENJAMIN FRANKLIN PARKWAY • PHILADELPHIA, PENNSYLVANIA 19103

ANALYTICAL APPROACH USED TO OBTAIN SEAL PERFORMANCE

Basically, seal performance can be subdivided into two major categories:

- Steady-state
- Dynamics

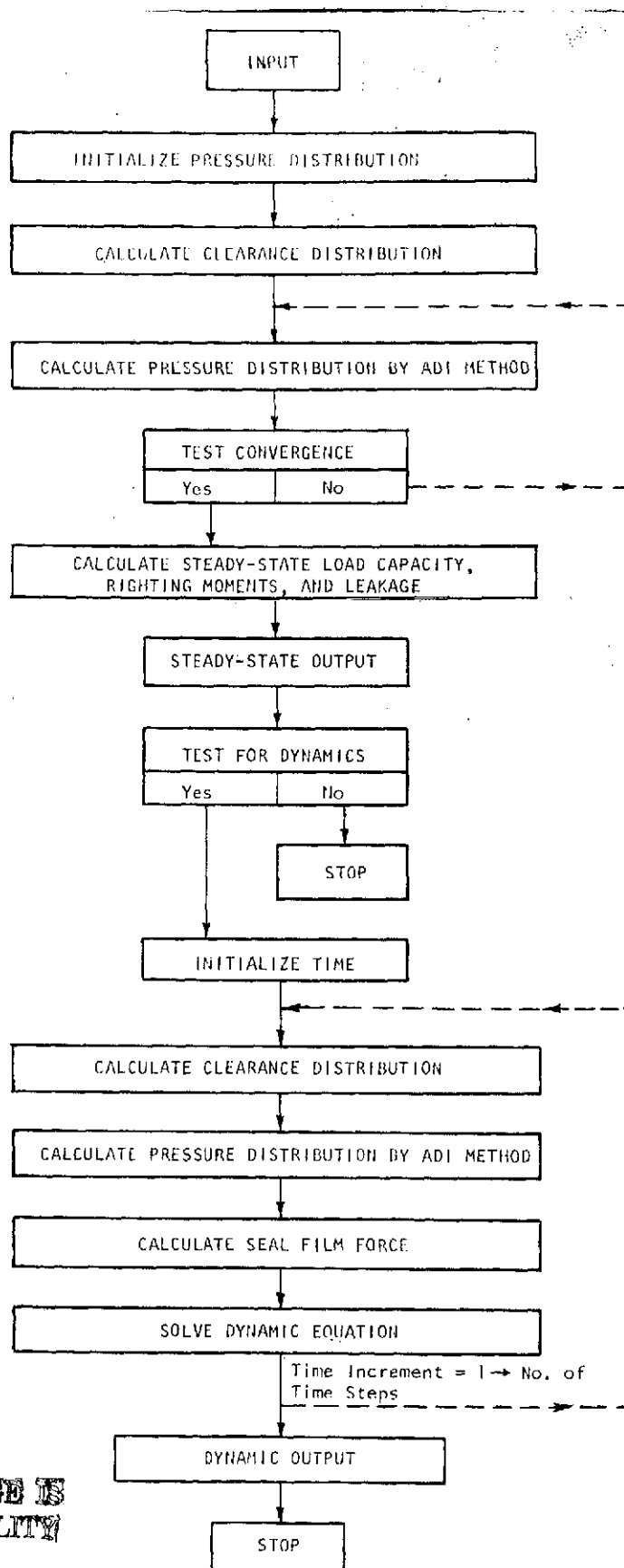
Steady-state performance consists of determining the load capacity, power loss and leakage for each operating condition. Dynamic performance involves obtaining the nose-piece response due to some forcing function such as swashing of the seal seat due to shaft motion, oscillating external forces, etc. The approach used to determine seal performance is shown in Figure A-1 which consists of the following major steps:

- Calculate the pressure profile in the primary seal film by numerical solution of the mass flux lubrication equation.
- Determine seal force, moment, power loss and leakage due to the gas film from the pressure distribution.
- Determine seal dynamic response by direct integration of the equations of motion coupled with the lubrication equation.

Calculation of Pressure Distribution for Steady-State Performance

Since the governing lubrication equation is non-linear for compressible flow, an iterative numerical scheme must be used to determine the pressure distribution. A finite difference diffusion method was the selected approach. It consists of the following:

1. Subdivide each seal pad and sealing dam into a grid network.
2. Form finite difference equations from the lubrication equation in terms of pressure at each point in this grid network.
3. Assume an initial pressure distribution.



ORIGINAL PAGE IS
OF POOR QUALITY

Figure A-1. Seal Performance Procedure

4. Calculate clearance distribution
5. Calculate a new pressure distribution at each time step using a numerical solution method. If its the first iteration, use the profile assumed in (3) above.
6. Repeat step (5) until the pressure solution converges. This is accomplished by comparing the new pressure distribution with the one from the previous time step.

GRID NETWORK

A typical variable grid network is shown in Figure A-2. One of the major advantages of using variable grid spacing is that it enables modeling a dense grid at regions of high pressure gradients and thus circumvents problems of numerical instability imposed by uniform grids of spacing that would not absorb excessive computer storage or computational time.

Referring to Figure A-2 the grid point or nodes are numbered sequentially in columns by the index L where:

$$L = I + (J-1)M, J = 1 \text{ to } N; I = 1 \text{ to } M$$

For the L^{th} node as shown in Figure A-2 and illustrated in more detail in Figure A-3, it is convenient to label the "neighboring" points as follows:

$L-1^{\text{th}}$ has the label NORTH

$L+1^{\text{th}}$ has the label SOUTH

$L-M^{\text{th}}$ has the label WEST

$L+M^{\text{th}}$ has the label EAST

GOVERNING EQUATIONS

The continuity equation applied to an elemental volume is

$$\frac{\partial}{\partial t} \int_V \rho \, dv + \int_S \rho \vec{V} \cdot \vec{n} \, ds = \dot{M} \quad [\text{A-1}]$$

where

$$\frac{\partial}{\partial t} \int_V \rho \, dv = \text{net mass flux entering region due to change in volume}$$

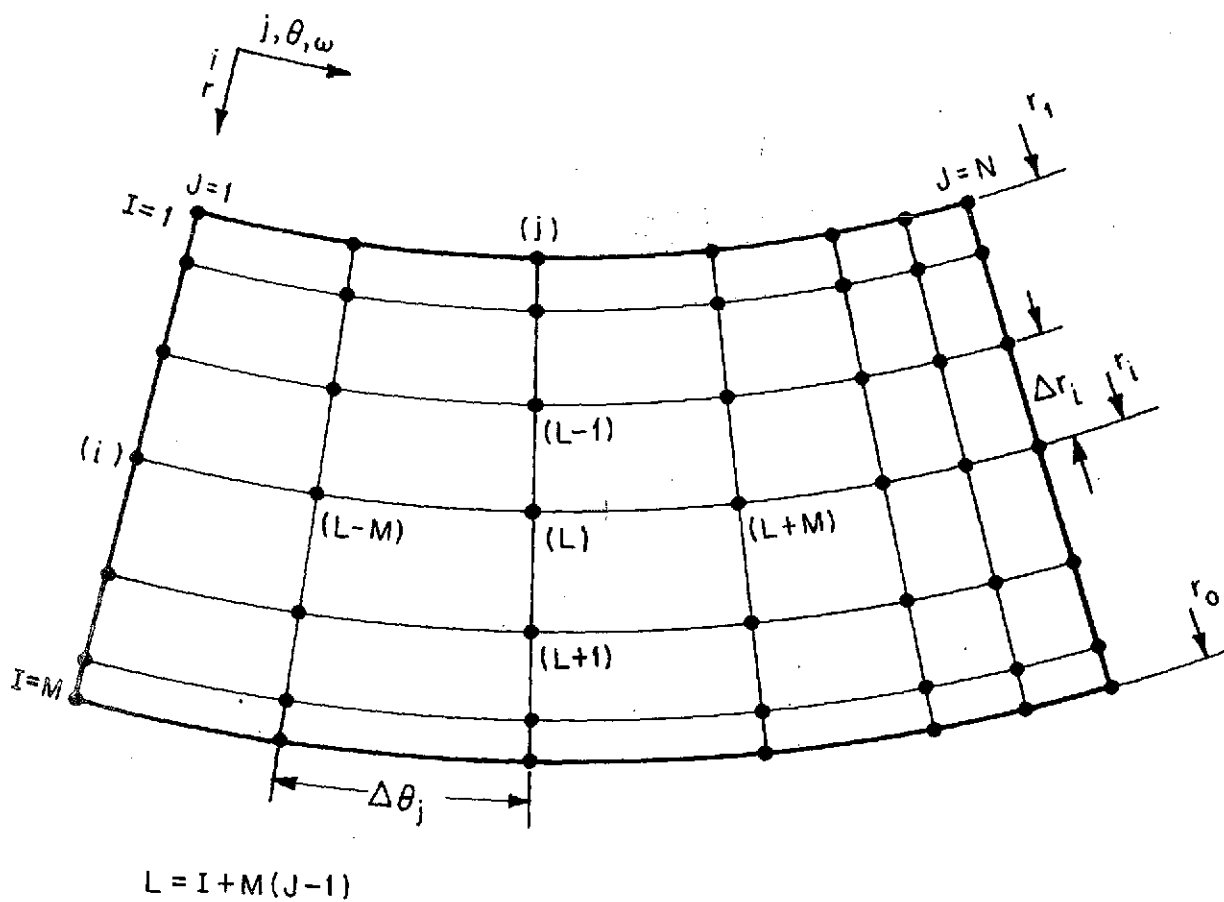


Figure A-2. Typical Grid Network

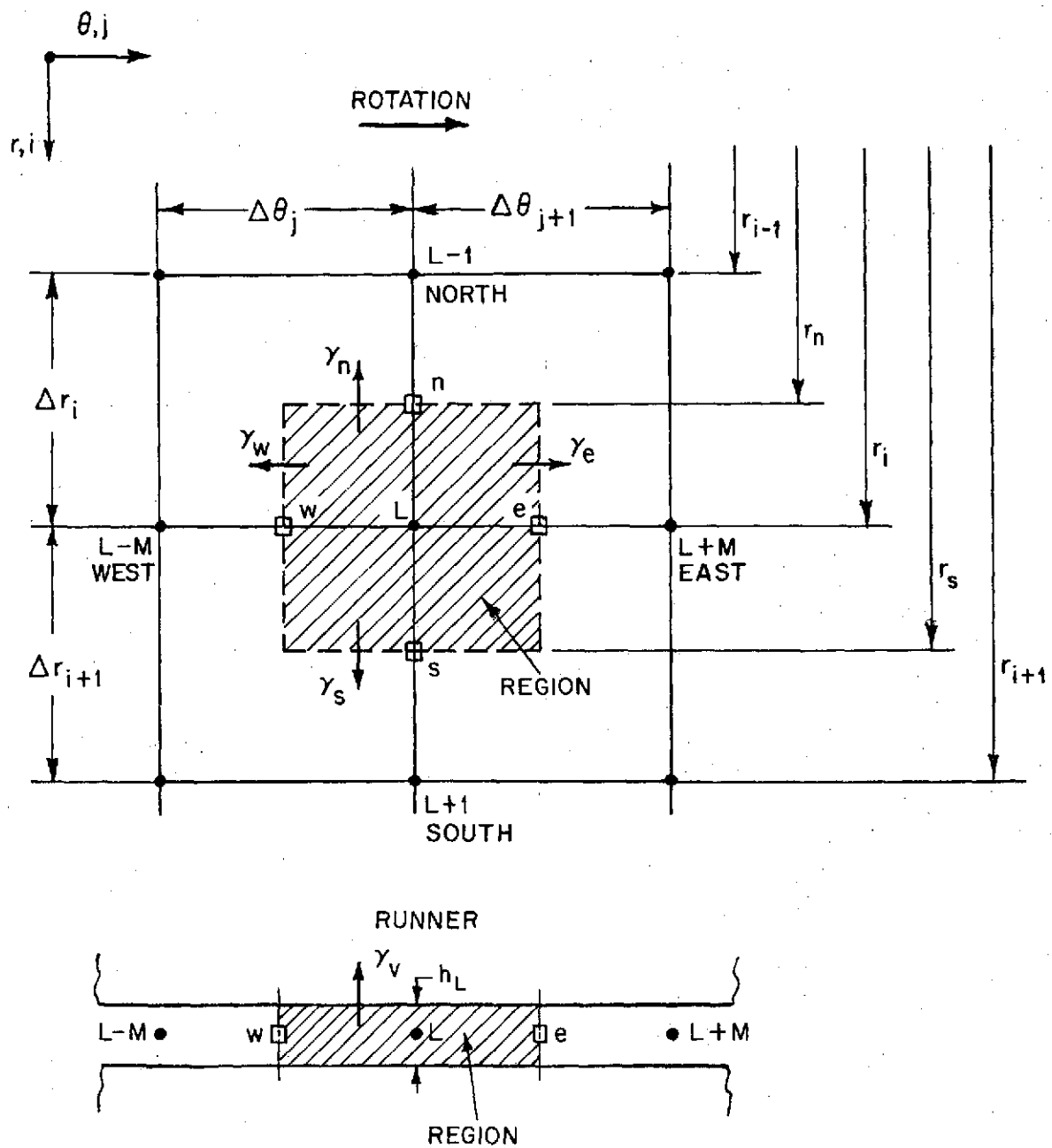


Figure A-3. Flow Balance Model

$$\int_S \rho \bar{V} \cdot \bar{n} ds = \text{net mass flux leaving boundary of region.}$$

\dot{M} = net mass flux entering due to external supply.
For the case under study this quantity is zero.

Applying the normal assumption of laminar lubrication, the velocity vector \bar{V} in polar coordinates (as derived from the Navier-Stokes equation) has the components

$$v_{\theta} = -\frac{\partial p}{r \partial \theta} \frac{h^2}{12\mu} + \frac{r\omega}{2}$$

$$v_r = -\frac{\partial p}{\partial r} \frac{h^2}{12\mu}$$

The mass density ρ by making the isothermal assumption can be expressed as

$$\rho = \frac{p}{G T_s}$$

Consider the region surrounding the L^{th} grid point illustrated in Figure A-3. This region is constructed so that its extremities encompass half the distance between the L^{th} point and its neighbors. A typical region has an area

$$\Delta a = \left[\frac{r_n + r_s}{2} \right] \left[\frac{\Delta \theta_{j+1} + \Delta \theta_j}{2} \right] \left[\frac{\Delta r_{i+1} + \Delta r_i}{2} \right]$$

Define

$$\bar{\Delta \theta} = \frac{\Delta \theta_{j+1} + \Delta \theta_j}{2}, \quad \bar{\Delta r} = \frac{\Delta r_{i+1} + \Delta r_i}{2}$$

Assuming that this region is "small", that is

$$\frac{\partial}{\partial t} \int_V \frac{p}{G T_s} dv = \frac{\partial}{\partial t} \left[\frac{p}{G T_s} h \Delta a \right]$$

$$\int_S \frac{p}{G T_s} \bar{V} \cdot \bar{n} ds = \frac{p}{G T_s} \bar{V} \cdot \bar{n} h \Delta \ell$$

where Δl is the length of the boundary. By applying Equation [A-1], which indicates that the net mass flux entering a given region must be equal to the net mass flux leaving a region, to the region in Figure A-3 the resultant flow balance becomes:

$$\gamma_v + \gamma_n + \gamma_s + \gamma_e + \gamma_w = 0 \quad [A-2]$$

where

$$\gamma_v = \frac{\Delta a}{GT_s} \frac{\partial}{\partial t} (ph_L)$$

$$\gamma_n = \frac{h_n^3 r_n \overline{\Delta \theta}}{12\mu GT_s} p \left. \frac{\partial p}{\partial r} \right|_n$$

$$\gamma_s = \frac{h_s^3 r_s \overline{\Delta \theta}}{12\mu GT_s} p \left. \frac{\partial p}{\partial r} \right|_s$$

$$\gamma_e = - \frac{h_e^3}{12\mu GT_s} \frac{\overline{\Delta r}}{r_i} p \left. \frac{\partial p}{\partial \theta} \right|_e + \frac{r_i \omega h_e \overline{\Delta r}}{2 GT_s} \left(\frac{p_L + p_{L+M}}{2} \right)$$

$$\gamma_w = \frac{h_w^3}{12\mu GT_s} \frac{\overline{\Delta r}}{r_i} p \left. \frac{\partial p}{\partial \theta} \right|_w - \frac{r_i \omega h_w \overline{\Delta r}}{2 GT_s} \left(\frac{p_L + p_{L-M}}{2} \right)$$

Parameters are non-dimensionalized as follows:

$$\begin{aligned} R &= r/r_o & \Delta A &= \Delta a/r_o^2 \\ H &= h/C & Q &= p^2 \\ T &= t\omega/2\Lambda & \Lambda &= \frac{6\mu \omega r_o^2}{p_a C^2} \\ P &= p/p_a \end{aligned}$$

By substituting the non-dimensional parameters, Equation [A-2] becomes

$$\begin{aligned} & \left. \frac{H_L}{P_L} \frac{\partial Q}{\partial T} \right|_L + \left. \frac{2Q_L}{P_L} \frac{\partial H}{\partial T} \right|_L + \frac{H_n^3 R_n \overline{\Delta \theta}}{\Delta A} \left. \frac{\partial Q}{\partial R} \right|_n - \frac{H_s^3 R_s \overline{\Delta \theta}}{\Delta A} \left. \frac{\partial Q}{\partial R} \right|_s - \frac{H_e^3 \overline{\Delta R}}{R_i \Delta A} \left. \frac{\partial Q}{\partial \theta} \right|_e \\ & + \frac{H_w^3 \overline{\Delta R}}{R_i \Delta A} \left. \frac{\partial Q}{\partial \theta} \right|_w + \frac{2\Delta R_i \overline{\Delta R}}{\Delta A} \left[\frac{1}{2} \left(\frac{Q_L}{P_L} + \frac{Q_{L+M}}{P_{L+M}} \right) H_e - \frac{1}{2} \left(\frac{Q_L}{P_L} + \frac{Q_{L-M}}{P_{L-M}} \right) H_w \right] = 0 \end{aligned} \quad [A-3]$$

Expanding this equation with two point finite differences for derivatives produces

$$\begin{aligned} & \frac{H_L}{P_L} \frac{Q_L - \tilde{Q}_L}{\Delta T} + \frac{2Q_L}{P_L} \frac{\partial H_L}{\partial T} + H_n^3 R_n \frac{\overline{\Delta \theta}}{\Delta A} \left(\frac{Q_L - Q_{L-1}}{\Delta R_i} \right) - H_s^3 R_s \frac{\overline{\Delta \theta}}{\Delta A} \left(\frac{Q_{L+1} - Q_L}{\Delta R_{i+1}} \right) \\ & + \frac{H_w^3 \overline{\Delta R}}{R_i \Delta A} \left(\frac{Q_L - Q_{L-M}}{\Delta \theta_j} \right) - \frac{H_e^3 \overline{\Delta R}}{R_i \Delta A} \left(\frac{Q_{L+M} - Q_L}{\Delta \theta_{j+1}} \right) + \frac{\Delta R_i \overline{\Delta R}}{\Delta A} \left[\left(\frac{Q_L}{P_L} + \frac{Q_{L+M}}{P_{L+M}} \right) H_e - \left(\frac{Q_L}{P_L} + \frac{Q_{L-M}}{P_{L-M}} \right) H_w \right] = 0 \end{aligned} \quad [A-4]$$

\tilde{Q} is the value of Q at previous time step

P is known from a previous interval

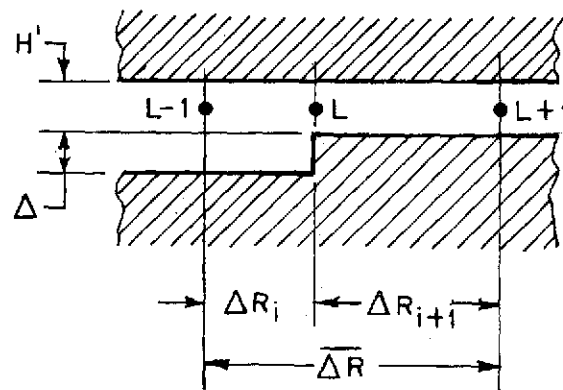
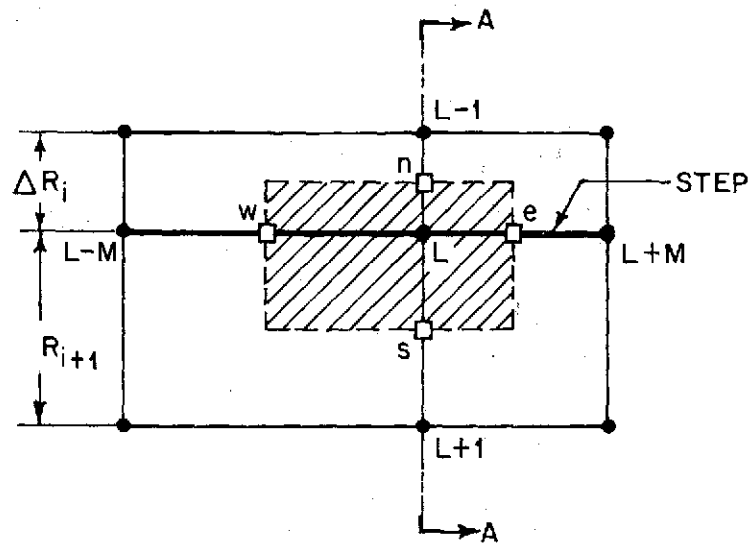
Since \tilde{Q} and P are assumed known, this is a linear equation at any given time step with independent variable Q .

If the L^{th} node occurs at either a circumferential or radial step, a discontinuity in clearance exists. For continuity to apply under these circumstances the following modification must be made to the clearance in Equation [A-4] depending on the location of the step:

- Step parallel to circumferential line for step region on L-1 side (see Figure A-4)

$$H = \frac{\Delta R_i}{\Delta R} \left(H' + \Delta \right) + \frac{\Delta R_{i+1}}{\Delta R} H'$$

$$H^3 = \frac{\Delta R_i}{\Delta R} \left(H' + \Delta \right)^3 + \frac{\Delta R_{i+1}}{\Delta R} H'^3$$



SECTION A-A

Figure A-4. Step Region Parallel to Circumferential Line on L-1 Side

where H' is the clearance calculated before the addition of the step height

For the step region on the $L+1$ side

$$H = \frac{\Delta R_{i+1}}{\Delta R} (H' + \Delta) + \frac{\Delta R_i}{\Delta R} (H')$$

$$H^3 = \frac{\Delta R_{i+1}}{\Delta R} (H' + \Delta)^3 + \frac{\Delta R_i}{\Delta R} (H')^3$$

This applies for H_L , H_e , H_w , H_e^3 , H_w^3 of Equation [A-4]

- Step parallel to a radial line

$$H = \frac{\Delta \theta_j}{\Delta \theta} (H' + \Delta) + \frac{\Delta \theta_{j+1}}{\Delta \theta} H'$$

$$H^3 = \frac{\Delta \theta_j}{\Delta \theta} (H' + \Delta)^3 + \frac{\Delta \theta_{j+1}}{\Delta \theta} H'^3$$

This applies for H_L , H_n^3 , H_s^3 of Equation [4]

- Corner nodes of pocket pad

Appropriate modifications are made to H_e , H_w , H_e^3 , H_w^3 , H_n^3 , H_s^3 but no change is made to H_L of Equation [A-4]

If the L^{th} grid point occurs at a joined boundary (this occurs in the 360° sealing dam for $J=1$, $I=2$ to $M-1$ and $J=N$, $I=2$ to $M-1$ nodes) the following modifications must be made to Equation [A-4]. Examine the node layout in Figure A-5

- $J=1$, $I=2$ to $M-1$ nodes

$$Q_{L-M} = Q_{I+(N-1)M}$$

$$P_{L-M} = P_{I+(N-1)M}$$

- $J=N$, $I=2$ to $M-1$ nodes

$$Q_{L+M} = Q_I$$

$$P_{L+M} = P_I$$

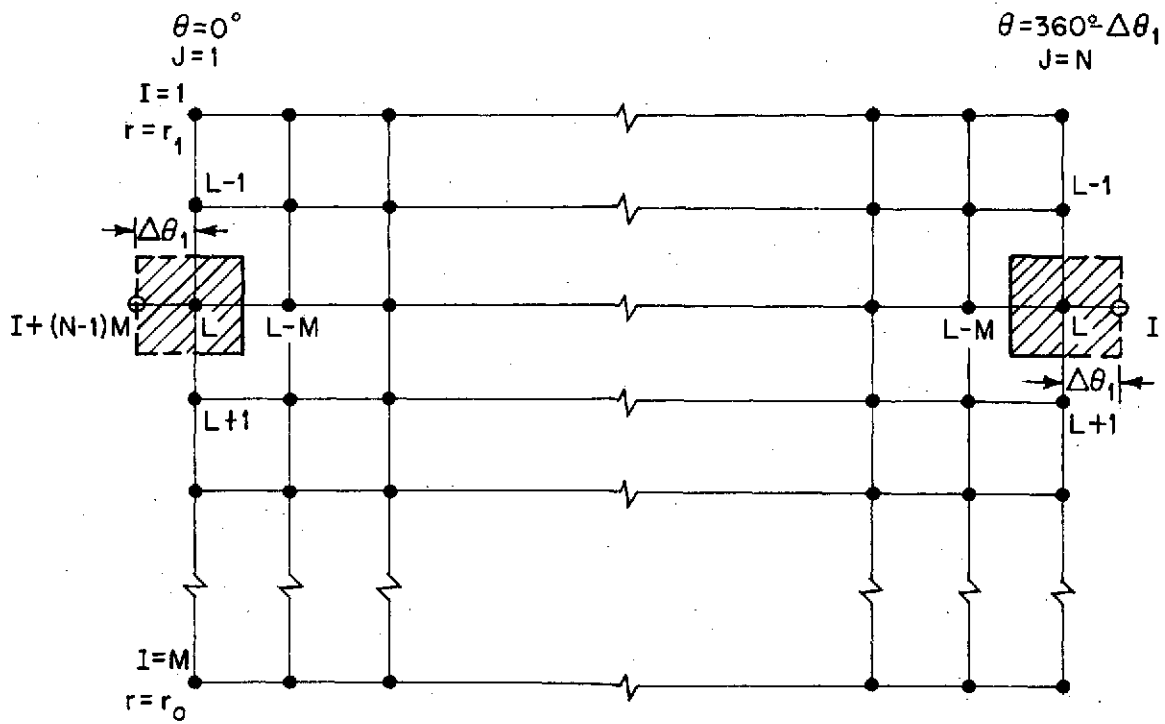


Figure A-5. Sealing Dam Boundary Nodes

Clearance Distribution

Using the coordinate system specified in Figure 2 the clearance distribution becomes:

$$h_L = C - zs_t + (\alpha s_{x_t} - \alpha r_{x_t}) r_i \sin \theta_j + (\alpha s_{y_t} - \alpha r_{y_t}) r_i \cos \theta_j \quad [A-5]$$

(time dependent terms have subscript t)

In the pocket region of a pad

$$h_L = h'_L + \delta$$

where

$$h'_L = \text{clearance based on Equation [A-5]}$$

Note that the clearance is a function of both spatial coordinates and time. The rate of change of clearance with respect to time is

$$\frac{\partial h_L}{\partial t} = - \frac{dzs}{dt} + \left(\frac{d\alpha s_{x_t}}{dt} - \frac{d\alpha r_{x_t}}{dt} \right) r_i \sin \theta_j + \left(\frac{d\alpha s_{y_t}}{dt} - \frac{d\alpha r_{y_t}}{dt} \right) r_i \cos \theta_j \quad [A-6]$$

For dynamic problems zs , αs_x , αs_y , $\frac{dzs}{dt}$, $\frac{d\alpha s_x}{dt}$, $\frac{d\alpha s_y}{dt}$ are determined from the equations of motion while αr_x , αr_y ,

$\frac{\partial \alpha r_x}{\partial t}$, $\frac{\partial \alpha r_y}{\partial t}$ are known quantities calculated from the swashing (nutation) of the runner

Pressure Solution Method

Equation [A-4] was solved by the alternating direction implicit (ADI) method (references 4 and 5).

The general finite-difference Equation [A-4] can be put into the form:

$$(A_{P_L} + A_{EW_L} + A_{NS_L}) Q_L + E_L Q_{L+M} + W_L Q_{L-M} + N_L Q_{L-1} + S_L Q_{L+1} = G_L \quad [A-7]$$

where

$$A_L = A_{P_L} + A_{EW_L} + A_{NS_L}$$

$$A_{P_L} = - \frac{H_L}{\Delta T P_L} - \frac{2}{P_L} \frac{\partial H_L}{\partial T}$$

$$A_{EW_L} = - \frac{H_e^3}{R_L \Delta \theta_{J+1}} \frac{\overline{\Delta R}}{\Delta A} - \frac{H_w^3}{R_i \Delta \theta_J} \frac{\overline{\Delta R}}{\Delta A} - \frac{\Lambda R_i \overline{\Delta R}}{P_L \Delta A} (H_e - H_w)$$

$$A_{NS_L} = - \frac{H_n^3 R_n \overline{\Delta \theta}}{\Delta R_i \Delta A} - \frac{H_s^3 R_s \overline{\Delta \theta}}{\Delta R_{i+1} \Delta A}$$

$$N_L = \frac{H_n^3 R_n \overline{\Delta \theta}}{\Delta A \Delta R_i}$$

$$S_L = \frac{H_s^3 R_s \overline{\Delta \theta}}{\Delta A \Delta R_{i+1}}$$

$$E_L = \frac{H_e^3 \overline{\Delta R}}{R_i \Delta A \Delta \theta_{J+1}} - \frac{\Lambda R_i \overline{\Delta R} H_e}{\Delta A P_e}$$

$$W_L = \frac{H_w^3 \overline{\Delta R}}{R_i \Delta A \Delta \theta_J} + \frac{\Lambda R_i \overline{\Delta R} H_w}{\Delta A P_w}$$

$$G_L = - \frac{H_L \tilde{Q}_L}{\Delta T P_L}$$

At any time step an equation like [A-7] can be written for each node in a given seal pad. If a node should fall on a boundary or region where the pressure is known then the coefficients of [A-7] become:

$$A_L = 1$$

$$N_L = S_L = W_L = E_L = 0$$

$$G_L = Q_{SP} \text{ where } Q_{SP} \text{ is the known value.}$$

The result is a system of linear equations with constant coefficients which can be represented in matrix form.

$$[COEF] \{Q\} = \{G\}$$

[A-8]

Figure A-6 illustrates the terms of this matrix equation.

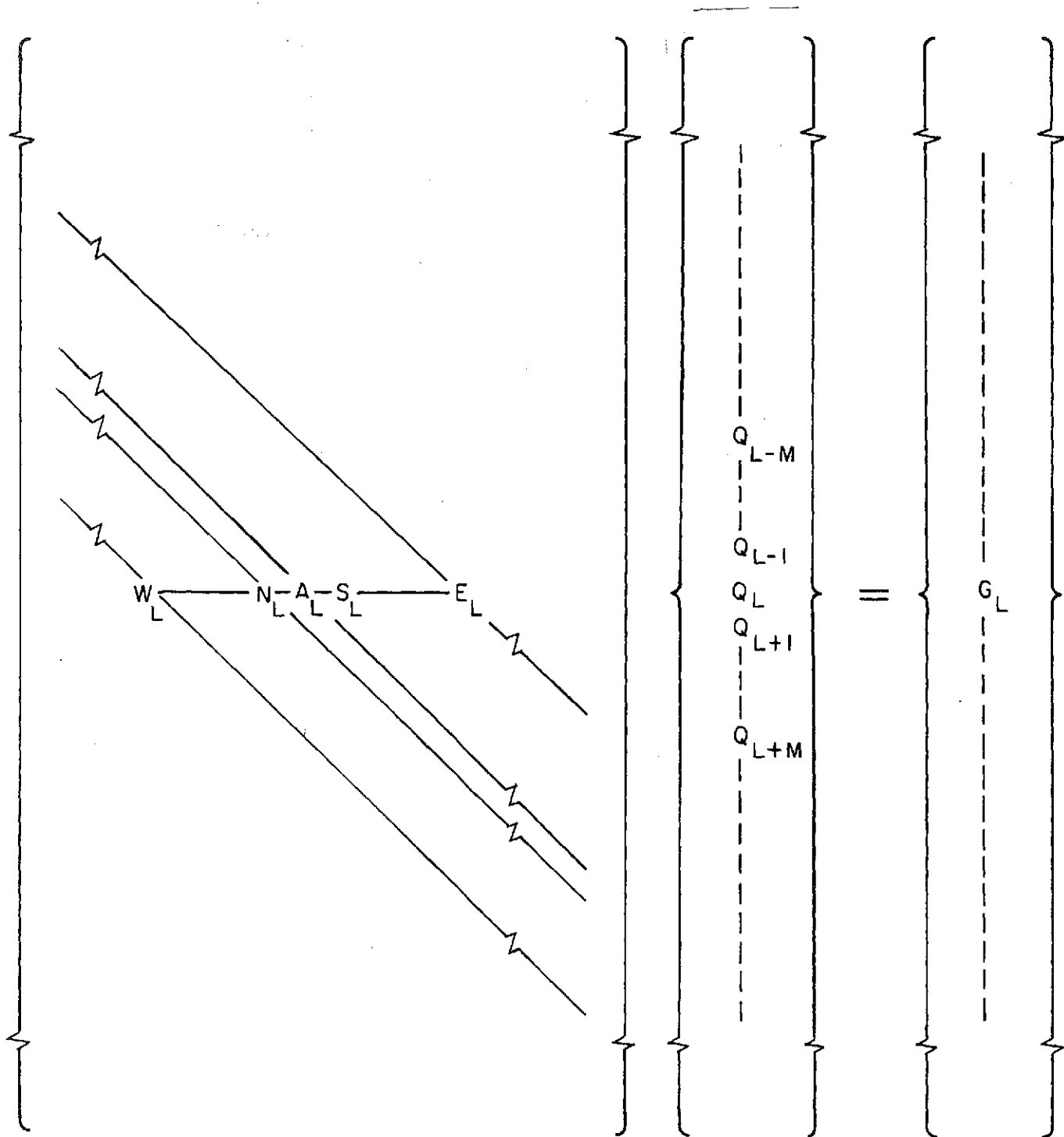


Figure A-6. Pressure Matrix Equation

- During the first half of a time cycle Equation [A-7] becomes

which produces for the system the tri-diagonal matrix equation of the form

- During the second half of the cycle

$$\left[\begin{array}{c} \vdots \\ N_L \\ \vdots \end{array} \right] \left[\begin{array}{c} \vdots \\ A'_L \\ \vdots \end{array} \right] \left[\begin{array}{c} \vdots \\ S_L \\ \vdots \end{array} \right] = \left[\begin{array}{c} Q_{L-1} \\ Q_L \\ Q_{L+1} \end{array} \right] \left[\begin{array}{c} \vdots \\ \text{RHS}_L \\ \vdots \end{array} \right] \quad [\text{A-12}]$$

The pressure solution procedure for this method is shown in the flow chart, Figure A-7.

STEADY STATE PERFORMANCE

Once the pressure profile is known, seal steady-state performance can be calculated by solving the following equations:

$$\bullet F_a = \int_{r_1}^{r_o} \int_0^\theta (p_L - p') r dr d\theta$$

$$\bullet T_{a_x}^* = \int_{r_1}^{r_o} \int_0^\theta (p_L - p') \sin(\theta) r^2 dr d\theta$$

$$\bullet T_{a_y}^* = \int_{r_1}^{r_o} \int_0^\theta (p_L - p') \cos(\theta) r^2 dr d\theta$$

$$\bullet M_{fr} = \int_{r_1}^{r_o} \int_0^\theta \frac{h_L}{2} \frac{\partial p_L}{\partial \theta} r dr d\theta + \mu \omega \int_{r_1}^{r_o} \int_0^\theta \frac{r^3}{h_L} dr d\theta$$

$$\bullet P_f = M_{fr} \frac{\omega}{6600}$$

where

$p' = p_s$ for step pads

$p' = p_a$ for sealing dam

*The coordinate system is shown in Figure 2.

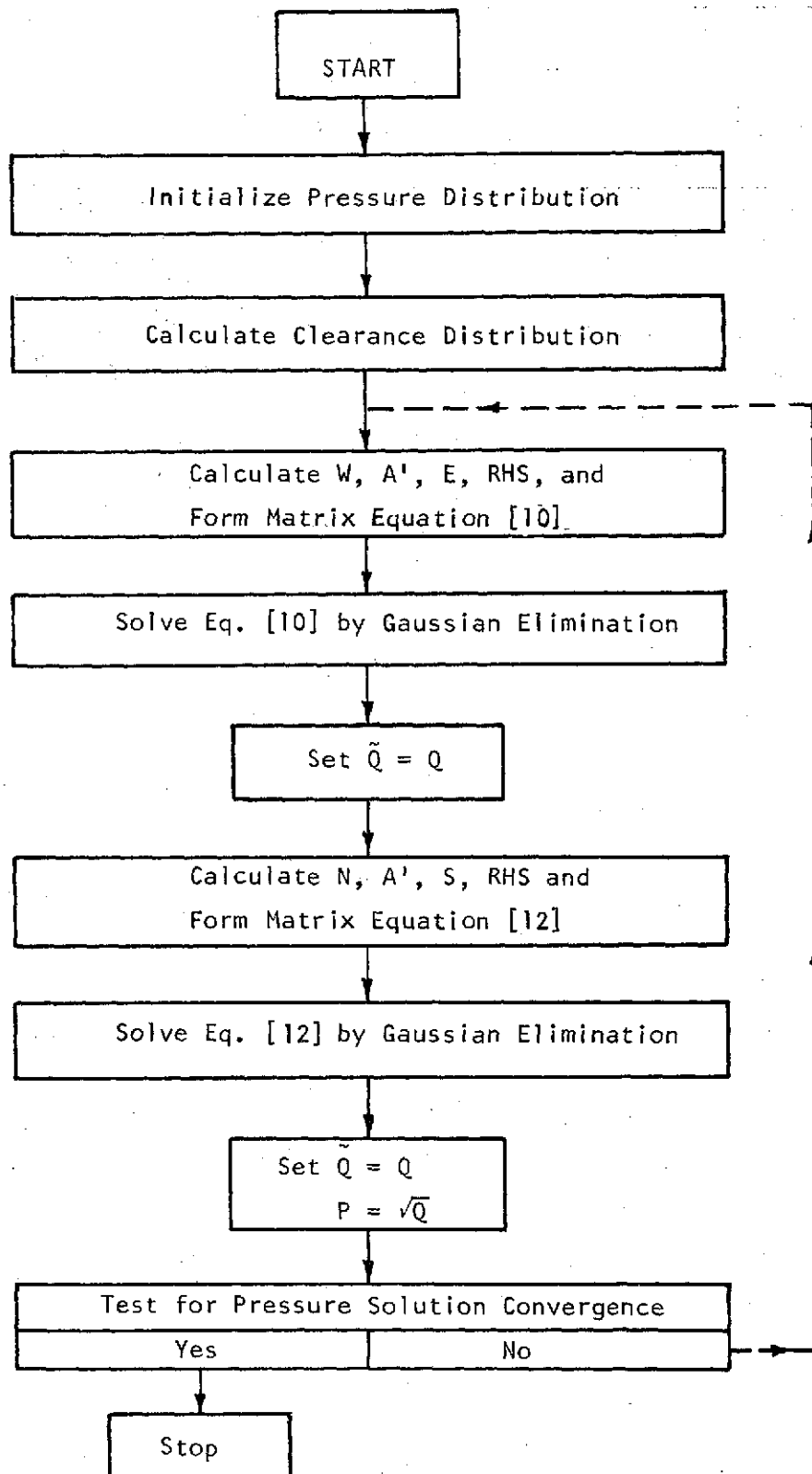


Figure A-7. Pressure Solution Flow Chart Using the ADI Method

The above equations are applied to each shrouded step pad and sealing ridge. Self acting load and moment capacity is obtained by summing up the individual results for each pad, while power loss is determined by adding up results for each pad and sealing ridge. Seal leakage is computed by

$$F_L = \frac{1}{24 GT_s} \int_0^{360} h_L^3 \frac{\partial p_L^2}{\partial r} \Big|_{r=r} r d\theta$$

r = outside radius of
sealing ridge

$$F_{SCFM} = 781.3 F_L$$

The above integrations are performed by numerical methods.

Dynamic Equations

The equations of motion for translation and rotation are as follows.

$$m_s \ddot{z}_{s_t} = F_a^* - F_{a_{eq}}^* + F_f$$

• Rotation

$$I_x \ddot{\alpha}_{s_x} = T_{a_x}^* + T_f$$

$$I_y \ddot{\alpha}_{s_y} = T_{a_y}^* + T_f$$

Treatment of Coulomb Friction

Coulomb frictional resistance was accounted for all degrees of freedom (axial and angular modes). A single subroutine was used with appropriate changes made to the dummy variables for each degree of freedom (reference 6).

The treatment is described for the angular modes, but if angular motions and torques are replaced by axial motions and forces, then the theory is equally applicable to the axial modes.

*These forces and moments are due to the hydrodynamic effect of the lift pad only. Change in force and moment due to the hydrodynamic effect on the sealing ridge are negligible.

The Coulomb friction is represented by a constant resisting torque applied by the secondary seal to the seal ring. The friction torque is a function of sealed pressure and coefficient of friction.

Consider a velocity vs. time plot as shown in Figure A-8.

There are three regions of accountability.

1. When accelerating, T_f and T_a are opposite and $|T_f| < |T_a|$.
2. When decelerating, T_f and T_a are of same sign and a finite velocity implies $|T_f| < |T_a|$.
3. If the velocity changes sign between successive time steps, then somewhere between motion has stopped and cannot start until $|T_a| < |T_f|$. Thus, there is a discontinuity in the velocity curve. If we followed the normal procedure without taking account of the finite stopping time, the velocity would be repositioned to B in Figure A-8 instead of point A. To get point A we proceed as follows:

From similar triangles

$$\frac{dt_1}{dt} = \frac{\dot{\alpha}}{\ddot{\alpha}' dt}$$

$$dt_2 = dt - dt_1 = dt \left[1 - \frac{\dot{\alpha}}{\ddot{\alpha}' dt} \right]$$

Since we are now operating on the negative side of the velocity the friction torque opposes the applied torque. If $|T_a| < |T_f|$ then

$$\ddot{\alpha}(t) = (-T_f + T_a)/I$$

and

$$\dot{\alpha}(t) = \ddot{\alpha}(t) dt \left[1 - \frac{\dot{\alpha}}{\ddot{\alpha} dt} \right]$$

and

$$\alpha(t) = \alpha(t-dt) + \left[1 - \frac{\dot{\alpha}}{\ddot{\alpha} dt} \right] \dot{\alpha} dt$$

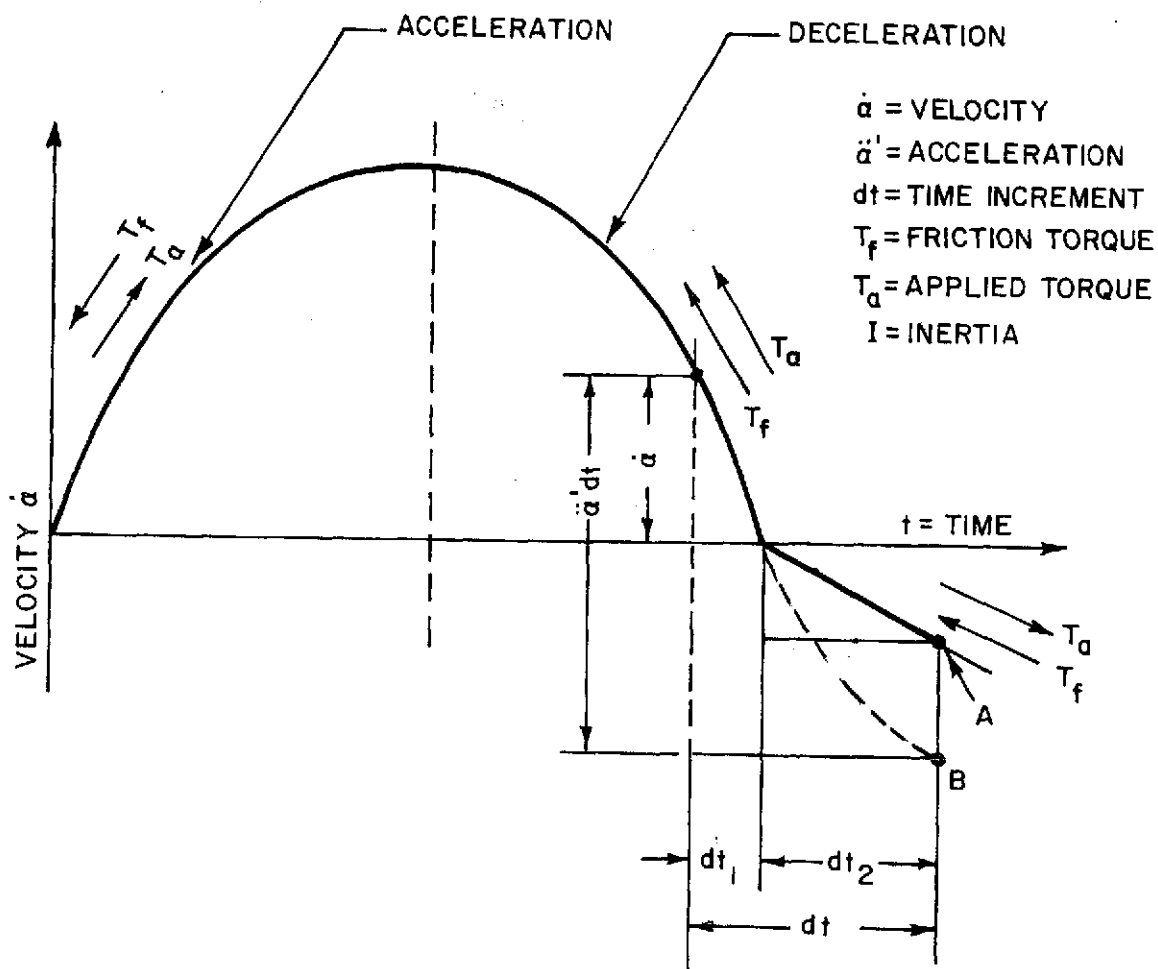


Figure A-8. Velocity vs. Time

If $|T_a| < |T_f|$ then

$$\ddot{\alpha}(t) = \dot{\alpha}(t) = 0$$

A simplified flow chart of the friction routine is shown on Figure A-9.

Dynamic Solution Method

The direct integration approach determines seal motions by simultaneously solving the equations of motions and the lubrication equation (reference 7). This method is straight-forward and easy to implement. It consists of the following steps:

1. Compute a pressure profile using the ADI method described for the equilibrium position and initialize velocities and accelerations.
2. Calculate the self-acting force and moments from the fluid film pressure profile.
3. Calculate seal motions and velocities from the dynamics equation in the following manner:

$$\frac{d^2 z_{s_t}}{dt^2} = \frac{1}{m_s} (\Sigma \text{ forces})$$

$$\frac{dz_{s_t}}{dt_{\text{new}}} = \frac{dz_{s_t}}{dt_{\text{old}}} + \frac{d^2 z_{s_t}}{dt^2} dt$$

$$z_{s_{t_{\text{new}}}} = z_{s_{t_{\text{old}}}} + \frac{dz_{s_t}}{dt} dt$$

where "new" refers to the present time and "old" refers to the time at the previous time step ($t_{\text{old}} = t_{\text{new}} - dt$) and dt is the time step increment. The same approach is used to determine the angular modes of the seal.

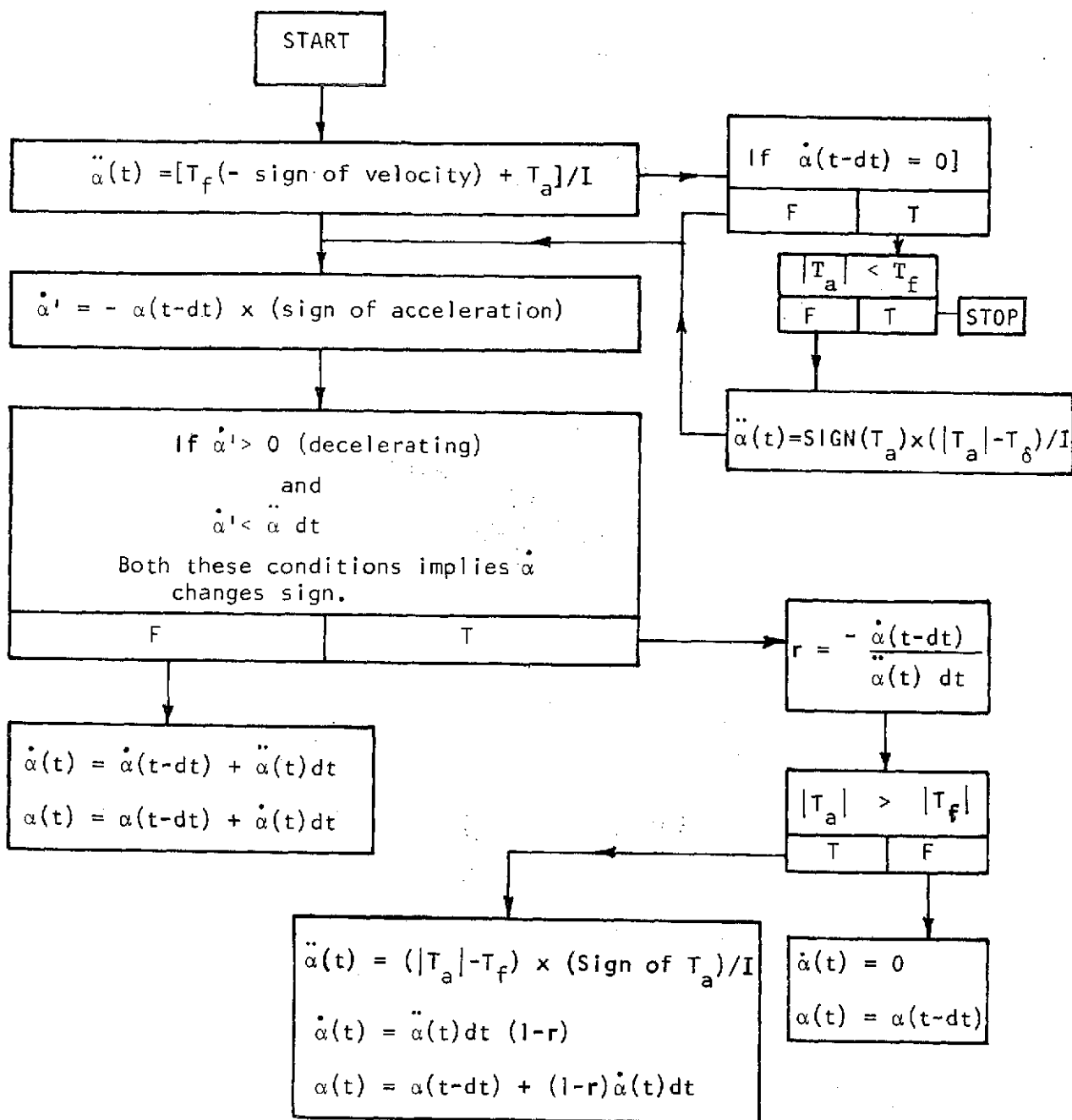
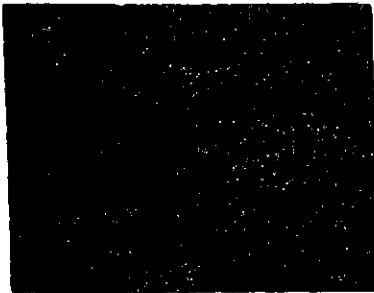


Figure A-9. Piston Ring Friction Flow Chart

4. Calculate a new clearance distribution and its time derivative from step 3 above and the nutation of runner (Equations A-5).
5. Compute a new pressure profile* based on new clearance distribution.

Repeat steps (2) through (5) for the desired number of time steps.
Save and plot the seal motions as a function of time.

*Note that the time step size dt is assumed small enough so that pressure iteration for each dynamic time step is not required.



F-C3452-1

Appendix

B

DYNAMIC RESPONSE RESULTS, CASES 1, 2, 3 AND 4



THE FRANKLIN INSTITUTE RESEARCH LABORATORIES
THE BENJAMIN FRANKLIN PARKWAY • PHILADELPHIA PENNSYLVANIA 19103

CASE 1a

Pressure = 300 psig (2068.5 kN/m²) Runout = 0.001 in. (25.4 μm)
Temperature = 1000°F (537.78°C) Friction = 0.0 lbs (0.0 N), 0.0 in.-lb (0.0 Nm)
Speed = 500 ft/sec (152.4 m/sec) Initial Clearance = 0.00032 in. (8.128 μm)
Nosepiece Wt. = 1.75 lbs (7.784 N)

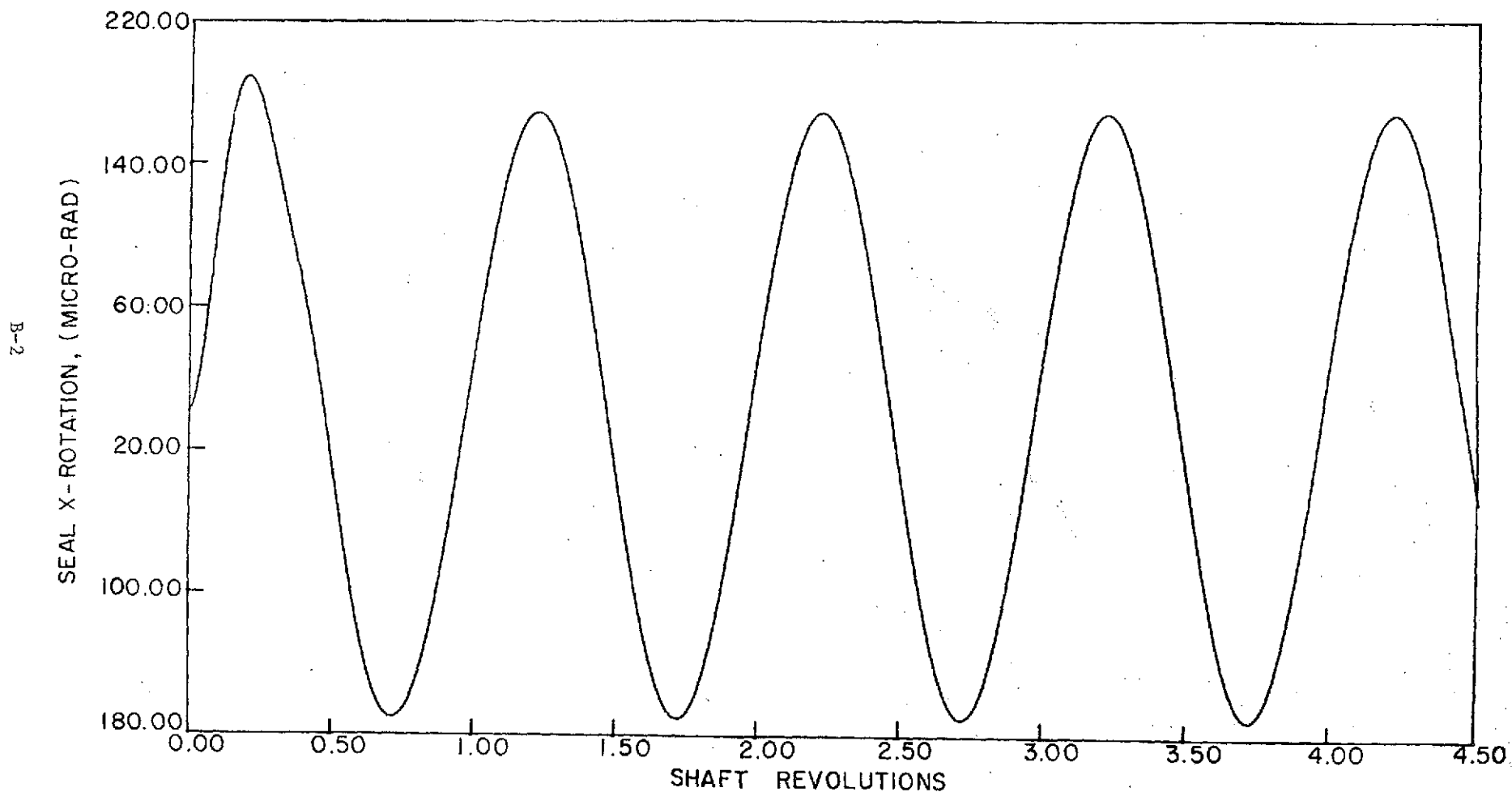


Figure B-1
Rotation About X-Axis vs. Shaft Revolutions, Case 1A

Pressure = 300 psig (2068.5 kN/m²) Runout = 0.001 in. (25.4 μ m)
Temperature = 1000°F (537.78°C) Friction = 0.0 lbs (0.0 N), 0.0 in.-lb (0.0 Nm)
Speed = 500 ft/sec (152.4 m/sec) Initial Clearance = 0.00032 in. (8.128 μ m)
Nosepiece Wt. = 1.75 lbs (7.784 N)

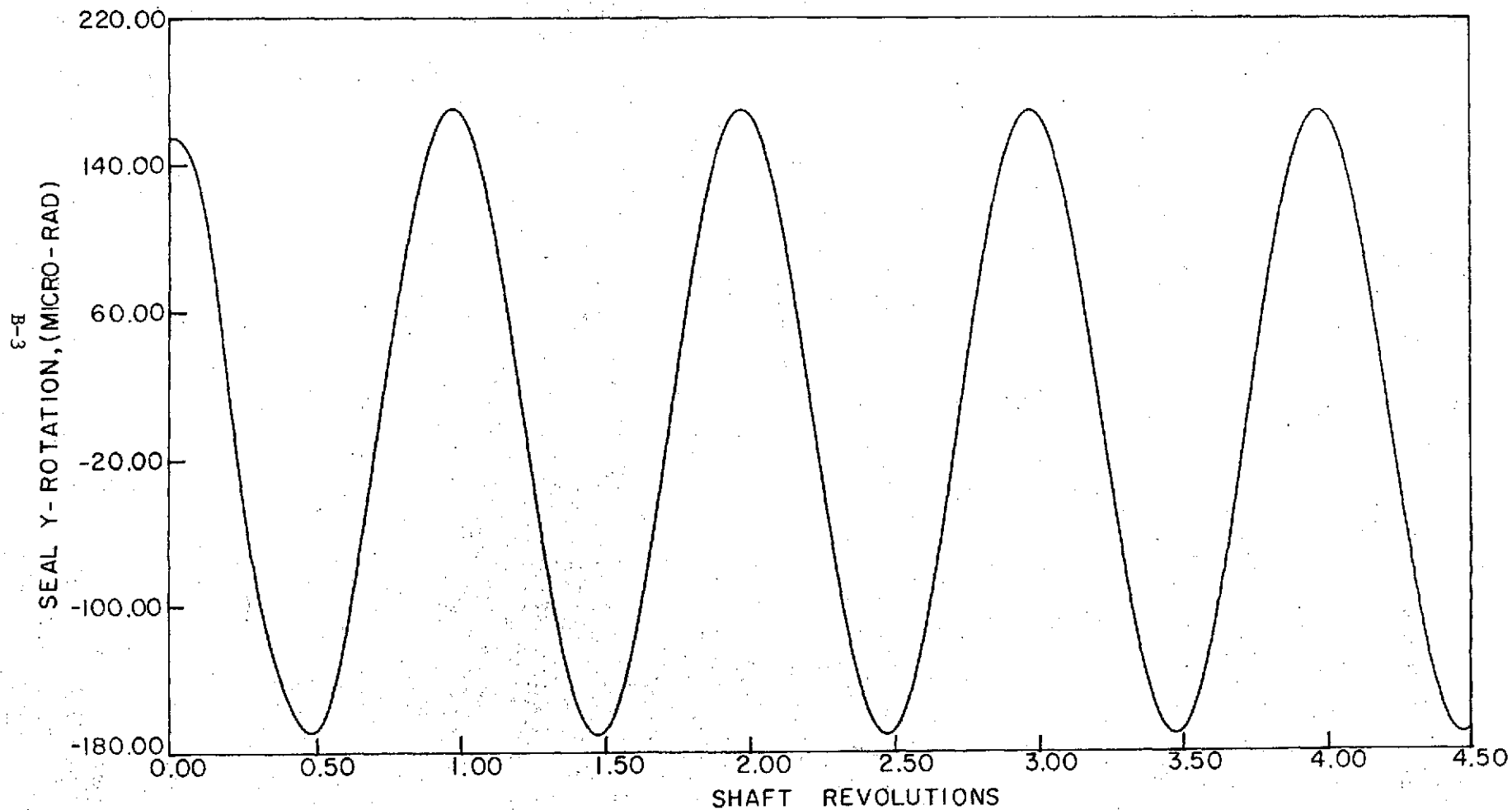


Figure B-2

Rotation About Y-Axis vs. Shaft Revolutions, Case 1A

Pressure = 300 psig (2068.5 kN/m²)
Temperature = 1000°F (537.78°C)
Speed = 500 ft/sec (152.4 m/sec)
Nosepiece Wt. = 1.75 lbs (7.784 N)

Runout = 0.001 in. (25.4 μm)
Friction = 0.0 lbs (0.0 N), 0.0 in.-lb (0.0 Nm)
Initial Clearance = 0.00032 in. (8.128 μm)

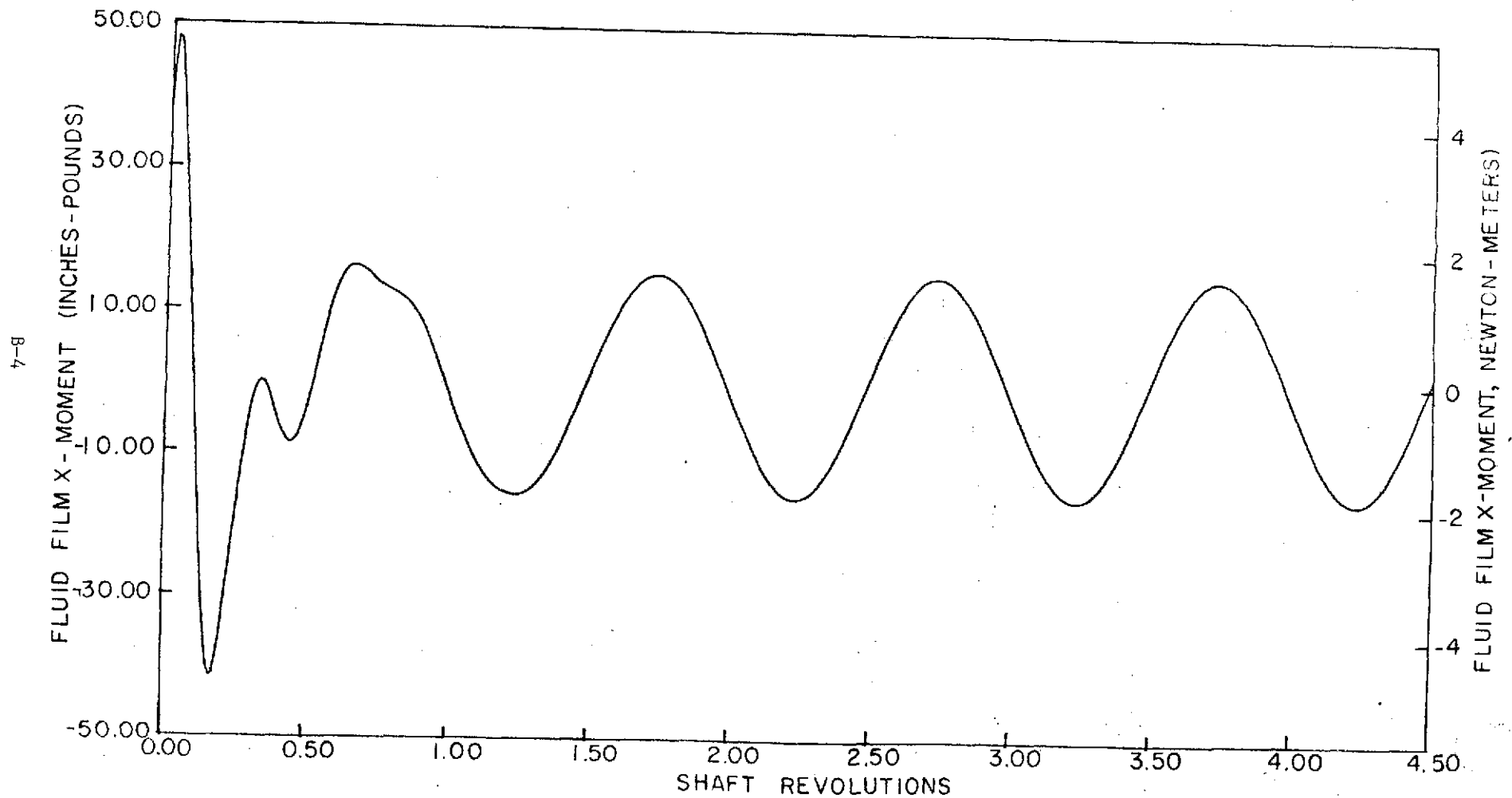


Figure B-3
Fluid-Film Moment About X-Axis vs. Shaft Revolutions, Case 1A

Pressure = 300 psig (2068.5 kN/m²) Runout = 0.001 in. (25.4 μm)
Temperature = 1000°F (537.78°C) Friction = 0.0 lbs (0.0 N), 0.0 in.-lb (0.0 Nm)
Speed = 500 ft/sec (152.4 m/sec) Initial Clearance = 0.00032 in. (8.128 μm)
Nosepiece Wt. = 1.75 lbs (7.784 N)

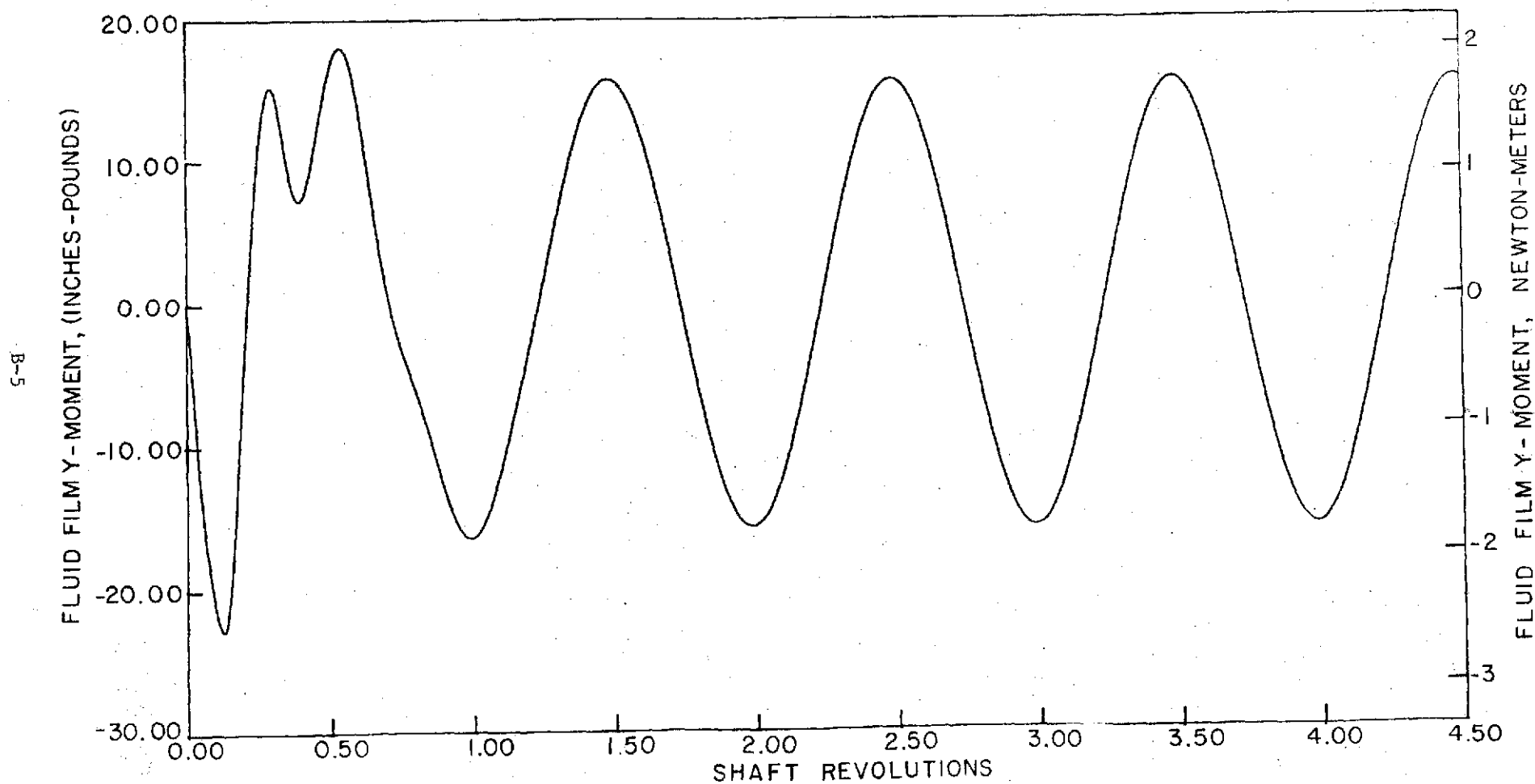


Figure B-4
Fluid-Film Moment About Y-Axis vs. Shaft Revolutions, Case 1A

CASE 1b

Pressure = 300 psig (2068.5 kN/m²)

Runout = 0.001 in. (25.4 μ m)

Temperature = 1000°F (537.78°C)

Friction = 6.0 lbs (26.688 N), 13.0 in.-lbs (1.4687 Nm)

Speed = 500 ft/sec (152.4 m/sec)

Initial Clearance = 0.00032 in. (8.128 μ m)

Nosepiece Wt. = 1.75 lbs (7.784 N)

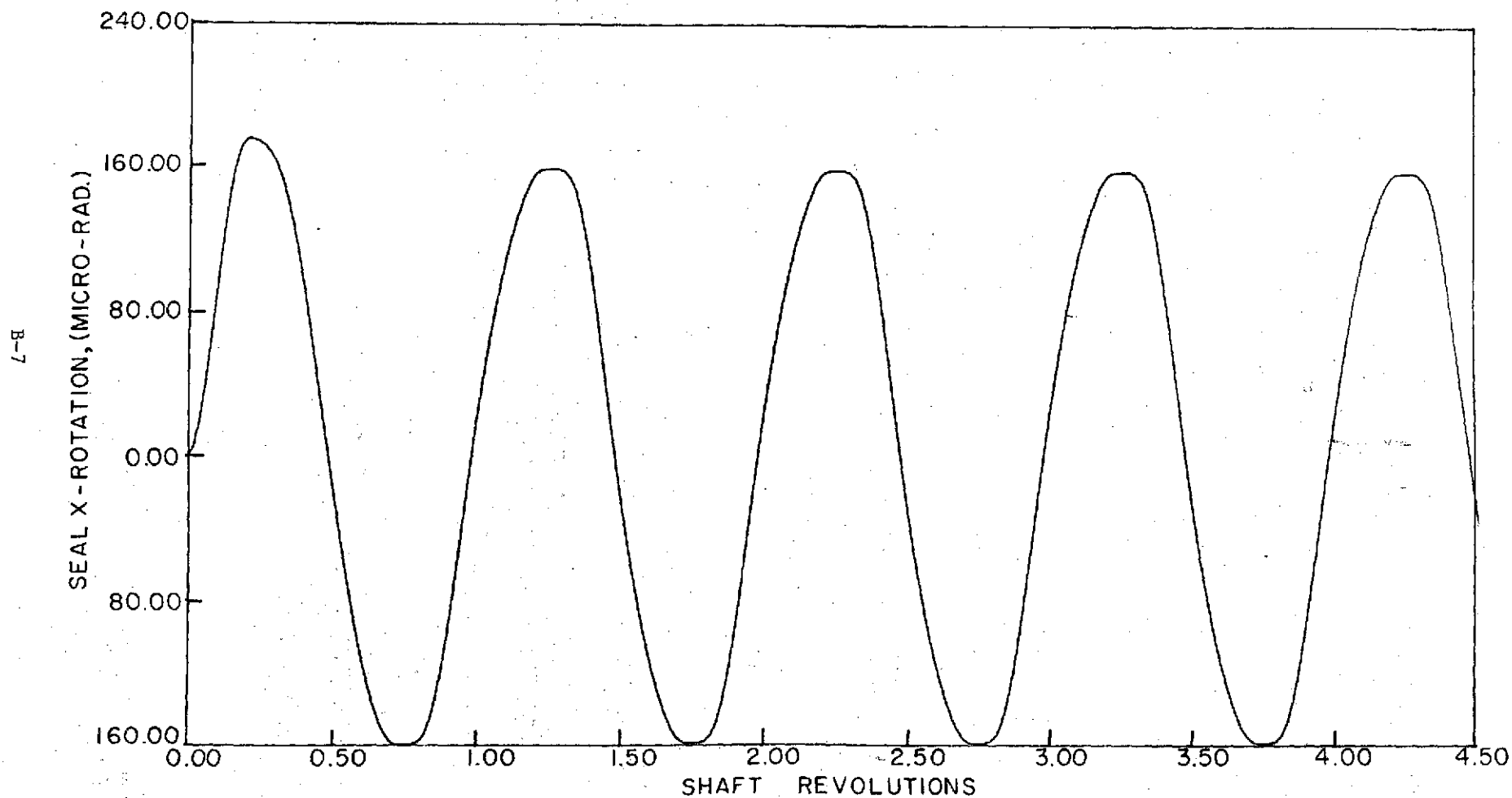


Figure B-5

Rotation About X-Axis vs. Shaft Revolutions, Case 1B

Pressure = 300 psig (2068.5 kN/m²)

Runout = 0.001 in. (25.4 μ m)

Temperature = 1000°F (537.78°C)

Friction = 6.0 lbs (26.688 N), 13.0 in.-lbs (1.4687 Nm)

Speed = 500 ft/sec (152.4 m/sec)

Initial Clearance = 0.00032 in. (8.128 μ m)

Nosepiece Wt. = 1.75 lbs (7.784 N)

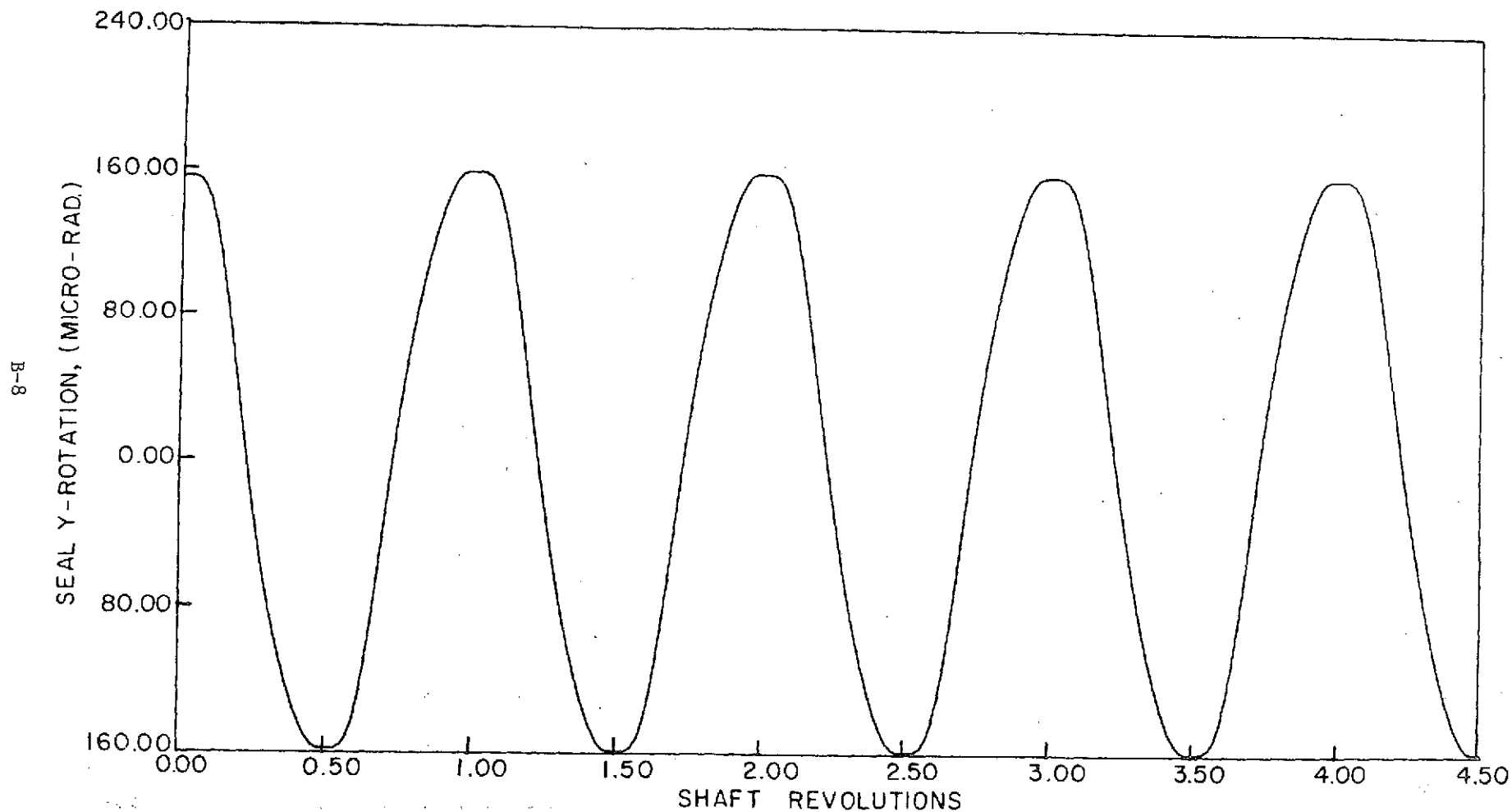


Figure B-6

Rotation About Y-Axis vs. Shaft Revolutions, Case 1B

Pressure = 300 psig (2068.5 kN/m²)

Runout = 0.001 in. (25.4 μ m)

Temperature = 1000°F (537.78°C)

Friction = 6.0 lbs (26.688 N), 13.0 in.-lbs (1.4687 Nm)

Speed = 500 ft/sec (152.4 m/sec)

Initial Clearance = 0.00032 in. (8.128 μ m)

Nosepiece Wt. = 1.75 lbs (7.784 N)

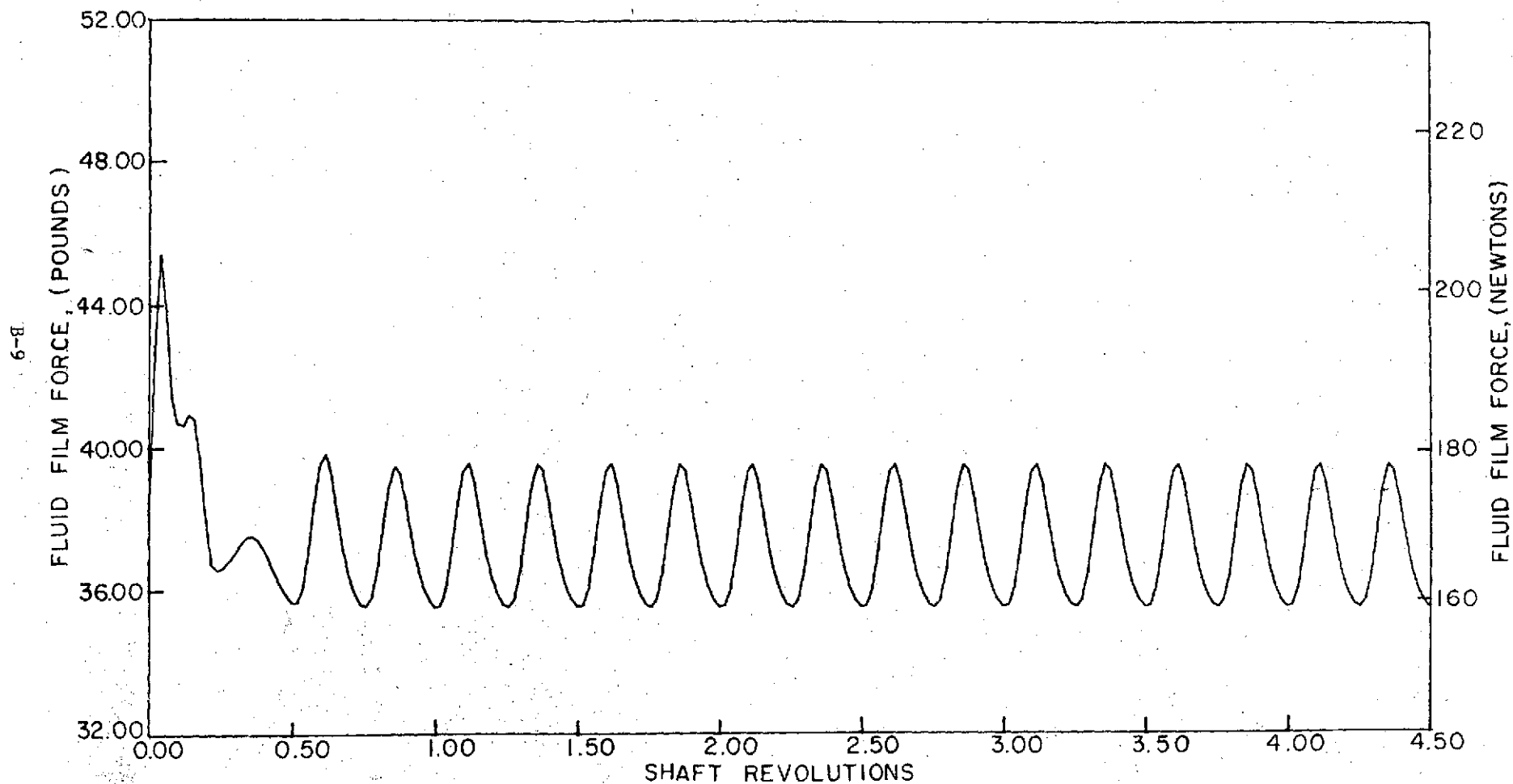


Figure B-7

Fluid-Film Force vs. Shaft Revolutions, Case 1B

Pressure = 300 psig (2068.5 kN/m²)

Runout = 0.001 in. (25.4 μ m)

Temperature = 1000°F (537.78°C)

Friction = 6.0 lbs (26.688 N), 13.0 in.-lbs (1.4687 Nm)

Speed = 500 ft/sec (152.4 m/sec)

Initial Clearance = 0.00032 in. (8.128 μ m)

Nosepiece Wt. = 1.75 lbs (7.784 N)

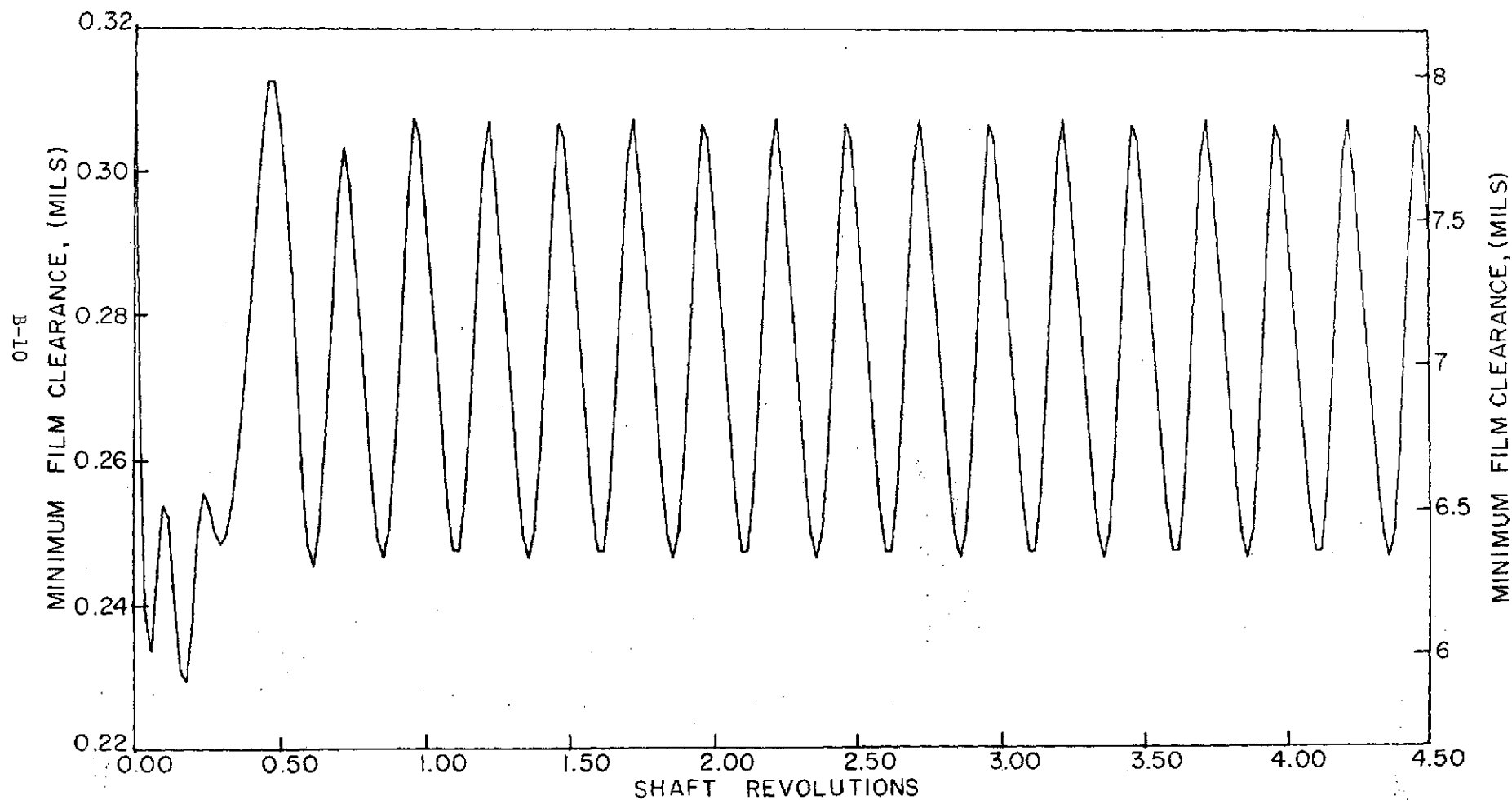


Figure B-8

Minimum Clearance vs. Shaft Revolutions, Case 1B

Pressure = 300 psig (2068.5 kN/m²)

Runout = 0.001 in. (25.4 μ m)

Temperature = 1000°F (537.78°C)

Friction = 6.0 lbs (26.688 N), 13.0 in.-lbs (1.4687 Nm)

Speed = 500 ft/sec (152.4 m/sec)

Initial Clearance = 0.00032 in. (8.128 μ m)

Nosepiece Wt. = 1.75 lbs (7.784 N)

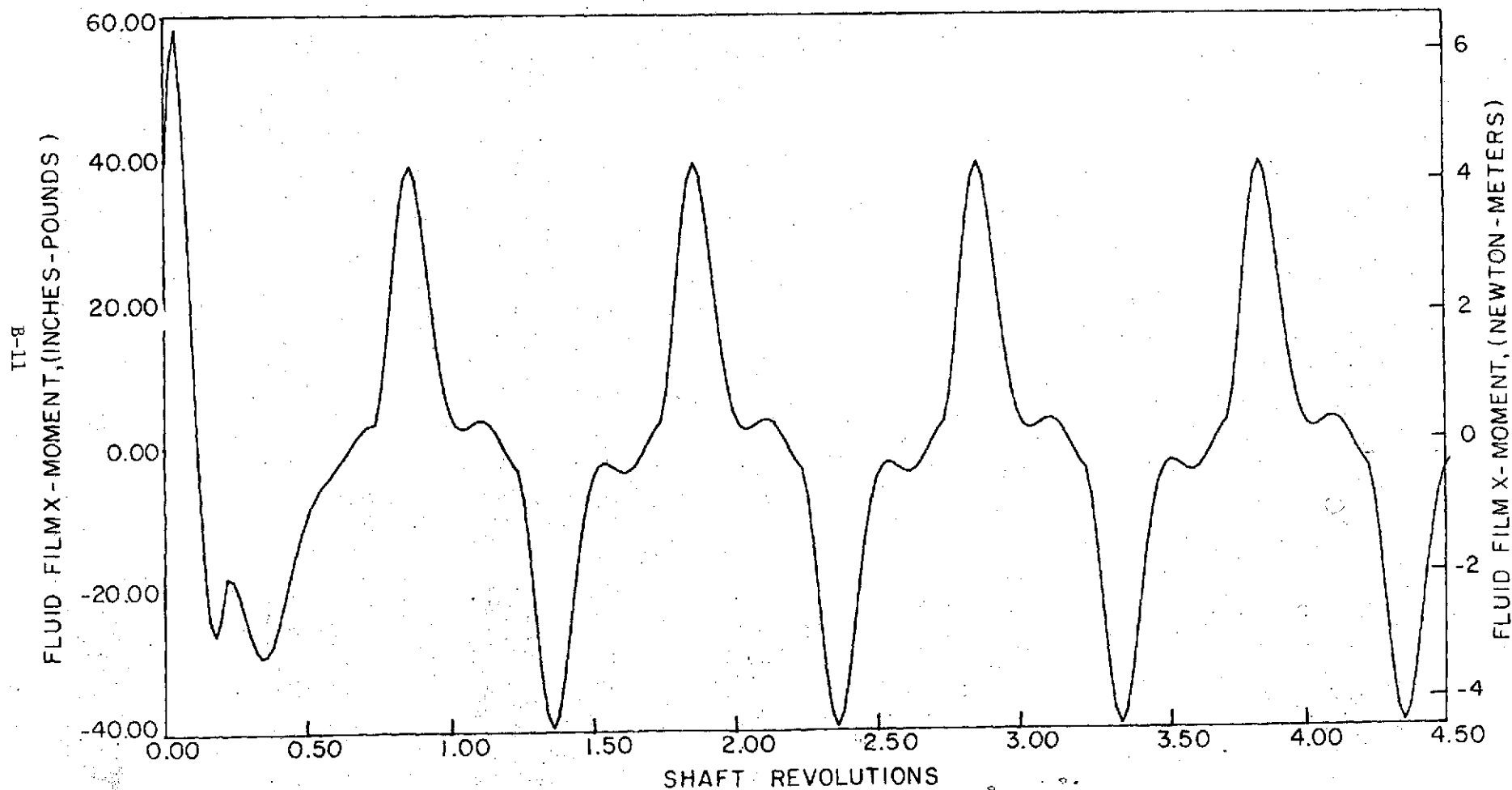


Figure B-9

Fluid-Film Moment About X-Axis vs. Shaft Revolutions, Case 1B

Pressure = 300 psig (2068.5 kN/m²)

Runout = 0.001 in. (25.4 μ m)

Temperature = 1000°F (537.78°C)

Friction = 6.0 lbs (26.688 N), 13.0 in.-lbs (1.4687 Nm)

Speed = 500 ft/sec (152.4 m/sec)

Initial Clearance = 0.00032 in. (8.128 μ m)

Nosepiece Wt. = 1.75 lbs (7.784 N)

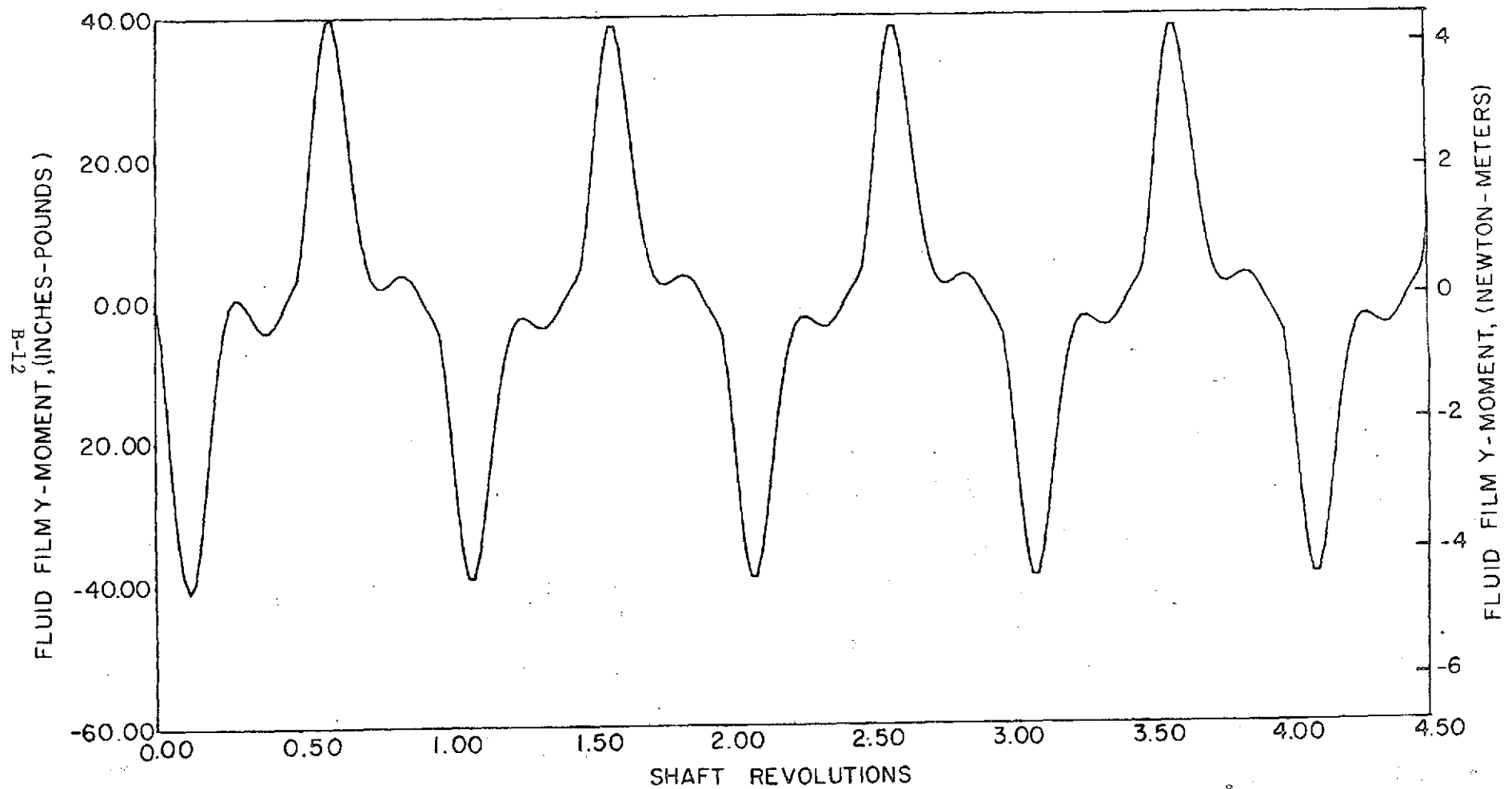


Figure B-10

Fluid-Film Moment About Y-Axis vs. Shaft Revolutions, Case 1B

Run 1c, Case 1

Pressure = 300 psig (2068.5 kN/m²)

Runout = 0.001 in. (25.4 μ m)

Temperature = 1000°F (537.78°C)

Friction = 14.0 lbs (62.272 N), 29.0 in.-lbs (3.276 Nm)

Speed = 500 ft/sec (152.4 m/sec)

Initial Clearance = 0.00032 in. (8.128 μ m)

Nosepiece Wt. = 1.75 lbs (7.784 N)

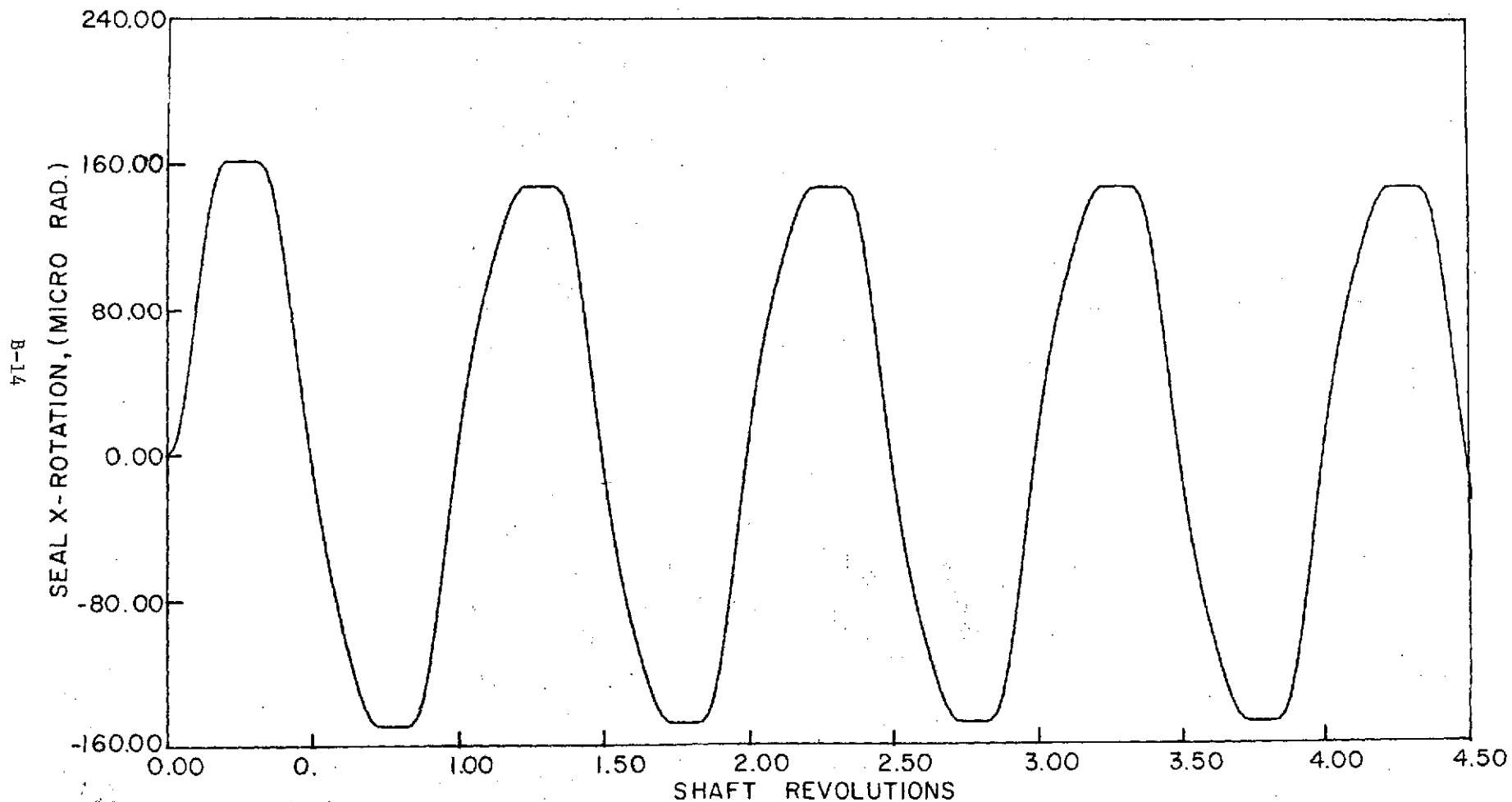


Figure B-11

Rotation About X-Axis vs. Shaft Revolutions, Run 1C, Case 1

Pressure = 300 psig (2068.5 kN/m²) Runout = 0.001 in. (25.4 μ m)
Temperature = 1000°F (537.78°C) Friction = 14.0 lbs (62.272 N), 29.0 in.-lbs (3.276 Nm)
Speed = 500 ft/sec (152.4 m/sec) Initial Clearance = 0.00032 in. (8.128 μ m)
Nosepiece Wt. = 1.75 lbs (7.784 N)

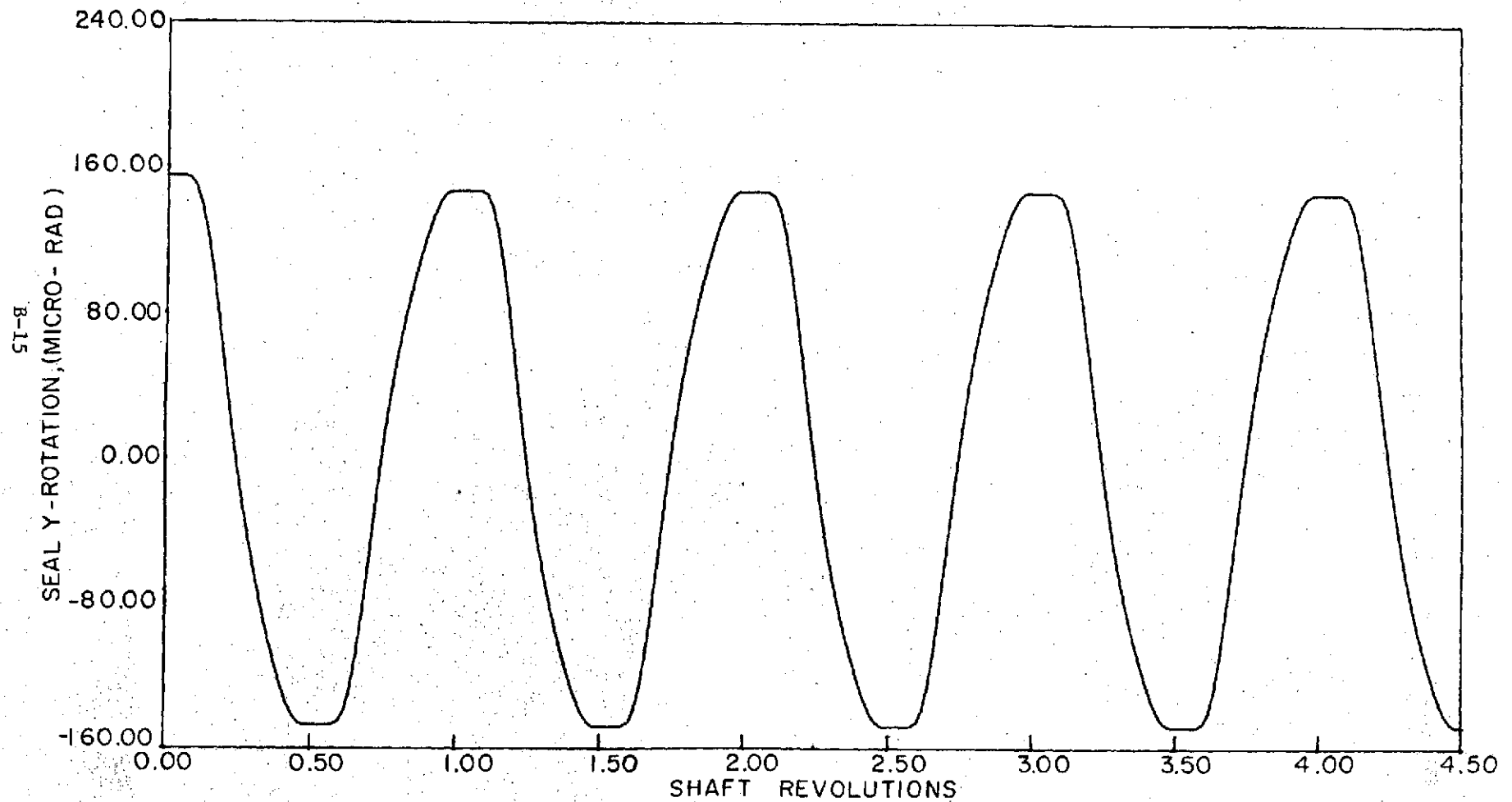


Figure B-12

Rotation About Y-Axis vs. Shaft Revolutions, Run 1C, Case 1

Pressure = 300 psig (2068.5 kN/m²)

Runout = 0.001 in. (25.4 μ m)

Temperature = 1000°F (537.78°C)

Friction = 14.0 lbs (62.272 N), 29.0 in.-lbs (3.276 Nm)

Speed = 500 ft/sec (152.4 m/sec)

Initial Clearance = 0.00032 in. (8.128 μ m)

Nosepiece Wt. = 1.75 lbs (7.784 N)

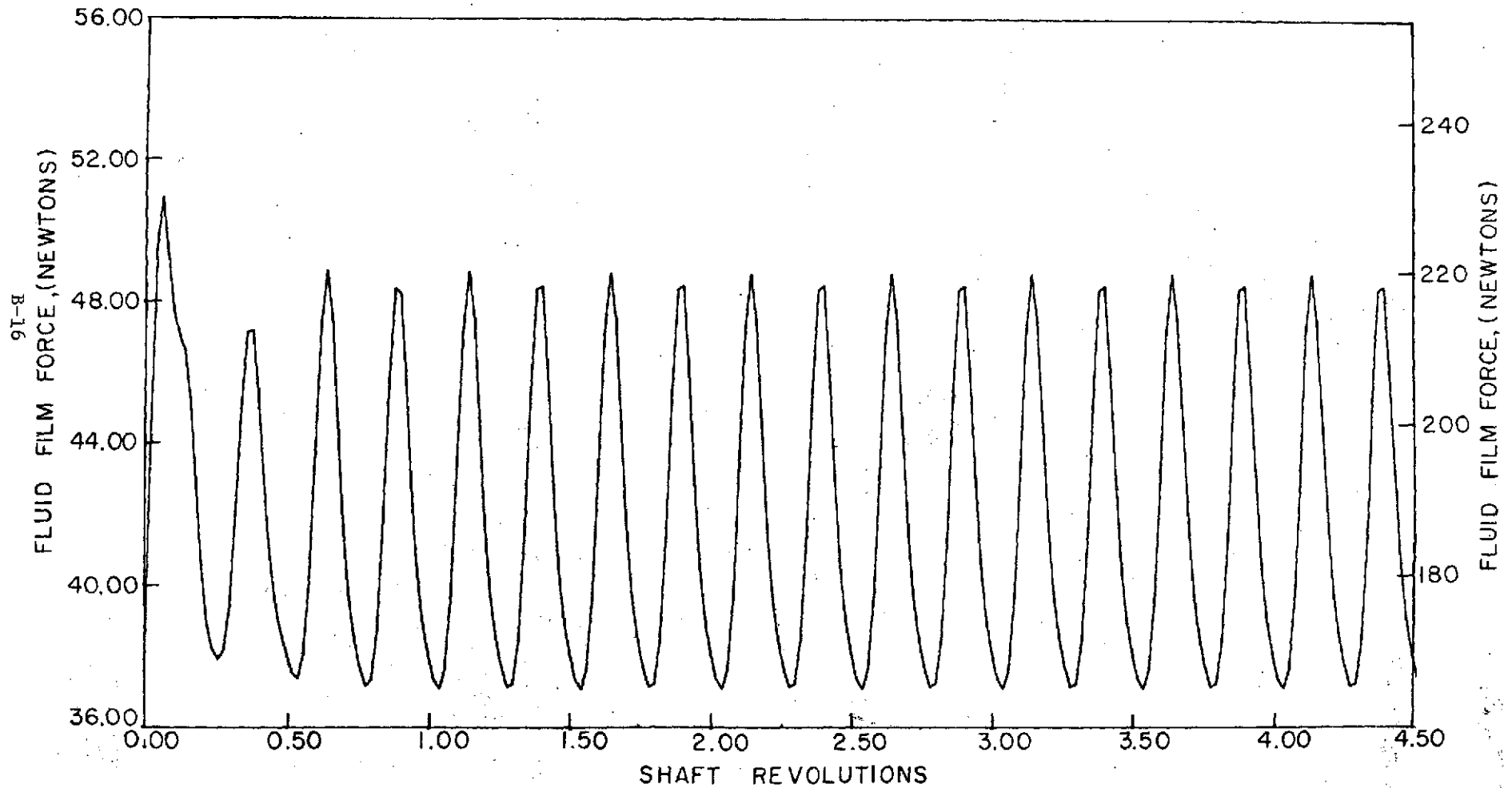


Figure B-13

Fluid-Film Force vs. Shaft Revolutions, Run 10, Case 1

Pressure = 300 psig (2068.5 kN/m²)

Runout = 0.001 in. (25.4 μ m)

Temperature = 1000°F (537.78°C)

Friction = 14.0 lbs (62.272 N), 29.0 in.-lbs (3.276 Nm)

Speed = 500 ft/sec (152.4 m/sec)

Initial Clearance = 0.00032 in. (8.128 μ m)

Nosepiece Wt. = 1.75 lbs (7.784 N)

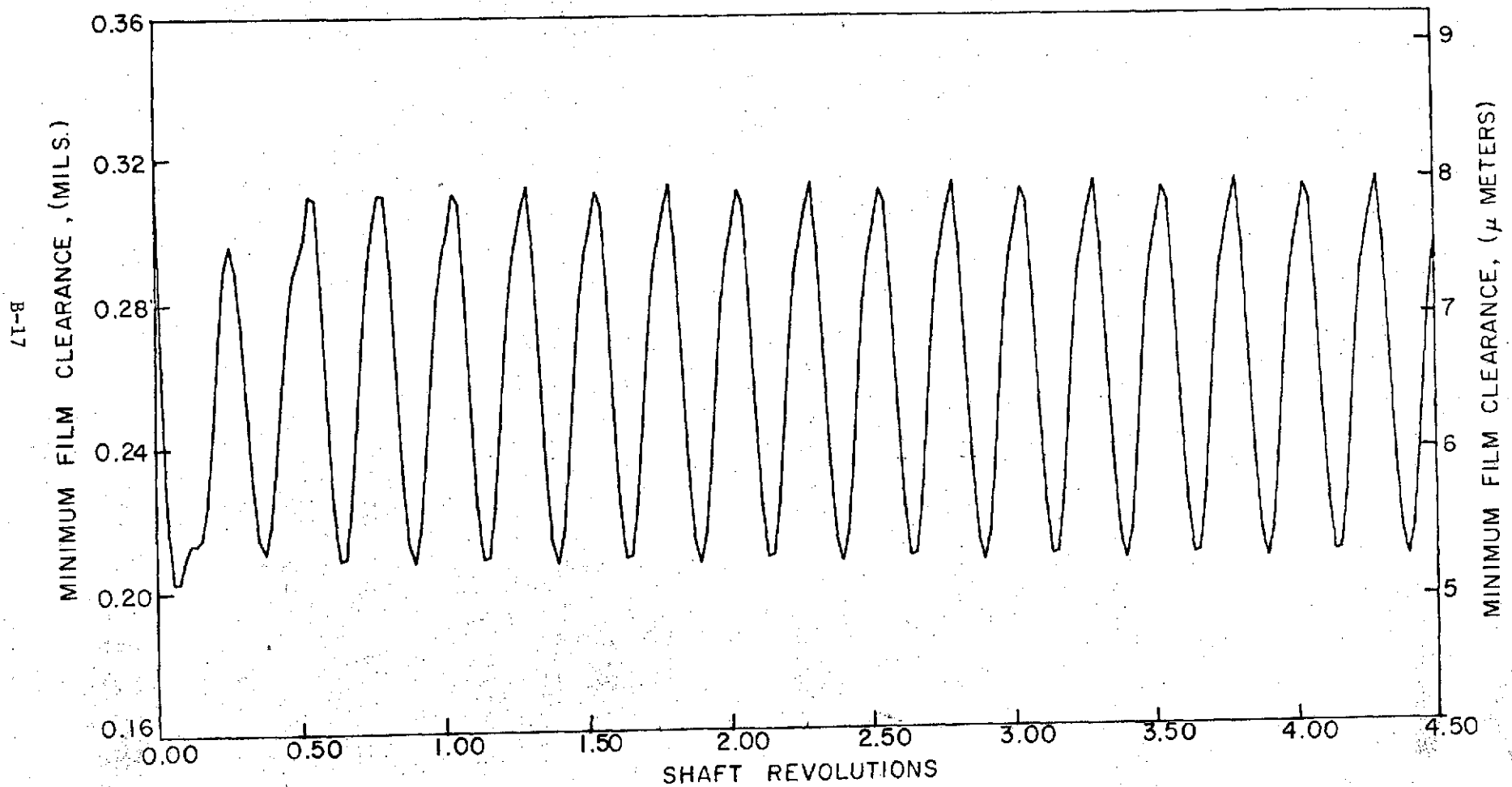


Figure B-14

Minimum Clearance vs. Shaft Revolutions, Run 1C, Case 1

Pressure = 300 psig (2068.5 kN/m²)

Runout = 0.001 in. (25.4 μ m)

Temperature = 1000°F (537.78°C)

Friction = 14.0 lbs (62.272 N), 29.0 in.-lbs (3.276 Nm)

Speed = 500 ft/sec (152.4 m/sec)

Initial Clearance = 0.00032 in. (8.128 μ m)

Nosepiece Wt. = 1.75 lbs (7.784 N)

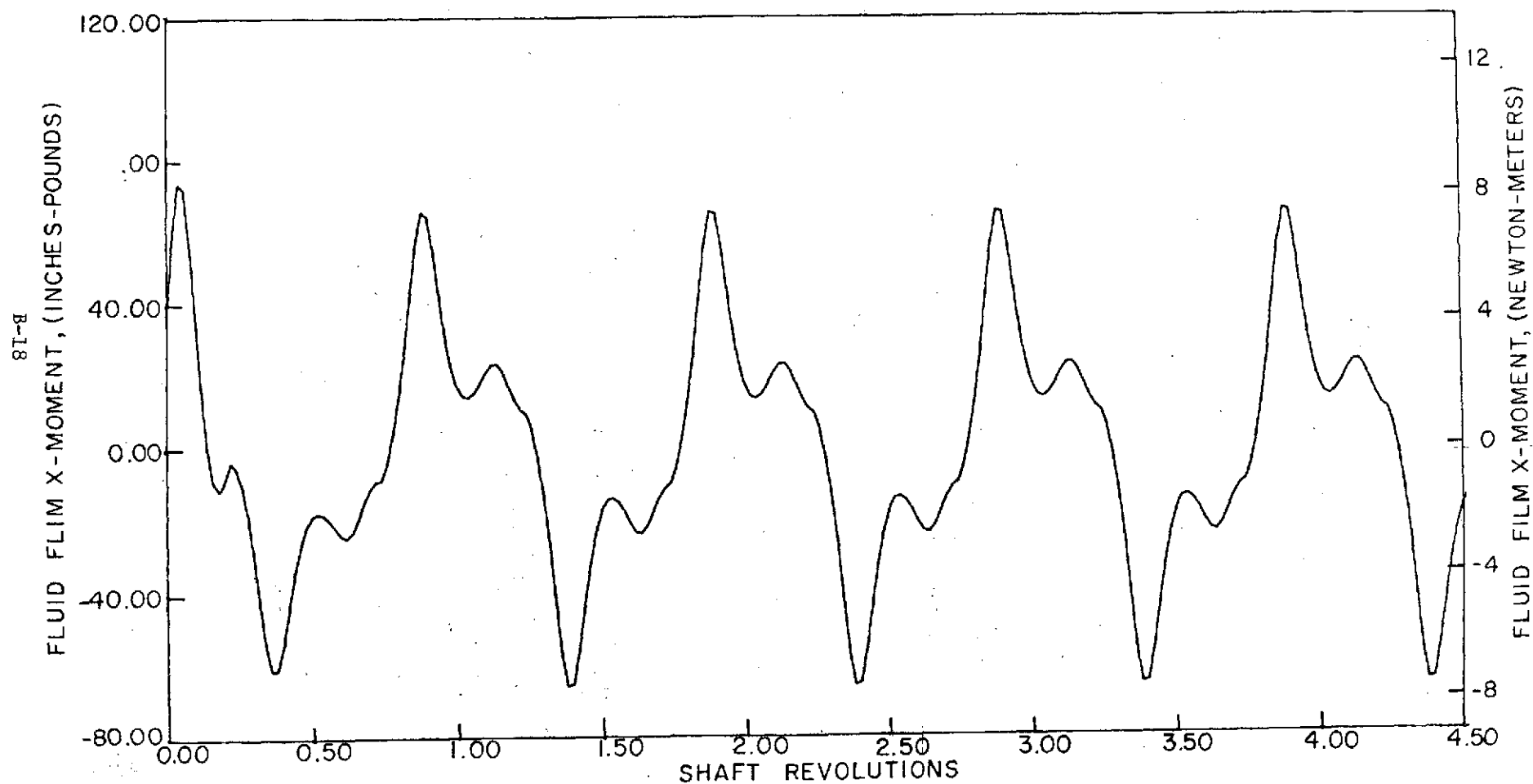


Figure B-15

Fluid-Film Moment About X-Axis vs. Shaft Revolutions, Run 1C, Case 1

Pressure = 300 psig (2068.5 kN/m²)

Runout = 0.001 in. (25.4 μ m)

Temperature = 1000°F (537.78°C)

Friction = 14.0 lbs (62.272 N), 29.0 in.-lbs (3.276 Nm)

Speed = 500 ft/sec (152.4 m/sec)

Initial Clearance = 0.00032 in. (8.128 μ m)

Nosepiece Wt. = 1.75 lbs (7.784 N)

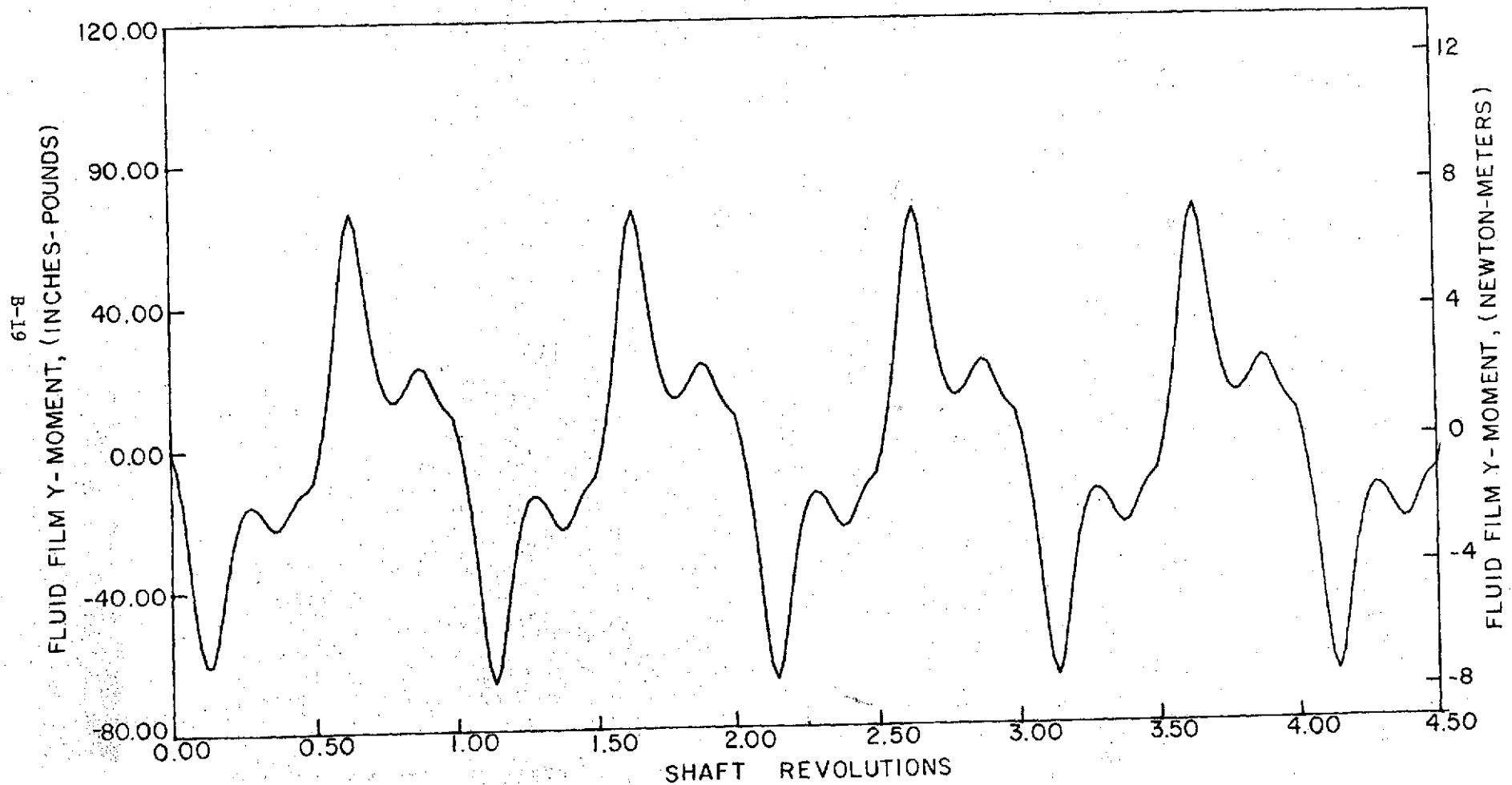


Figure B-16

Fluid-Film Moment About Y-Axis vs. Shaft Revolutions, Run 1C, Case 1

Run 2a, Case 1

B-20

C-2

Pressure = 300 psig (2068.5 kN/m²)

Runout = 0.0015 in. (38.1 μ m)

Temperature = 1000°F (537.78°C)

Friction = 0.0 lbs (0.0 N), 0.0 in.-lbs (0.0 Nm)

Speed = 500 ft/sec (152.4 m/sec)

Initial Clearance = 0.00032 in. (8.128 μ m)

Nosepiece Wt. = 1.75 lbs (7.784 N)

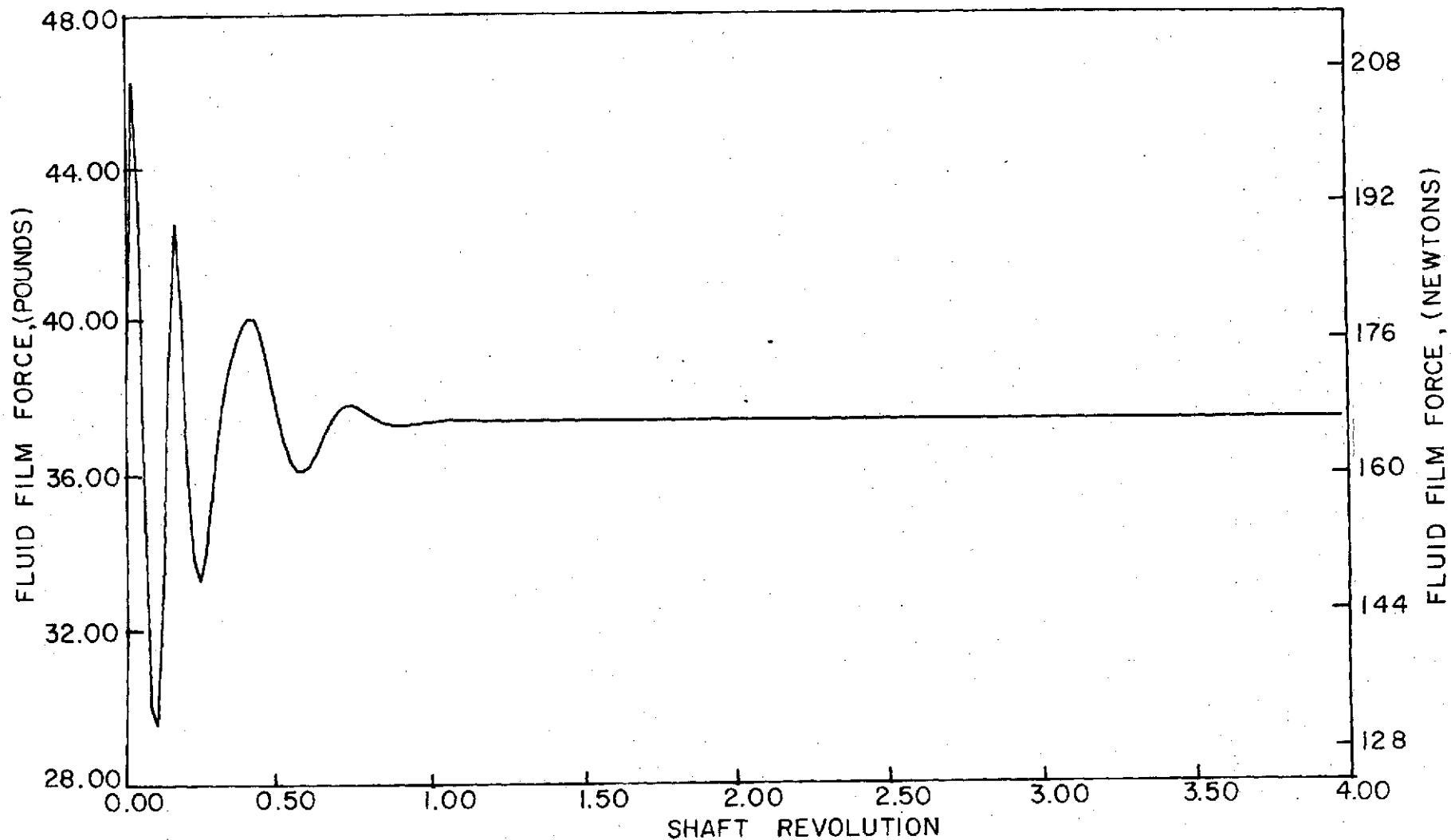


Figure B-17

Fluid-Film Force vs. Shaft Revolutions, Run 2A, Case 1

B-21

Pressure = 300 psig (2068.5 kN/m²)
Temperature = 1000°F (537.78°C)
Speed = 500 ft/sec (152.4 m/sec)
Nosepiece Wt. = 1.75 lbs (7.784 N)

Runout = 0.0015 in. (38.1 μm)
Friction = 0.0 lbs (0.0 N), 0.0 in.-lbs (0.0 Nm)
Initial Clearance = 0.00032 in. (8.128 μm)

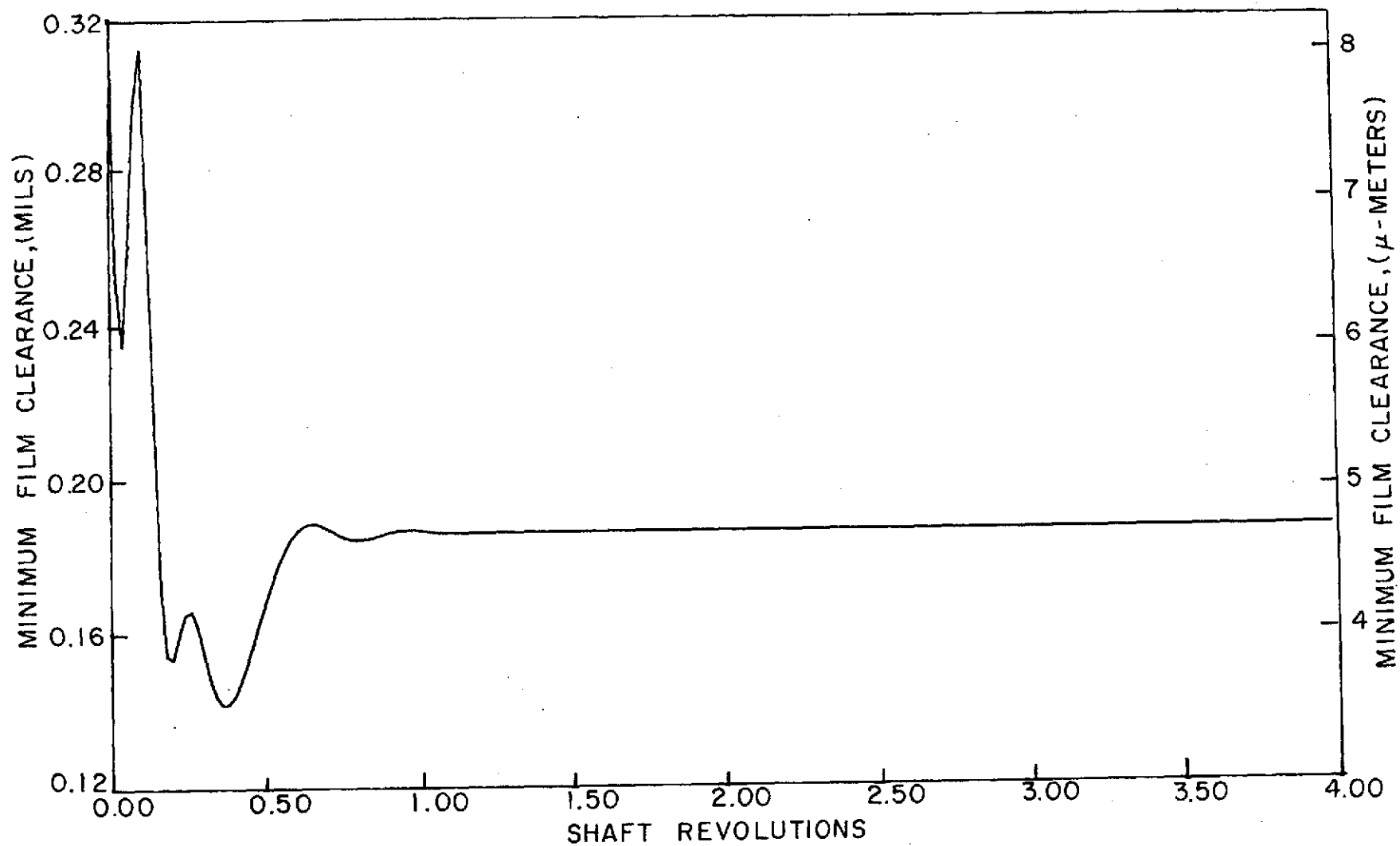


Figure B-18

Minimum Clearance vs. Shaft Revolutions, Run 2A, Case 1

Pressure = 300 psig (2068.5 kN/m²)

Runout = 0.0015 in. (38.1 μm)

Temperature = 1000°F (537.78°C)

Friction = 0.0 lbs (0.0 N), 0.0 in.-lbs (0.0 Nm)

Speed = 500 ft/sec (152.4 m/sec)

Initial Clearance = 0.00032 in. (8.128 μm)

Nosepiece Wt. = 1.75 lbs (7.784 N)

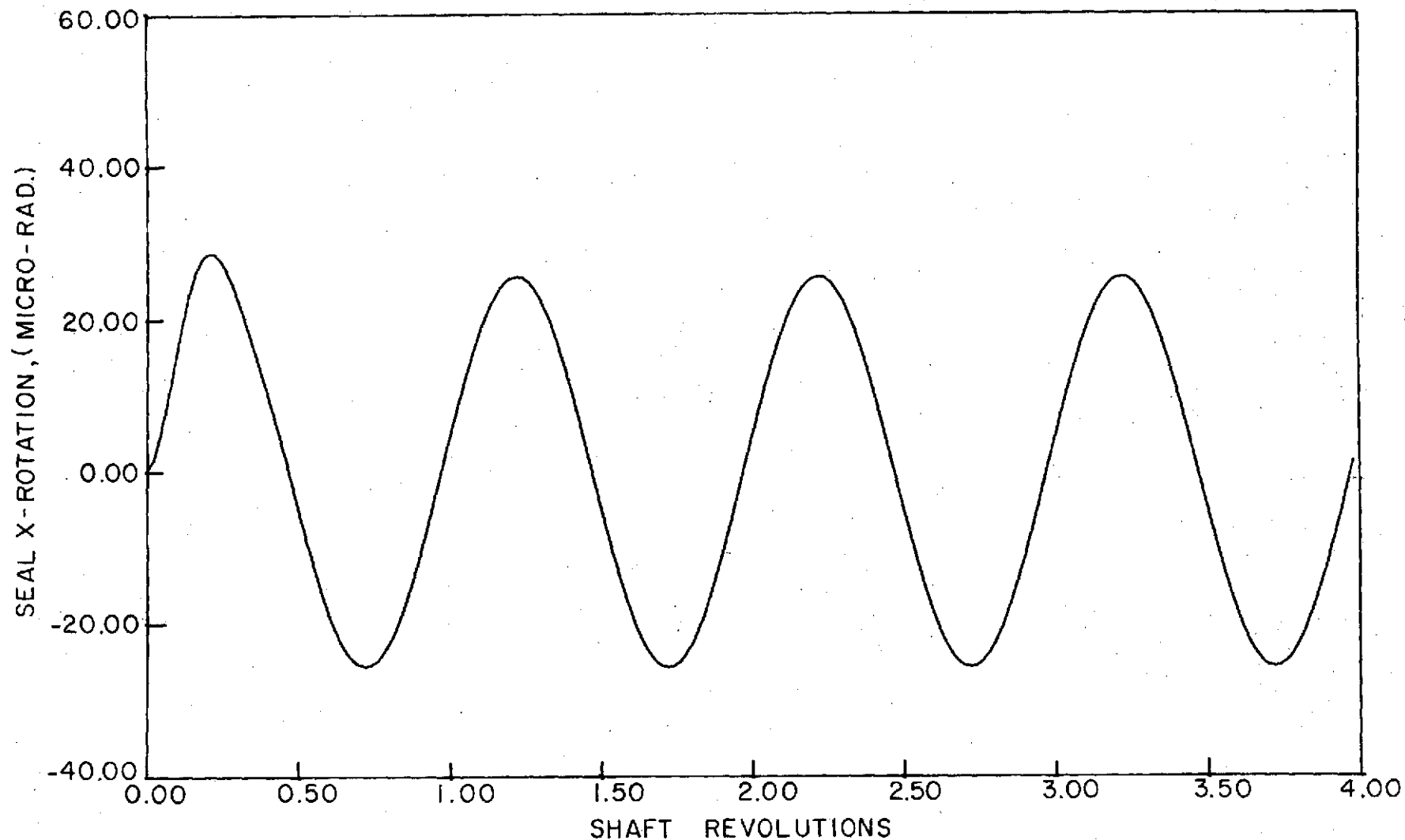


Figure B-19

Rotation About X-Axis vs. Shaft Revolutions, Run 2A, Case 1

Pressure = 300 psig (2068.5 kN/m²)
Temperature = 1000°F (537.78°C)
Speed = 500 ft/sec (152.4 m/sec)
Nosepiece Wt. = 1.75 lbs (7.784 N)

Runout = 0.0015 in. (38.1 μm)
Friction = 0.0 lbs (0.0 N), 0.0 in.-lbs (0.0 Nm)
Initial Clearance = 0.00032 in. (8.128 μm)

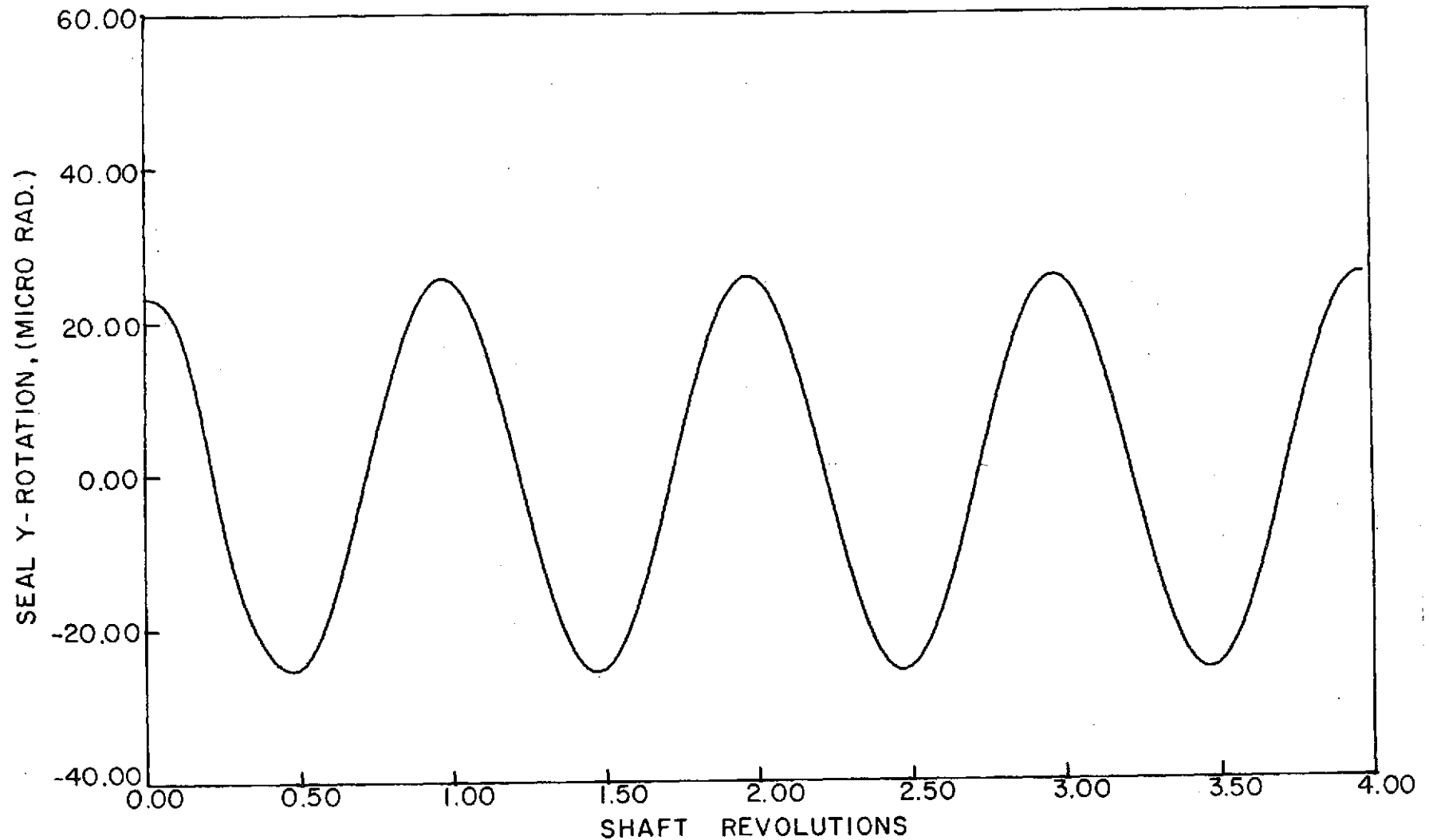


Figure B-20

Rotation About Y-Axis vs. Shaft Revolutions, Run 2A, Case 1

Pressure = 300 psig (2068.5 kN/m²)

Runout = 0.0015 in. (38.1 μ m)

Temperature = 1000°F (537.78°C)

Friction = 0.0 lbs (0.0 N), 0.0 in.-lbs (0.0 Nm)

Speed = 500 ft/sec (152.4 m/sec)

Initial Clearance = 0.00032 in. (8.128 μ m)

Nosepiece Wt. = 1.75 lbs (7.784 N)

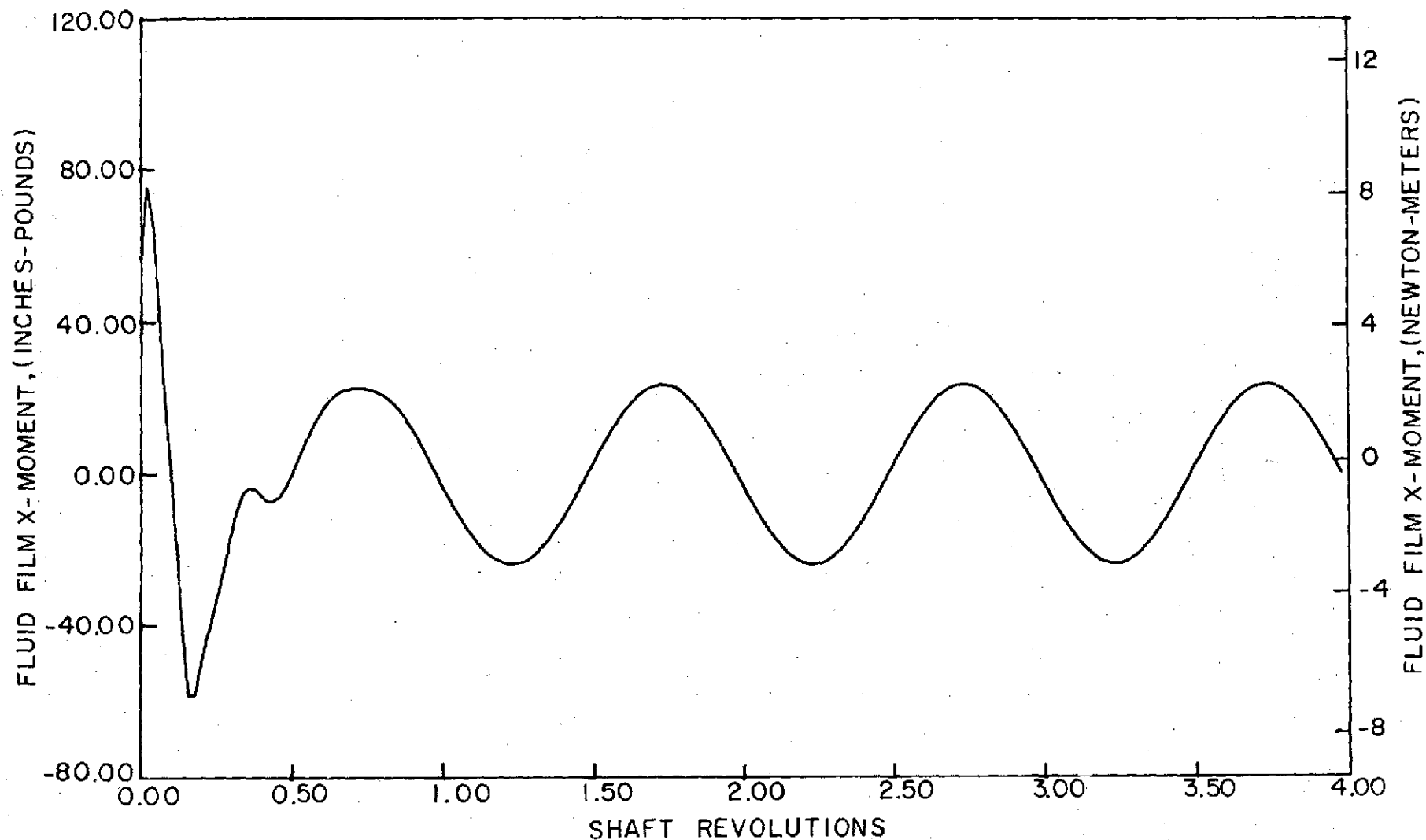


Figure B-21

Fluid-Film Moment About X-Axis vs. Shaft Revolutions, Run 2A, Case 1

Pressure = 300 psig (2068.5 kN/m²)
Temperature = 1000°F (537.78°C)
Speed = 500 ft/sec (152.4 m/sec)
Nosepiece Wt. = 1.75 lbs (7.784 N)

Runout = 0.0015 in. (38.1 μm)
Friction = 0.0 lbs (0.0 N), 0.0 in.-lbs (0.0 Nm)
Initial Clearance = 0.00032 in. (8.128 μm)

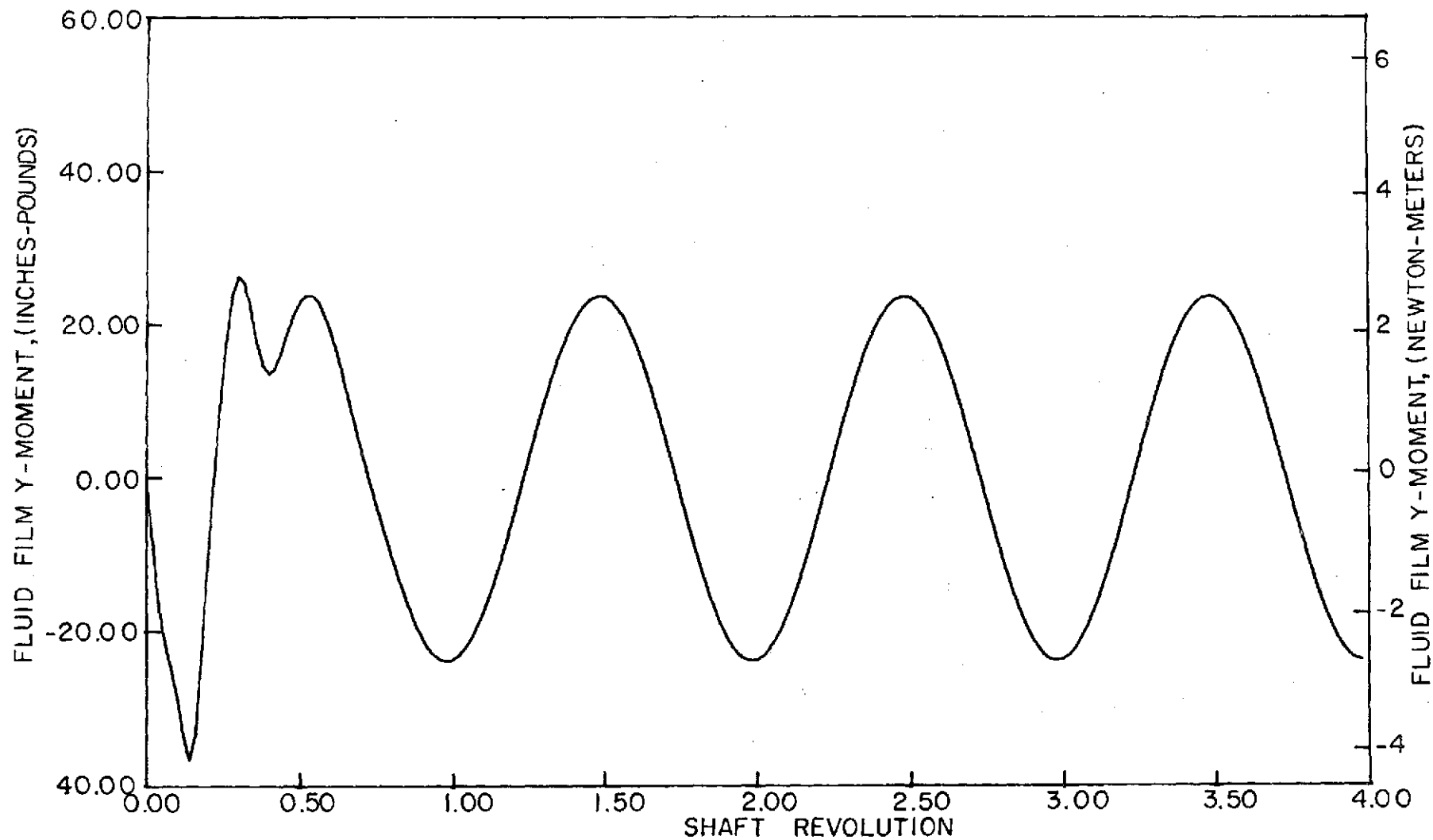


Figure B-22

Fluid-Film Moment About Y-Axis vs. Shaft Revolutions, Run 2A, Case 1

Run 3a, Case 1

Pressure = 300 psig (2068.5 kN/m²)
Temperature = 1000°F (537.78°C)
Speed = 500 ft/sec (152.4 m/sec)
Nosepiece Wt. = 1.75 lbs (7.784 N)

Runout = 0.002 in. (50.8 μm)
Friction = 0.0 lbs (0.0 N), 0.0 in.-lbs (0.0 Nm)
Initial Clearance = 0.00032 in. (8.128 μm)

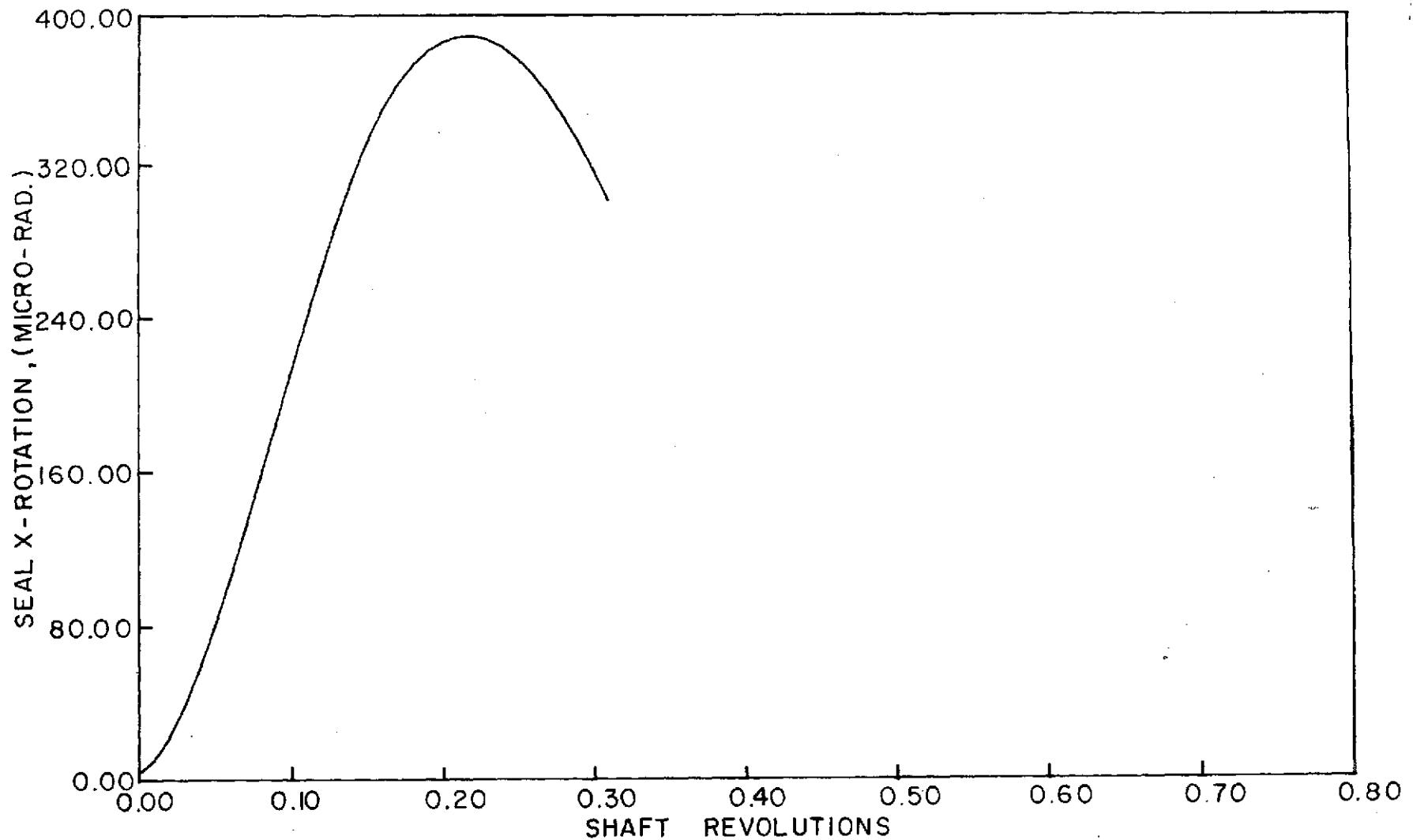


Figure B-23

Rotation About X-Axis vs. Shaft Revolutions, Run 3A, Case 1

Pressure = 300 psig (2068.5 kN/m²)

Runout = 0.002 in. (50.8 μ m)

Temperature = 1000°F (537.78°C)

Friction = 0.0 lbs (0.0 N), 0.0 in.-lbs (0.0 Nm)

Speed = 500 ft/sec (152.4 m/sec)

Initial Clearance = 0.00032 in. (8.128 μ m)

Nosepiece Wt. = 1.75 lbs (7.784 N)

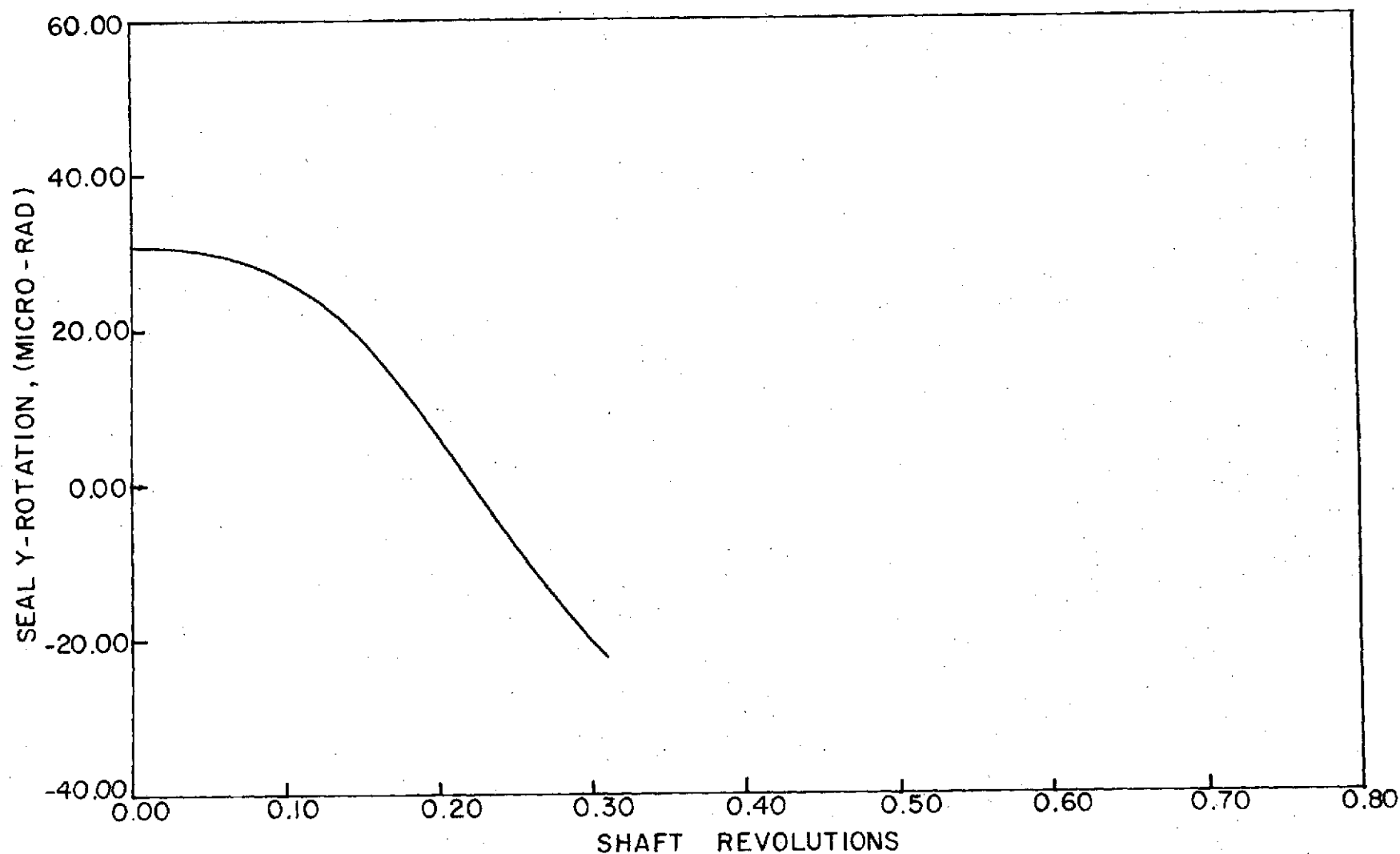


Figure B-24

Rotation About Y-Axis vs. Shaft Revolutions, Run 3A, Case 1

Pressure = 300 psig (2068.5 kN/m²)
Temperature = 1000°F (537.78°C)
Speed = 500 ft/sec (152.4 m/sec)
Nosepiece Wt. = 1.75 lbs (7.784 N)

Runout = 0.002 in. (50.8 μm)
Friction = 0.0 lbs (0.0 N), 0.0 in.-lbs (0.0 Nm)
Initial Clearance = 0.00032 in. (8.128 μm)

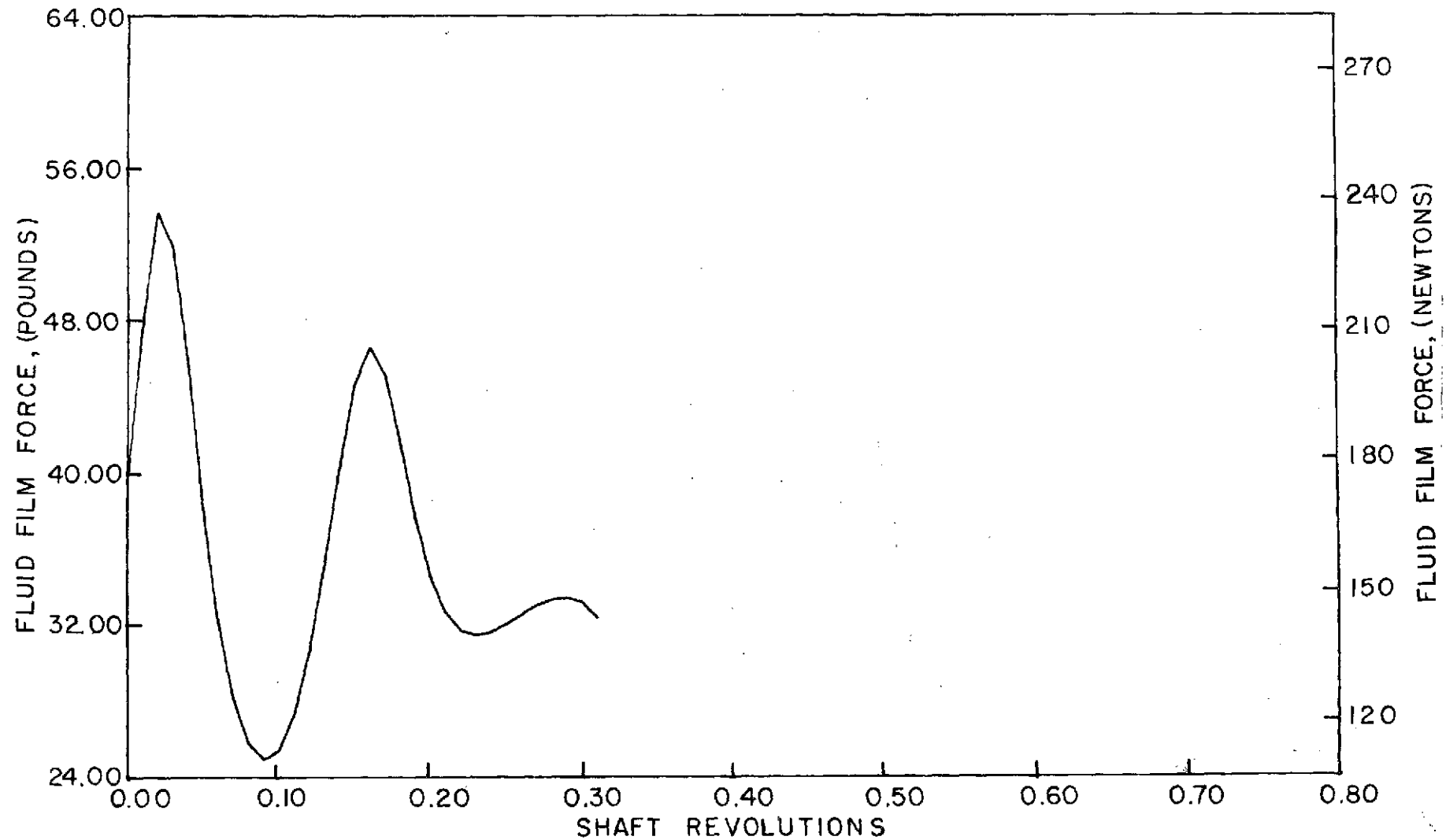


Figure B-25
Fluid-Film Force vs. Shaft Revolutions, Run 3A, Case 1

Pressure = 300 psig (2068.5 kN/m²)

Runout = 0.002 in. (50.8 μm)

Temperature = 1000°F (537.78°C)

Friction = 0.0 lbs (0.0 N), 0.0 in.-lbs (0.0 Nm)

Speed = 500 ft/sec (152.4 m/sec)

Initial Clearance = 0.00032 in. (8.128 μm)

Nosepiece Wt. = 1.75 lbs (7.784 N)

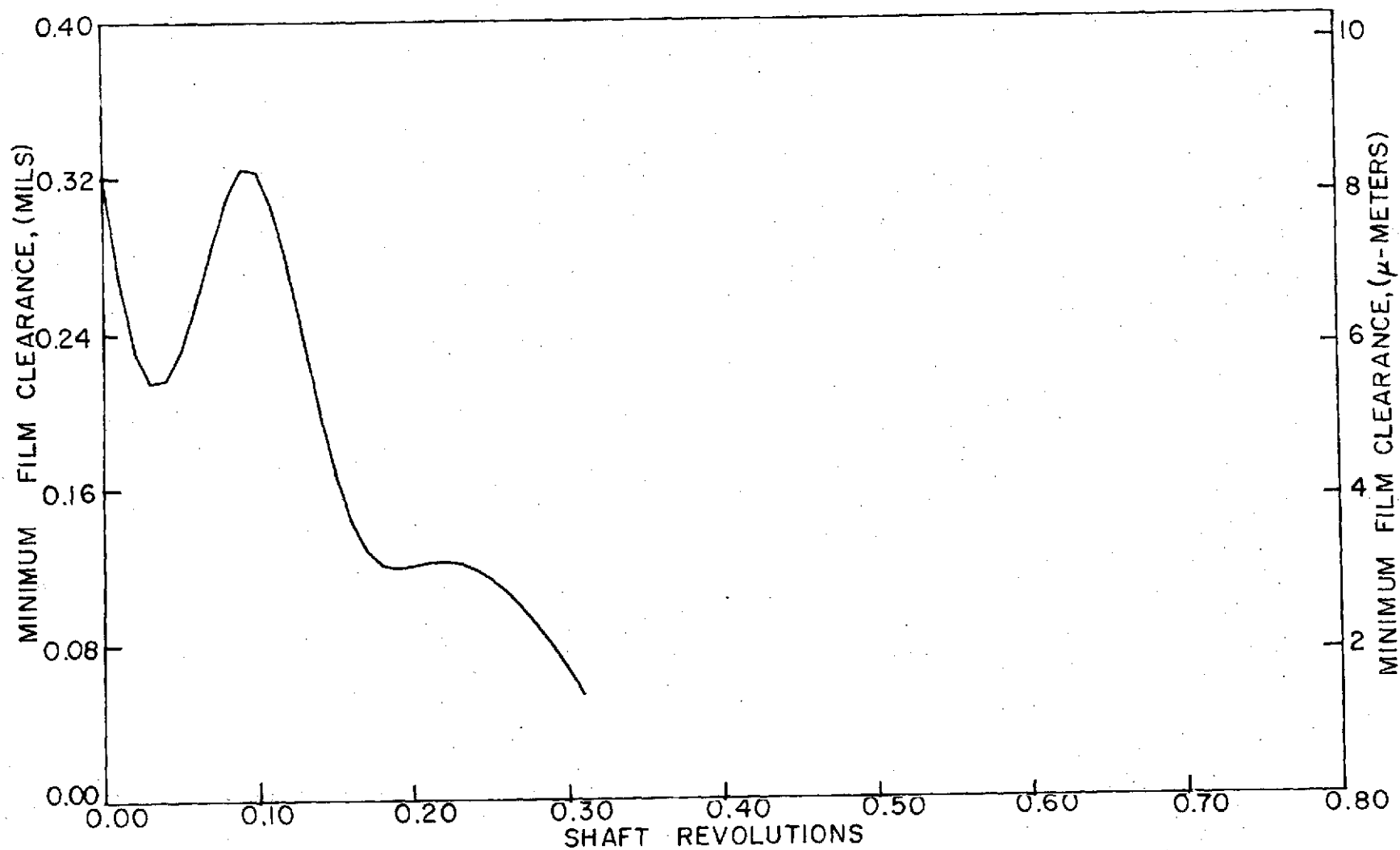


Figure B-26

Minimum Clearance vs. Shaft Revolutions, Run 3A, Case 1

Pressure = 300 psig (2068.5 kN/m²)

Runout = 0.002 in. (50.8 μ m)

Temperature = 1000°F (537.78°C)

Friction = 0.0 lbs (0.0 N), 0.0 in.-lbs (0.0 Nm)

Speed = 500 ft/sec (152.4 m/sec)

Initial Clearance = 0.00032 in. (8.128 μ m)

Nosepiece Wt. = 1.75 lbs (7.784 N)

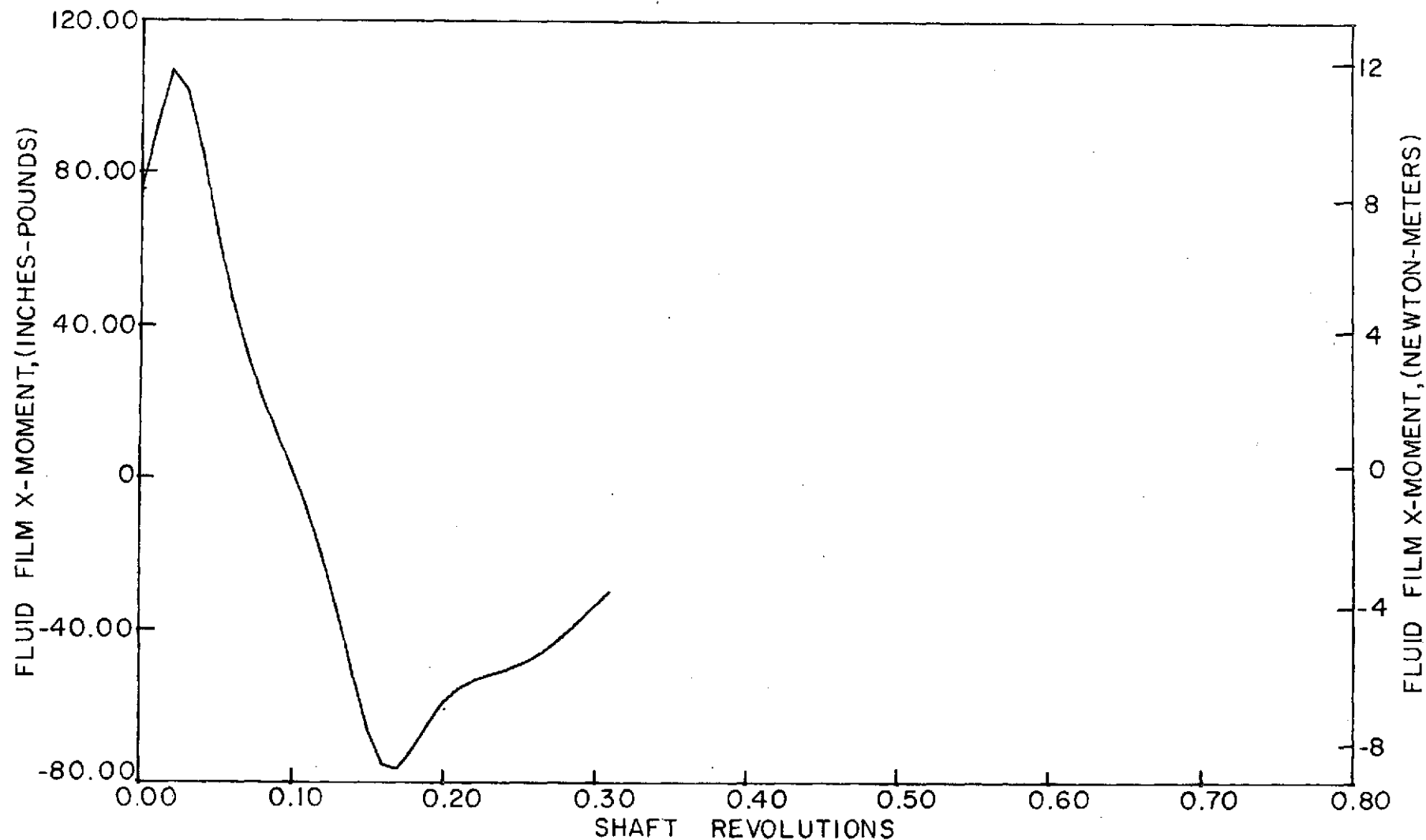


Figure B-27

Fluid-Film Moment About X-Axis vs. Shaft Revolutions, Run 3A, Case 1

Pressure = 300 psig (2068.5 kN/m²)
Temperature = 1000°F (537.78°C)
Speed = 500 ft/sec (152.4 m/sec)
Nosepiece Wt. = 1.75 lbs (7.784 N)

Runout = 0.002 in. (50.8 μm)
Friction = 0.0 lbs (0.0 N), 0.0 in.-lbs (0.0 Nm)
Initial Clearance = 0.00032 in. (8.128 μm)

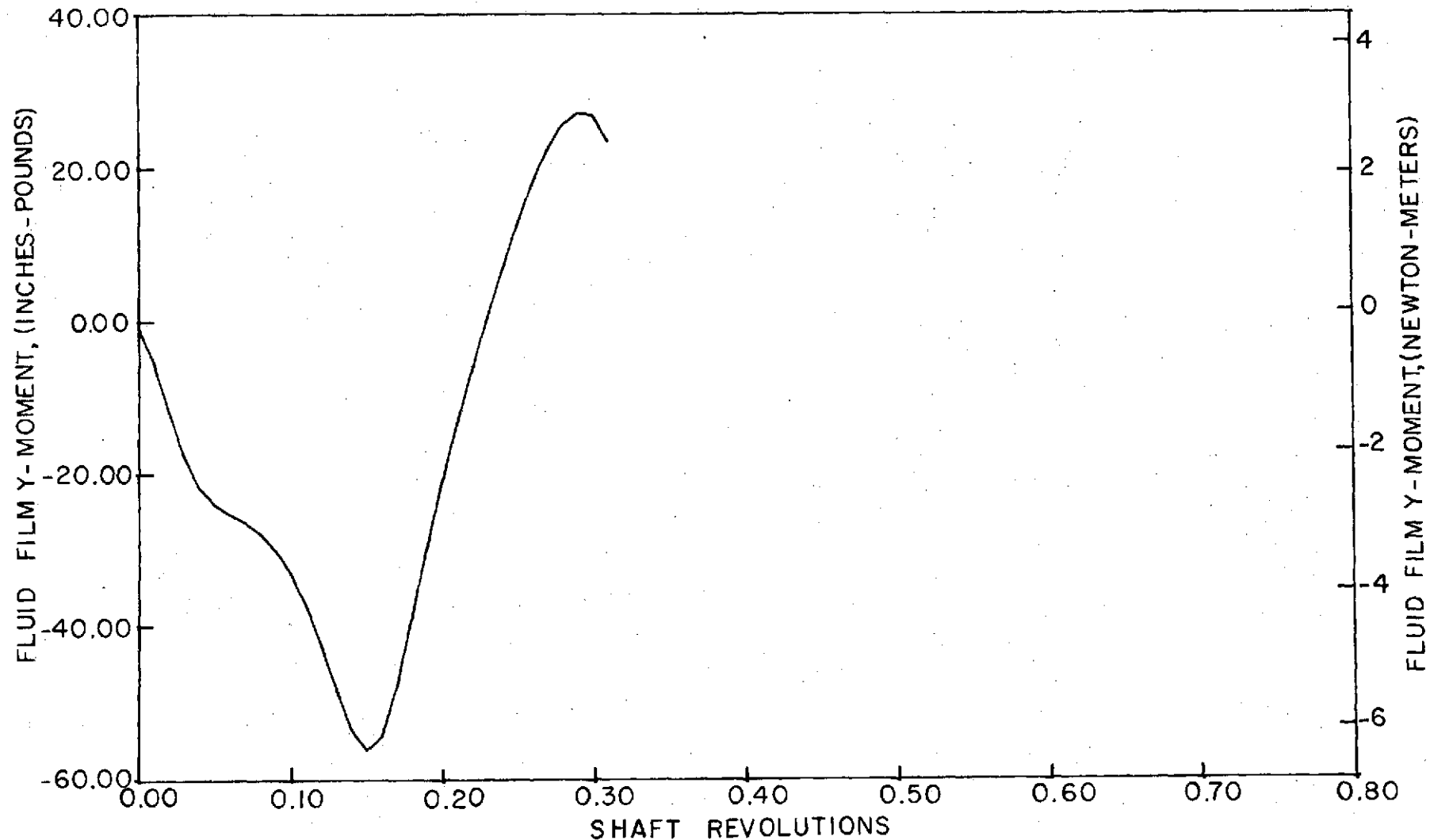


Figure B-28

Fluid-Film Moment About Y-Axis vs. Shaft Revolutions, Run 3A, Case 1

Run 3d, Case 1

Pressure = 300 psig (2068.5 kN/m²)
Temperature = 1000°F (537.78°C)
Speed = 500 ft/sec (152.4 m/sec)
Nosepiece Wt. = 1.75 lbs (7.784 N)

Runout = 0.002 in. (50.8 μm)
Friction = 6.0 lbs (26.688 N), 13.0 in.-lbs (1.4687 Nm)
Initial Clearance = 0.00032 in. (8.128 μm)

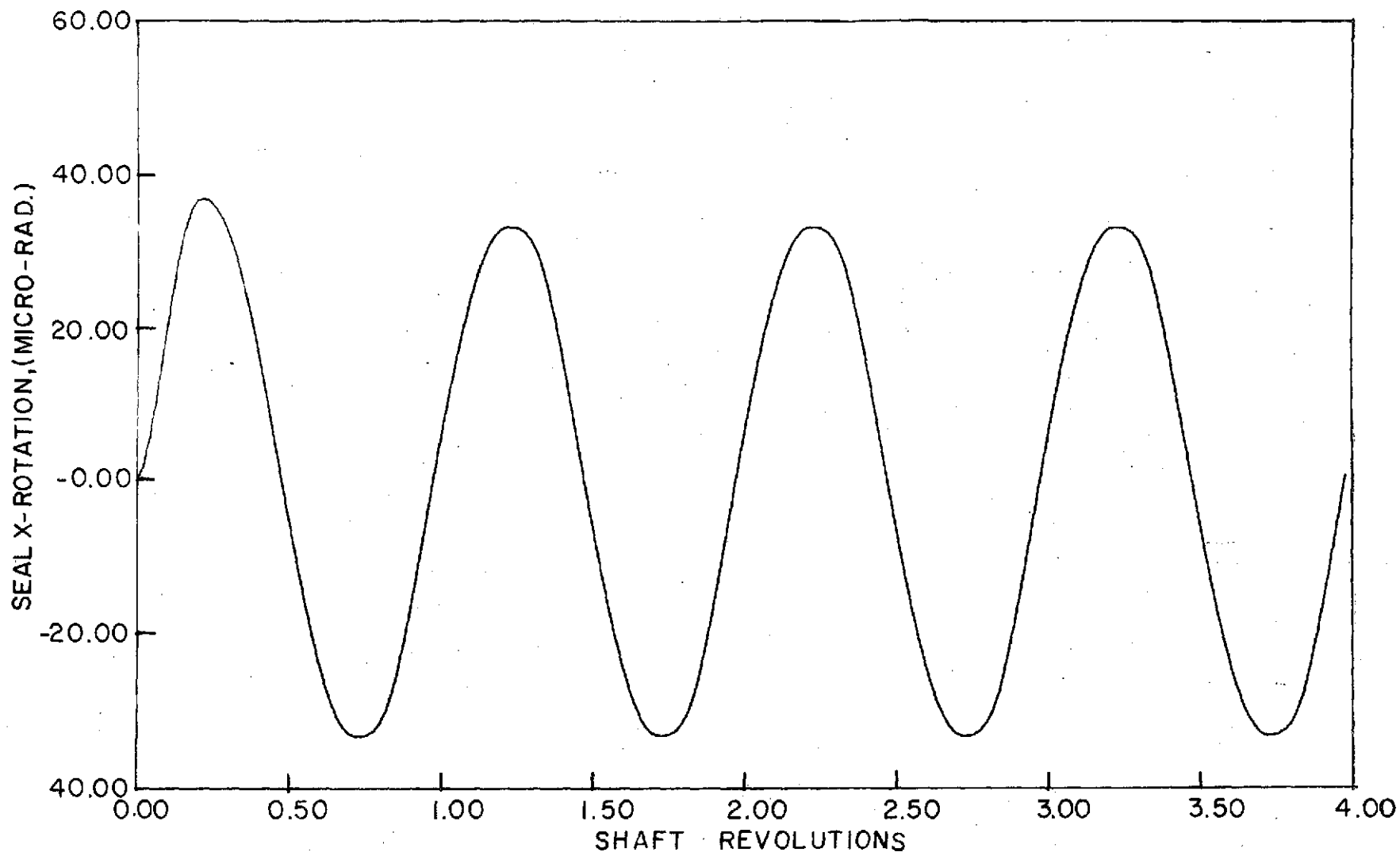


Figure B-29
Rotation About X-Axis vs. Shaft Revolutions, Run 3D, Case 1

Pressure = 300 psig (2068.5 kN/m²)

Runout = 0.002 in. (50.8 μ m)

Temperature = 1000°F (537.78°C)

Friction = 6.0 lbs (26.688 N), 13.0 in.-lbs (1.4687 Nm)

Speed = 500 ft/sec (152.4 m/sec)

Initial Clearance = 0.00032 in. (8.128 μ m)

Nosepiece Wt. = 1.75 lbs (7.784 N)

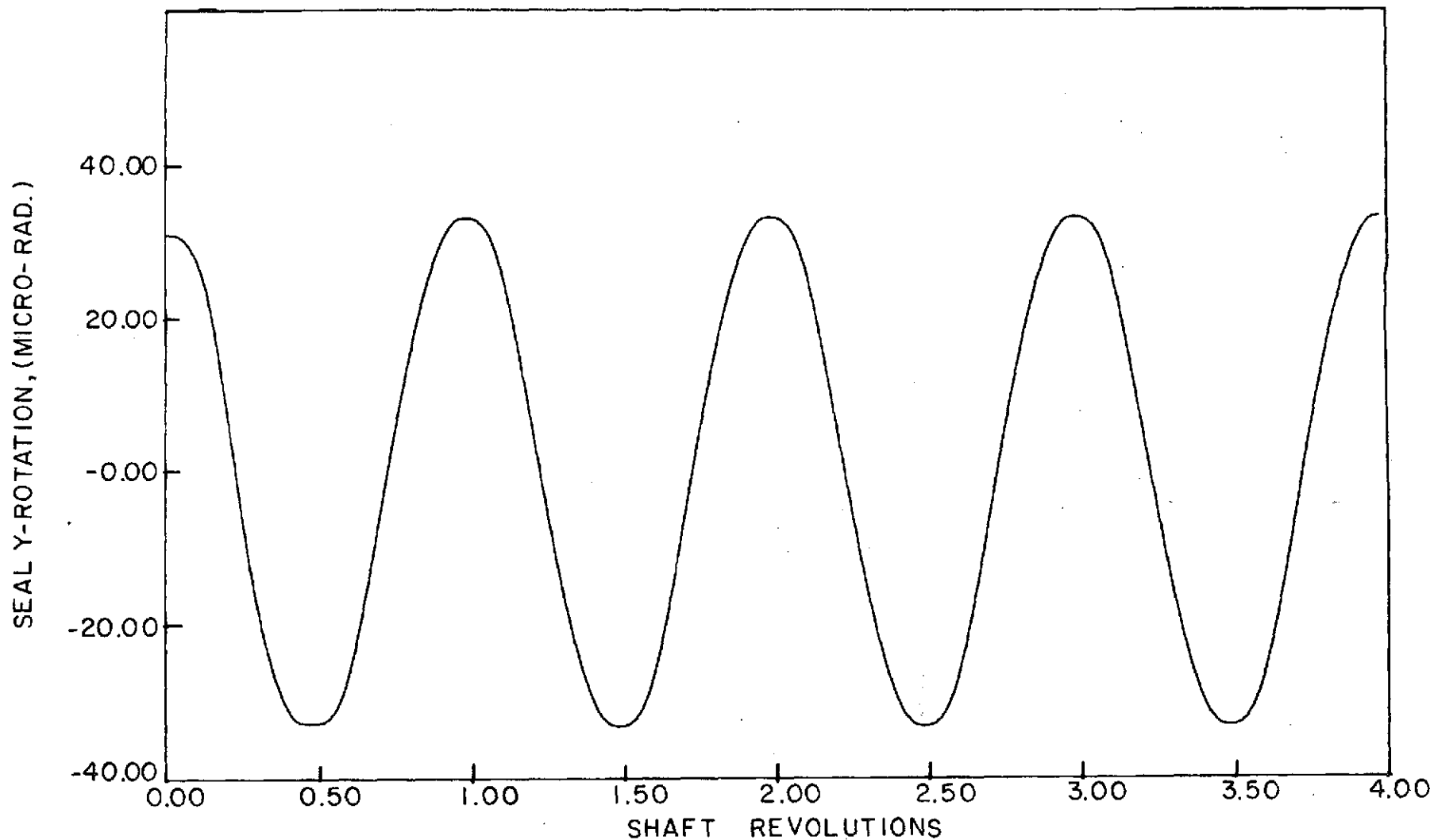


Figure B-30

Rotation About Y-Axis vs. Shaft Revolutions, Run 3D, Case 1

Pressure = 300 psig (2068.5 kN/m²)

Runout = 0.002 in. (50.8 μm)

Temperature = 1000°F (537.78°C)

Friction = 6.0 lbs (26.688 N), 13.0 in.-lbs (1.4687 Nm)

Speed = 500 ft/sec (152.4 m/sec)

Initial Clearance = 0.00032 in. (8.128 μm)

Nosepiece Wt. = 1.75 lbs (7.784 N)

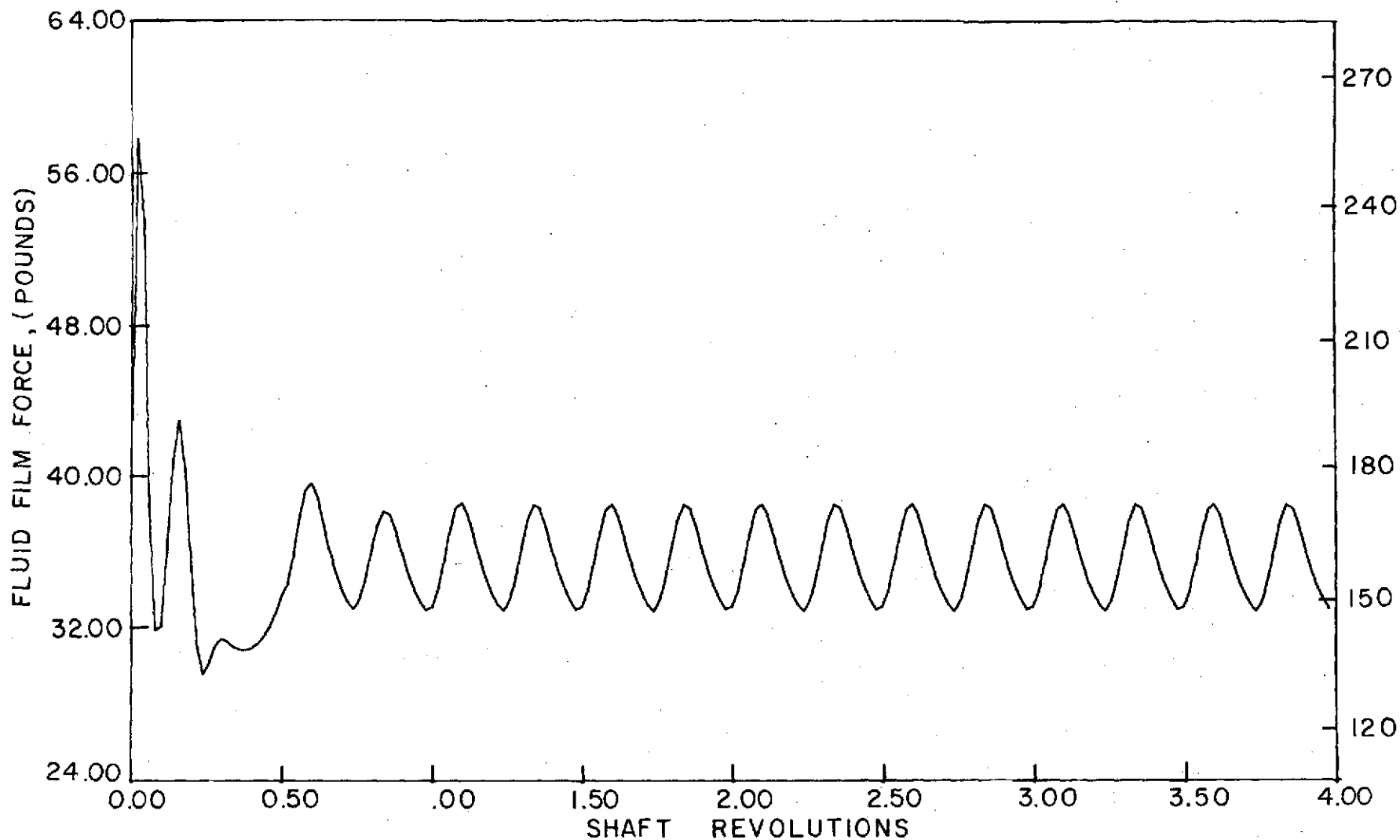


Figure B-31

Fluid-Film Force vs. Shaft Revolutions, Run 3D, Case 1

Pressure = 300 psig (2068.5 kN/m²)
Temperature = 1000°F (537.78°C)
Speed = 500 ft/sec (152.4 m/sec)
Nosepiece Wt. = 1.75 lbs (7.784 N)

Runout = 0.002 in. (50.8 μm)
Friction = 6.0 lbs (26.688 N), 13.0 in.-lbs (1.4687 Nm)
Initial Clearance = 0.00032 in. (8.128 μm)

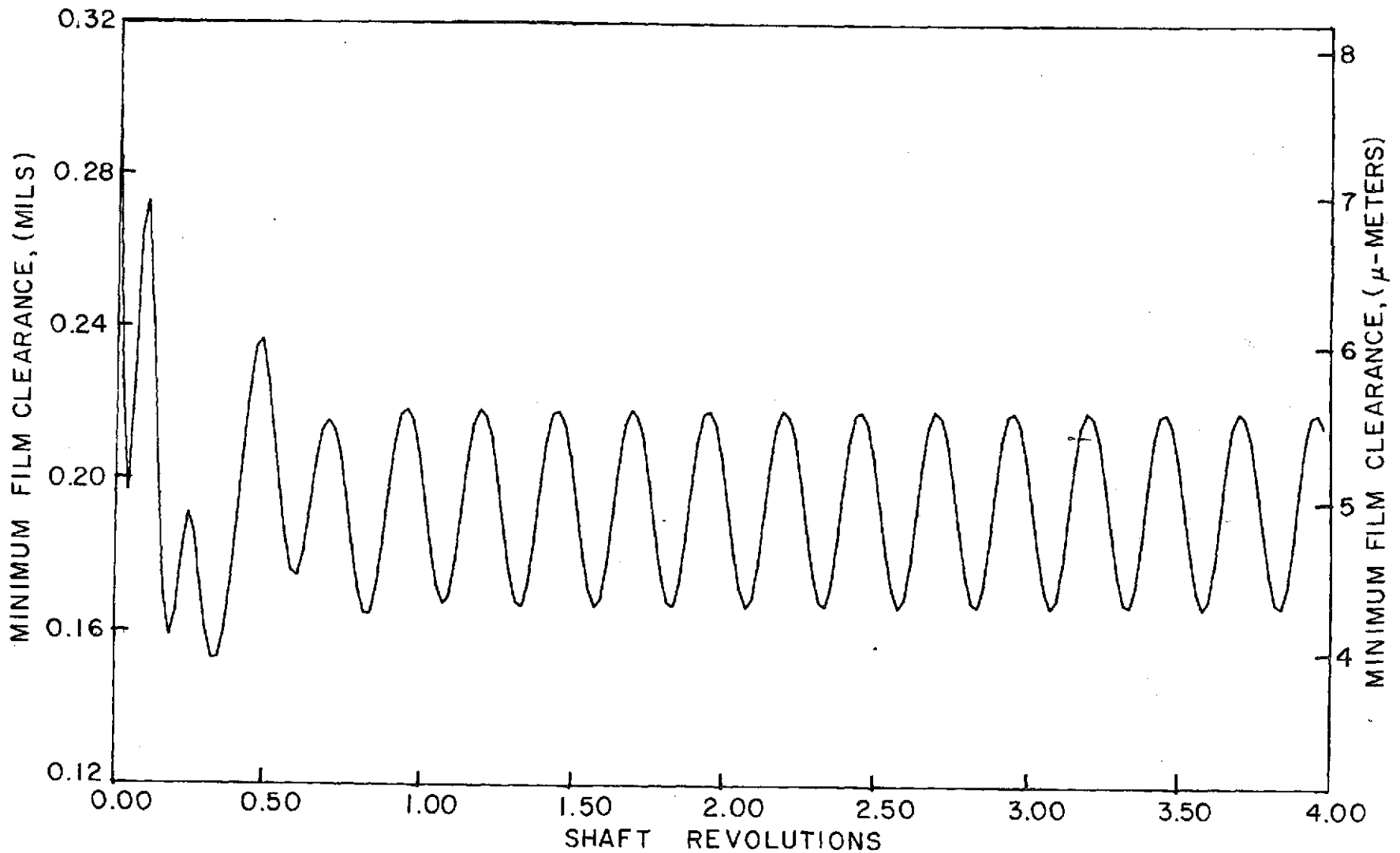


Figure B-32

Minimum Clearance vs. Shaft Revolutions, Run 3D, Case 1

Pressure = 300 psig (2068.5 kN/m²)

Runout = 0.002 in. (50.8 μm)

Temperature = 1000°F (537.78°C)

Friction = 6.0 lbs (26.688 N), 13.0 in.-lbs (1.4687 Nm)

Speed = 500 ft/sec (152.4 m/sec)

Initial Clearance = 0.00032 in. (8.128 μm)

Nosepiece Wt. = 1.75 lbs (7.784 N)

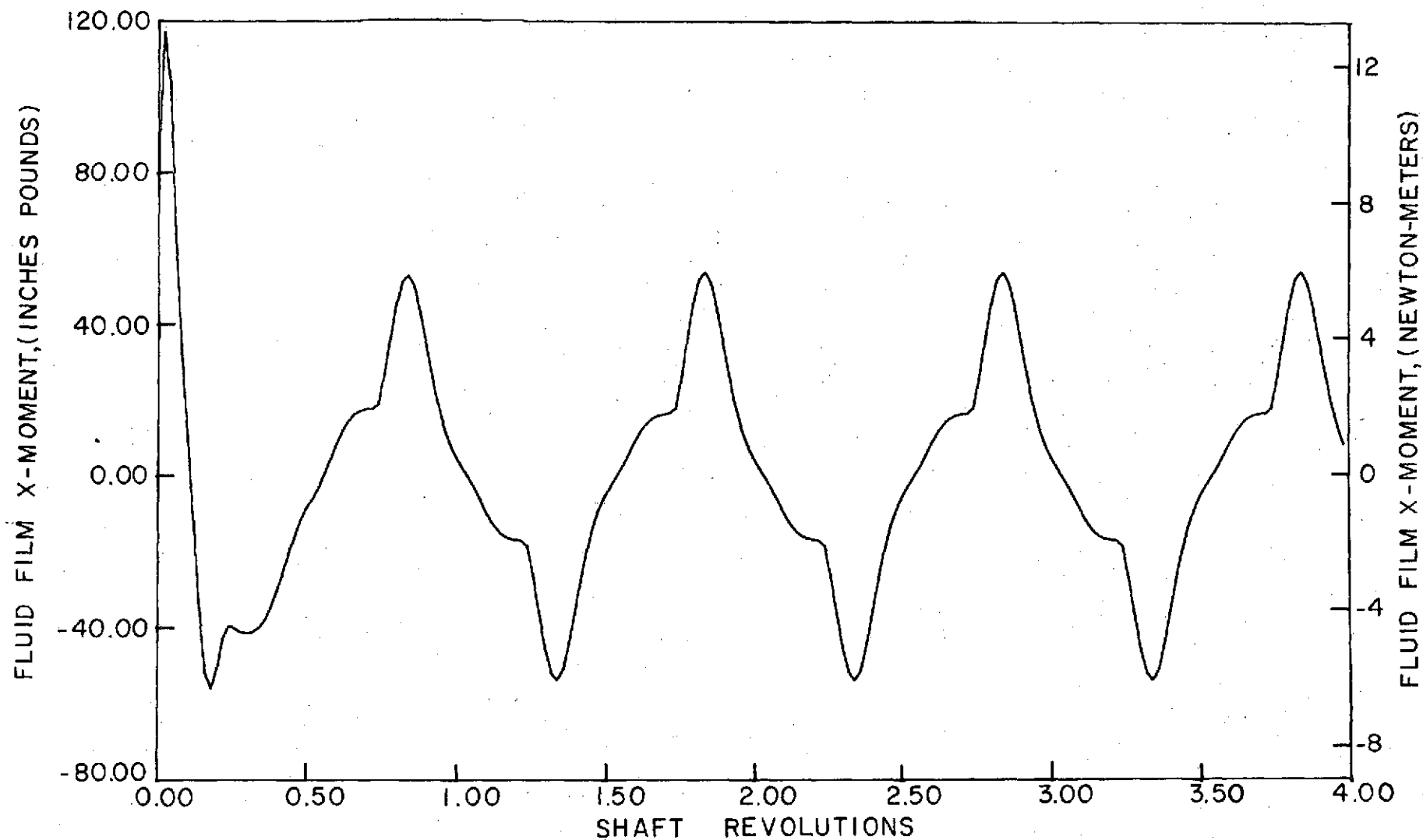


Figure B-33

Fluid-Film Moment About X-Axis vs. Shaft Revolutions, Run 3D, Case 1

Pressure = 300 psig (2068.5 kN/m²) Runout = 0.002 in. (50.8 μm)
Temperature = 1000°F (537.78°C) Friction = 6.0 lbs (26.688 N), 13.0 in.-lbs (1.4687 Nm)
Speed = 500 ft/sec (152.4 m/sec) Initial Clearance = 0.00032 in. (8.128 μm)
Nosepiece Wt. = 1.75 lbs (7.784 N)

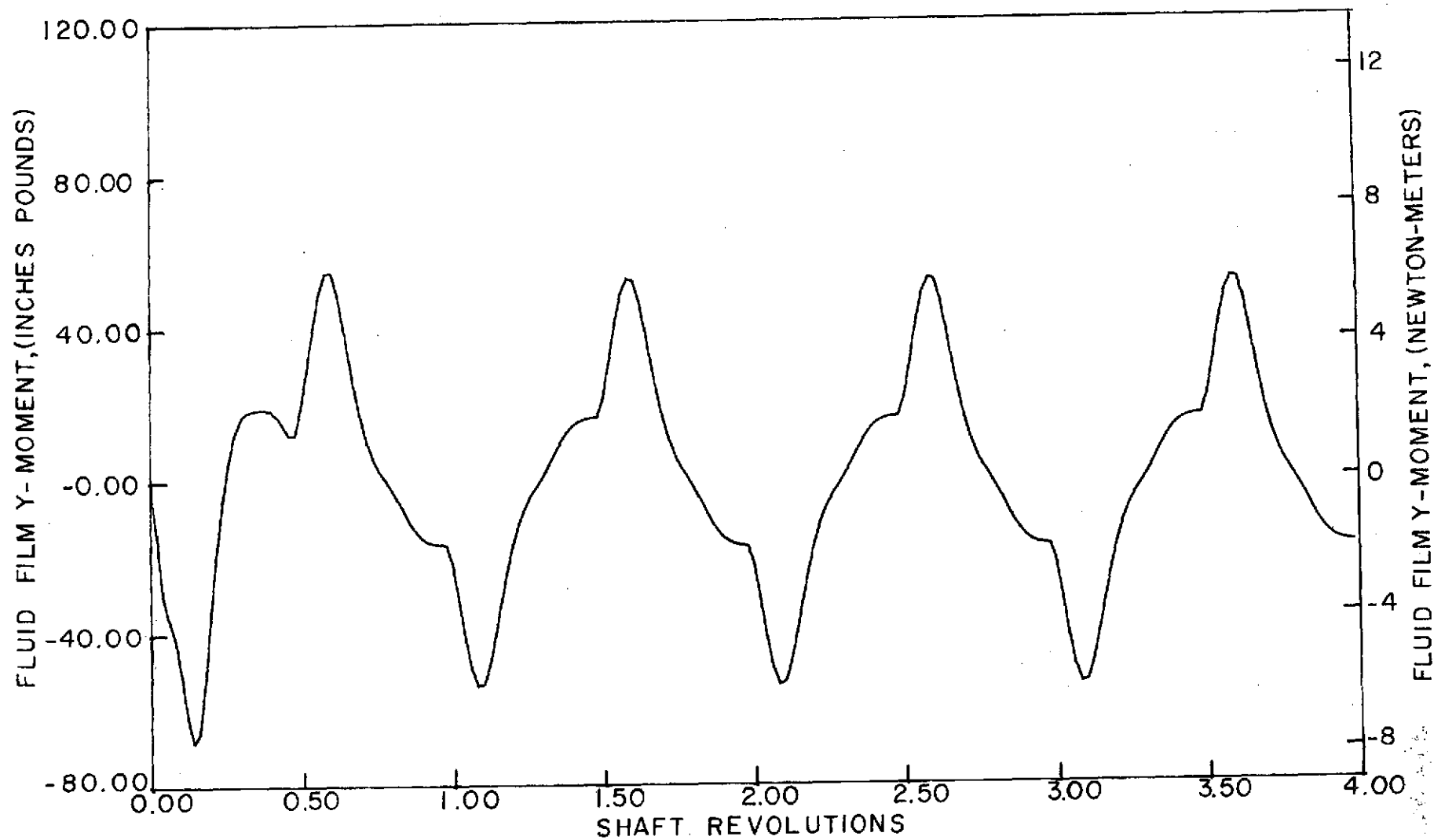


Figure B-34
Fluid-Film Moment About Y-Axis vs. Shaft Revolutions, Run 3D, Case 1

Run 4a, Case 1

Pressure = 300 psig (2068.5 kN/m²)

Runout = 0.0025 in. (63.5 μ m)

Temperature = 1000°F (537.78°C)

Friction = 0.0 lbs (0.0 N), 0.0 in.-lbs (0.0 Nm)

Speed = 500 ft/sec (152.4 m/sec)

Initial Clearance = 0.00032 in. (8.128 μ m)

Nosepiece Wt. = 1.75 lbs (7.784 N)

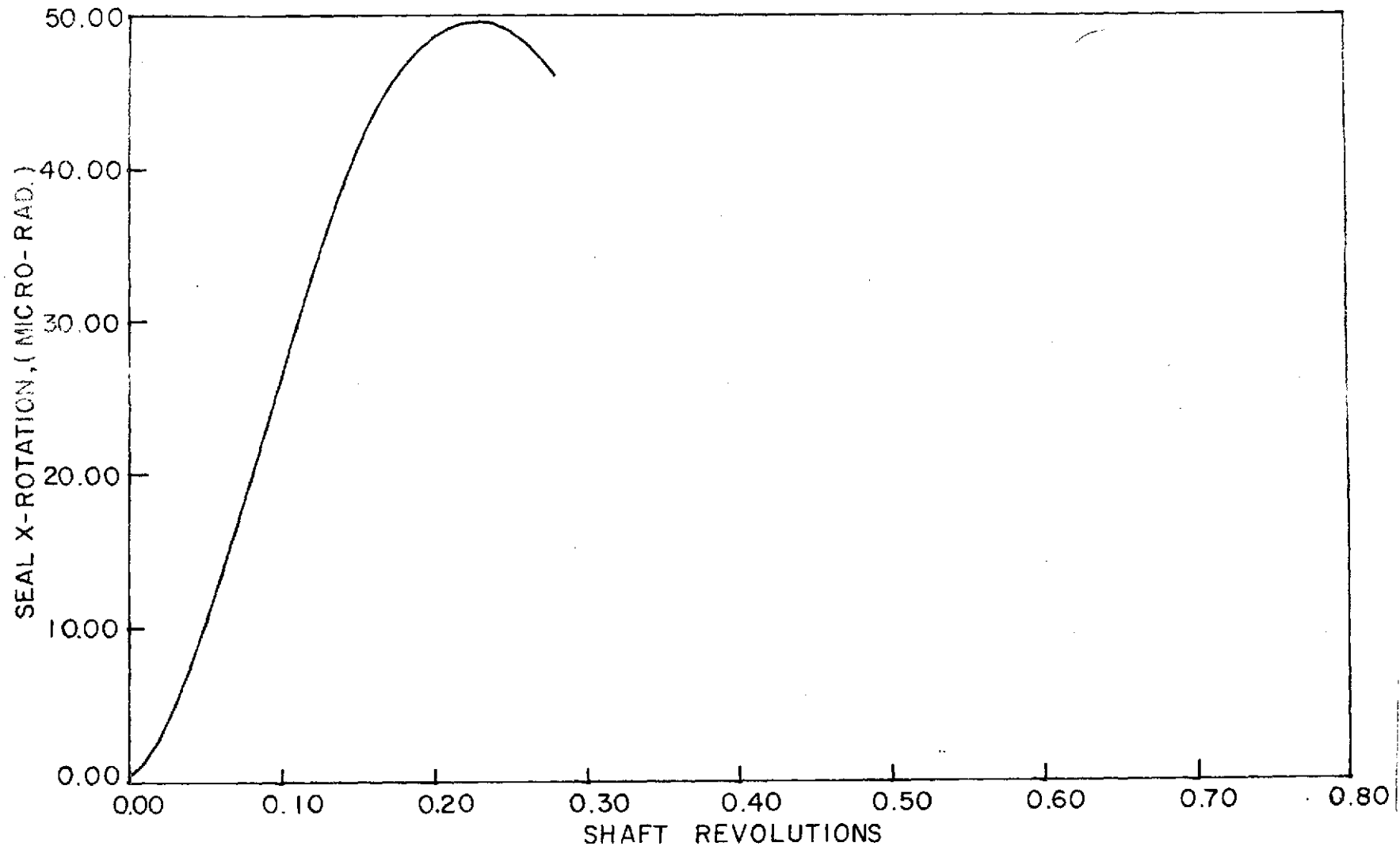


Figure B-35

Rotation About X-Axis vs. Shaft Revolutions, Run 4A, Case 1

Pressure = 300 psig (2068.5 kN/m²)

Runout = 0.0025 in. (63.5 μ m)

Temperature = 1000°F (537.78°C)

Friction = 0.0 lbs (0.0 N), 0.0 in.-lbs (0.0 Nm)

Speed = 500 ft/sec (152.4 m/sec)

Initial Clearance = 0.00032 in. (8.128 μ m)

Nosepiece Wt. = 1.75 lbs (7.784 N)

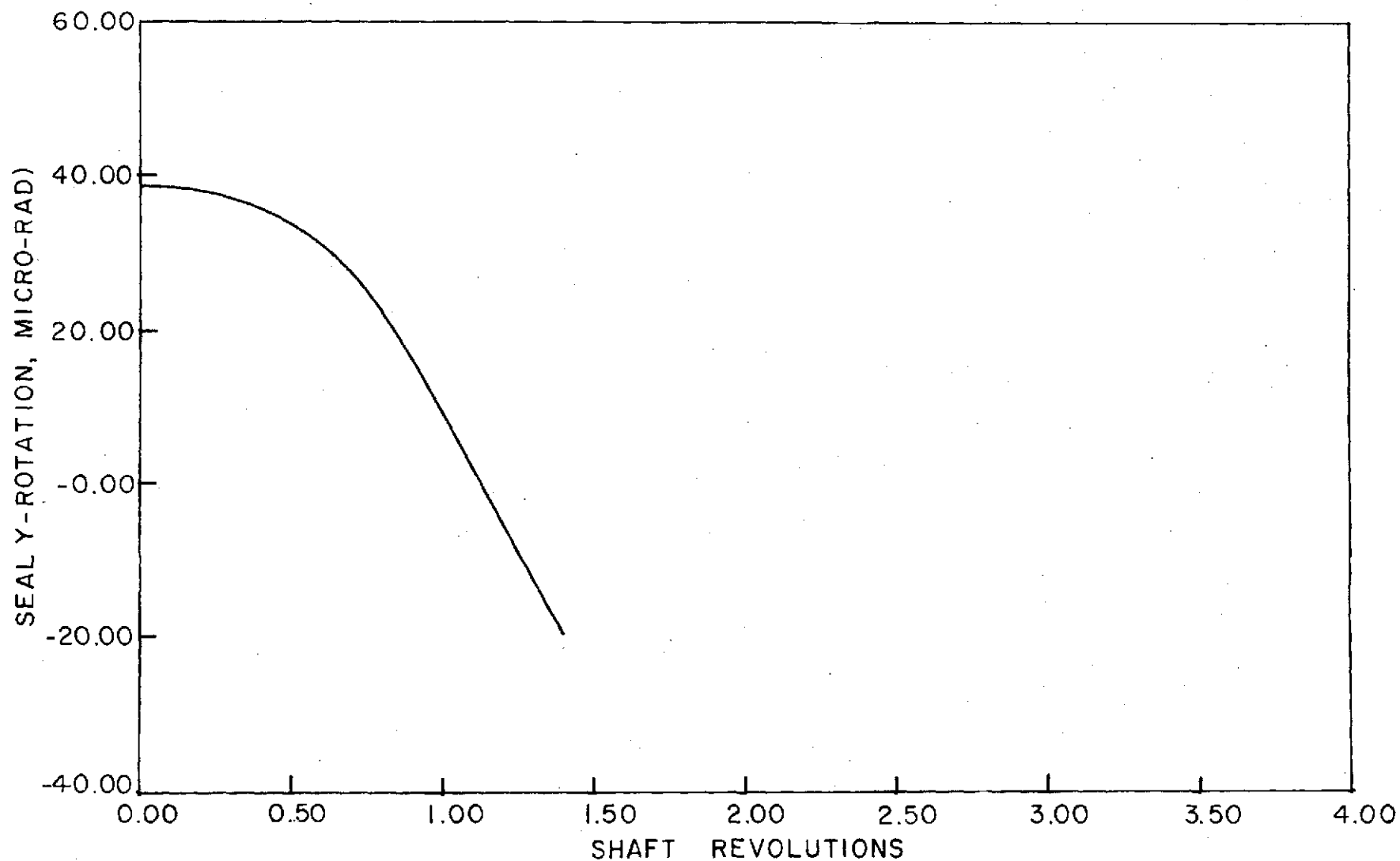


Figure B-36

Rotation About Y-Axis vs. Shaft Revolutions, Run 4A, Case 1

Pressure = 300 psig (2068.5 kN/m²)

Runout = 0.0025 in. (63.5 μm)

Temperature = 1000°F (537.78°C)

Friction = 0.0 lbs (0.0 N), 0.0 in.-lbs (0.0 Nm)

Speed = 500 ft/sec (152.4 m/sec)

Initial Clearance = 0.00032 in. (8.128 μm)

Nosepiece Wt. = 1.75 lbs (7.784 N)

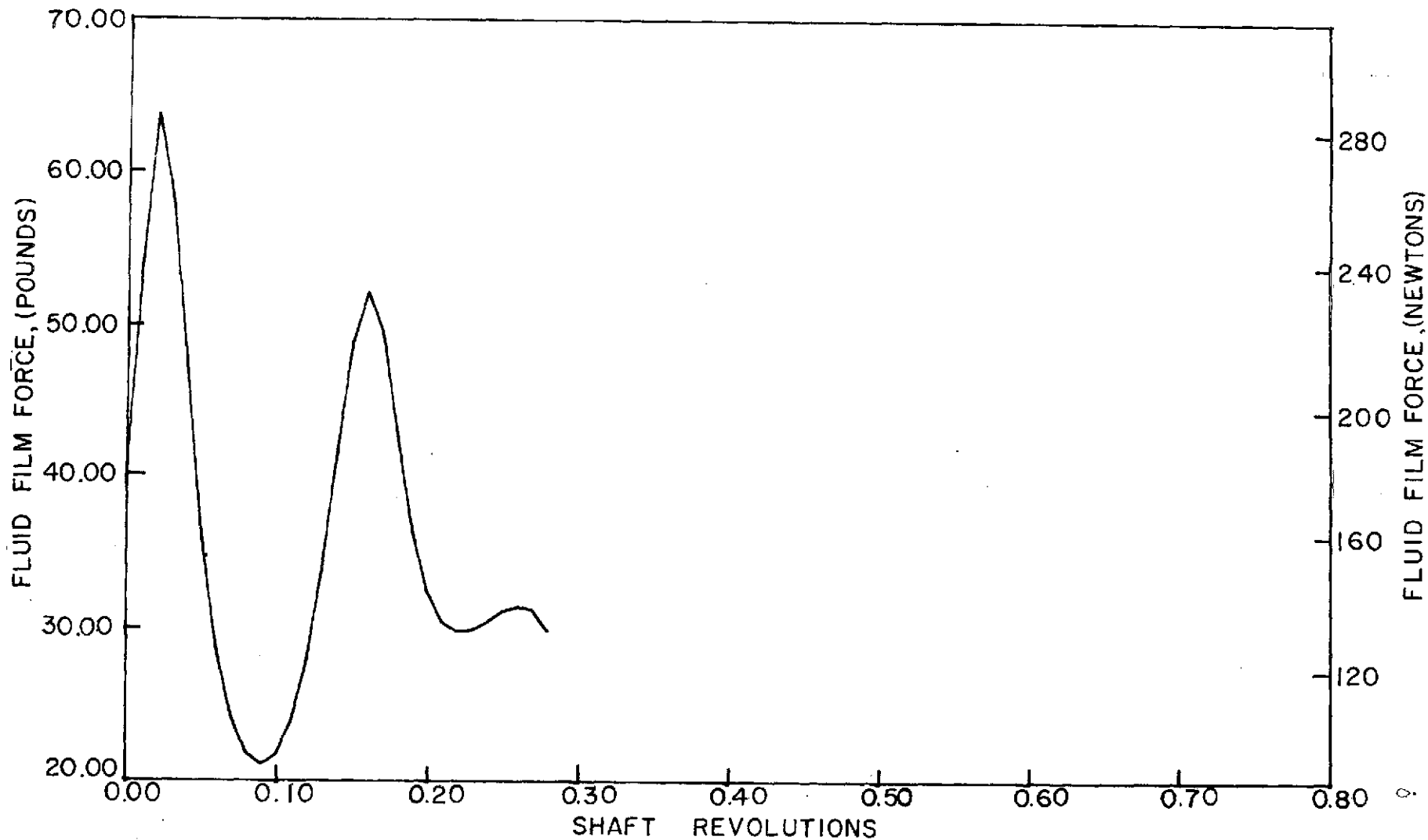


Figure B-37

Fluid-Film Force vs. Shaft Revolutions, Run 4A, Case 1

Pressure = 300 psig (2068.5 kN/m²)
Temperature = 1000°F (537.78°C)
Speed = 500 ft/sec (152.4 m/sec)
Nosepiece Wt. = 1.75 lbs (7.784 N)

Runout = 0.0025 in. (63.5 μm)
Friction = 0.0 lbs (0.0 N), 0.0 in.-lbs (0.0 Nm)
Initial Clearance = 0.00032 in. (8.128 μm)

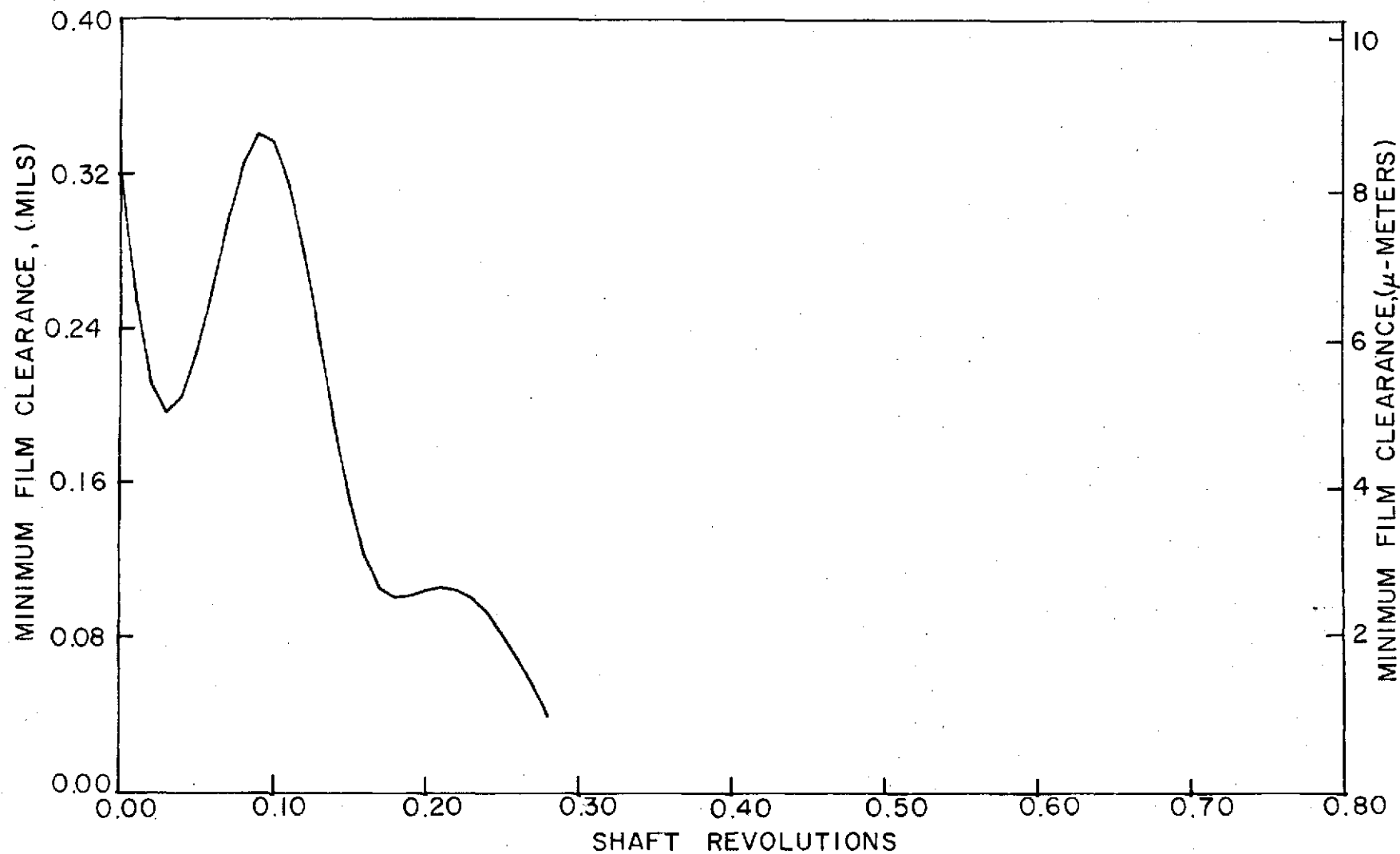


Figure B-38

Minimum Clearance vs. Shaft Revolutions, Run 4A, Case 1

Pressure = 300 psig (2068.5 kN/m²)
Temperature = 1000°F (537.78°C)
Speed = 500 ft/sec (152.4 m/sec)
Nosepiece Wt. = 1.75 lbs (7.784 N)

Runout = 0.0025 in. (63.5 μm)
Friction = 0.0 lbs (0.0 N), 0.0 in.-lbs (0.0 Nm)
Initial Clearance = 0.00032 in. (8.128 μm)

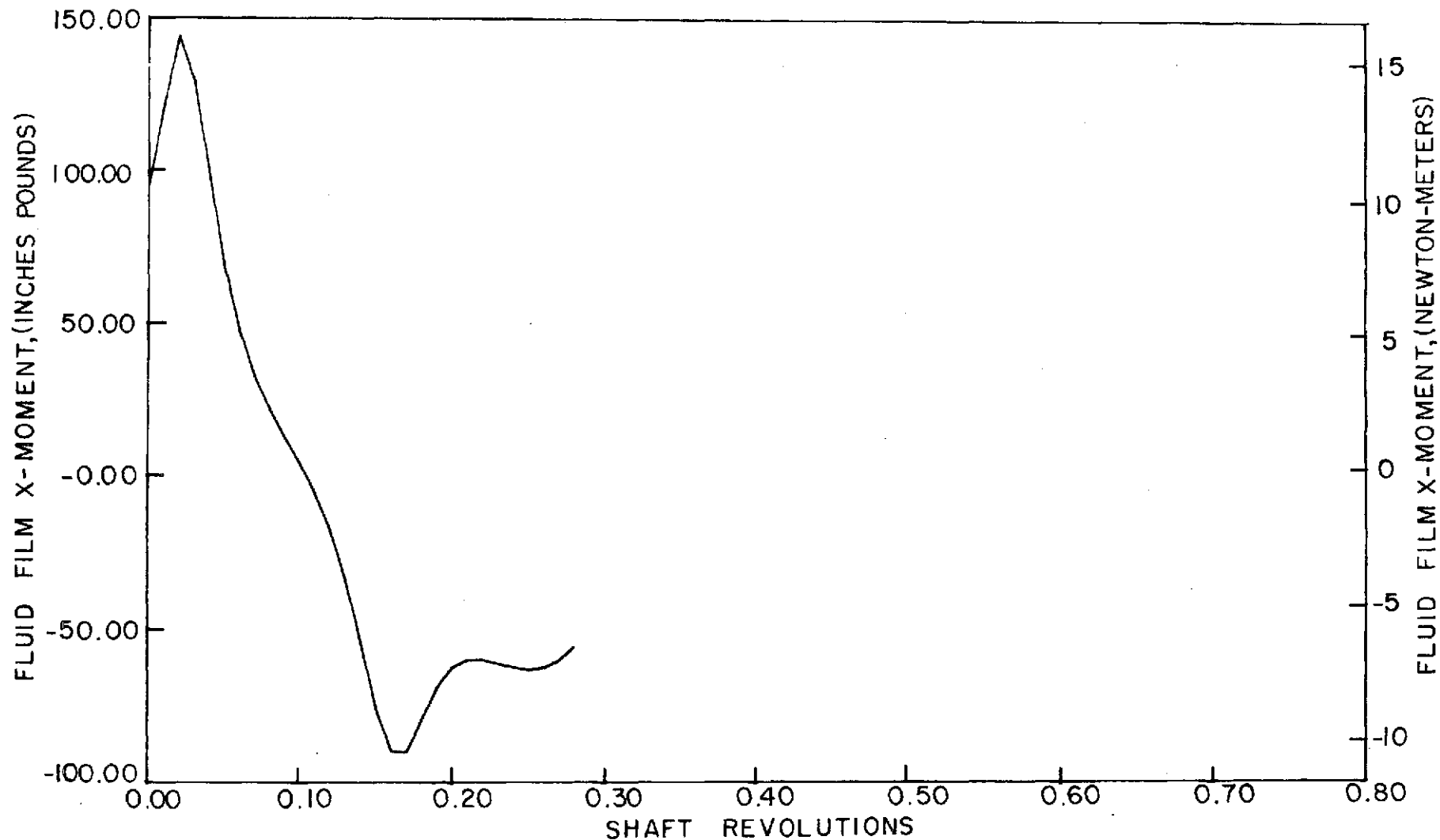


Figure B-39

Fluid-Film Moment About X-Axis vs. Shaft Revolutions, Run 4A, Case 1

Pressure = 300 psig (2068.5 kN/m²)
Temperature = 1000°F (537.78°C)
Speed = 500 ft/sec (152.4 m/sec)
Nosepiece Wt. = 1.75 lbs (7.784 N)

Runout = 0.0025 in. (63.5 μm)
Friction = 0.0 lbs (0.0 N), 0.0 in.-lbs (0.0 Nm)
Initial Clearance = 0.00032 in. (8.128 μm)

B-47

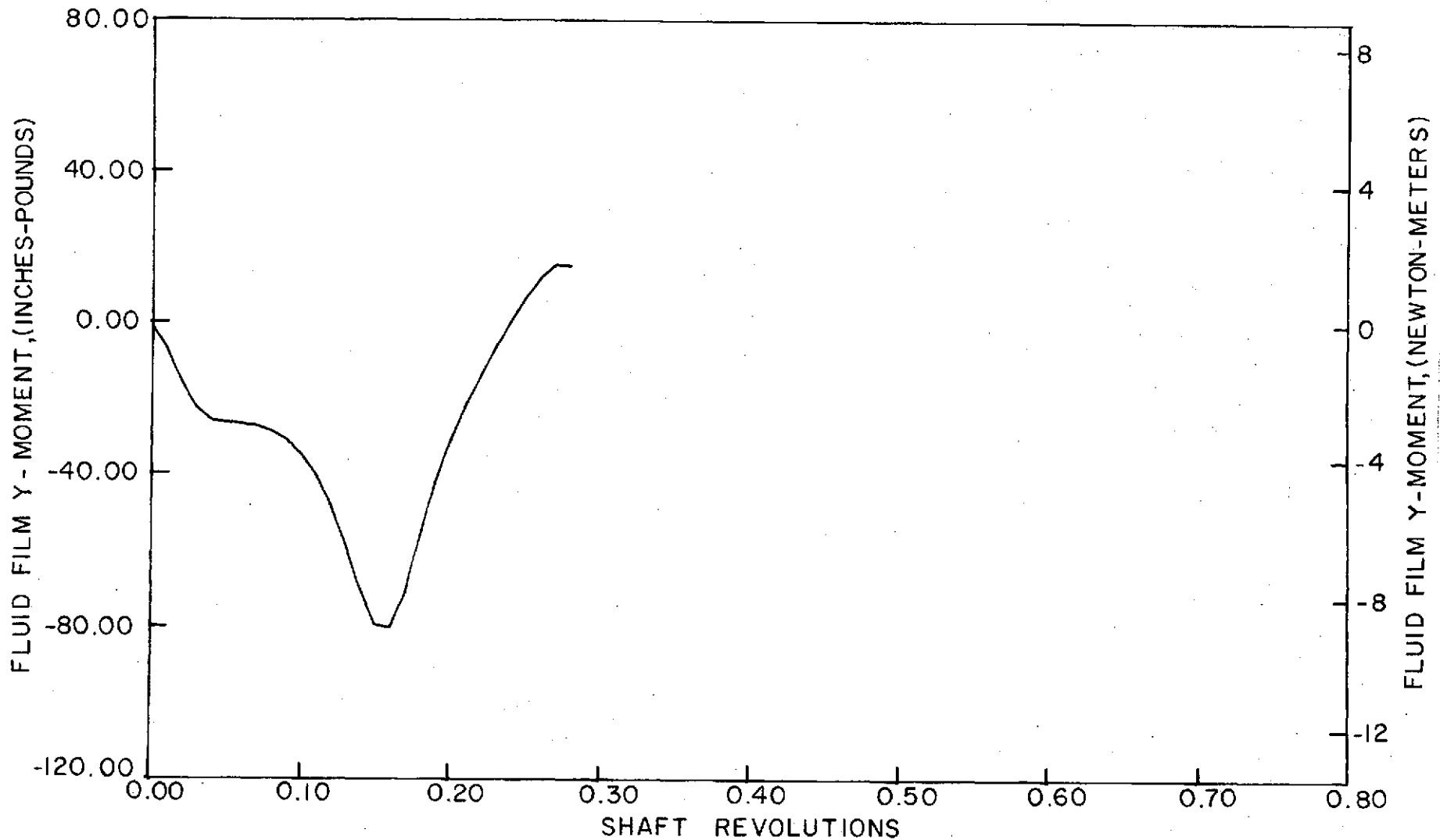


Figure B-40
Fluid-Film Moment About Y-Axis vs. Shaft Revolutions, Run 4A, Case 1

Run 5a, Case 1

Pressure = 300 psig (2068.5 kN/m²)
Temperature = 1000°F (537.78°C)
Speed = 500 ft/sec (152.4 m/sec)
Nosepiece Wt. = 1.75 lbs (7.784 N)

Runout = 0.0025 in. (63.5 μm)
Friction = 4.0 lbs (17.792 N), 52.0 in.-lbs (5.875 Nm)
Initial Clearance = 0.00032 in. (8.128 μm)

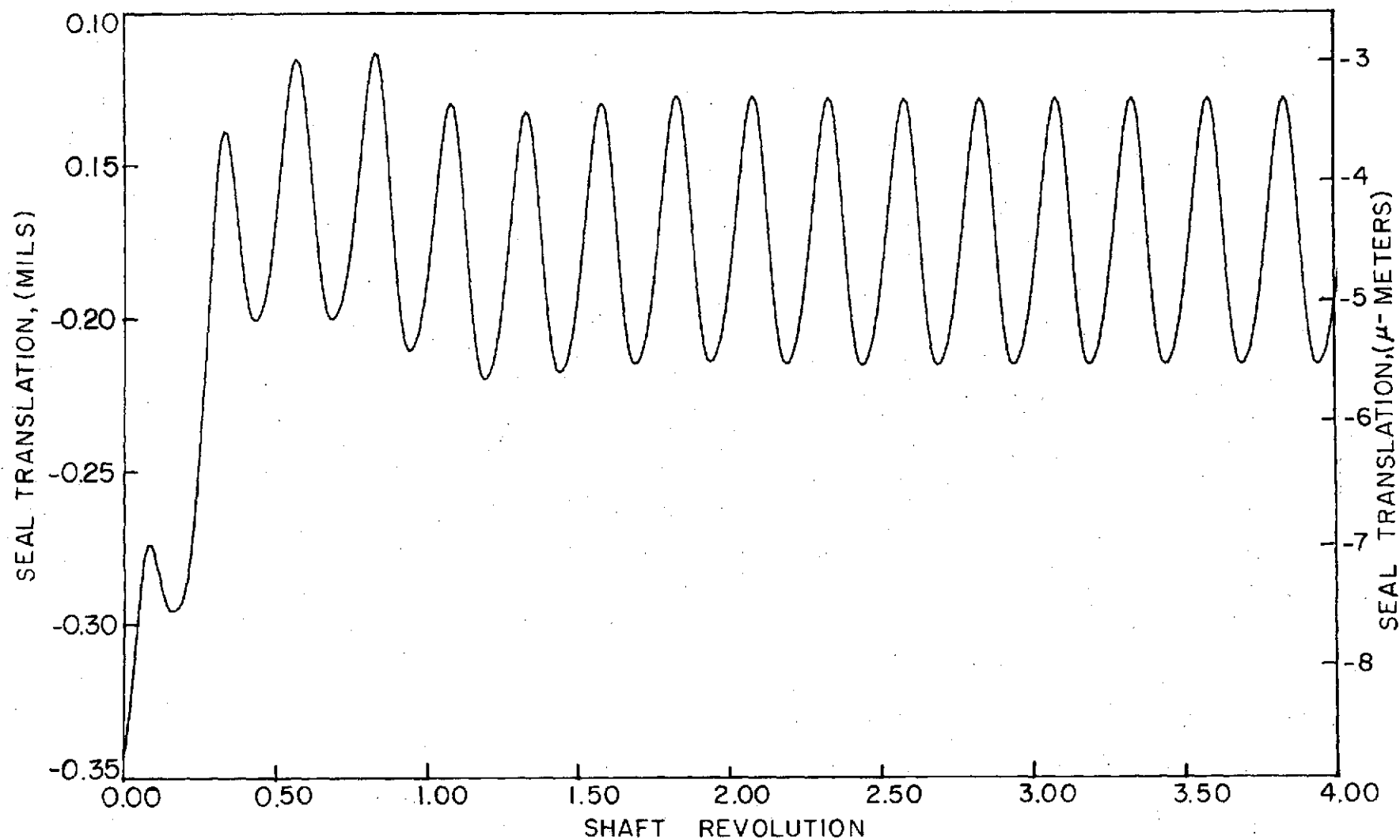


Figure B-41

Seal Translation vs. Shaft Revolutions, Case 1, Run 5A

Pressure = 300 psig (2068.5 kN/m²)

Runout = 0.0025 in. (63.5 μ m)

Temperature = 1000°F (537.78°C)

Friction = 4.0 lbs (17.792 N), 52.0 in.-lbs (5.875 Nm)

Speed = 500 ft/sec (152.4 m/sec)

Initial Clearance = 0.00032 in. (8.128 μ m)

Nosepiece Wt. = 1.75 lbs (7.784 N)

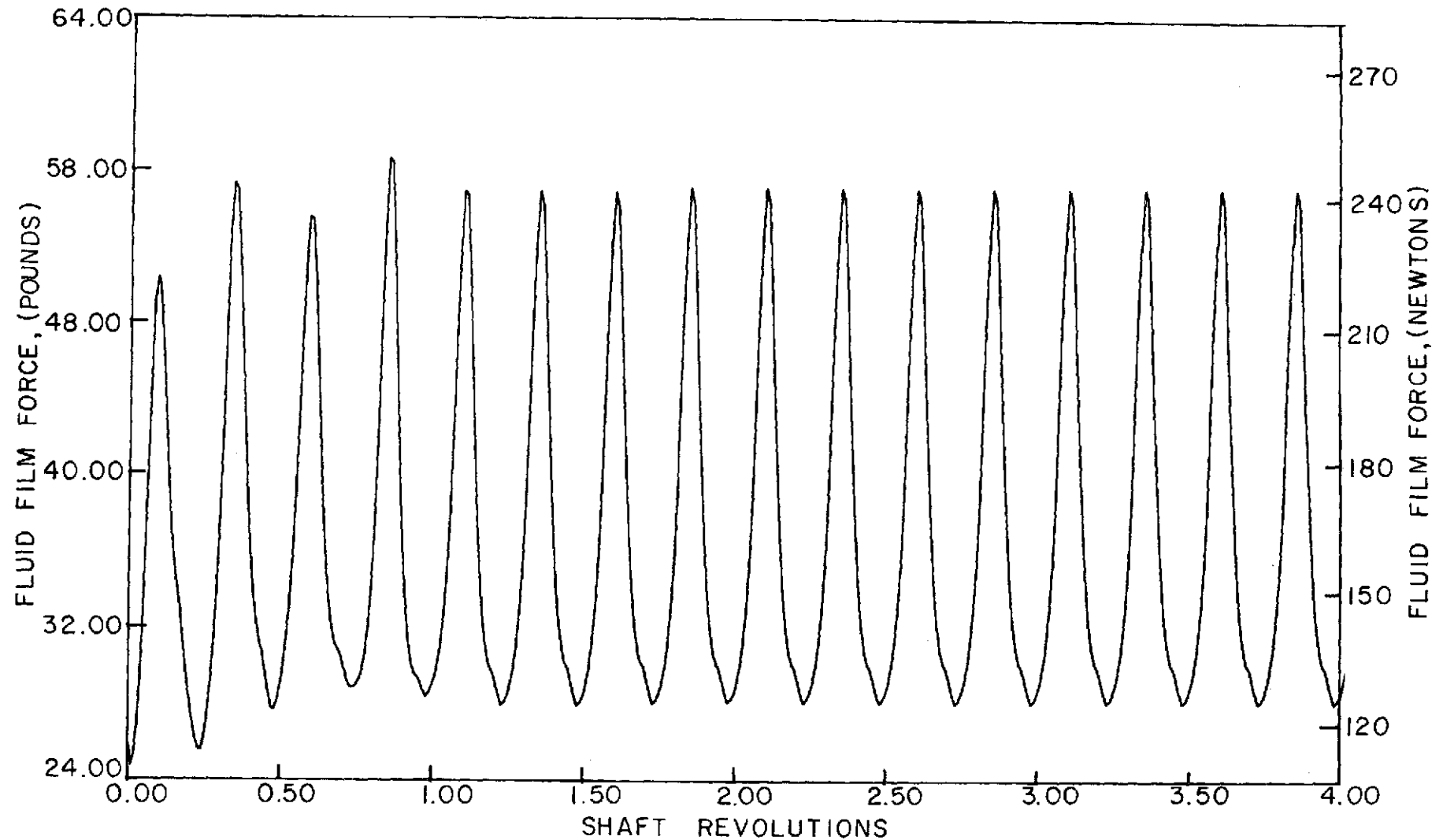


Figure B-42

Fluid-Film Force vs. Shaft Revolutions, Case 1, Run 5A

Pressure = 300 psig (2068.5 kN/m²)
Temperature = 1000°F (537.78°C)
Speed = 500 ft/sec (152.4 m/sec)
Nosepiece Wt. = 1.75 lbs (7.784 N)

Runout = 0.0025 in. (63.5 μm)
Friction = 4.0 lbs (17.792 N), 52.0 in.-lbs (5.875 Nm)
Initial Clearance = 0.00032 in. (8.128 μm)

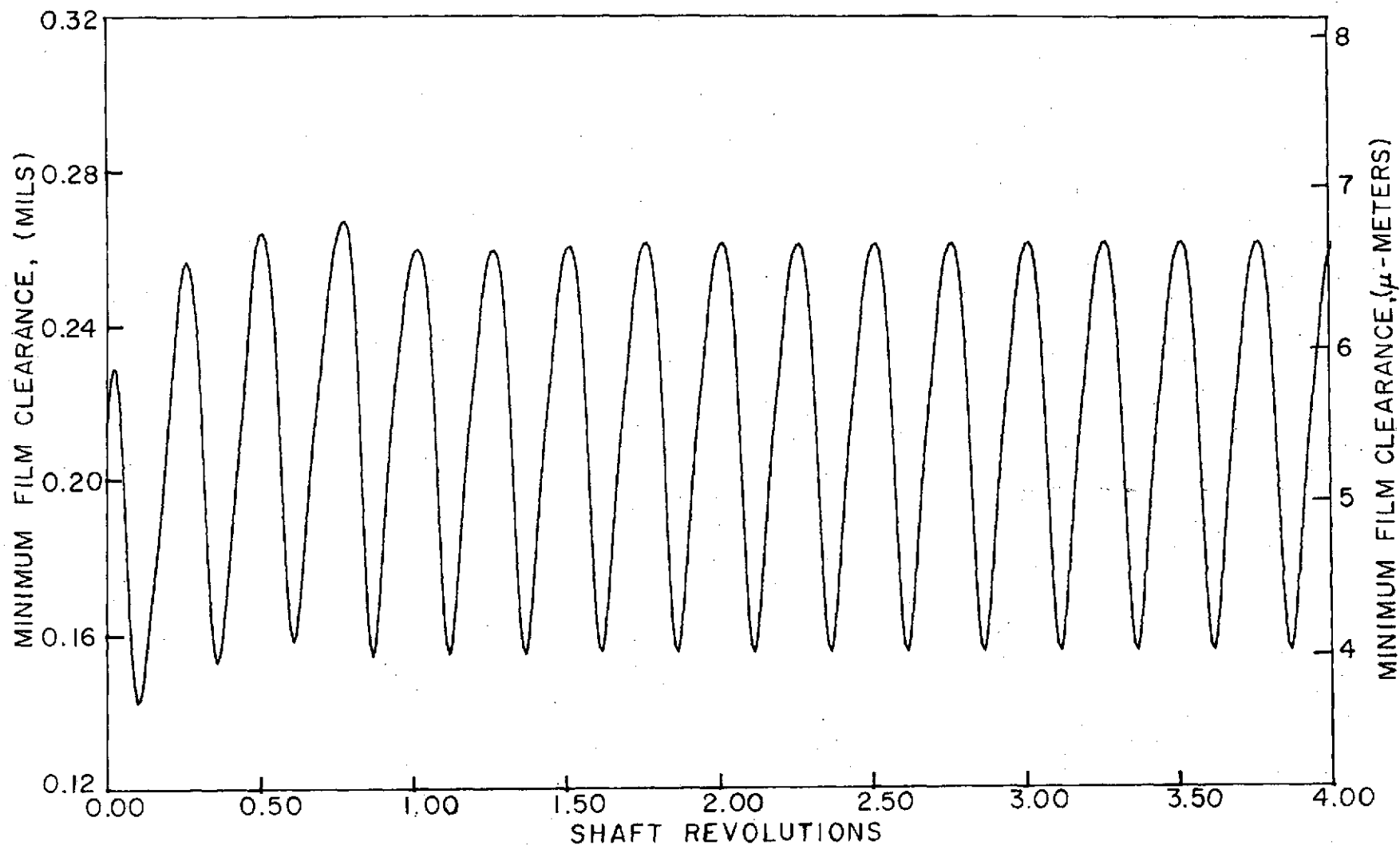


Figure B-43

Minimum Clearance vs. Shaft Revolutions, Case 1, Run 5A

Pressure = 300 psig (2068.5 kN/m²)
Temperature = 1000°F (537.78°C)
Speed = 500 ft/sec (152.4 m/sec)
Nosepiece Wt. = 1.75 lbs (7.784 N)

Runout = 0.0025 in. (63.5 μm)

Friction = 4.0 lbs (17.792 N), 52.0 in.-lbs (5.875 Nm)

Initial Clearance = 0.00032 in. (8.128 μm)

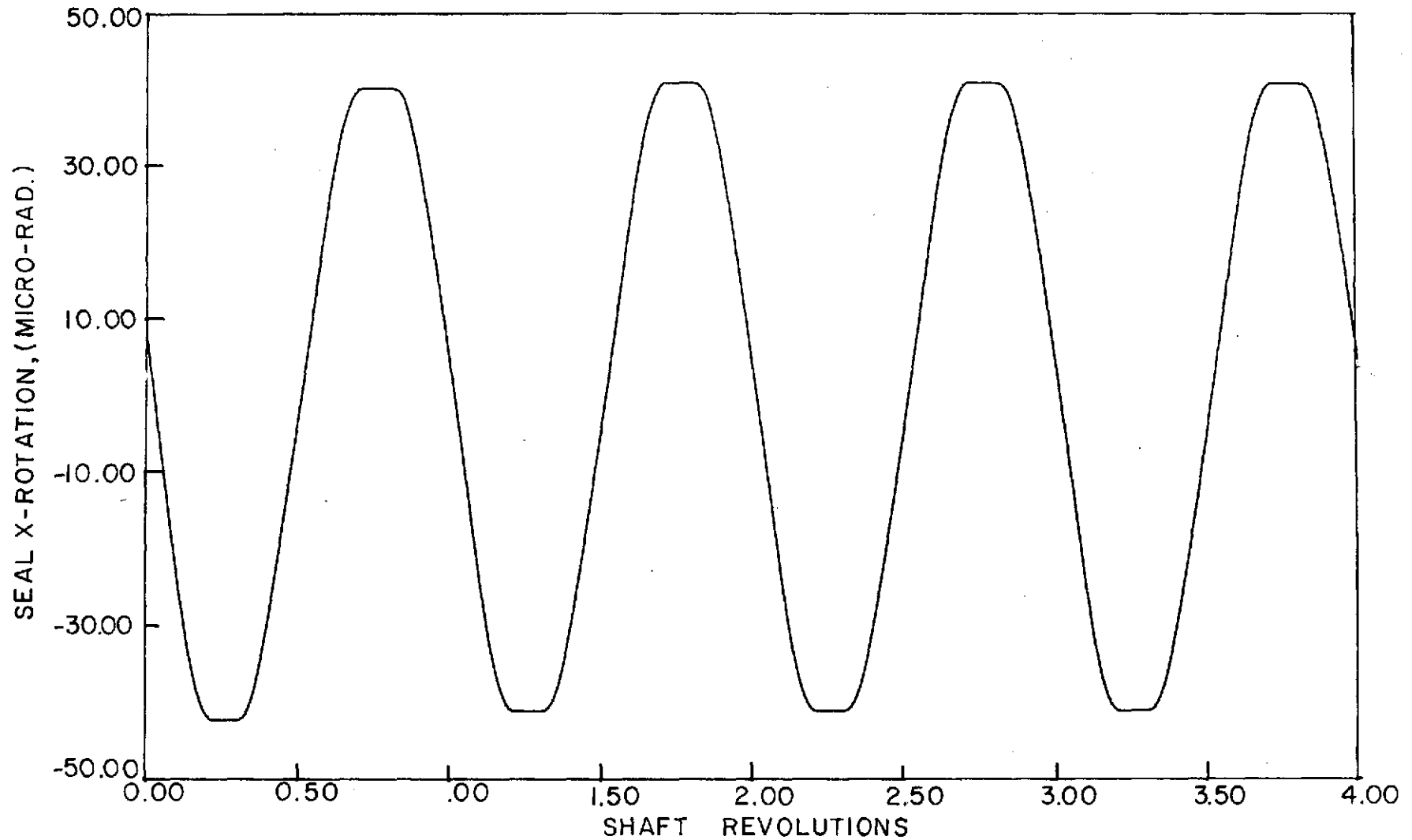


Figure B-44

Rotation About X-Axis vs. Shaft Revolutions, Case 1, Run 5A

Pressure = 300 psig (2068.5 kN/m²)
Temperature = 1000°F (537.78°C)
Speed = 500 ft/sec (152.4 m/sec)
Nosepiece Wt. = 1.75 lbs (7.784 N)

Runout = 0.0025 in. (63.5 μm)
Friction = 4.0 lbs (17.792 N), 52.0 in.-lbs (5.875 Nm)
Initial Clearance = 0.00032 in. (8.128 μm)

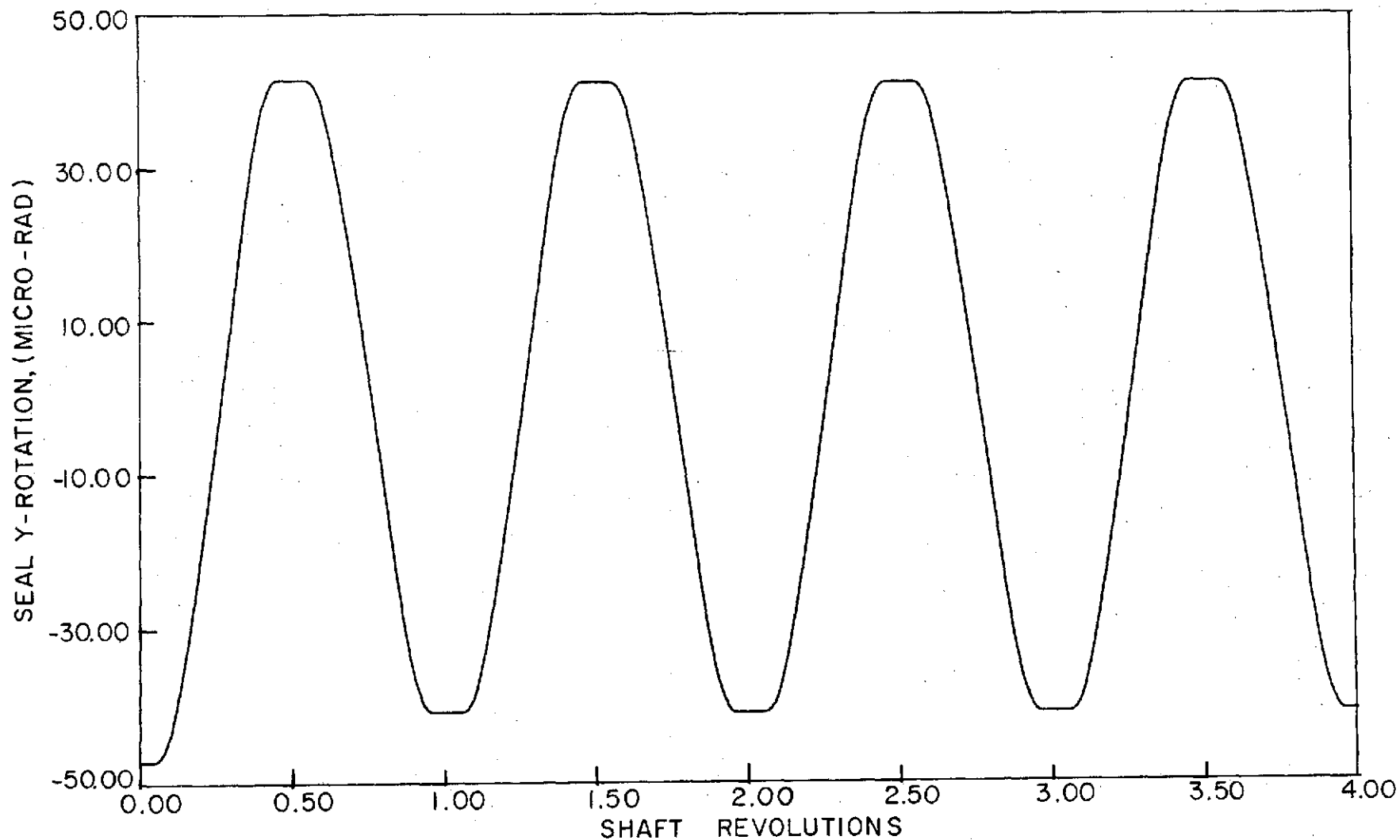


Figure B-45
Rotation About Y-Axis vs. Shaft Revolutions, Case 1, Run 5A

Pressure = 300 psig (2068.5 kN/m²)
Temperature = 1000°F (537.78°C)
Speed = 500 ft/sec (152.4 m/sec)
Nosepiece Wt. = 1.75 lbs (7.784 N)

Runout = 0.0025 in. (63.5 μm)
Friction = 4.0 lbs (17.792 N), 52.0 in.-lbs (5.875 Nm)
Initial Clearance = 0.00032 in. (8.128 μm)

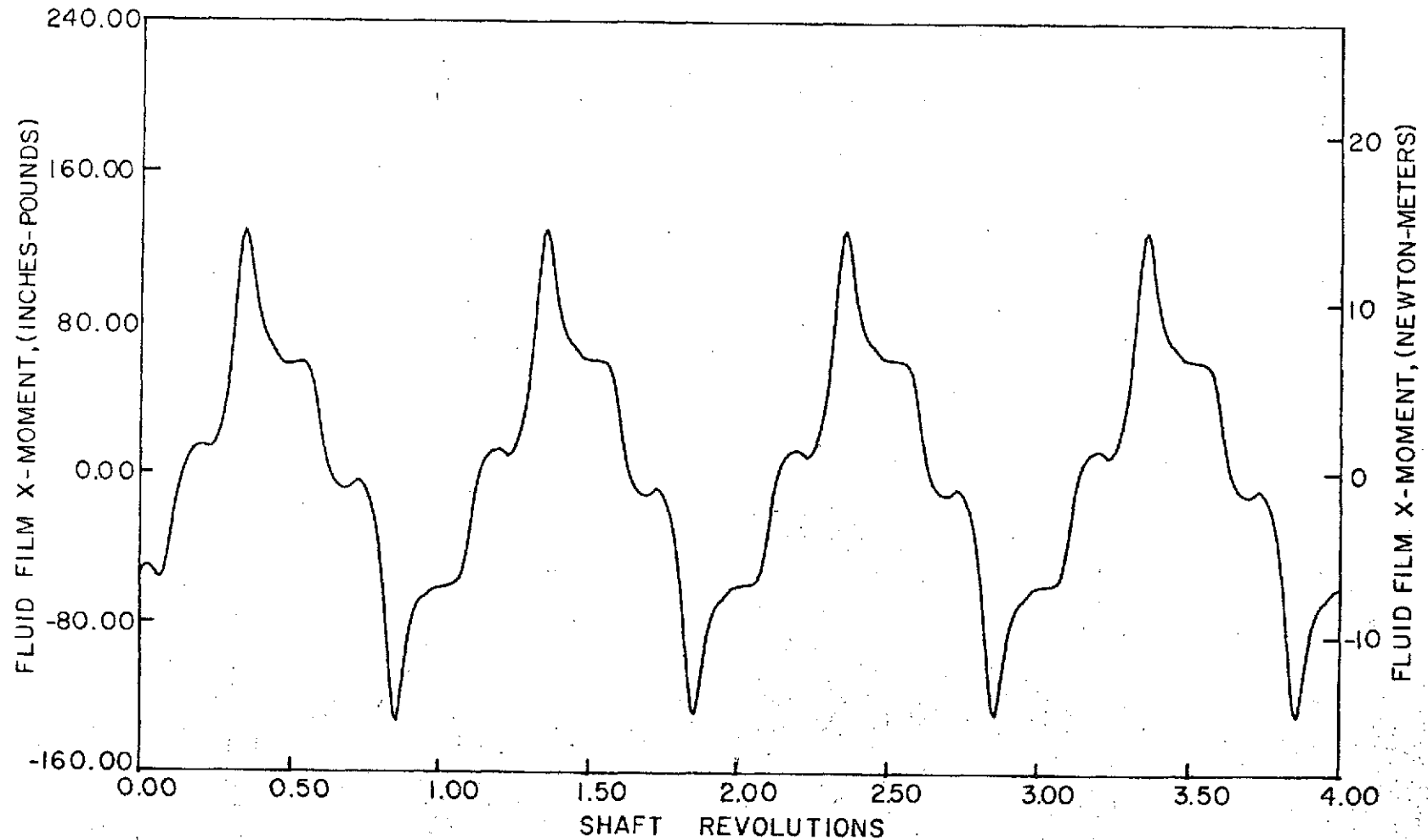


Figure B-46

Fluid-Film Moment About X-Axis vs. Shaft Revolutions, Case 1, Run 5A

Pressure = 300 psig (2068.5 kN/m²)

Runout = 0.0025 in. (63.5 μ m)

Temperature = 1000°F (537.78°C)

Friction = 4.0 lbs (17.792 N), 52.0 in.-lbs (5.875 Nm)

Speed = 500 ft/sec (152.4 m/sec)

Initial Clearance = 0.00032 in. (8.128 μ m)

Nosepiece Wt. = 1.75 lbs (7.784 N)

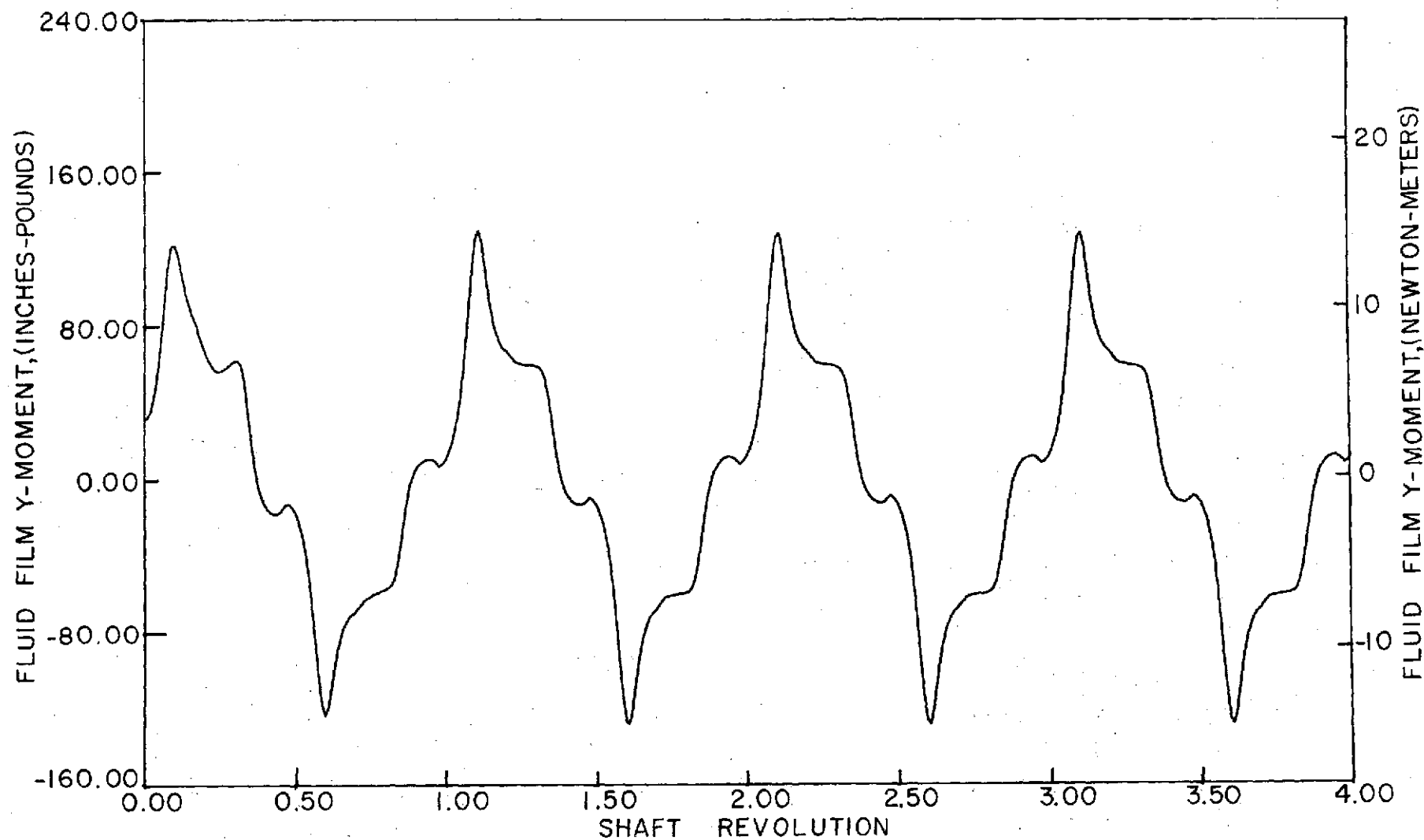
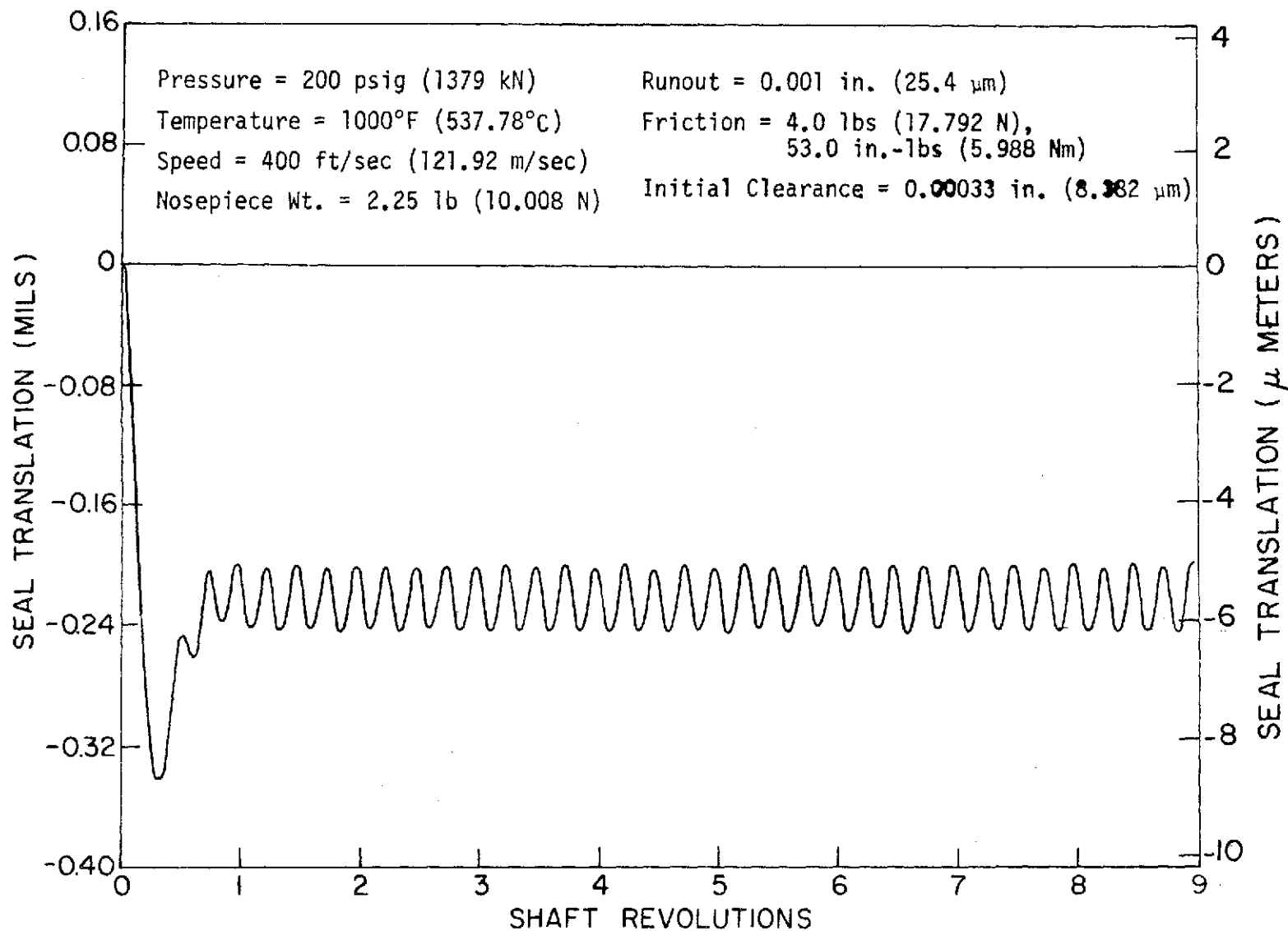


Figure B-47

Fluid-Film Moment About Y-Axis vs. Shaft Revolutions, Case 1, Run 5A

Figure B-48 . Seal Translation vs. Shaft Revolutions for Case 2



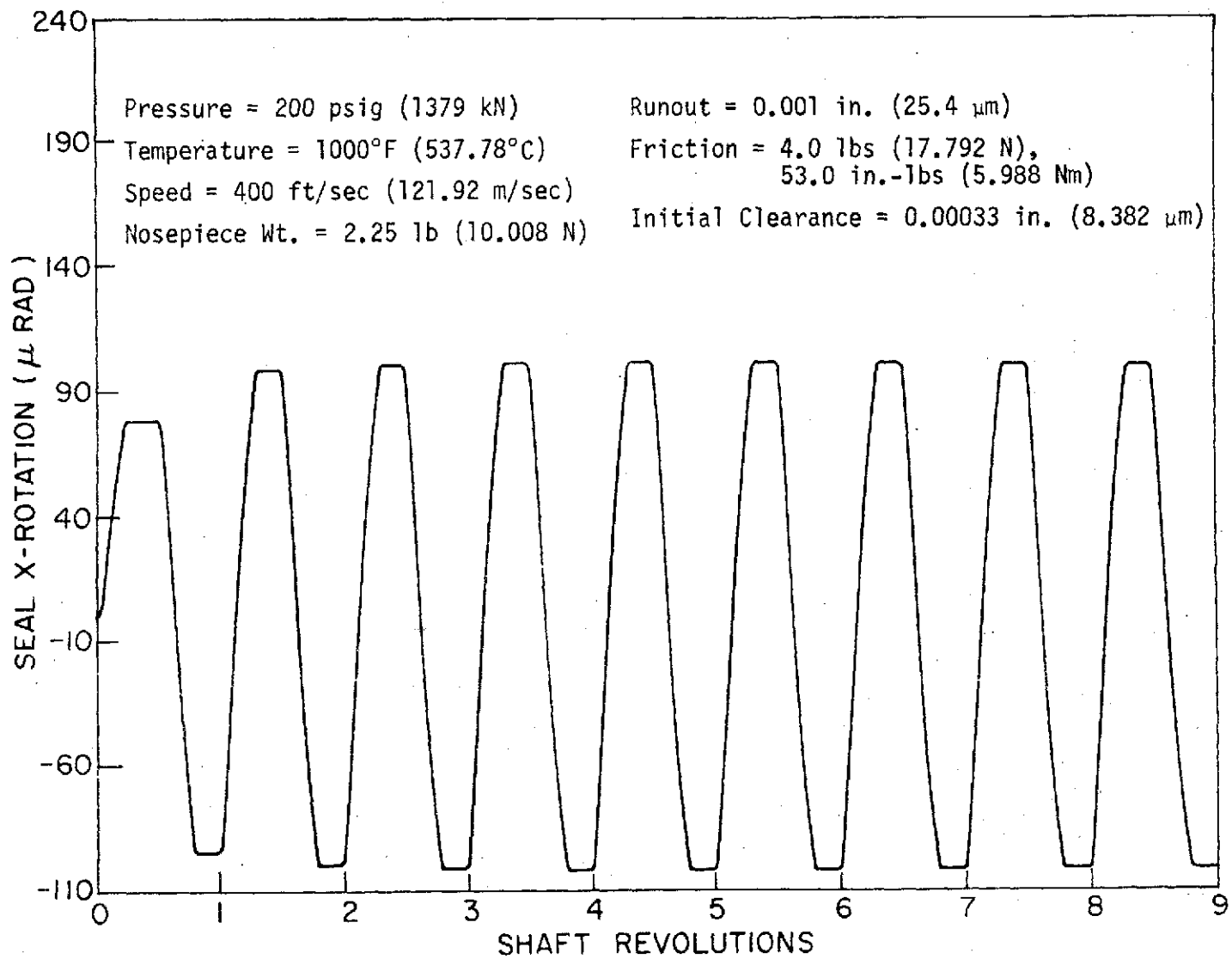


Figure B-49 . Seal Rotation about X-Axis vs. Shaft Revolutions for Case 2

Figure B-50 . Seal Rotation about Y-Axis vs. Shaft Revolutions for Case 2

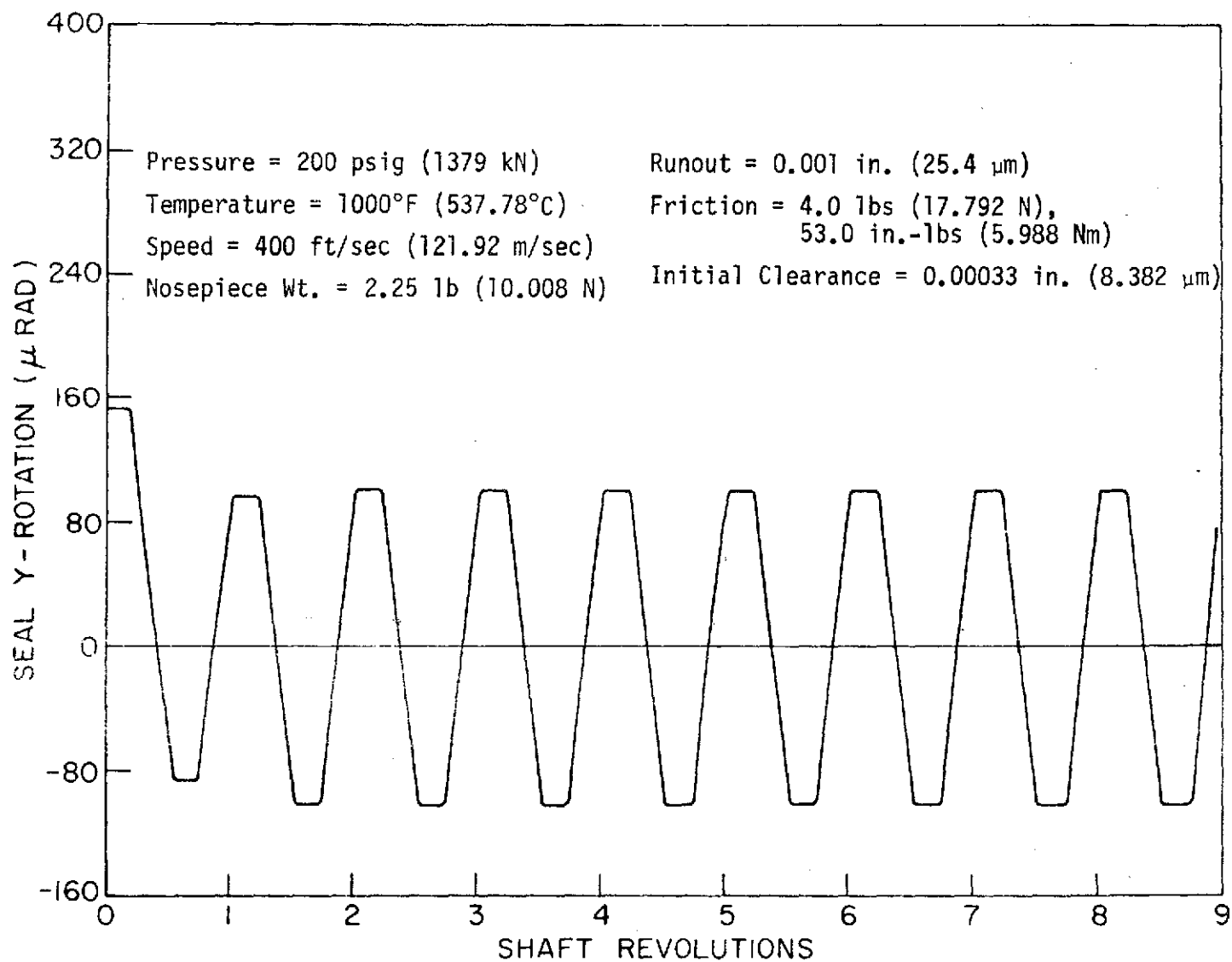


Figure B-51 . Minimum Film Thickness vs. Shaft Revolutions for Case 2

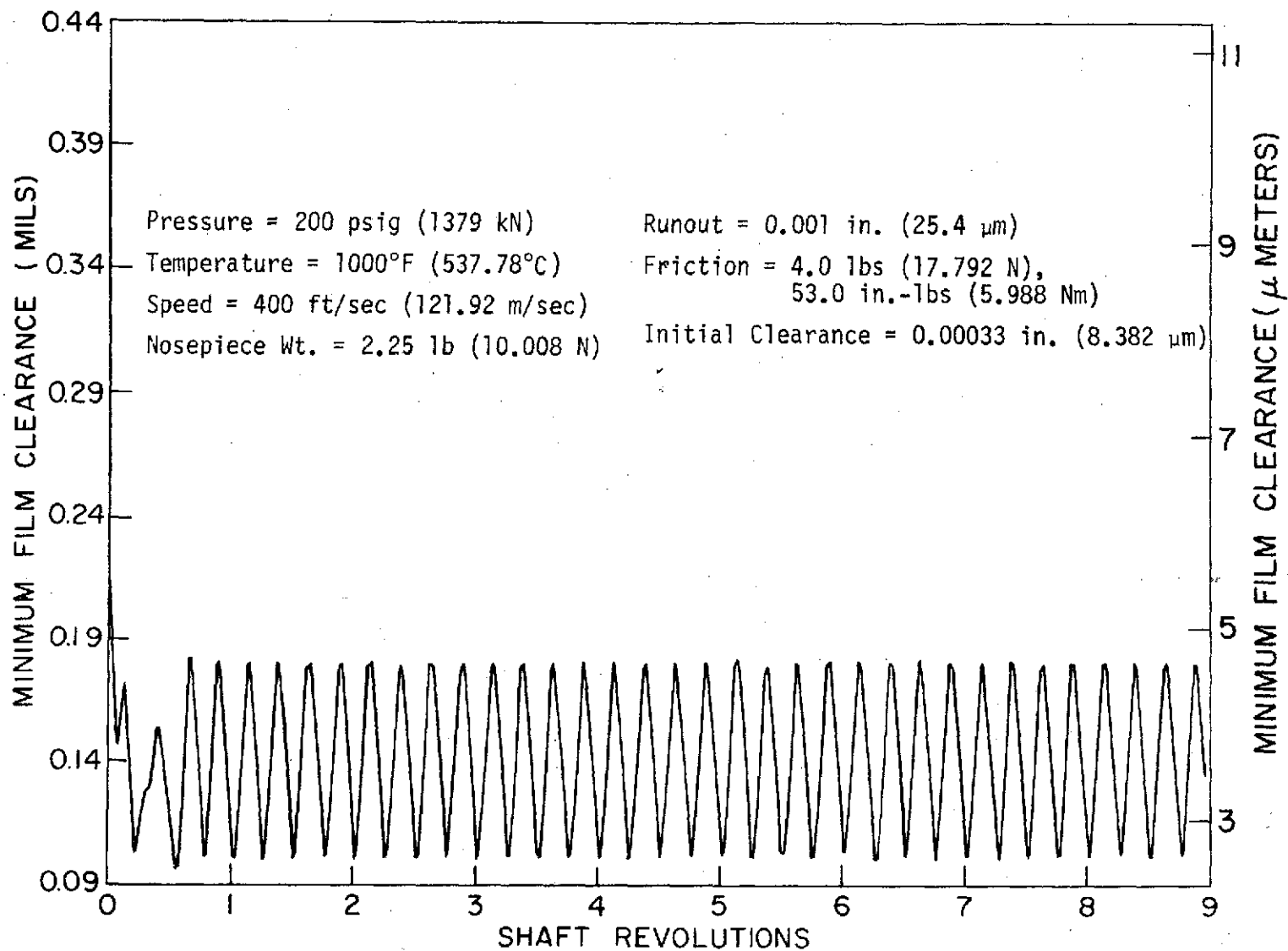
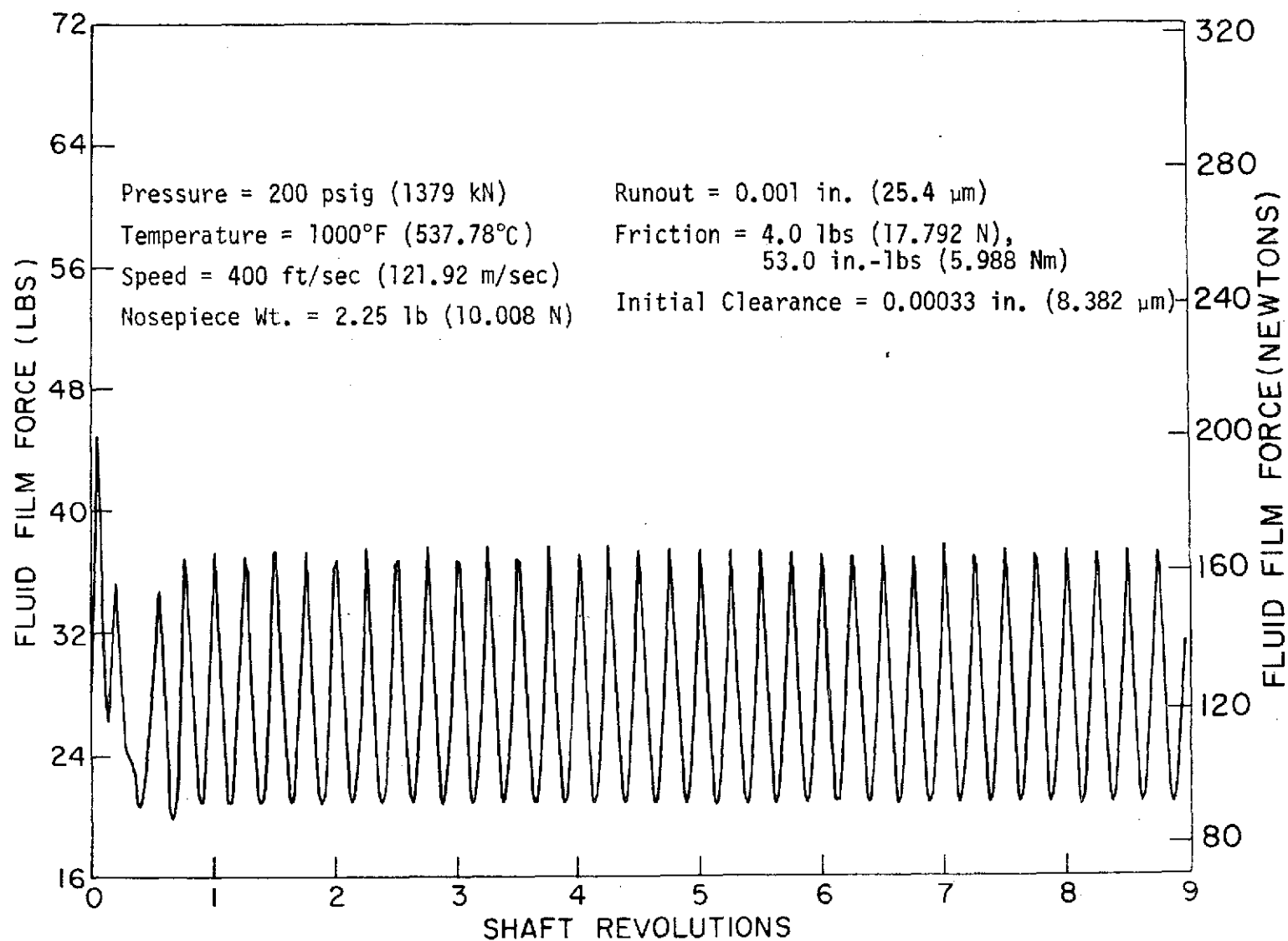


Figure B-52. Fluid Film Force vs. Shaft Revolutions for Case 2



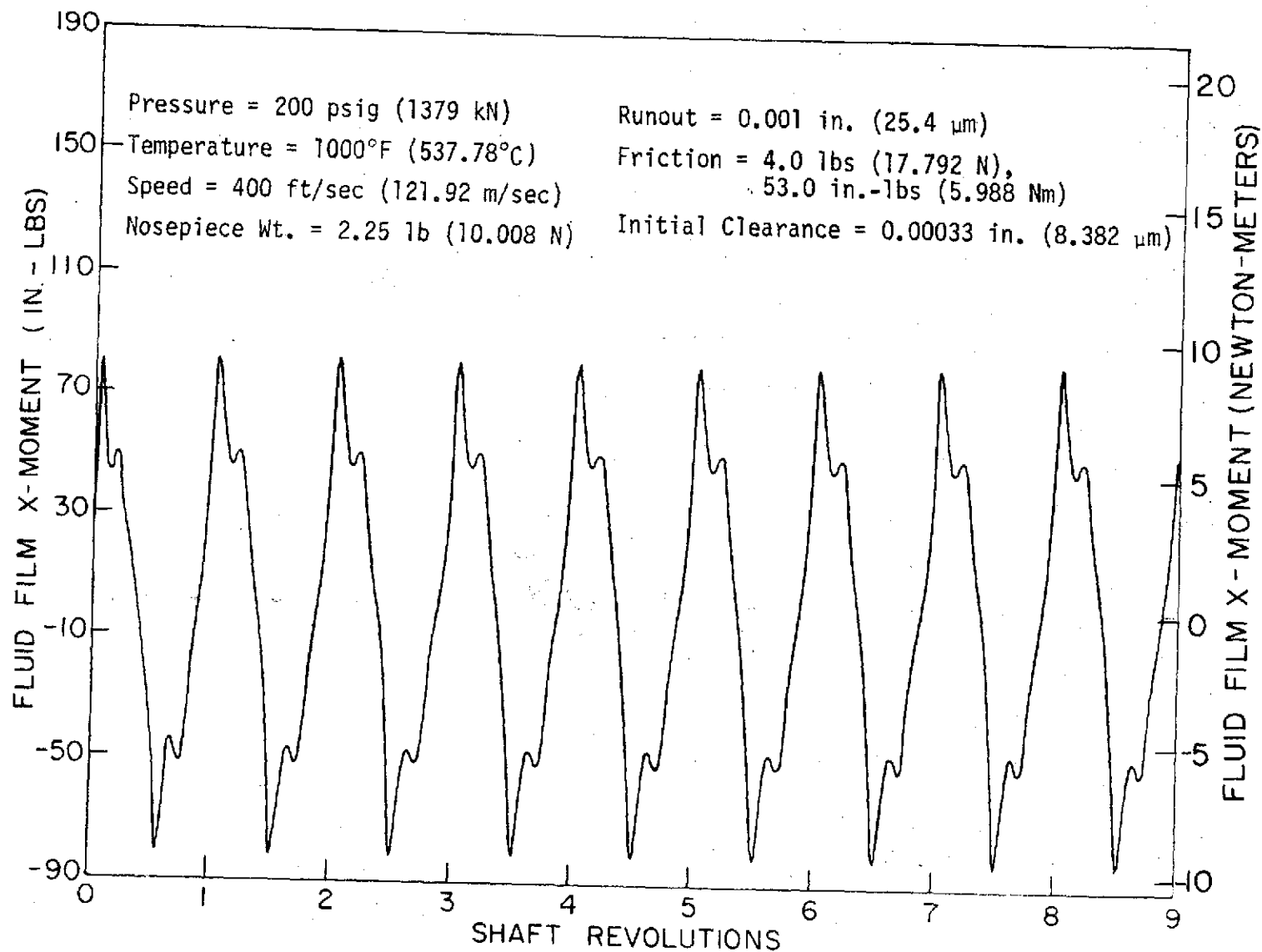


Figure B-53. Fluid Film Moment about X-Axis vs. Shaft Revolutions for Case 2

Figure B-54 . Fluid Film Moment about Y-Axis vs. Shaft Revolutions for Case 2

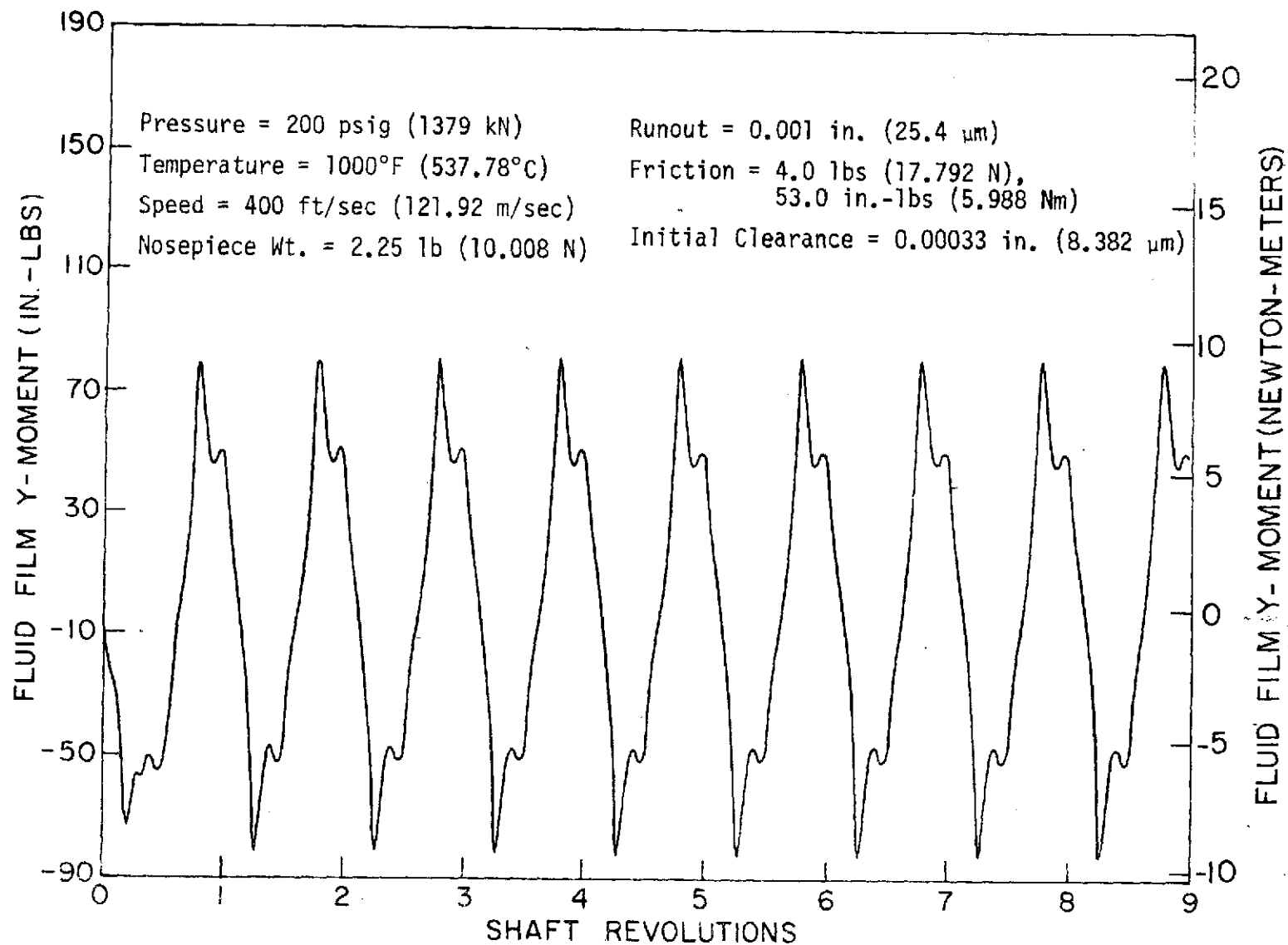
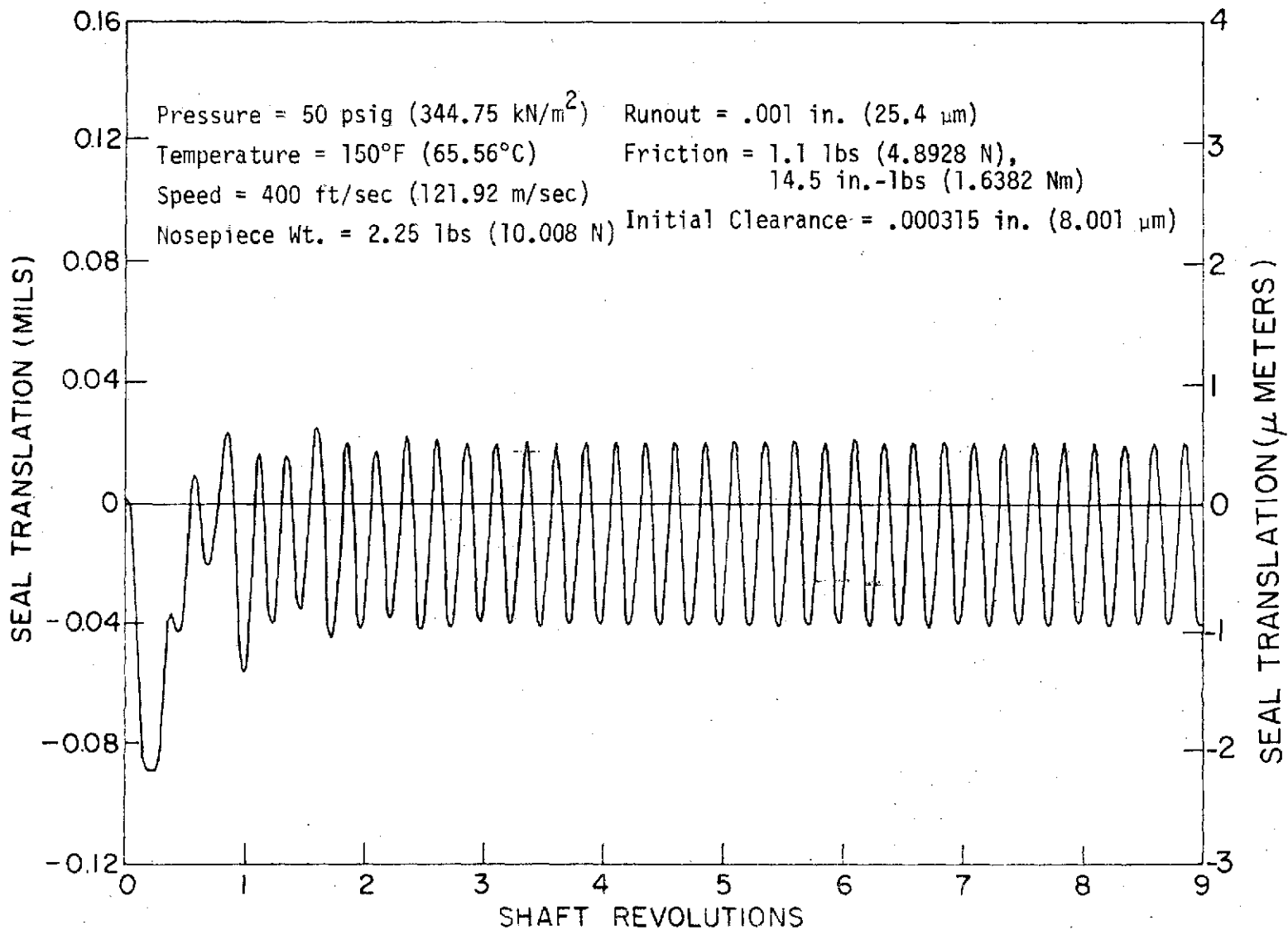


Figure B-55. Seal Translation vs. Shaft Revolutions for Case 3



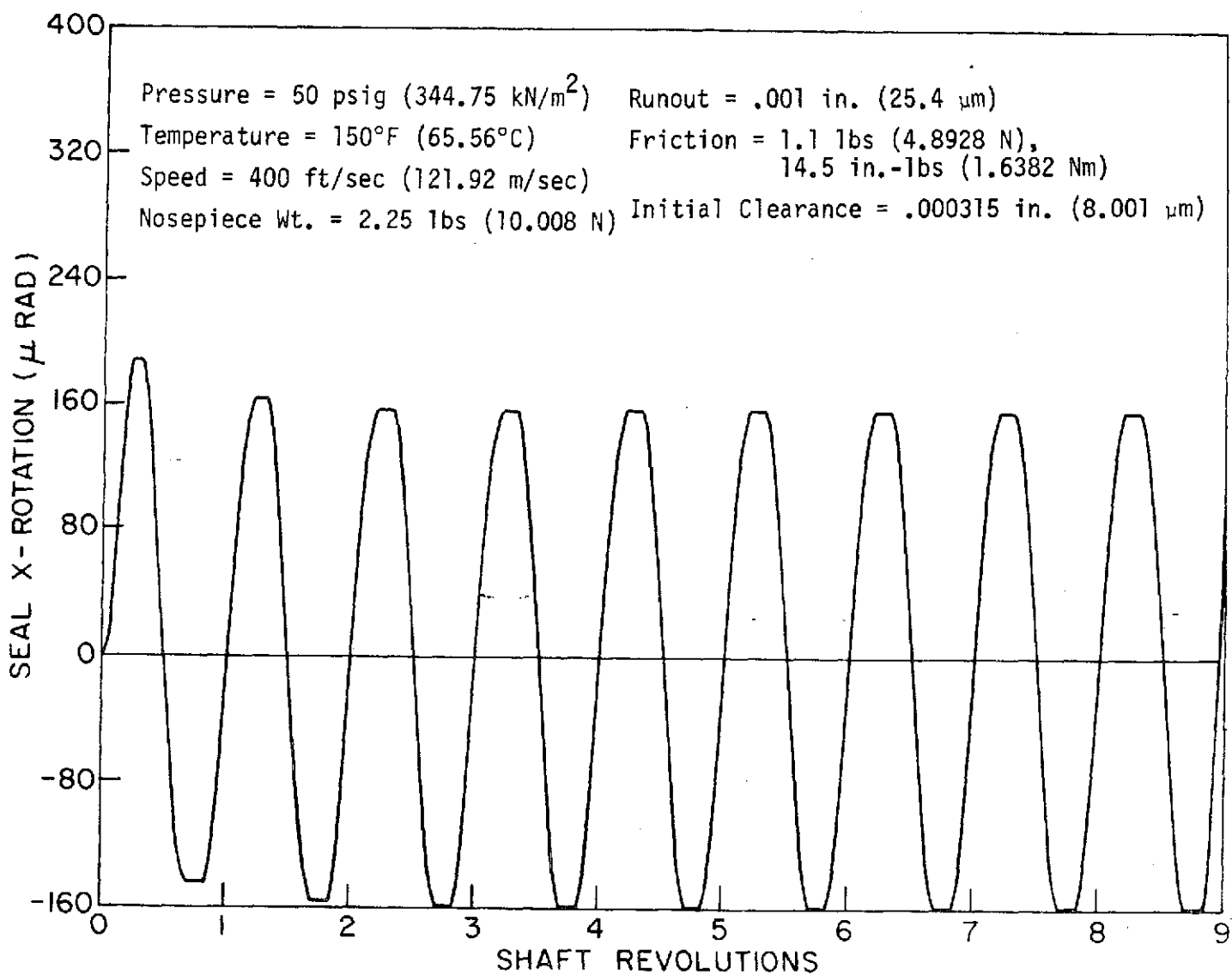


Figure B-56. Seal Rotation about X-Axis vs. Shaft Revolutions for Case 3

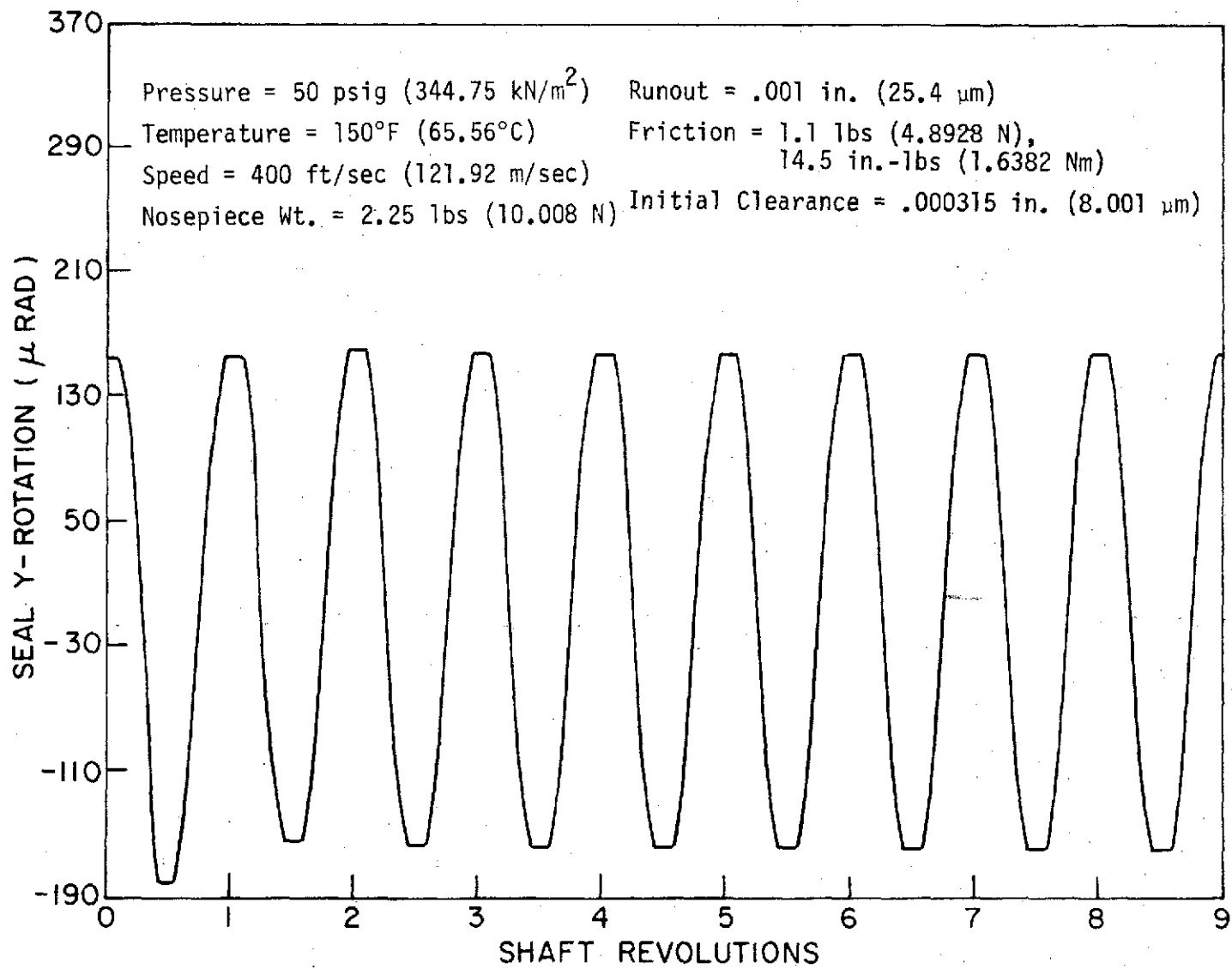


Figure B-57. Seal Rotation about Y-Axis vs. Shaft Revolutions for Case 3

Figure B-58 . Minimum Film Thickness vs. Shaft Revolutions for Case 3

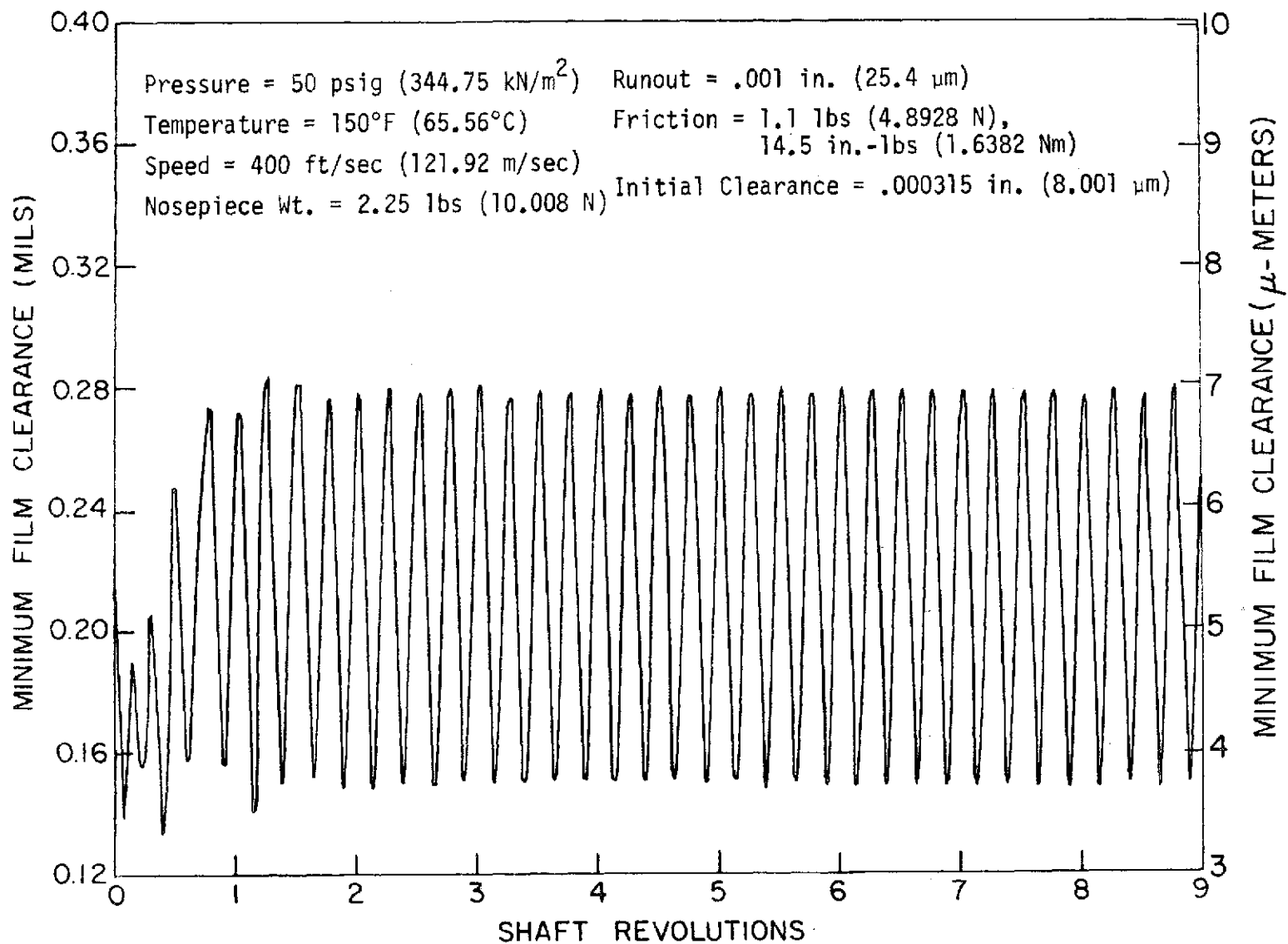


Figure B-59. Fluid Film Force vs. Shaft Revolutions for Case 3

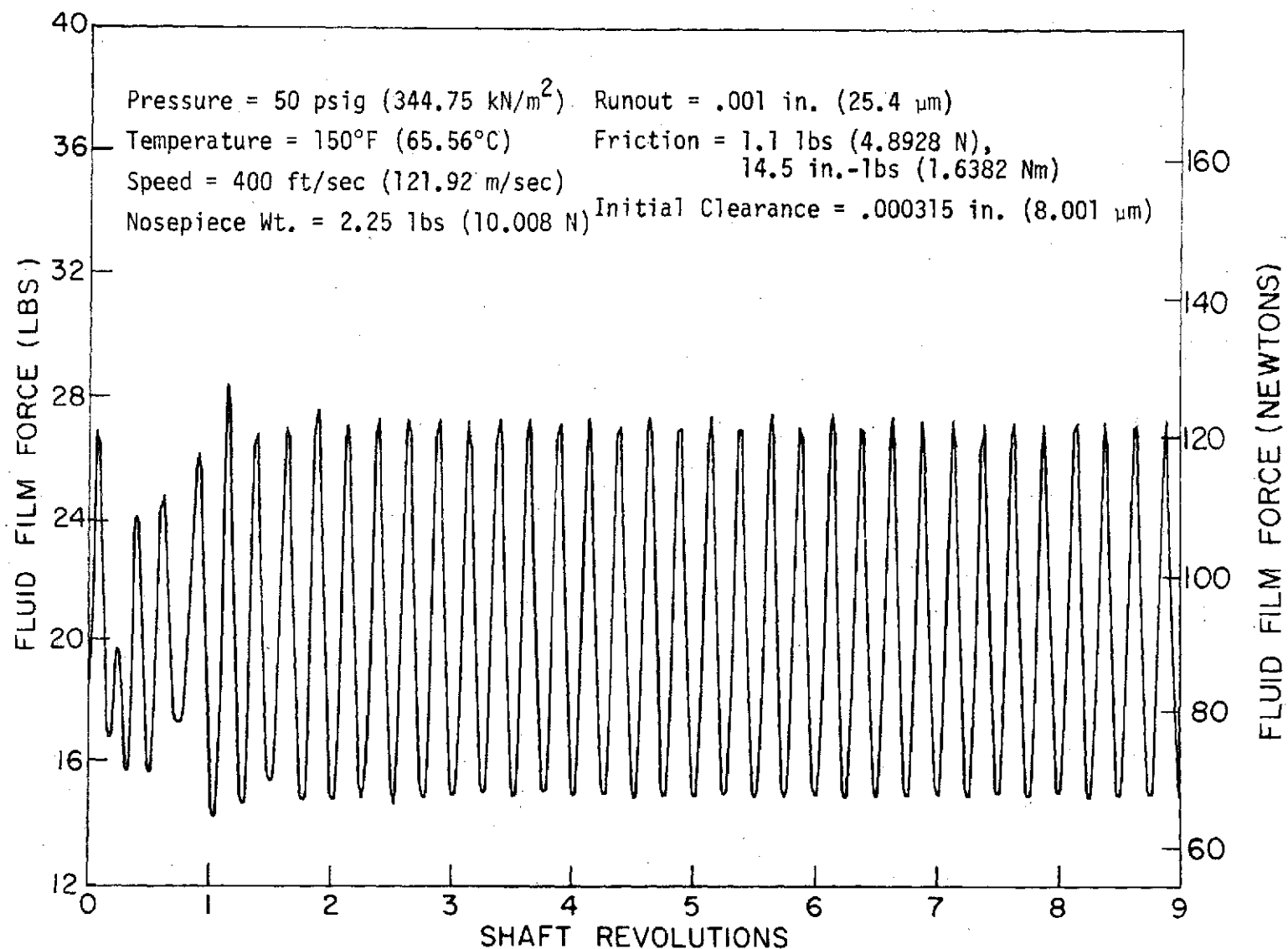


Figure B-60. Fluid Film Moment about X-Axis vs. Shaft Revolutions for Case 3

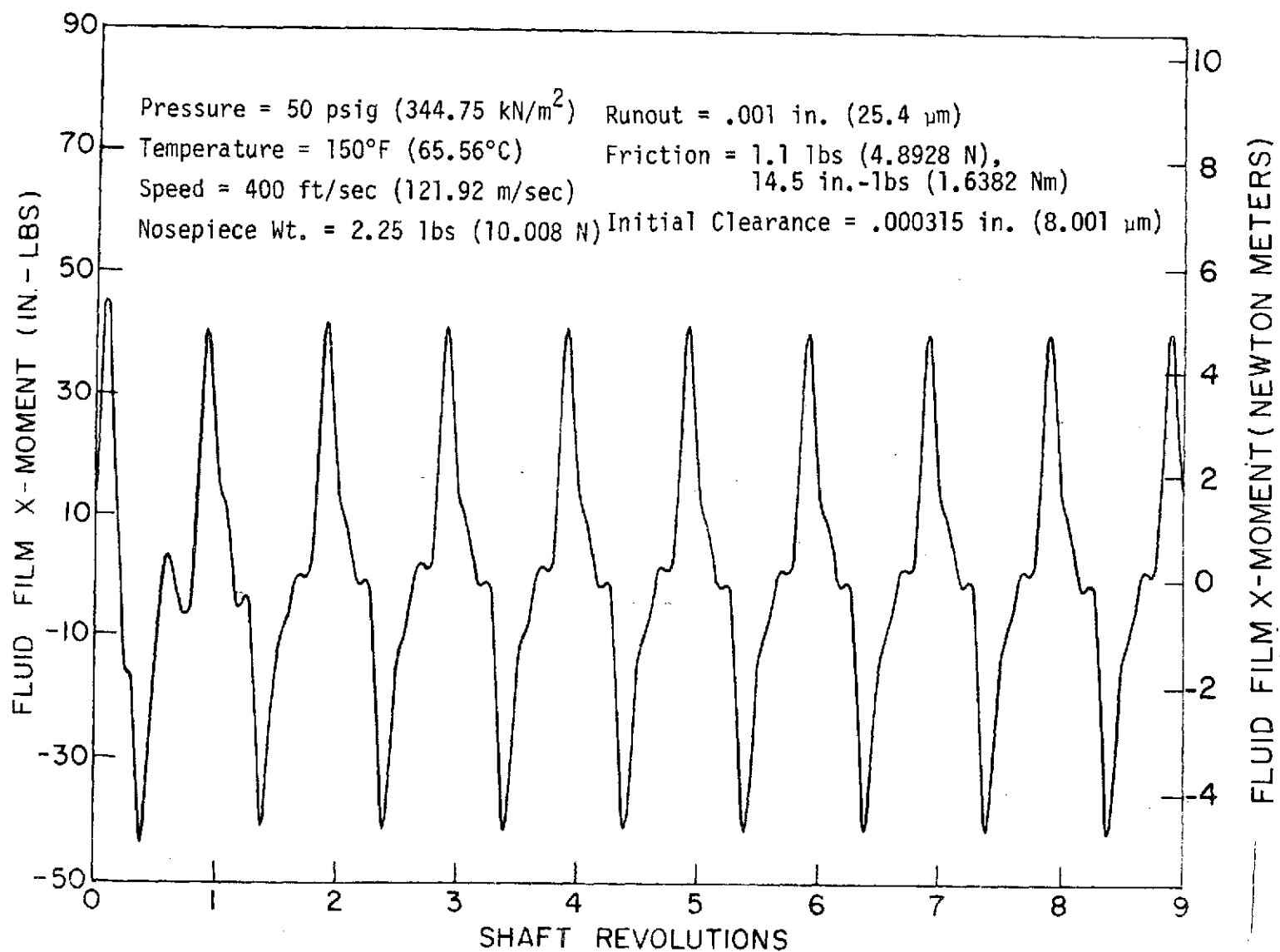
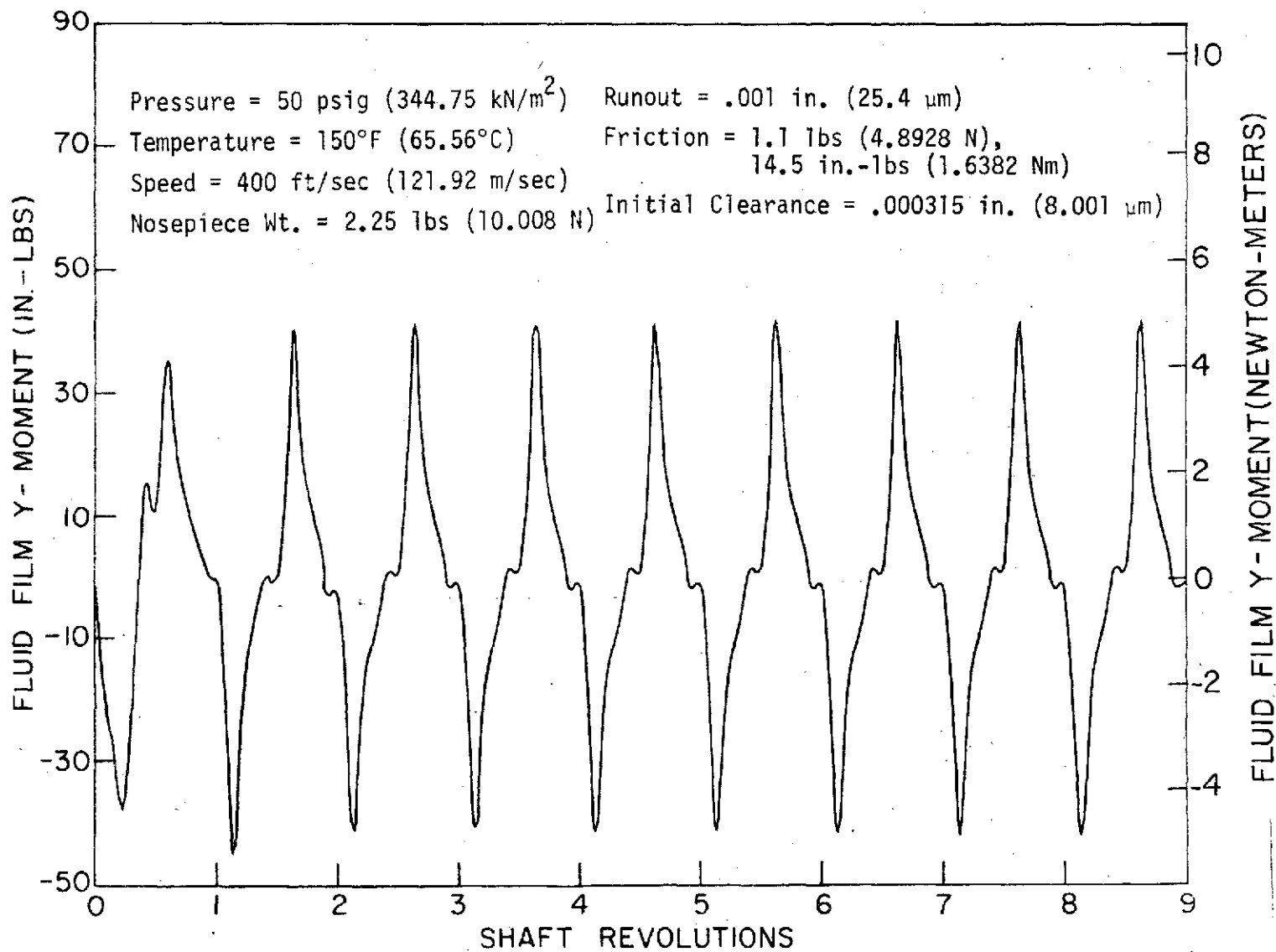


Figure B-61. Fluid Film Moment about Y-Axis vs. Shaft Revolutions for Case 3



SEAL TRANSLATIONS (μ -METERS)

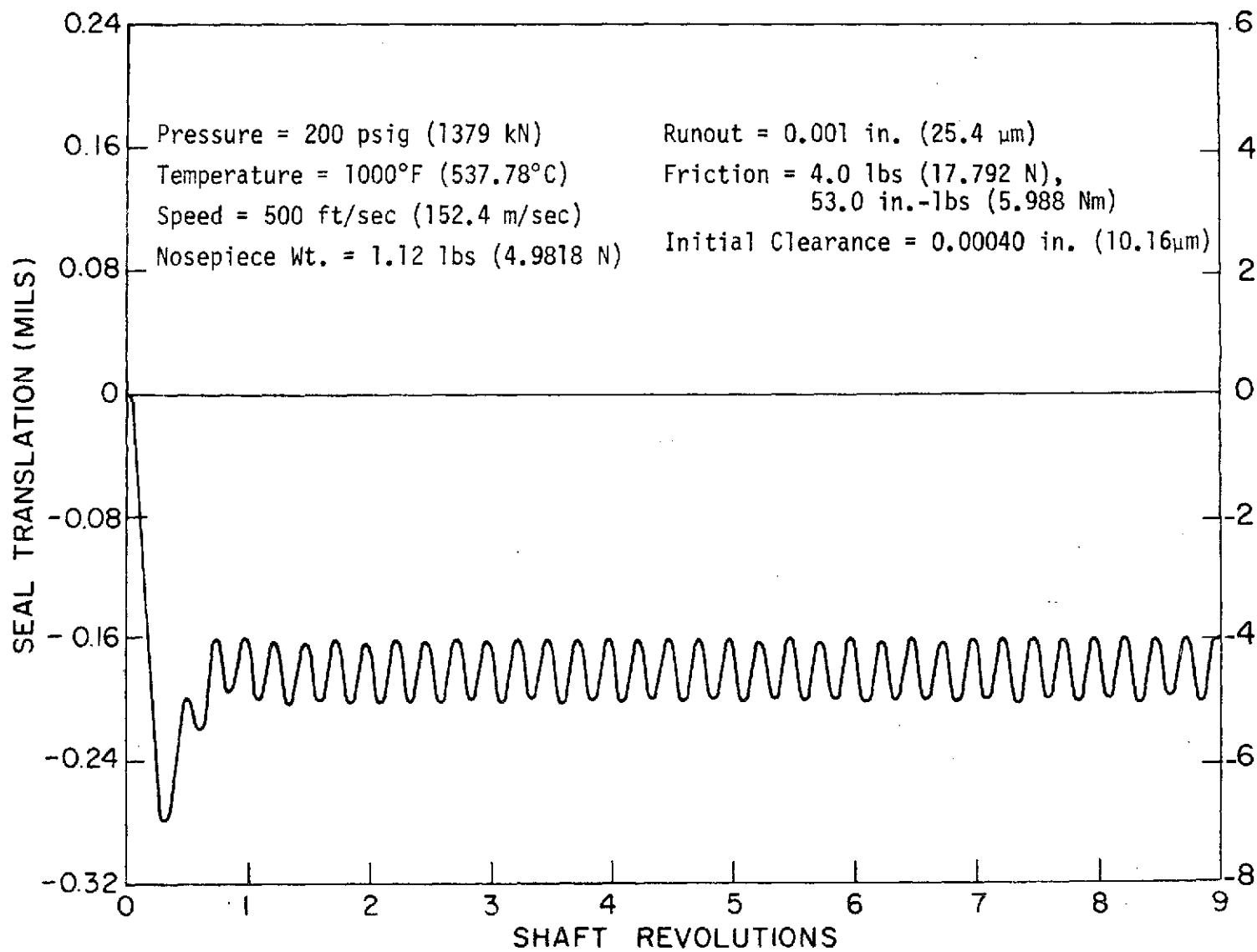


Figure B-62. Seal Translation vs. Shaft Revolutions for Case 4

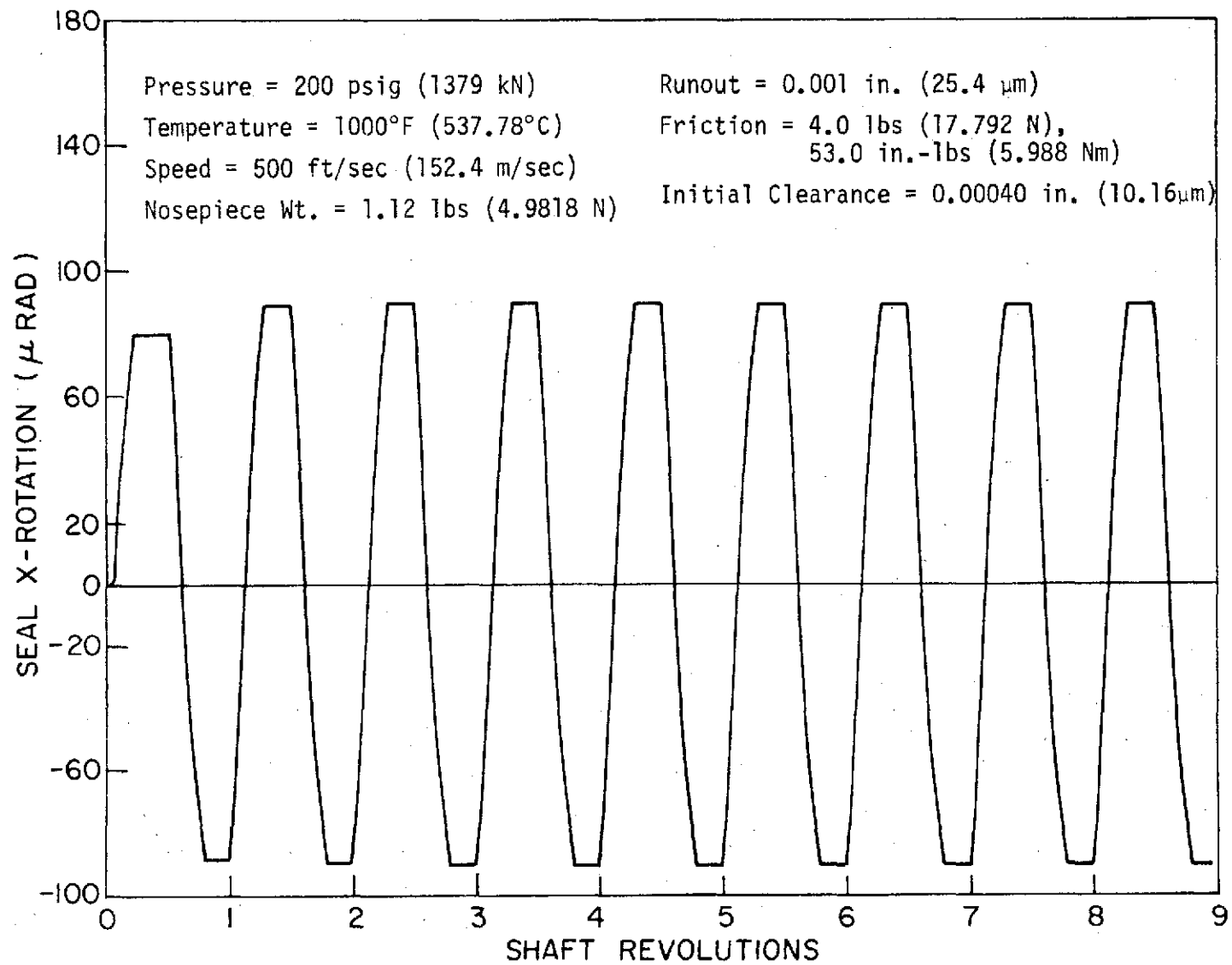


Figure B-63. Seal Rotation about X-Axis vs. Shaft Revolutions for Case 4

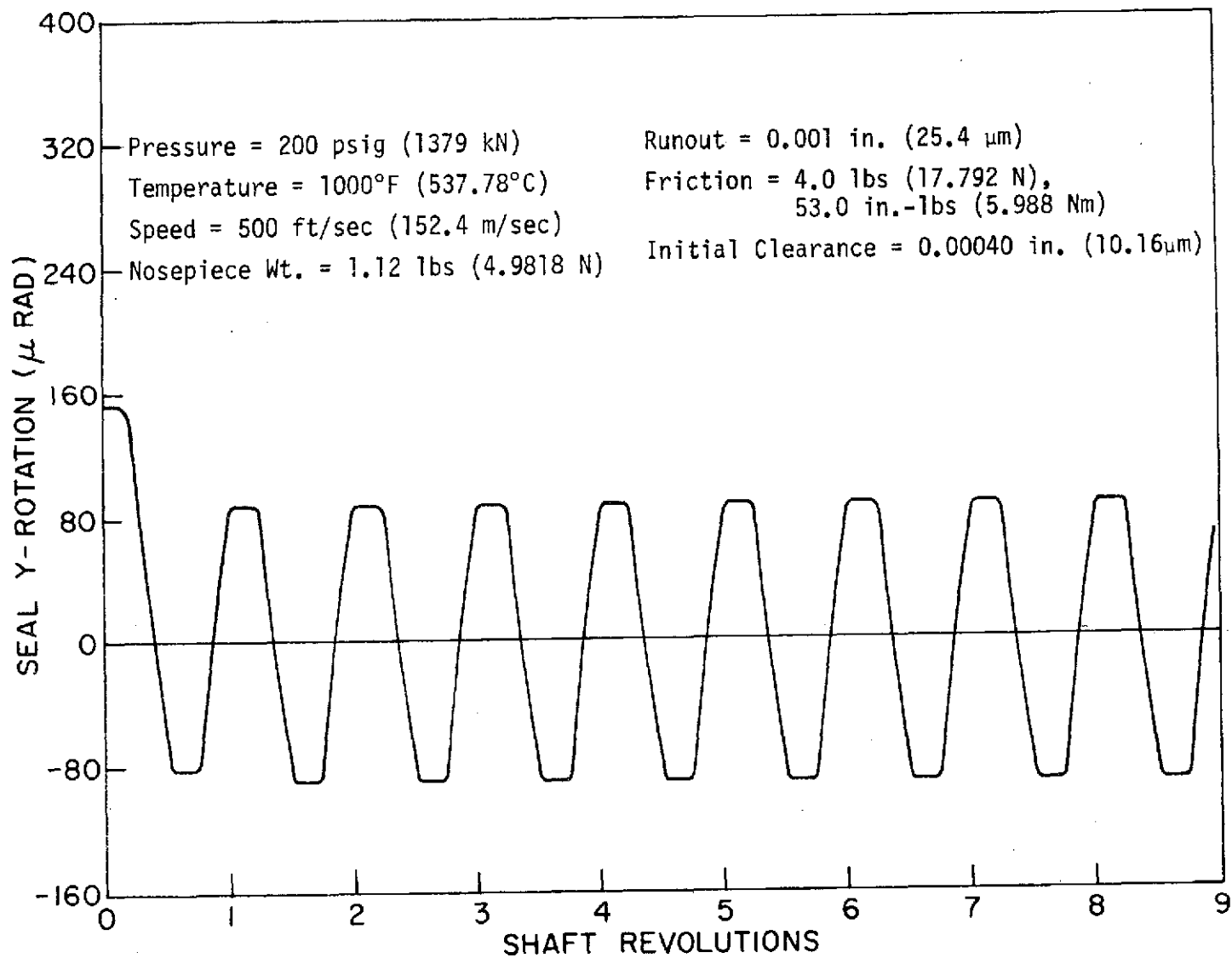


Figure B-64. Seal Rotation about Y-Axis vs. Shaft Revolutions for Case 4

Figure B-65. Minimum Film Thickness vs. Shaft Revolutions for Case 4

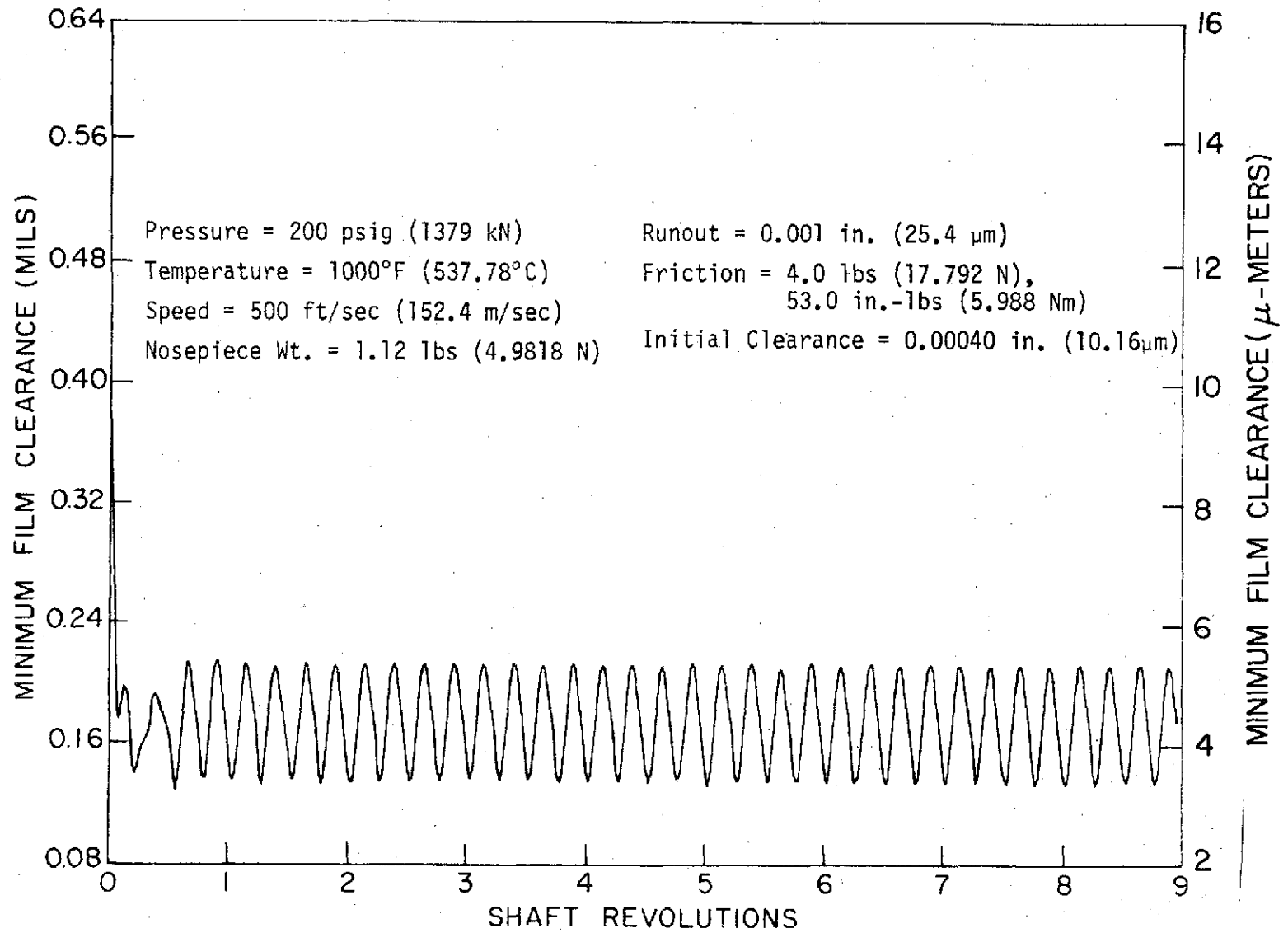


Figure B-66. Fluid Film Force vs. Shaft Revolutions for Case 4

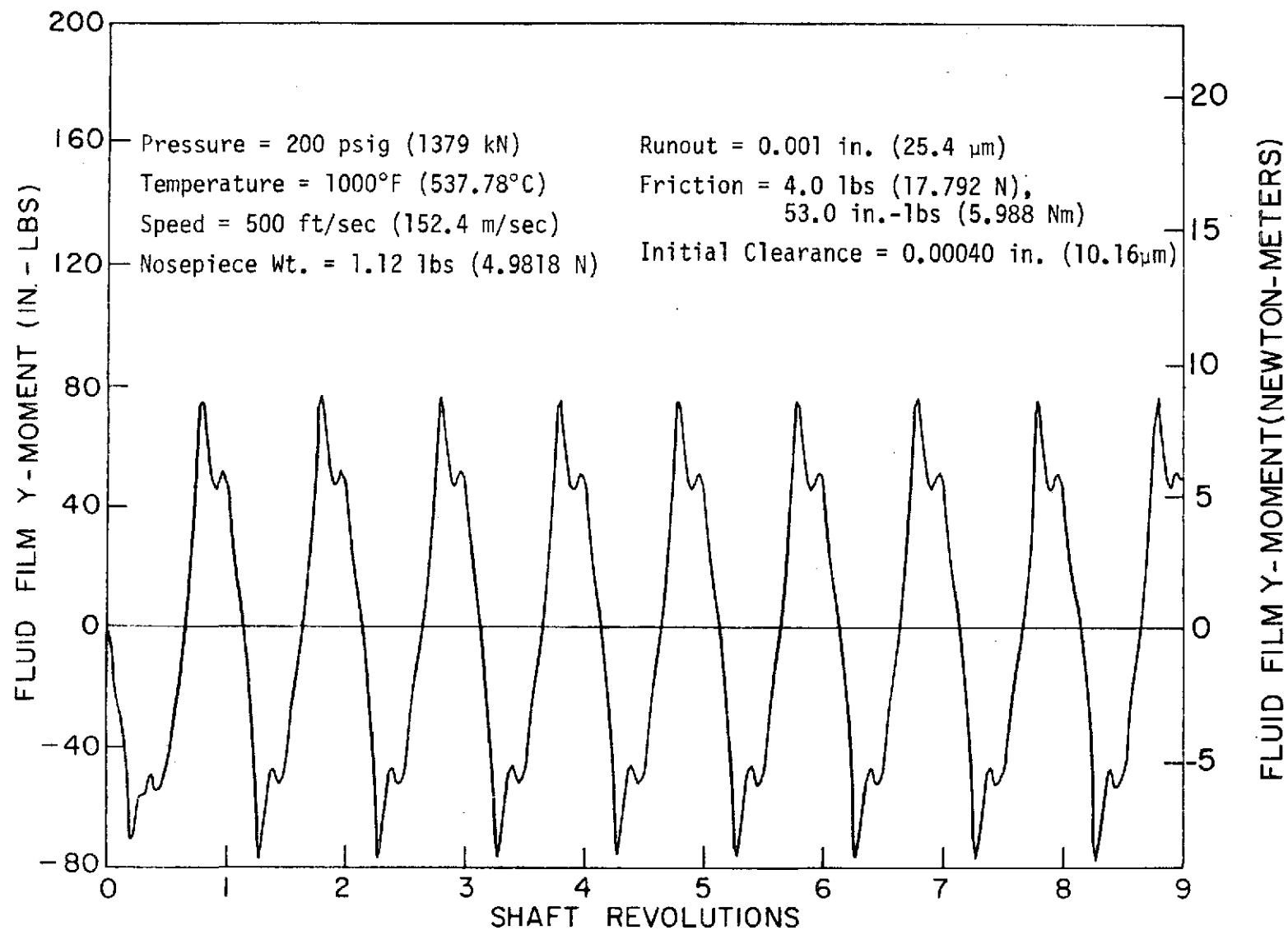


Figure B-67. Fluid Film Moment about X-Axis vs. Shaft Revolutions for Case 4

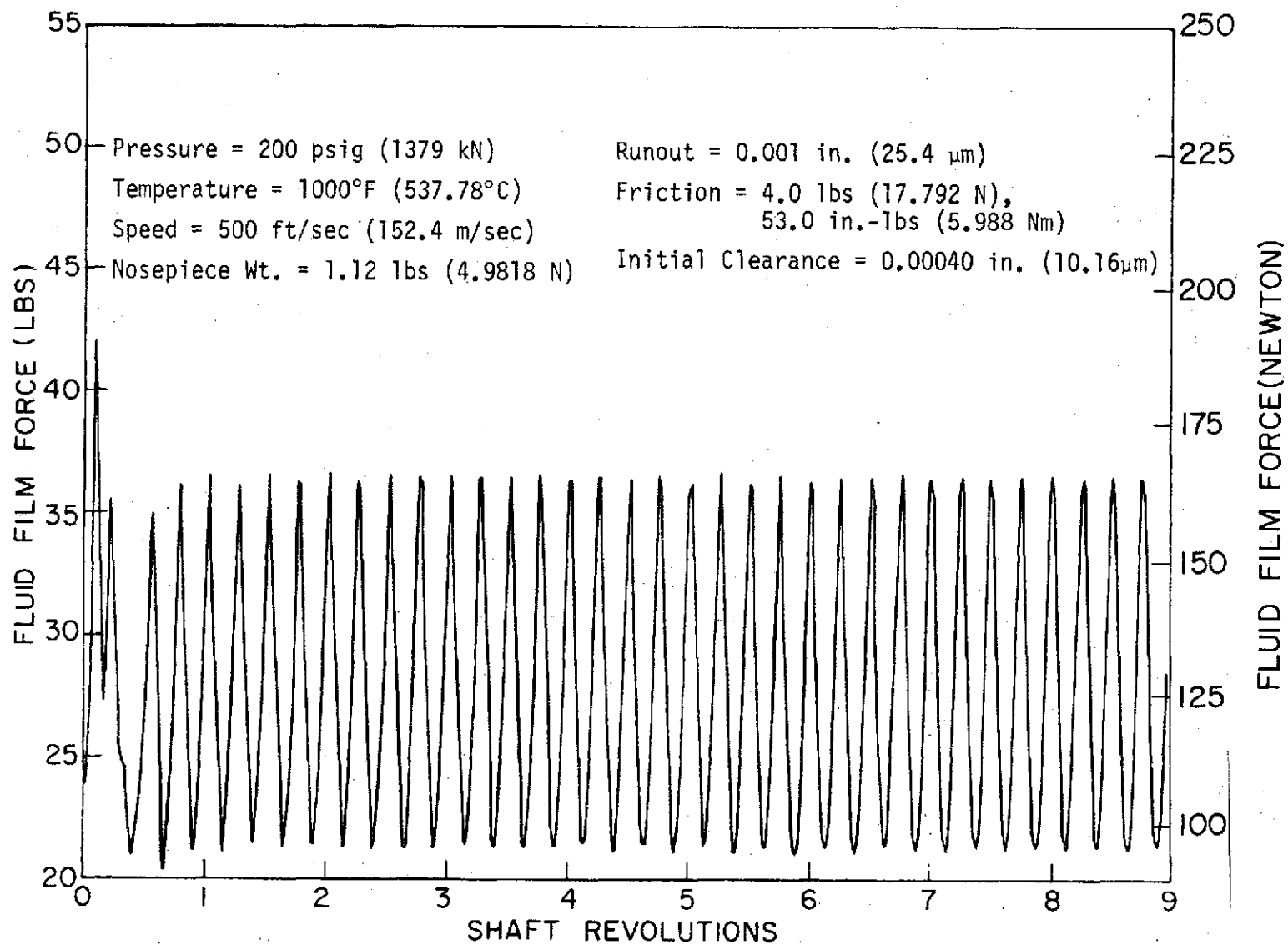
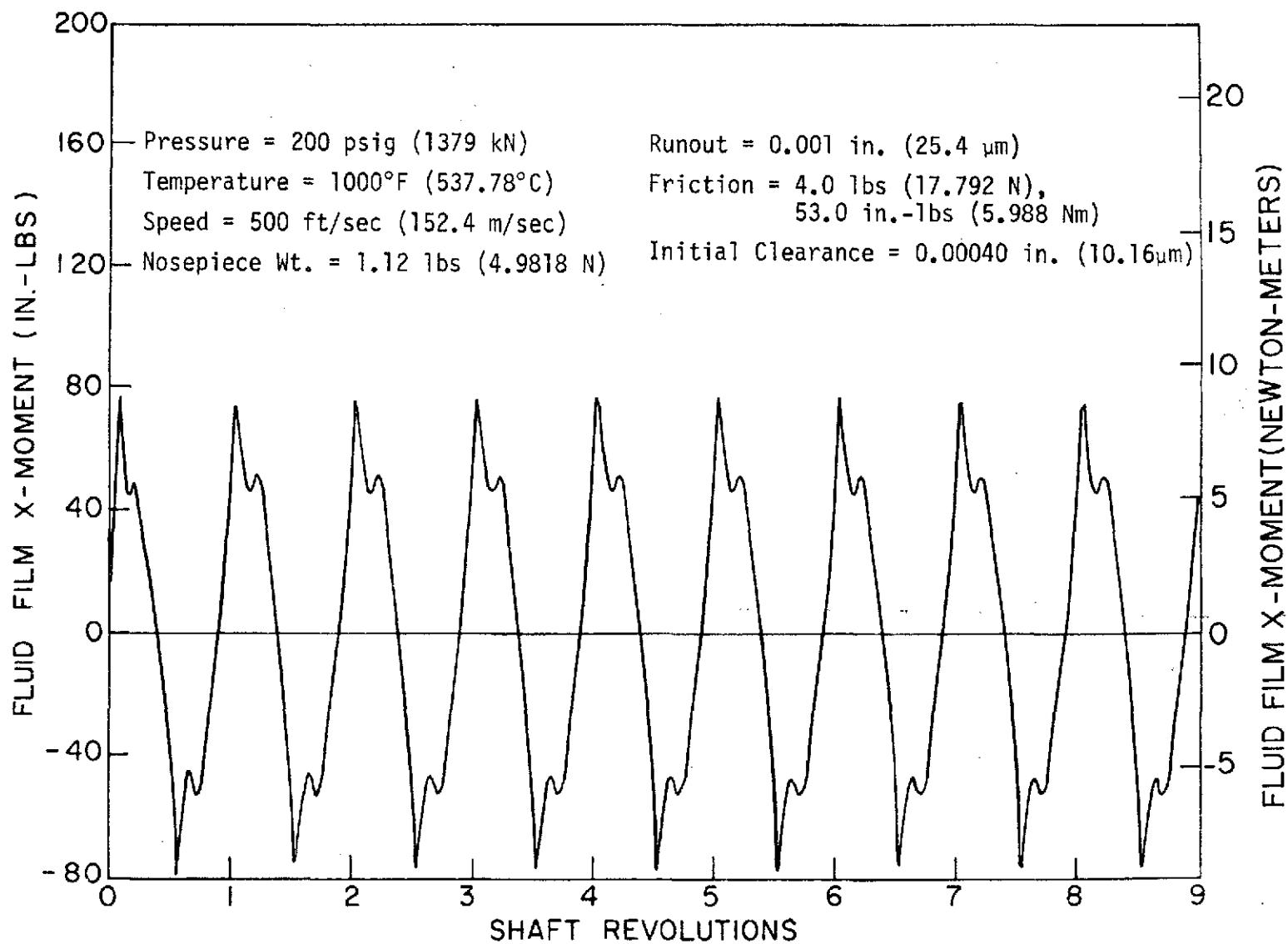



Figure B-68. Fluid Film Moment about Y-Axis vs. Shaft Revolutions for Case 4





F-C3452-1

Appendix

C

COMPUTATION OF PISTON RING FRICTION



THE FRANKLIN INSTITUTE RESEARCH LABORATORIES
THE BENJAMIN FRANKLIN PARKWAY • PHILADELPHIA PENNSYLVANIA 19103

Secondary Seal Ring Friction

Reference 9 gives one procedure used to compute secondary seal ring friction. This approach considers a load balance on the piston ring (Figure C-1) to determine the net radial force acting on the seal carrier. The radial force due to the spring effect of the piston ring is assumed negligible. In this case,

$$F_R = F_3 - F_1 - \eta_{ST} (F_2 - F_4)$$

where η_{ST} is the static coefficient of friction from Case 1 of Table I

$$F_1 = 388.22\text{N (87.22 lbs)}$$

$$F_2 = 1099.99\text{N (247.3 lbs)}$$

$$F_3 = 549.33\text{N (123.50 lbs)}$$

$$F_4 = 384.71\text{N (86.49 lbs)}$$

$$\begin{aligned} F_R &= 549.33 - 388.22 - \eta_{ST} (1099.9 - 384.71) \left| (123.50 - 87.28 - \eta_{ST} (247.3 - 86.49)) \right. \\ &= 161.11 - 715.24 \eta_{ST} \left| (26.22 - 160.8 \eta_{ST}) \right| \end{aligned}$$

Therefore for coefficient of sliding friction greater than .1 (static friction approximately equal to .2) the net radial force would be zero. This obviously is not true.

If the piston ring were allowed to seat first against the seal carrier then the radial force is only a fraction of F_1 and F_3 . It is believed that this case more accurately represents the actual physical cases. Therefore,

$$F_R = F_3 - F_1 = 161.11\text{N (36.22 lb)}$$

The friction force becomes

$$F_{fr} = \eta F_R = 161.11\eta \text{ (36.22}\eta\text{)}$$

where

η is the sliding coefficient of friction

F_R is the radial force (161.11N (36.22 lbs))

F_{fr} is the axial friction force

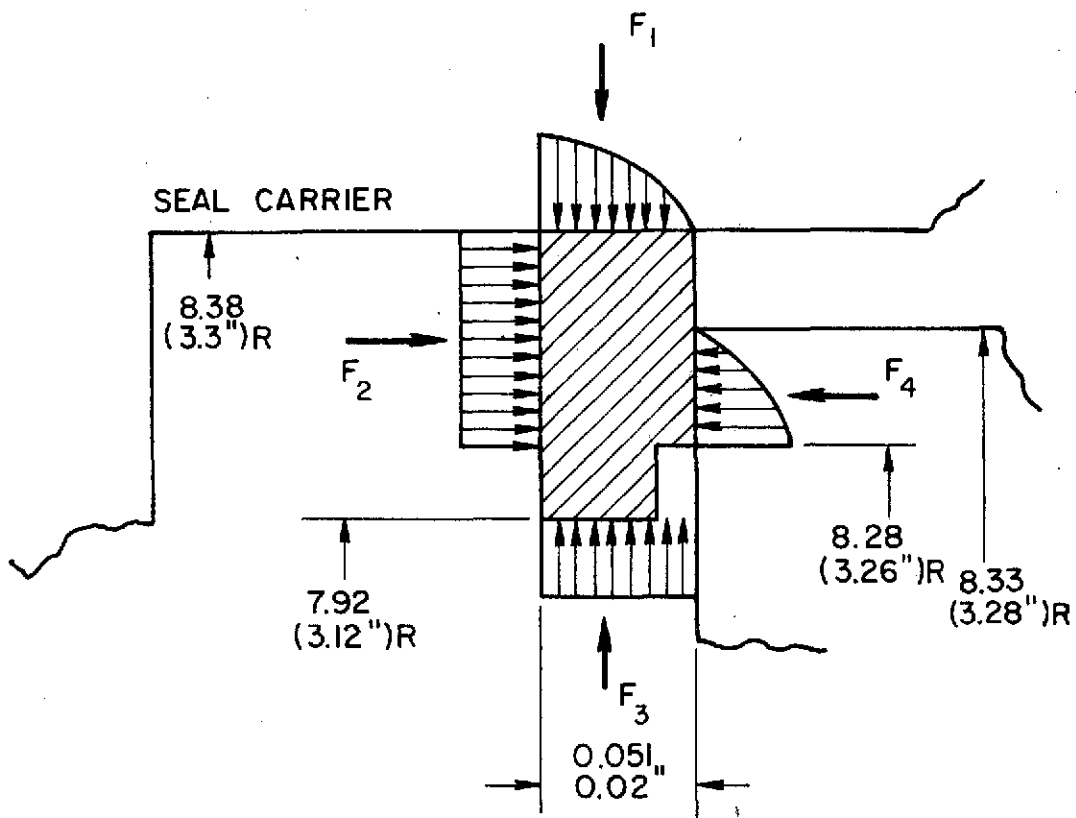


Figure C-1. Force Balance on Piston Ring Secondary Sealing Surfaces

Frictional moments can then be determined by examining the friction force per unit area ($\eta F_r/A$) applied to an incremental area (dA) shown in Figure C-2. The friction force applied to this area becomes

$$dF_{fr} = \eta F_r$$

$A = 2\pi rL$ contact area

r = radius of piston ring
8.38 cm (3.3 in.)

L = axial length of contact
.051 cm (.02 in.)

η = coefficient of sliding friction

$dA = Lr d\theta$

The friction moment about the x axis which is equivalent to the moment about the y axis becomes

$$M_{fr} = 2 \int_0^{\pi} r \sin \theta dF_r$$

M_{fr} is the friction moment

$$= \frac{r F_r \eta}{\pi} \int_0^{\pi} \sin \theta d\theta$$

$$M_{fr} = 2.1 F_{Fr}$$

Therefore the friction levels are

η	f_{fr}		M_{fr}	
	<u>N</u>	<u>lbs</u>	<u>N-m</u>	<u>in.-lbs</u>
0	0.0	0	0.0	0
.03	4.45	1	.226	2
.11	17.79	4	.904	8
.17	26.69	6	1.47	13
.22	35.58	8	1.92	17
.30	48.93	11	2.60	23
.39	62.27	14	3.28	29
.77	124.54	28	6.67	59
> 1	177.92	40	9.49	84
> 1	222.4	50	11.86	105

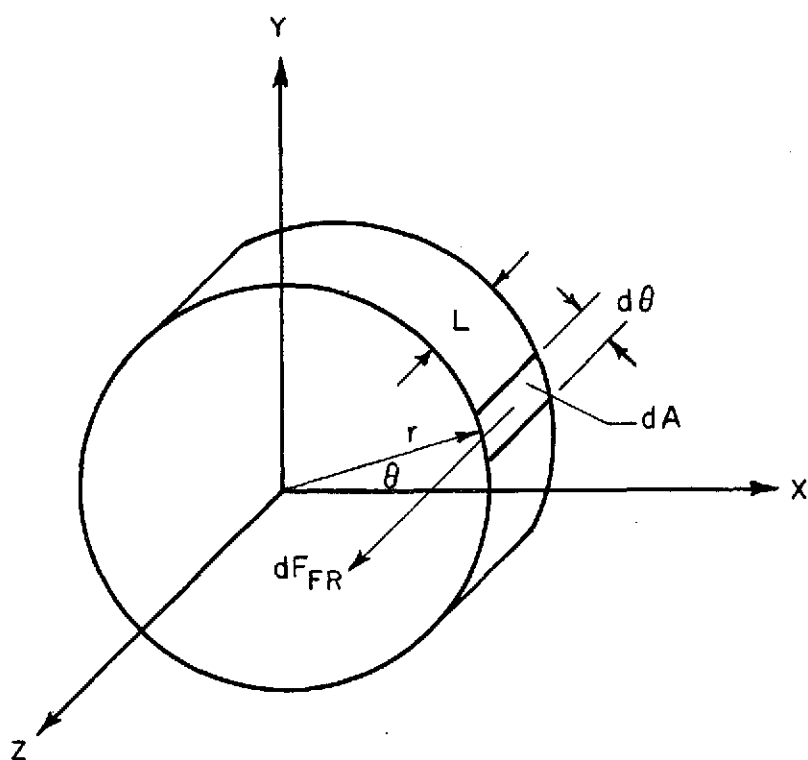


Figure C-2. Friction Moment - Secondary Seal